Loughborough University

Thesis Access Form

Copy No.....**Location**.....

Author.....**Samuel James Allen**.....

Title.....**Optimisation of Performance in the Triple Jump Using Computer Simulation**.....

Status of access OPEN

Moratorium Period:.....years, ending...../.....200.....

Conditions of access approved by (CAPITALS):M.R. YEADON.....

Supervisor (Signature).....MRYeadon.....

Department of...**School of Sport, Exercise and Health Sciences**.....

Author's Declaration: *I agree the following conditions:*

Open access work shall be made available (in the University and externally) and reproduced as necessary at the discretion of the University Librarian or Head of Department. It may also be digitised by the British Library and made freely available on the Internet to registered users of the EThOS service subject to the EThOS supply agreements.

*The statement itself shall apply to **ALL** copies including electronic copies:*

This copy has been supplied on the understanding that it is copyright material and that no quotation from the thesis may be published without proper acknowledgement.

Restricted/confidential work: All access and any photocopying shall be strictly subject to written permission from the University Head of Department and any external sponsor, if any.

Author's signature.....Sam Allen.....Date.....08/10/09.....

users declaration: for signature during any Moratorium period (Not Open work): ***I undertake to uphold the above conditions:***			
Date	Name (CAPITALS)	Signature	Address

OPTIMISATION OF PERFORMANCE IN THE TRIPLE JUMP USING COMPUTER SIMULATION

by

Samuel James Allen

A Doctoral Thesis

Submitted in partial fulfilment of the requirements for the award of Doctor of Philosophy of Loughborough University

October 2009

Loughborough University

CERTIFICATE OF ORIGINALITY

This is to certify that I am responsible for the work submitted in this thesis, that the original work is my own except as specified in acknowledgments or in footnotes, and that neither the thesis nor the original work contained therein has been submitted to this or any other institution for a degree.

..... (Signed)

08/10/09 ..... (Date)

ABSTRACT

OPTIMISATION OF PERFORMANCE IN THE TRIPLE JUMP USING COMPUTER SIMULATION

Samuel James Allen, Loughborough University, 2009

While experimental studies can provide information on what athletes are doing, they are not suited to determining what they should be doing in order to improve their performance. The aim of this study was to develop a realistic computer simulation model of triple jumping in order to investigate optimum technique. A 13-segment subject-specific torque-driven computer simulation model of triple jumping was developed, with wobbling masses within the shank, thigh, and torso. Torque generators were situated at each hip, shoulder, knee, ankle, and ball joint. Kinetic and kinematic data were collected from a triple jump using a force plate and a Vicon motion analysis system. Strength characteristics were measured using an isovelocity dynamometer from which torque-angle and torque-angular velocity relationships were calculated. Segmental inertia parameters were calculated from anthropometric measurements. Viscoelastic parameters were obtained by matching an angle-driven model to performance data for each phase, and a common set for the three contact phases was determined. The torque-driven model was matched to performance data for each phase individually by varying torque generator activation timings using a genetic algorithm. The matching produced a close agreement between simulation and performance, with differences of 3.8%, 2.7%, and 3.1% for the hop, step, and jump phases respectively. The model showed good correspondence with performance data, demonstrating sufficient complexity for subsequent optimisation of performance. Each phase was optimised for jump distance with penalties for excessive angular momentum at take-off. Optimisation of each phase produced an increase in jump distance from the matched simulations of 3.3%, 11.1%, and 8.2% for the hop, step, and jump respectively. The optimised technique showed a symmetrical shoulder flexion consistent with that employed by elite performers. The effects of increasing strength and neglecting angular momentum constraints were then investigated. Increasing strength was shown to improve performance, and angular momentum constraints were proven to be necessary in order to reproduce realistic performances.

PUBLICATIONS

Conference presentations:

ALLEN, S.J., 2007. Contributions to performance in the triple jump, *IAAF Elite Coaches Conference,* 2007.

ALLEN, S.J., KING, M.A. and YEADON, M.R., 2009. Evaluation of a computer simulation model of triple jumping, *Proceedings of the XXII Congress of the International Society of Biomechanics,* 5-9 July 2009, [CD-ROM].

ALLEN, S.J., KING, M.A. and YEADON, M.R., 2009. Optimisation of performance in triple jumping, *Proceedings of the 12th International Symposium on Computer Simulation in Biomechanics,* 2-4 July 2009, pp5-6.

ALLEN, S.J., KING, M.A. and YEADON, M.R., 2006. Issues in determining accurate joint torques by quasi-static and inverse dynamic analyses, *Proceedings of the Biomechanics Interest Group of the British Association of Sport and Exercise Sciences,* 2006, pp4.

ACKNOWLEDGEMENTS

I would like to thank my supervisors, Prof. Fred Yeadon and Dr Mark King, for their guidance and support throughout this project. Special mention must also go to Dr. Steph Forrester who has often acted as a third supervisor in all but name. I would also like to acknowledge the financial support of the School of Sport, Exercise and Health Sciences. I would like to express my gratitude to Andrew Bell for acting as subject in this study. Finally, I would like to thank everyone in the Sports Biomechanics and Motor Control Research Group and associates (Matt, Mike, Lesley, Peter, Jono, Andy, David, Emma, Chris, Behzat, Felix, Idafe, Martin, Neale, Phil, Monique, Helen, David, Roger, Mickael, Filipe, Akiko, John, Alec, Sarah, Gheorghe, Jo, and Bob) who have provided assistance and friendship during my time in Loughborough.

DEDICATION

To Claire, and My Family

TABLE OF CONTENTS

LIST OF FIGURES

LIST OF TABLES

CHAPTER 1

INTRODUCTION

1.1 CHAPTER OVERVIEW

In this chapter an introduction to the triple jump is given. Previous literature on triple jumping is discussed and the purpose of the study is outlined. Research questions are posed and described with reference to the literature. Lastly an overview of the thesis is given with brief descriptions of each chapter.

1.2 THE AREA OF STUDY

The triple jump is an athletic event comprising a run up followed by three consecutive phases (Figure 1.1): The hop, a take-off from one foot, landing on the same foot; the step, a take-off from one foot, landing on the other foot; and the jump, a take-off from one foot, landing in the sand pit, usually on two feet.

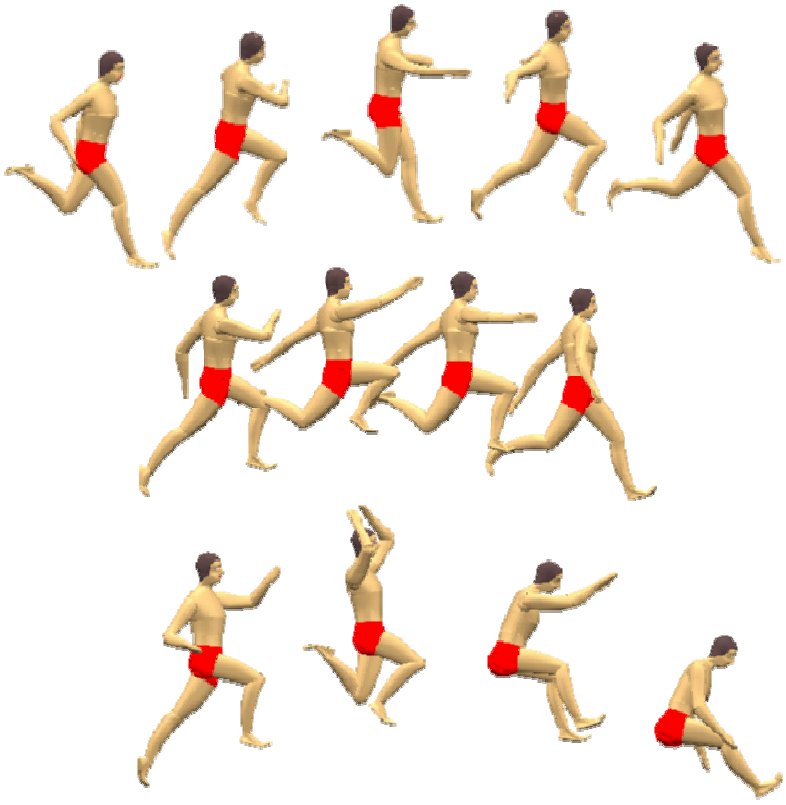

Figure 1.1 The three phases of a triple jump.

1.3 PREVIOUS LITERATURE

There have been a number of studies investigating human jumping activities. These can be split broadly into those that are experimental and those that are theoretical in nature. The experimental studies can be further split into those dealing with athletic events involving an approach run followed by a take-off from one leg: the high; long; and triple jumps, (Dapena and Chung, 1988; Lees et al., 1993; Hay, 1992). And those concerned with more general two-legged jumping motions with no approach run: squat; countermovement; and drop jumps (Viitasalo et al., 1998). The theoretical studies can again be split into two categories: predictive (Wakai and Linthorne, 2002; Yu and Hay, 1996); and analytical (Alexander, 1990, 1992; Hatze, 1981; Anderson and Pandy, 1999; van Soest et al., 1993). Predictive models have been used to attempt to mathematically predict behaviour from the interaction of a few parameters, without attempting to model the system as a whole, whereas analytical models have attempted, with the use of computers and with obvious simplifications, to model the entire system.

The majority of studies of triple jumping have been concerned with attempting to determine the optimum ratio of each phase to the total distance jumped (Figure 2.7) (Miller and Hay, 1986; Hay 1992, 1993, 1995, 1997, 1999; Yu and Hay, 1996; Yu, 1999). Hay (1992) stated that the identification of the optimum phase ratio for an athlete, 'should take priority over all other problems of triple jump technique because, without a solution to this problem, all others must be considered in ignorance'. From 1911 to 1985 a general trend away from a hop-dominated technique with a small step phase (39%:22%:37%) towards a more balanced (37-39%:28-30%:31-33%) and latterly jump-dominated technique (34-35%:28-30%:36-37%) was seen (Hay, 1993). Hay (1999) observed that roughly half the competitors in the final of the 1996 Olympic Games employed hop-dominated techniques and half employed other techniques. Therefore, despite the number of studies in this area, these results indicate that no consensus has been reached either in the scientific community or the athletic community as to whether optimum phase ratios for triple jumping exist, and, if so, what they are.

Hay (1993) stated that the peak ground reaction forces (GRFs) recorded during the support phase of the step in triple jumping are, 'much greater than a human limb is exposed to in

any other voluntary activity for which data could be found'. These forces range from 12.6 times bodyweight in college level triple jumpers (Ramey and Williams, 1985), through 15.4 times bodyweight (Perttunen et al., 2000), to 14.0-22.3 times bodyweight (Amadio, 1985). Hay (1993) stated that even 22.3 times bodyweight may be an underestimate of the forces elite triple jumpers undergo, since the largest jump distance recorded by Amadio (1985) was 15.35 m, nearly 3 m less than the current male world record of 18.29 m. Perhaps unsurprisingly considering these high forces in the stance leg, epidemiological studies have shown the most common sites of injury in triple jumpers are the ankle, knee, hip, and lower back (Kutsar, 1988).

Hay (1992), in his comprehensive review of triple jump biomechanics, considered various kinematic variables such as: take-off, flight, and landing distances; and the heights of the centre of mass (COM) at touchdown and take-off. He found that the results for all these measures were highly variable, with no consistent trends presenting themselves. Hay (1992) also considered various technical issues such as the optimal use of the free leg, and the contentious issue of whether to employ a single-arm or double-arm technique, or some combination of the two.

Other studies have investigated the effects of angular momentum (Yu and Hay, 1995) and the contribution of the free limbs (Yu and Andrews, 1998) to performance. Yu and Hay, (1996) and Yu (1999) produced mathematical models to investigate the optimum horizontal-to-vertical velocity conversion ratios.

It is evident that there are a number of unanswered questions raised in the literature on triple jumping, the overriding one being what the optimum phase ratios for any given athlete are, and which factors determine these ratios. In addition to this, another controversial issue is what the optimum arm technique is. Also, although the magnitude of the GRFs are reasonably well documented for triple jumpers of various abilities, little attempt has been made to determine the internal forces and moments acting on the support leg of the triple jumper (Hay, 1993).

1.4 STATEMENT OF PURPOSE

All the studies described above used experimental data to describe kinematic and kinetic features of the triple jump in subjects ranging from novices to elite performers. This method of investigation is useful for providing information on what techniques various athletes currently employ, but is not well suited to predicting what techniques athletes should employ in order to maximise the distance of their jumps. With this in mind the purpose of this study was to develop a torque-driven computer simulation model of triple jumping in order to investigate optimum technique. Anthropometric, strength, and performance data will be obtained from a national standard triple jumper in order that the model may be subject-specific. Subject-specific viscoelastic parameters will be derived by matching an angle-driven model to performance data. The torque-driven model will then be evaluated against performance data to ensure that it is a good representation of the activity being modelled. The technique employed by the model will be optimised in order to maximise the distance jumped in each phase individually. This will enable conclusions to be drawn on the components of optimal technique. Since the technique of the model will be optimised for each phase individually, only components of optimal technique at each phase will be commented on. However, the model will also be capable of simulating all three phases sequentially, and this will allow future investigations into factors such as optimal phase ratios and projection angles.

1.5 RESEARCH QUESTIONS

Q1. How close to optimum was the technique of the subject in this study?

A subject-specific computer simulation model of triple jumping will allow an investigation into the effectiveness of the technique of the subject from which data were collected. The anthropometry, mass and inertia, and strength of the model will represent that obtained from measurements of the subject. Kinematic data of the subject performing a triple jump will provide a detailed representation of the technique he currently employs. A subsequent optimisation of the torque generator activation timings governing the movement of the model in order to maximise the distance jumped in each phase will allow a subject-specific performance improvement to be calculated.

Q2. What is the optimum arm technique for triple jump performance?

Hay (1992) stated that, 'that the arm action used at take-off into each of the three phases has been the source of considerable debate over the last 2-3 decades'. The debate centres on the relative merits of the single-arm technique, where the arms move in an asymmetric fashion, mirroring the action of the contralateral leg as they do in running, or the double-arm technique where both arms start in a hyperextended position behind the body and are flexed throughout the take-off. Hay (1992) observed that numerous points have been raised in the course of the debate but no quantitative data have been presented to back them up. He concluded that this extended debate has been useful in identifying factors that may bear on the issue but little progress was likely to be made towards an understanding without carefully designed experiments, appropriate data, and a rational interpretation of the findings. A computer simulation model of triple jumping will facilitate the optimisation of arm technique and allow a quantifiable understanding of the merits of this technique.

Q3. How would an increase in strength affect triple jump performance?

Athletes spend hours in the gym in an attempt to increase the strength of muscles that span various joints, believing that this will facilitate a performance improvement. However the isolated effects of these changes in strength on performance are hard to gauge. Bobbert and van Soest (1994) found that increases in strength resulted in a decrement in vertical jump performance if original muscle activation timings were maintained; however, after a re-optimisation of these muscle activation timings, performance increased in line with strength increases. The effects of an increase in strength on triple jump performance can be quantified using the computer simulation model of triple jumping.

Q4. What influence do angular momentum constraints have on simulations of the triple jump?

In all human jumping activities there has to be a consideration of the effects of angular momentum generated during take-off on the ability to achieve a requisite landing orientation. This is likely to be particularly marked in triple jumping in comparison to jumps with only one take-off phase, since not only does the athlete have to land, but on

two occasions, also coordinate another single leg take-off involving extremely high and potentially damaging GRFs. Wilson et al. (2007) found that including constraints on angular momentum at take-off in their model of running vertical jumping decreased the height jumped by 0.16 m. They concluded that these constraints should be included if models of jumping are to produce realistic results. The computer simulation model will allow the effects of these angular momentum constraints on triple jump performance to be ascertained.

1.6 CHAPTER ORGANISATION

Chapter 2 comprises a critical review of the literature in human jumping activities. In this review experimental and theoretical studies are considered in separate sections. The review of experimental studies is further split based on the types of activity they investigated: high, long, and triple jumps; and squat, drop, and countermovement jumps. The review of theoretical studies is also split based on whether they were predictive or analytical in nature.

Chapter 3 includes a critical review of literature relevant to the construction of the simulation model of triple jumping. This comprises a review of simulation models of jumping in the literature, soft tissue motion, muscle models, and optimisation algorithms. The construction of the simulation model of triple jumping is then described. This details the rigid and wobbling elements of the model, torque generators, and spring-dampers.

Chapter 4 describes the methods used to collect performance, strength, and anthropometric data from a triple jumper, and the subsequent parameter determination. This performance data comprises kinematic and kinetic data from a number of partial and complete triple jumps. Methods for the calculation of joint angles and the filtering of force data are explained. The protocol for obtaining strength data is outlined and the method for the calculation of torque / angle / angular velocity functions is described. The collection of anthropometric data and method for calculation of segmental inertia parameters are then detailed.

Chapter 5 includes a review of literature on the evaluation of simulation models of jumping and optimisation algorithms. A description of methods for the calculation of subject-specific viscoelastic parameters using an angle-driven model of each phase of the triple jump is given. The methods for the evaluation of a torque-driven model are then described. The results of this evaluation are reported and discussed in the form of: the components of phase distances; joint angles; joint torques; and torque generator activation timings.

Chapter 6 contains a review of literature on the optimisation of models of jumping. The methods for optimisation of the torque-driven model of each phase of triple jumping are described. The results of the optimisation of technique are then reported and analysed in the form of: the components of phase distance; joint angles; joint torques and torque generator activation timings; work / impulse analyses; and GRFs.

Chapter 7 provides a summary of the thesis. This includes a consideration of the techniques of kinematic, kinetic, and anthropometric data collection, and potential areas for improvement in future studies. Improvements to the structure of the model with regard to the calculation of viscoelastic parameters are discussed. The evaluation and optimisation of the model are then summarised and briefly discussed. Research questions posed in Chapter 1 are then answered with reference to the results of the optimisation of technique. Lastly, future applications of the model are described.

CHAPTER 2

REVIEW OF LITERATURE

2.1 CHAPTER OVERVIEW

In this chapter research literature on jumping activities is reviewed. Literature pertaining to other specific areas of this thesis, such as data collection techniques, model evaluation, and model optimisation, will be included within the relevant chapters for ease of reference. Initially, experimental studies focusing specifically on the high, long, and triple jumps are discussed, followed by a brief overview of studies investigating squat, drop, and countermovement jumps. Theoretical models of jumping of a predictive nature are then considered. Theoretical models of jumping that incorporate computer simulation are included in Chapter 3.

2.2 EXPERIMENTAL JUMPING STUDIES

A number of research studies have been performed using data from various human jumping activities in an attempt to outline factors that affect performance. These studies can be split into those dealing with one-legged jumps that utilise an approach run, usually athletic events: the high; long; and triple jumps (Dapena and Chung, 1988; Lees et al., 1994; Hay, 1993). And those concerned with non-sports-specific two-legged jumps with no approach run: squat; countermovement; and drop jumps (Viitasalo et al., 1998). There has been considerable experimental research done on squat, countermovement, and drop jumps (Komi and Bosco, 1978; Bosco and Komi, 1979; Hudson 1986; Bobbert et al., 1986, 1987a, 1987b; Bobbert and Ingen Schenau, 1988), the majority of this was considered to be beyond the scope of this review. Since this study is concerned with the computer simulation of the triple jump the review of experimental literature will concentrate on the high, long, and triple jumps. There is a consideration of two-legged jumps in the review of computer simulation studies in Chapter 3.

Although they are slightly different in nature, very close parallels can be drawn between technical issues in high and long jumping, and those in triple jumping. Each involves an approach run followed by a take-off from one leg, requiring a generation of vertical velocity facilitated by the horizontal approach velocity.

2.2.1 High jump

Leg angles during take-off

Greig and Yeadon (2000) investigated the effects of various kinematic parameters at the point of touchdown of the foot in the take-off stride on the performance of high jumpers. They found that the optimum velocity of approach for the high jumper studied was 7.0 m/s which was towards the upper end of the range of velocities observed. They also found that optimum performance was achieved with a minimum amount of knee flexion and with a leg plant angle of 34° from the vertical (Figure 2.1).

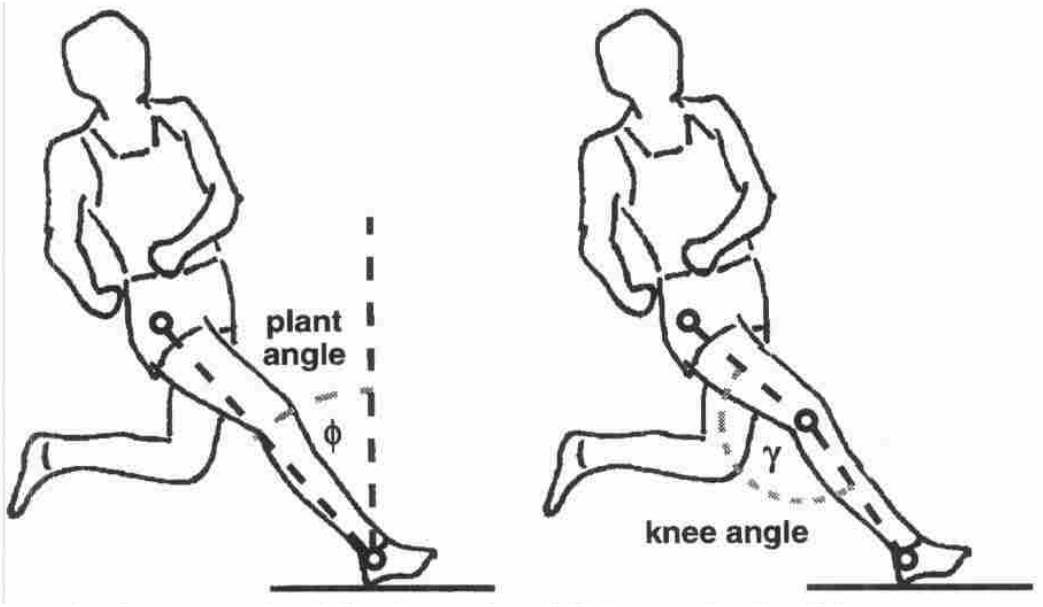

Figure 2.1 The plant angle and knee angle of a high jumper at touchdown (adapted from Greig and Yeadon, 2000).

The jump performance was shown to be most sensitive to changes in the leg plant angle and the amount of knee flexion. An increase in approach velocity was correlated with a larger knee angle and a larger plant angle at touchdown. A regression equation relating leg plant angle and approach velocity to jump height was shown to account for 79% of the

variation in jump height. This indicated that optimum high jump performance would be achieved at the highest velocities at which the athlete was capable of maintaining a minimum amount of knee flexion whilst using a large plant angle.

Vertical and radial motions of the body

Dapena and Chung (1988) investigated the effects of the vertical and radial motions of the body during the take-off of a high jump. They found that the radial velocity of the COM with respect to the supporting foot was generally more negative or less positive than the vertical velocity throughout the take-off phase. This initial negative radial velocity indicated that the muscles around the joints of the stance leg were likely to be in eccentric conditions. They stated that, immediately after the foot hits the ground at take-off, the COM velocity has a positive vertical direction and hence, unlike counter-movement jumps, the eccentric component of the muscular contractions can contribute directly to the positive vertical velocity of the COM, rather than reducing the negative vertical velocity. Dapena and Chung (1988) stated that this technique has its drawbacks in that the resultant impulse from the GRF acts, on average, at 67° from the horizontal and hence the vertical impulse is 8% smaller than the resultant impulse. Dapena and Chung (1988) also showed that the flexion of the arms and swinging leg reduced the radial distance of the COM from the hip joint during the initial period of ground contact when this distance was decreasing. This led to a cushioning of the stance leg from the impact peak of the GRF. This could possibly allow it to resist excessive flexion. Later in the ground contact when the radial distance of the COM to the hip joint was increasing, the arms and swinging leg were shown to act to increase this distance. This would put the joints of the stance leg in slower concentric conditions, facilitating a larger GRF later in the ground contact. This indicates that simulation models of jumping need both a free leg and arms in order to properly model the effects of the free limbs on the COM movement and subsequent loading of the stance leg.

Contribution of lower extremity joints

Stefanyshyn and Nigg (1998) looked at the contribution of the lower extremity joints to mechanical energy in running vertical and horizontal jumps (Figure 2.2). They found a similar contribution of the metatarsophalangeal (MTP) joint and knee joint to each type of jump; the MTP joint absorbed approximately 15-16% of the total energy absorbed by the

lower extremity, and the knee generated 25% of the total lower extremity energy and absorbed 31% and 28% of the energy in the vertical and horizontal jumps respectively. The ankle and hip, however, had different contributions. The ankle is the largest energy generator and absorber in both types of jump; in the vertical jump it generated 53% and absorbed 36% of the total energy generated and absorbed, but in the horizontal jump it generated and absorbed 49% and 47% respectively. This indicated a much larger eccentric portion in the horizontal jump. The hip was a net energy generator in both jumps, but its . However, the model will also be capable of simulating all three phases sequentially, and he hip absorbed less energy than the other joints and less during horizontal jumping than vertical jumping: 10% versus 16%.

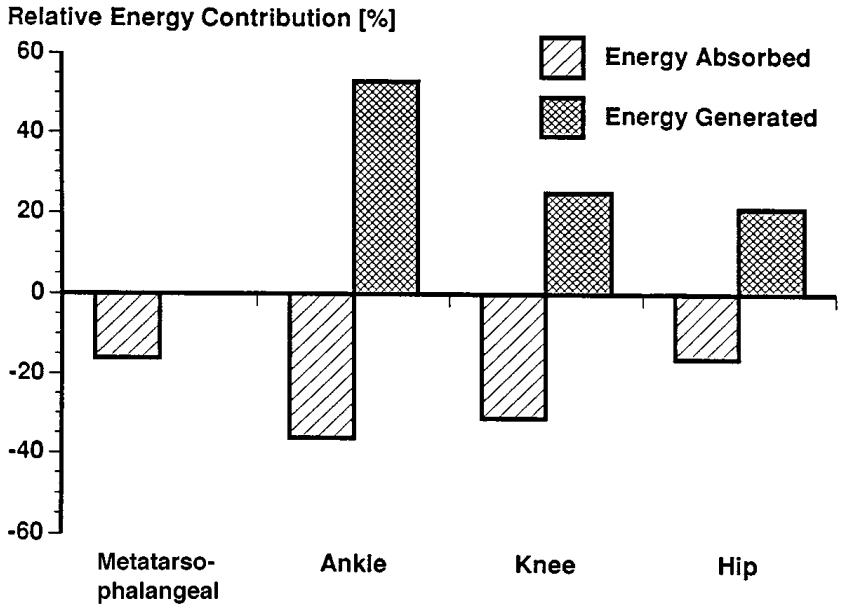

Figure 2.2 Energy contributions at various joints in the high jump (adapted from Stefanyshyn and Nigg, 1998).

It would be tempting to conclude that the most important joint in both long and high jumping is the ankle; however the ability of other joints to facilitate these energy changes is sometimes overlooked in energy analyses. Greig and Yeadon, (2000) indicated that the best high jumps were achieved with minimum knee flexion, in this instance the joint may not change its angle and hence may have a small relative energy contribution, but may still exert a large angular impulse in order to maintain this joint angle. Greig and Yeadon (2000) showed that the maintenance of this joint angle was important in high jump

performance. Therefore work / energy analyses should only be used in conjunction with other measures in order to obtain a more thorough understanding of a sporting technique.

2.2.2 Long jump

Leg angles during take-off

Graham-Smith and Lees (2005) and Lees et al. (1994) performed kinematic analyses of the long jump take-off in 3-D and 2-D respectively. Lees et al. (1994) analysed competitors in the world student games and found an average knee angle at touchdown of 166° which decreased to 147° at maximum knee flexion. The average hip angle at touchdown was 158°. So, on average, these long jumpers exhibited a more flexed knee with the leg planted closer to the vertical than the optimum high jumper analysed by Greig and Yeadon (2000). This was probably indicative of the different demands of the events, the long jump requires a higher approach velocity and, as such, it is harder to maintain extension in the knee, and would be harder still if the plant angle were further from the vertical.

Graham-Smith and Lees (2005) found few variables correlated linearly with jump distance. They cited the homogenous nature of athletes studied as the reason why these correlations were not apparent, intimating that they probably would be apparent if subjects with a wider range of abilities were studied. It can sometimes be difficult to obtain statistically significant results from analyses involving athletes operating at or near their optimum technique in competitions, because the range of performances is often very small (Yeadon and Challis, 1994). The effects of a small variation in one variable can therefore be masked by co-variation of other variables, leading to seemingly unrelated outcomes. This is a problem that computer simulation models are ideally suited to overcoming, allowing the effects of the manipulation of individual variables in isolation to be quantified, which is impossible to achieve in experimental studies.

Bridgett and Linthorne (2006) set out to investigate the validity of the simulation models of the long jump take-off constructed by Alexander (1990), and Seyfarth et al. (2000). In order to do this they looked at the change in the take-off technique of a long jumper over a range of approach velocities brought about by intervention. It was found that the models were in reasonable agreement with the experimental results, however there were areas where they were not in agreement. The hip angle of the subject at touchdown decreased

linearly with increasing approach velocity, and, whilst both models predicted a decreasing hip angle with increasing approach velocity, they overestimated the optimum leg angle at touchdown (Figure 2.3). This may be related to the invariant knee angles of the simulation models at touchdown. Bridgett and Linthorne (2006) noted that optimum take-off angles decreased with increasing run-up speed. This was in line with Seyfarth et al. (2000). However they underestimated the optimum take-off angle. The knee angle of the subject at touchdown increased linearly with approach velocity, whereas the simulation models had a set knee angle of 170°. Bridgett and Linthorne (2006) suggested that a model of the long jump take-off should include this knee angle as a technique variable. These results indicate that, whilst the models of Alexander (1990) and Seyfarth (2000) were useful in providing general trends in the variation of optimum long jump technique with changes in different parameters, they were not complex enough to accurately reproduce the magnitude or specific form of these variations (Figure 2.3). In order to reproduce these changes more accurately a more detailed simulation model would be required.

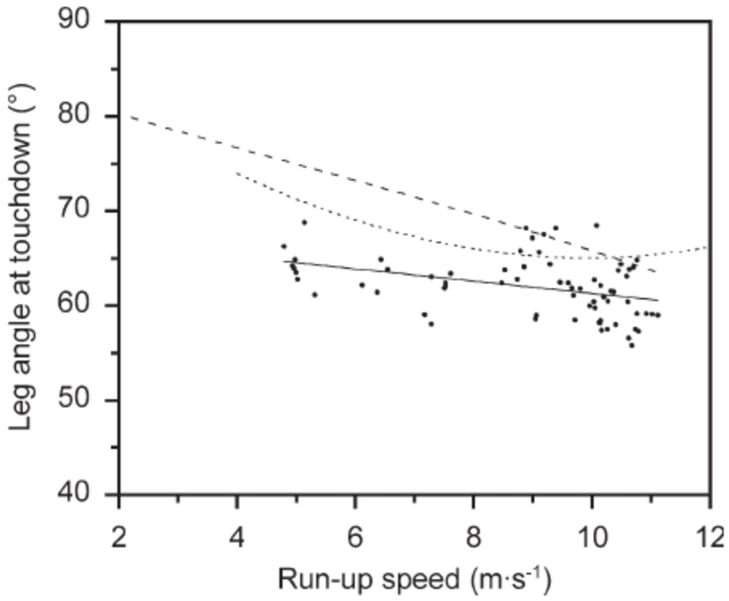

Figure 2.3 Leg angle changes with run-up speed with a line of best fit (solid line), and the results of the models of Alexander (1990) (long-dashed line), and Seyfarth (2000) (short-dashed line) (adapted from Bridgett and Linthorne, 2006).

Energy changes during take-off

Lees et al. (1994) also performed an analysis of energy changes during the take-off of a long jump. They found that, from touchdown to the point of maximum knee flexion, 6.3

J/kg were lost from the original kinetic energy. They hypothesised that some energy was dissipated by inefficient muscular mechanisms and upwards of 100 J could be stored in the elastic structures of the body. During knee extension 2.7 J/kg of energy was created, indicating that only 40% of the kinetic energy lost during knee flexion was regained. Lees et al. (1994) attributed 64% of the vertical velocity at take-off to what they called the 'pivot', essentially the mechanical effect of the body rotating about the contact point on the foot. This indicated that most of the vertical velocity was gained while the knee was still flexing. Lees et al. (1994) stated that Dapena and Chung (1988) held a contrasting view to Lees et al. (1993) in their analysis of the long jump take-off. They claimed that Lees et al. (1993) emphasised eccentric muscular activity as contributing directly to vertical velocity during the initial flexion of the knee, whereas Dapena and Chung (1988) emphasised the initial eccentric conditions as being important only in priming the muscles for subsequent concentric activity. However in the view of this author this was not apparent in the discussion of Dapena and Chung (1988) and both they and Lees et al. (1993, 1994) acknowledged the importance of eccentric muscle actions in contributing directly to changes in vertical velocity.

Bridgett and Linthorne (2006), in their evaluation of the models of Alexander (1990) and Seyfarth et al. (2000), found that mechanical energy was gained at speeds below 8 m/s and lost at speeds above this, and that take-off duration decreased with increasing approach speed. This was due to the increased velocity of the COM but was offset somewhat by an increased range of motion at the hip. The take-off duration was underestimated considerably by both models. The underestimation of take-off duration was likely to be due to the fact neither model incorporated a foot segment, therefore the distance from the COM to the floor was limited by the length of the thigh and shank and could not be increased by ankle plantar flexion as it is in humans.

Costa and McNitt-Gray (1999) investigated the kinetics of the long jump take-off. They found that athletes exhibiting the largest increase in vertical velocity did so by doing more positive work at the hip than those showing smaller increases. They hypothesised that, to achieve this positive work at the hip, the athletes had to maintain a small negative, or near-zero, net joint moment at the knee. It seems unlikely that an athlete could maintain a net joint moment of near zero, as this would result in an angular acceleration of near zero and the knee inevitably flexes and extends during a jump take-off.

Muscular activity during take-off

Kakihana and Suzuki (2001) investigated electromyographic (EMG) activity, GRFs, and kinematics during the take-off phases of running jumps, at a range of approach velocities, by two male long jumpers. One jumper consistently achieved a higher vertical velocity than the other over the range of approach velocities. They concluded that the jumper achieving the larger vertical velocity did so by using a backward trunk lean at touchdown and take-off, a smaller range of motion of the thigh throughout the support phase, more extended knee and ankle angles at touchdown, and a more flexed knee angle at take-off (Figure 2.4).

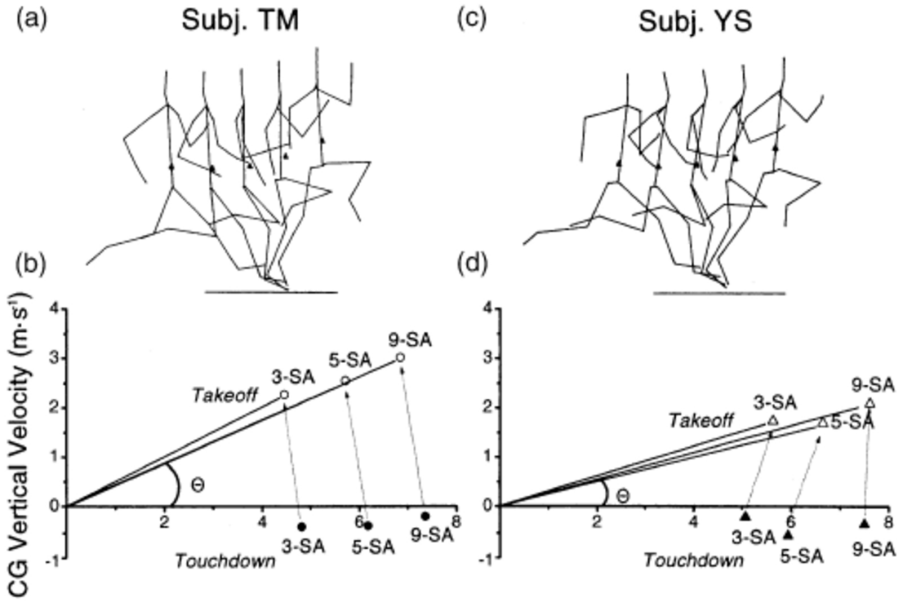

Figure 2.4 Visual representation and velocity vectors of long jump take-offs by two subjects (adapted from Kakihana and Suzuki, 2001).

This jumper also experienced a greater horizontal breaking impulse and smaller horizontal propulsion impulse. There were no substantial differences in the distances jumped between the subjects in this study, where they had limited length run-ups, but the subject who generated more vertical velocity had a personal best 83 cm further than the other subject who achieved a much smaller vertical velocity, so might be expected to be a better technician. The lack of differences between these two subjects despite the difference in personal bests might be related to the finding of Bridgett and Linthorne (2006) that mechanical energy is gained at speeds below 8 m/s and lost above this speed. Since the velocities in the study of Kakihana and Suzuki (2001) are all below 8 m/s (Figure 2.4) it

may be that the techniques of the two subjects were suited to different approach velocities and that an ability to generate greater vertical velocities might have become more of a benefit at higher approach velocities. The muscles showing the greatest EMG activity were rectus femoris, vastus medialis, lateral gastrocnemius, and tibialis anterior, whilst the biceps femoris were less active. However no measurement was taken of the gluteals, which might have been expected to contribute substantially to hip extension.

Hay et al. (1999) investigated the changes in muscle-tendon lengths during the take-off of a long jump (Figure 2.5). They investigated whether maximum knee flexion was a valid indicator of when muscles change their modes of action; they found that this was not the case for most muscles. Hay et al. (1999) also looked at six different muscle groups and seven measures of their action during the take-off. They then correlated these measures with the change in vertical velocity in order to gauge how each contributed to jump height. Figure 2.5 indicates that both the hamstrings and gluteus maximus lengthened throughout take-off. The biarticular rectus femoris muscle lengthened throughout take-off and the vastii muscles very slightly lengthened (0.3 ± 0.1 cm) then shortened. Both the soleus and gastrocnemius quite distinctly lengthened then shortened. In line with the findings of Dapena and Chung (1988), and Lees et al. (1993, 1994), Hay et al. (1999) found that all but one of the seven measures that were significantly related to the change in vertical velocity were measures of the eccentric phase, suggesting that the fast eccentric actions early in the take-off allowed the generation of large vertical forces and thus gains in vertical velocity. The only concentric muscle action related to the vertical velocity was the change in length of the hamstring muscles. This could be more of an indicator of the greater plant angle in the better jumps, which could have a mechanical effect unrelated to the muscle actions at the hip. The measures only give the muscle-tendon length and therefore do not necessarily represent the length of the contractile components, which might not show quite as much variation in length as Figure 2.5 suggests.

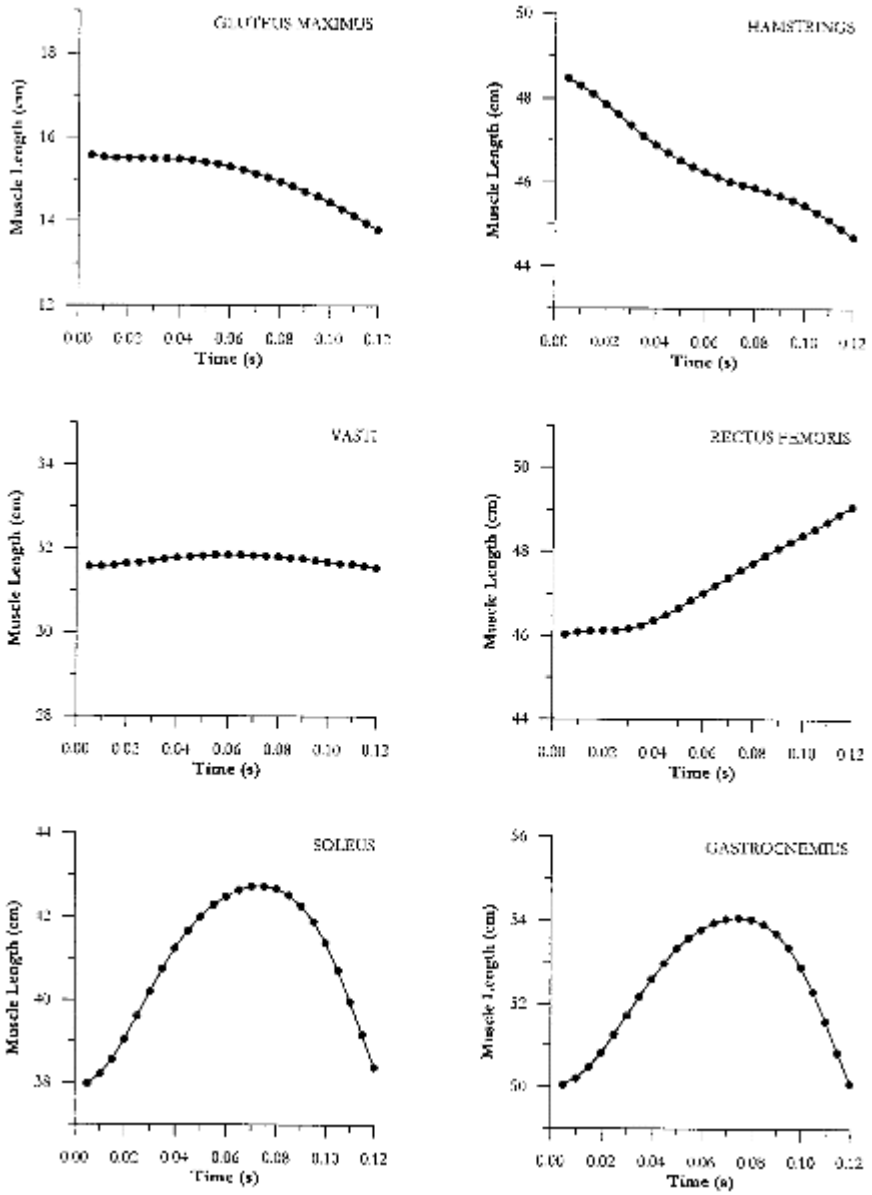

Figure 2.5 Muscle lengths during a long jump take-off (adapted from Hay et al., 1999).

Both Hay et al. (1999) and Stefanyshyn and Nigg (1998) found an important role of the triceps surae (gastrocnemius and soleus) in the take-off of a running jump. Hay et al. (1999) found that five of the seven measures of muscle activity that were significantly correlated to vertical velocity were measures of the activity of the triceps surae. Also, as mentioned above, Stefanyshyn and Nigg (1998) found the ankle joint generated and absorbed the most energy of all the joints in the lower extremity and concluded that the development of the gastrocnemius and soleus muscles was a key factor in achieving success in the running jumps. Stefanyshyn and Nigg (1998) also stated that the requirement of large hip extensor moments (400-650 Nm in their study) during take-off

indicated that the development of the hip extensor muscles was also important. Surprisingly Stefanyshyn and Nigg (1998) did not mention the contribution of knee joint torques as being of particular importance in the running jumps studied.

Landing leg motions at take-off

Hay (1987) mentioned two schools of thought concerning the placement of the foot at take-off; the 'active landing' where the foot is moving backwards relative to the body COM, and the 'locking' placement of the foot where it is not moving relative to the body COM. He stated that the latter is associated with a greater increase in vertical velocity and the former with a greater conservation of horizontal velocity; however he did not provide any empirical data to back this up. Hay (1987) cited Tiupa et al. (1982) who noted that the 'locking' technique could be considered more beneficial, since an increase in vertical velocity is more beneficial than an increase in horizontal velocity. Tiupa et al. (1982) investigated this and found correlations between the distance jumped and an increase in vertical velocity, and a decrease in horizontal velocity, respectively, during the period in which the centre of pressure (COP) was approaching the hip joint. However, increases in velocity components while the COP-to-hip distance increased were not correlated with the length of jump. This finding is in agreement with previously mentioned studies that found eccentric muscle actions early on in the contact phase greatly influenced jump performance (Dapena and Chung, 1988; Stefanyshyn and Nigg, 1998; Lees at al., 1993, 1994; Hay et al., 1999).

Koh and Hay (1990a) investigated the motions of the landing leg in the last three strides of the approach run in long jumpers. They used a mathematical model of muscle action which they validated with a physical model of the leg. Koh and Hay (1990a) found that 'active' landings - i.e. the mathematical model showed that muscle action reduced the forward horizontal velocity of the landing foot - were used in each stride. But the landing stride was less active than the two previous strides. The range of touchdown velocities of the foot relative to the COM were -10.45 m/s to -7.50 m/s, -9.34 m/s to -6.98 m/s, and -8.95 m/s to -5.38 m/s for the three strides. They did not find any statistically significant correlations of the measures of landing leg motions with measures of performance. They noted that this did not support the notion that either a highly active landing or a blocking landing is necessary to promote jump performance. However, they stated that there is some indication that a less active landing leg motion plays a role in lowering the COM in

the second to last stride and that this lowering increases the distance of the jump. They also stated there was some indication that placing the landing foot well forward of the body at the end of the last stride increased the distance of the jump. This may have been achieved by increasing the vertical velocity of the COM which they concluded is more important to jump performance than minimising the loss in horizontal velocity.

Angular momentum in flight

Hay (1993) considered the control of angular momentum in flight. In investigating angular momentum during take-off, Hay (1993) stated that roughly half the angular momentum that an athlete has about the transverse axis at take-off is gained in the approach. This leaves the athlete with a relatively large amount of forward somersaulting angular momentum which needs to be controlled in flight or it will lead to an inefficient landing with the feet well below the body. Hay (1993) considered various techniques for minimising the effect of this angular momentum on the orientation of the body in the air. He mentioned the 'sail' as being ineffective, and the 'hitch-kick' and 'hang' techniques as being more effective, at ensuring a good landing position, which he suggested is one where the hips are fully flexed and the trunk is forward over the legs.

Herzog (1986) investigated the sail and 2½ hitch-kick techniques in the flight phase of a long jump (Figure 2.6). The subject performing the sail technique had a lower forward somersault angular momentum at take-off than the subject performing the hitch-kick technique (4.17 $kg.m^2/s$ vs 11.05 $kg.m^2/s$). Herzog (1986) stated that neither athlete managed to fully compensate for the forward rotation of the head and trunk segment as this segment had positive values of angular momentum (0.78 $kg.m^2/s$ and 1.14 $kg.m^2/s$ for the sail and hitch-kick respectively). In this instance, with all other things being equal, the landing with more forward angular momentum should allow the athlete to plant their feet further in front of their COM without falling backwards into the sand. Therefore it would seem that the best technique to adopt would be one with a high whole-body forward somersault angular momentum and an airborne technique that would negate the effect of this angular momentum on the head and trunk, allowing a suitable landing orientation to be achieved. The hitch-kick would seem to be the best candidate as it is associated with greater forward angular momentum at take-off than the hang (21.4 $kg.m^2/s$ vs 16.9 $kg.m^2/s$, Ballreich and Bruggemann, 1986; 20.31 $kg.m^2/s$ vs 14.22 $kg.m^2/s$, Ramey, 1973) and the sail (11.05 $kg.m^2/s$ vs 4.17 $kg.m^2/s$, Herzog, 1986) and can successfully negate the effect of

the forward angular momentum on the head and trunk if executed properly (Herzog, 1986). These results indicated that the technique employed by athletes in the airborne phase can influence the distance of their jump. Therefore when attempting to simulate horizontal jumps, some account should be taken of airborne motions when calculating the distance of the jump, if this phase is not explicitly modelled.

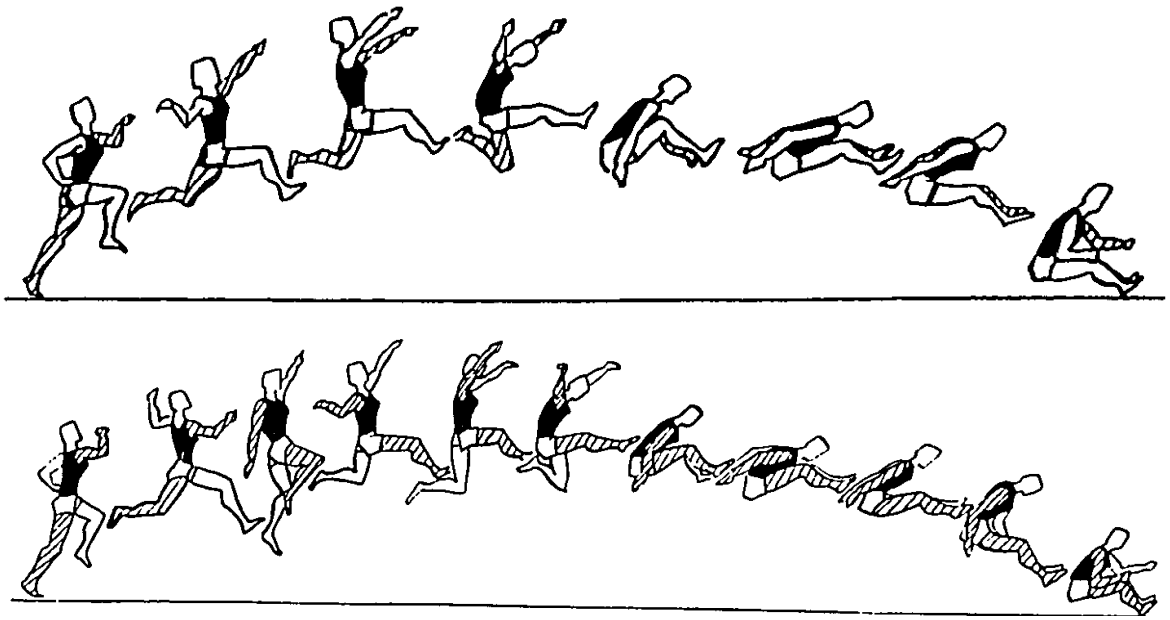

Figure 2.6 The sail (top) and hitch-kick techniques (bottom) in the flight phase of long jumping (adapted from Herzog, 1986).

Landing techniques

Hay (1987) provided a review of landing techniques He cited a study by McIntosh and Hayley (1952) who analysed an athlete performing two types of landing techniques: 'jack-knife' where the trunk and arms are inclined towards the feet; and 'extended' where the trunk is inclined backwards with the hands beside the hips. McIntosh and Hayley (1952) noted that neither technique allowed the feet to contact the sand beyond the projected point of contact of the COM, but that the extended technique allowed them to contact 8 cm before it, in comparison to the jack-knife which contacted 40 cm before. This led to a consideration of the relative importance of landing technique on distance jumped. Hay (1987) cited Bruggemann et al. (1982) who found no correlation between a measure of landing efficiency determined by McIntosh and Hayley (1982), and the distance jumped by 26 male long jumpers, and Hay (1986) who also found no correlation between COM height at landing and distance jumped. Both indicated little effect of the quality of landing on

distance jumped. However, Hay (1987) again cited Bruggemann (1982) who found a correlation between the height of the COM at landing and the distance jumped, and Hay (1986) who found a correlation between these variables for a world class jumper. This could be an issue associated with inter-subject and intra-subject correlations (Yeadon and Challis, 1994); where intra-subject correlations may indicate that limiting the height of the COM at landing is important in maximising the jump distance of an individual subject, inter-subject differences may mask this effect when considering this relationship across a number of subjects.

2.2.3 Triple jump

Phase / effort ratios

There have been a number of studies concerned with the choice of phase ratio – the ratio of the distance of each phase of the triple jump to the total distance jumped (Figure 2.7) – by elite jumpers (Miller and Hay, 1986; Hay 1992, 1993, 1995, 1997, 1999; Yu and Hay, 1996; Yu 1999).

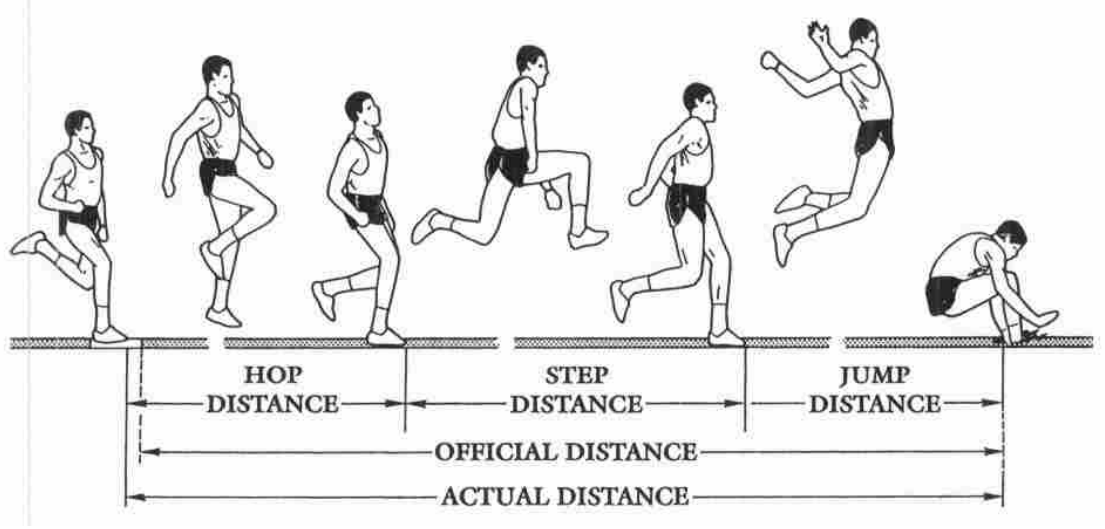

Figure 2.7 Phase, official, and actual distances in the triple jump (adapted from Hay, 1999)

Hay (1992) defined the three triple jump techniques with respect to phase ratios as being: (1) hop-dominated – where the hop percentage is at least 2% greater than the next largest phase percentage; (2) jump-dominated – where the jump percentage is at least 2% greater than the next largest phase percentage; and (3) balanced – where the largest phase percentage is less than 2% greater than the next largest phase percentage. Hay (1993) described the relative distribution of distance over the three phases as a percentage of the

total distance covered, tabulating these relative distances for world record performances from 1911 to 1985. This tabulation showed a general trend away from a hop-dominated technique with a small step phase (39%:22%:37%) towards a more balanced (37-39%:28-30%:31-33%) and latterly jump-dominated technique (34-35%:28-30%:36-37%) over time, with the step phase always being the shortest of the three phases. Hay (1993) noted world record advances over the last three decades considered in the analysis seemed to have involved a search for the ideal hop and jump percentages to go with a step of approximately 30%. Hay (1999) investigated the phase ratios employed by finalists in the 1996 Olympic Games. He found that balanced and jump-dominated techniques were just as effective as hop-dominated techniques, with roughly half the competitors employing hop-dominated techniques and half employing other techniques. The best distances of four of the top eight finishers were achieved with relatively short hop percentages in comparison to their other jumps. This often led to an increased jump percentage, suggesting that a reduction in hop percentage led to an increase in jump percentage and total distance jumped. This may be unsurprising given the nature of the event, with errors propagating over the three phases. Therefore a successful jump could have the same hop length but a smaller hop percentage than a less successful one. In this instance an absolute measure of phase length might be more informative.

Yu and Hay (1996), and Yu (1999), produced theoretical models (Section 2.3.1) in an attempt to relate the distance achieved in each phase of the triple jump to the total distance covered, in order that an optimum phase or 'effort' ratio could be obtained.

Biomechanical loading

A few studies have attempted to clarify the extent of the mechanical loading on limbs during triple jumping (Amadio, 1985; Ramey and Williams, 1985; Perttunen et al., 2000). Perttunen et al. (2000) found mean peak forces of 15.2 ± 3.3 times bodyweight in the braking portion of the step contact phase in jumps with a range of 11.37 – 15.24 m. This is in agreement with the range of 14.0-22.3 times bodyweight (Amadio, 1985) found in elite male jumpers, and higher than the maximum value of 12.6 times bodyweight found in male and female college-level jumpers (Ramey and Williams, 1985). The lower values recorded by Ramey and Williams (1985) can be explained by the shorter distances jumped by their subjects (~12 m for men, and ~9 m for women). Perttunen et al. (2000) found that higher

peak plantar pressures were significantly correlated to increased jump distances, indicating that higher forces are likely to occur in longer jumps. Hay (1993) stated that even the maximum measured value of 22.3 times bodyweight may be an underestimate of the forces elite triple jumpers undergo, since the largest jump distance recorded by Amadio (1985) was 15.35 m, which is nearly 3 m less than the current male world record of 18.29 m. Peaks of 2.6-3.0 times bodyweight were found in the horizontal direction (Ramey and Williams, 1985). These are less than the 7.0 times bodyweight found by Perttunen et al. (2000) and can again be explained by the difference in the distances jumped by the subjects in the two studies.

Arm techniques

Hay (1992) stated that, 'the arm action used at take-off into each of the three phases has been the source of considerable debate over the last 2-3 decades'. Two main techniques exist: the single-arm technique, where the arms move asymmetrically, as they do in sprinting; and the double-arm technique where the arms start in a hyperextended position and are flexed symmetrically throughout the take-off. Hay (1992) observed that numerous points have been raised in the course of the debate: that the double-arm technique causes a loss of speed in the hop take-off; that athletes that have greater 'jumping power' and who are not fast must use the double-arm technique; but that no quantitative data have been presented to support them. Hay (1992) concluded that the extended debate over arm actions had been useful in identifying factors that may bear on the issue; but that 'little further progress towards an understanding of these issues is likely to be made in the absence of carefully designed experiments, appropriate data and a rational interpretataion of the findings'. A computer simulation model of triple jumping would be ideally equipped to provide answers to these questions, since a quantifiable comparison of the two techniques could be made.

Angular momentum

Yu and Hay (1995) found significant non-linear correlations between side-somersaulting angular momentum at the take-off of the step and actual distance jumped, and also between the changes in this angular momentum during the support phase of the step and actual distance jumped. They predicted an optimum magnitude of 0.0069 $kg.m^2/s$ 'towards the free leg' (which diagrams indicate was anti-clockwise when viewed from the front with the right leg in contact with the ground). They also stated that the side-somersault angular

momentum at the take-off of the hop should also be 0.0069 kg.m^2/s and that the change in angular momentum during the support phase of the step should be minimised. They concluded that the changes in angular momenta and velocities during support phases were important in triple jump performance.

Contribution of free limbs

There have been some attempts to assess the contribution of the movement of free limbs (i.e. those not in contact with the ground) and performance in the triple jump (Yu and Hay, 1995; Yu and Andrews, 1998). Yu and Andrews (1998) investigated the relationship between free limb motions and triple jump performance in 13 subjects at the US Olympic trials. They found that free limb motions were associated with decreases in the forward horizontal velocity of the whole-body COM, and increases in the vertical velocity of the COM, but were not significantly correlated to changes in the corresponding velocity components of the whole-body COM, except when an extreme outlier was included in the analysis. They also found that, despite creating some angular momentum components about the COM during the support phases, the free limb motions did not affect the changes in whole-body angular momentum. Finally they concluded that neither the changes in velocity or angular momentum of the body due to free limb motions were related to the actual distance of the triple jump. These results indicate that free limb motions may not be important to triple jump performance. However, as with Graham-Smith and Lees (2005), the lack of statistical significance could just be a feature of analysing homogenous subjects, operating close to their optimum technique, in a competition environment (Yeadon and Challis, 1994). A comprehensive model of a triple jump should allow the effects of free limb motions to be isolated and quantified.

Landing leg motions at take-off

Koh and Hay (1990b) investigated the motions of the landing leg in the last three stance phases of triple jumpers competing in the US national championships. They showed roughly similar results to their analysis of long jumping, in that there were again no statistically significant correlations of measures of landing leg motions with measures of performance. They did note however, that the touchdown of the jump stance phase was the least active of the landings in the triple jump, and that there was some indication that a relatively active landing in this phase was linked to large effective distances. The elite jumpers in their study showed more active landings in this phase than the athletes of lesser

ability. Koh and Hay (1990b) concluded that it seemed active landings were beneficial but difficult to achieve or use effectively.

Take-off angles

Aagaard et al. (online) measured various parameters, including take-off angles, COM velocity, and COM height, in finalists in the men's triple jump in the 1995 world athletics championships, during which the world record was broken twice by the same athlete. In the second world record performance of 18.29 m they measured take-off angles of 16˚, 14.5˚ and 19˚ for the hop, step, and jump phases respectively (Table 2.1). The range of angles measured in the final for all athletes was 11-16˚ in the hop, 11-17˚ in the step and 16-22˚ in the jump. So the athlete breaking the world record employed a take-off angle at the top of the range for all athletes in the hop phase and in the centre of this range for the other two phases.

Table 2.1 Various kinematic parameters of a world record jump (adapted from Aagaard et al., online)

Phase	Height of COM at heel strike (m)	Minimum height of COM (m)	Height of COM at toe off (m)	Velocity at heel strike (m/s)	Minimum velocity (m/s)	Velocity at toe off (m/s)	Take-off angle (°)
Hop	1.00	1.00	1.20	9.60	9.26	9.60	16
Step	0.98	0.97	1.07	9.10	8.04	8.04	14.5
Jump	0.97	0.96	1.18	7.80	6.70	7.10	19

COM positions at take-off and landing

The COM positions incorporate the take-off and landing distances (Figure 2.7) and the vertical position of the COM. Hay (1992) found that the results from studies reporting take-off and landing distances showed remarkably little agreement with respect to either magnitudes or trends from one phase to the next. Hay and Miller (1985) found significant negative correlations between the take-off distance of the jump and the official distance. They concluded from this that a velocity with a greater vertical component would result in a better jump. They similarly found significant negative correlations between the landing distance of the jump and the official distance. Thus the less the landing distance the

greater the jump. They found this hard to explain, speculating that it may be due to less angular momentum being generated in the more successful jumps, therefore the athlete could not afford to place their feet too far in front of their COM. Studies reporting COM heights at take-off also showed variable results. The only consistent relationship being that the height of the take-off for the step is the lowest of the three phases, and the height of touchdown of all three phases is invariably 10 cm lower than the preceding height of take-off (Hay, 1992).

Times of support

Hay (1992) in his review of literature on triple jumping reported contact times of 0.12-0.14 s, 0.15-0.18 s, and 0.16-0.19 s for the hop, step, and jump take-offs respectively. This is in agreement with the findings of Perttunen et al., (2000) who reported mean contact times of 0.139 s, 0.157 s, and 0.177 s for the three phases. This trend for contact times increasing from phase to phase was borne out statistically, in that the support time for the step is significantly longer than that of the hop, and the jump significantly longer than that of the step (Fukashiro et al., 1981). This increase in contact time is likely to be related to the decrease in horizontal velocity during each phase (Hay, 1993). Significant negative correlations have been observed between each support time and the distance of the triple jump (Matveyev, 1985). Although Hay (1992) stated that this is probably due to the decrease in contact time with increasing approach velocity, rather than a causal relationship in itself. Fukashiro et al. (1981) found a positive correlation between the support time for the step and the total distance jumped, for which they stated no logical explanation could be found. This could be due to various factors; a high vertical velocity in the hop take-off could lead to a longer hop phase and a 'more vertical' velocity vector at the touchdown of the step phase, possibly leading to an increased ground contact time. Alternatively better athletes may contact the ground with their COM further behind their COP, leading to the radius of COM with respect to the COP passing through a larger angle during the stance phase.

Energy changes during each support phase

Fukashiro et al. (1981) investigated the mechanical energy changes during the triple jump. They found that 4% of mechanical energy was lost during the hop take-off, followed by approximately 15% for the step, and for the jump. The loss in mechanical energy during the step and jump was largely due to the large amount of negative work during the first

half of each contact phase due to high initial negative vertical velocities (Figure 2.8). The loss in horizontal velocity with each phase seen in Figure 2.8 has been reported by numerous investigators (Hay, 1992). The pattern of vertical velocities shown in Figure 2.8 is also typical, with the jump take-off invariably having the highest value, and the step take-off the lowest.

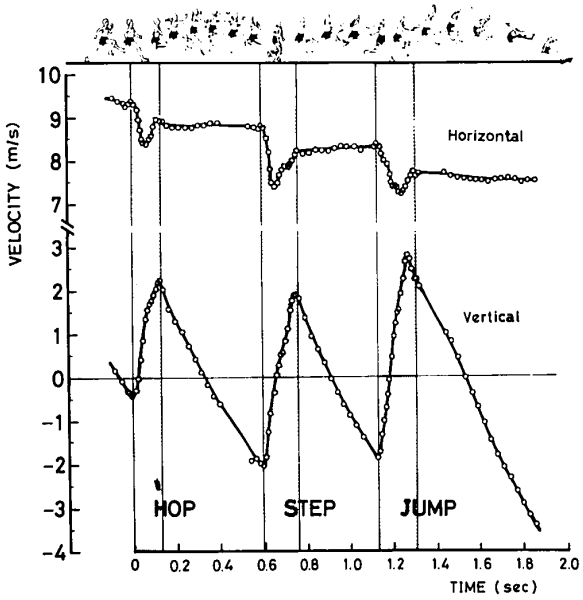

Figure 2.8 Graph showing velocity profiles for a triple jump (adapted from Fukashiro et al., 1981).

2.2.4 Two-legged jumps

This section is limited to one specific study on drop jumping in triple jumpers since the results were of direct relevance to this study.

Pre-impact muscle activation

Viitasalo et al. (1998) tested highly trained triple jumpers against controls in drop jumps from 40 cm and 80 cm. The triple jumpers jumped 32% and 34% higher than the controls in the 40 cm and 80 cm conditions respectively. They also showed smaller braking and total contact times and higher average and peak GRFs. The EMGs of the triple jumpers showed an earlier pre-activity of the vastus lateralis and gastrocnemius muscles when compared to the controls. Viitasalo et al. (1998) stated that myoelectrical activity has been found to be highly correlated with contact time, contact force, and angular velocity in

trained athletes. They found earlier mean muscular pre-activations of triple jumpers than controls (146 ms and 140 ms vs 92 ms and 92 ms in the gastrocnemius, and 78 ms and 88 ms vs 45 ms and 50 ms in the vastus lateralis).

The findings of Perttunen et al. (2000) were in agreement with this; they found that the high impact loading associated with the triple jump requires well-developed pre-landing motor control similar to that for other high-impact, stretch-shortening cycle exercises. They noted that this could be seen as high and fast EMG development just before the touchdown and during the braking phase, and that the high pre-landing and braking activity of the leg extensor muscles might prevent unnecessary yielding of the jumper during the braking phase (Yeadon et al., accepted for publication), resulting in a better performance. This was borne out statistically with an increased pre-activity of the gastrocnemius muscle being significantly correlated to increased jump distance (Figure 2.9).

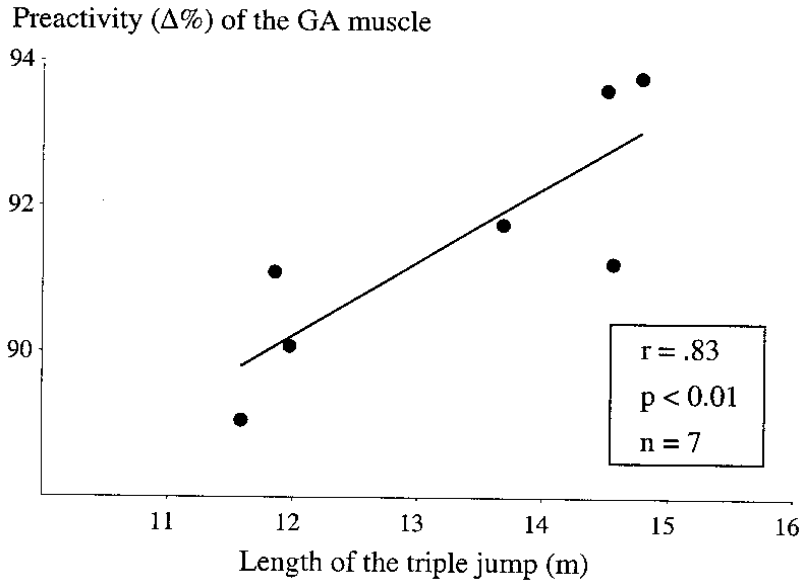

Figure 2.9 Graph showing distance jumped against preactivity of the gastrocnemius muscle (adapted from Perttunen et al., 2000).

These results indicate that simulations of jumping incorporating an impact should allow muscular co-contraction at the initiation of the simulation.

2.3 THEORETICAL JUMPING STUDIES

There have been a number of theoretical models of human jumping activities which can be split into two categories:

- Predictive (Yu and Hay, 1996; Yu, 1999; Wakai and Linthorne, 2002; Linthorne et al., 2005);
- Analytical (Alexander, 1990, 1992; Hatze, 1981; Wilson et al., 2004; Pandy et al., 1990; van Soest et al., 1993).

These predictive models were used to attempt to mathematically (often statistically) predict the behaviour of a system, or a portion of a system, representing a jumping performance from the interaction of a few parameters, without attempting to model the whole system dynamically. Whereas the analytical models integrated the system, which in these cases was invariably a multi-body torque-driven mathematical representation of a human performing a jump, backwards or forwards over small time steps in order to obtain the state of the system at another point in time. A discussion of analytical models is included in Section 3.2, therefore only predictive models will be discussed here.

2.3.1 Predictive models of jumping

Wakai and Linthorne (2002, 2005) investigated the optimum take-off angle in the standing long jump, producing a mathematical model where the jump distance comprised three portions: the take-off distance; flight distance; and landing distance. The take-off speed was modelled as a linear relationship between a constant applied muscular force and take-off angle. From this an optimum angle of 23° was predicted for maximum jump distance which is considerably less than the 35° preferred by athletes. Wakai and Linthorne (2002) justified this by saying that a jumper may achieve a near maximal jump distance using a range of take-off angles from 15-35°.

Linthorne et al. (2005) extended the work of Wakai and Linthorne (2002) to optimum take-off angles in running long jumps. As with the standing long jump, the total distance comprised the take-off distance, flight distance, and landing distance. The mathematical

model combined the equation of a projectile in free flight with measured relations from three athletes between take-off speed, take-off height, and take-off angle. This led to take-off angle predictions of approximately 21-25° which were in good agreement with the competition take-off angles of the three jumpers. Unlike Wakai and Linthorne's (2002) results for standing long jump, Linthorne et al. (2005) concluded that to achieve good performances the athlete must jump at close to the optimum angle.

In an attempt to optimise phase ratios Yu and Hay (1996) hypothesised that there is a linear relationship between the gain in vertical velocity and the concomitant loss of horizontal velocity during each of the three foot contacts that is a function of what they called the 'horizontal to vertical velocity conversion factor'- A_1. Having calculated this relationship for each subject, Yu and Hay (1996) then optimised the ratio of each phase in order to maximise the total distance jumped. They calculated this ratio for approach velocities between 8.5 m/s and 11.5 m/s and found that the optimum phase ratio was sensitive to A_1, when A_1 was between 0.5 and 0.9. They suggested that a hop-dominated technique should be employed if A_1 is less than 0.5 and a jump-dominated technique should be employed if A_1 is greater than 0.9. This relies on the assumption that the value of A_1 is independent of approach velocity, which is questionable. The optimised solutions employed phase ratios that were outside the range of those used by elite triple jumpers.

Yu (1999) expanded on this work by using a slightly different regression equation in order to determine the horizontal velocity loss at each phase. Yu (1999) concluded that athletes with a smaller A_1 were more efficient - that is they lose a smaller amount of horizontal velocity for a unit increase in vertical velocity. But an optimisation of phase ratios indicated that athletes who have a larger A_1 jumped further than those with a smaller A_1. This would seem counterintuitive since, all other things being equal, the athlete losing the least horizontal velocity for a unit gain in vertical velocity will jump the furthest. However Yu (1999) did not consider initial horizontal or vertical velocity when analysing this relationship, merely the change in these values (Figure 2.10). He also did not consider the magnitude of values for which he determined his relationship for each athlete. Hence it could be that athletes showing smaller values of A_1 do so because they have lower levels of initial horizontal and / or vertical velocity. Therefore they may seem more efficient but do not jump as far.

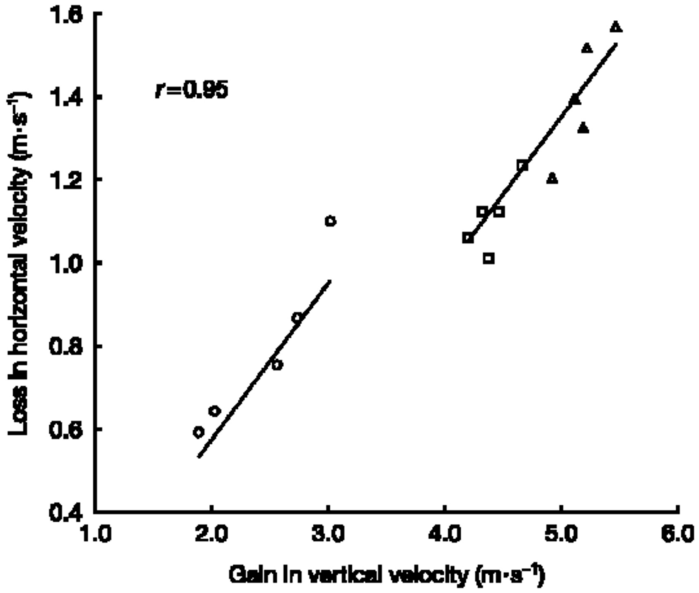

Figure 2.10 Graph showing the relationships between the gain in vertical velocity and loss in horizontal velocity during three phases of a triple jump (adapted from Yu, 1999).

2.4 SUMMARY OF LITERATURE

A number of factors raised in the experimental literature can inform the construction of a computer simulation modelling athletic jumping events. Dapena and Chung (1988) found that, in addition to more predictable effects on angular momentum, movements of free limbs affected the movement of the COM during a high jump take-off which had subsequent effects on the loading of the stance leg. This indicates that a model of jumping requires arms and a swinging leg in order to accurately ascertain the mechanical loading on the stance leg during take-off. Herzog (1986) showed that body configuration changes have an effect on the whole-body orientation during the flight phase of a long jump and, as such, a simulation model should incorporate some measure of configuration changes in flight in order to obtain realistic angular momentum values at take-off. Viitasalo et al. (1998) showed that triple jumpers have earlier muscular pre-activations than controls in drop jumping. A computer simulation model of triple jumping should therefore allow a suitably high level of muscular activation at touchdown in each phase. The analysis of Stefanyshyn and Nigg (1998) showed that the ankle generated the most energy in a long and high jump take-off; this might lead to the belief that the ankle was the most important joint in both types of jump. However Greig and Yeadon (2000) found that limiting knee

flexion was strongly associated with improved performance in high jumping. If the knee did not flex or extend it would not do any work, and would seem unimportant in a work / energy analysis. Therefore, when analysing technique, various factors should be considered to properly ascertain how actions at various joints contribute to performance. The predictive models studied attempted to predict features of optimal technique based on measured relationships. The problem with such studies is that observed relationships are only valid for the range of values measured, thus extrapolating these relationships outside these values can lead to optimised solutions that do not relate well to those techniques used by athletes (Yu and Hay, 1996; Wakai and Linthorne, 2002). The results of these predictive models indicate that theoretical studies of sports techniques should incorporate suitable simulation models with realistic input parameters that have been evaluated against performance data in order to avoid spurious optimal techniques being calculated.

2.5 CHAPTER SUMMARY

In this chapter literature relating to experimental studies involving specific athletic jumping events (the long, high, and triple jumps) was described. Theoretical studies, specifically those using predictive methods, were also outlined and critiqued. The literature was then summarised with particular consideration of those issues relevant to the construction of a computer simulation model of triple jumping and subsequent analysis of technique. The next chapter will describe the construction of this simulation model.

CHAPTER 3

CONSTRUCTION OF A COMPUTER SIMULATION MODEL OF TRIPLE JUMPING

3.1 CHAPTER OVERVIEW

In this chapter literature on analytical models of jumping is reviewed, there is also a brief consideration of literature on soft tissue movement, muscle models and optimisation algorithms. The development of a computer simulation model of triple jumping using Autolev^{TM} is described comprising a description and justification of the structure and function of the model.

3.2 ANALYTICAL MODELS OF JUMPING IN THE LITERATURE

3.2.1 Models of one-legged jumps

Alexander (1990, 1992) used a simple model to investigate optimum approach speeds and leg angles in the long and high jump take-offs. The model comprised a rigid trunk and a massless two-segment leg with the model's mass concentrated wholly in the trunk, with the COM at the hip. Whilst the foot was in contact with the ground, a torque generator exerted a torque at the knee. This torque generator comprised a contractile component and a series elastic component, was fully activated whilst the foot was in contact with the ground, and followed muscular mechanics similar to those outlined by Hill (1938). Alexander (1990, 1992) found that, according to his model, a typical male high jumper should run up at 7 m/s with a leg angle of 45°, whereas a long jumper should run up as fast as possible with a steeper leg angle. The disparity in approach velocity was explained by virtue of the fact that horizontal velocity is more important in long jumping than high jumping and the more shallow leg angle in high jumping allows a longer foot contact and hence a greater vertical impulse and a greater production of vertical velocity.

Linthorne and Kemble (1998) adapted Alexander's (1990) model by implementing anthropometric values from male and female athletes. They investigated the sensitivity of an athlete's performance to deviations from the optimum technique, and the dependence of this optimum technique on leg strength and leg length. Linthorne and Kemble (1998) found that male athletes should run up faster and have a greater leg angle at touchdown than women due to their longer legs and greater leg strength. They predicted that an increase in an athlete's leg strength would only benefit them if they ran up faster and planted with an increased leg angle at touchdown.

Chow and Hay (2005) investigated the effects of the approach velocity, vertical GRF, and change in angular momentum about a transverse axis, on long jump performance. They produced a two-dimensional inverted-pendulum-plus-foot model which was driven by GRFs scaled from the literature. They performed sensitivity analyses by varying these parameters and computing the jump performance. They found that jump distances were most sensitive to approach velocity; a 10% increase resulting in a 10% increase in jump distance, whereas a 10% increase in vertical GRF resulted in only a 7.2% increase in jump distance. However, when the cumulative effect of both these factors was considered they found that a 10% increase in both factors resulted in a 20.4% increase in jump distance. They also found that jump performance was overestimated if angular momentum was not considered in the analysis. This indicates that it is important to account for the angular momentum requirements of the activity when modelling human jumping activities.

Seyfarth et al. (1999) investigated the forces acting on the centre of gravity during the take-off phase of the long jump. They produced a model comprising a linear spring with the ability of lengthening to represent the leg, and a distal mass representing the COM, coupled by nonlinear visco-elastic elements. They found that this did not allow an accurate representation of the passive peak observed in the GRFs in long jumping. They therefore added a second mass representing the COM of the stance leg to account for this (Figure 3.1). This is an example of an oversimplification leading to a model that did not properly represent the activity it was attempting to simulate. Seyfarth (1999) found that high stiffness values for the leg spring allowed a number of different strategies to achieve distances close to the theoretical maximum. However the optimum angle of attack - the angle the thigh makes with the horizontal - requires only a relatively low stiffness of the leg.

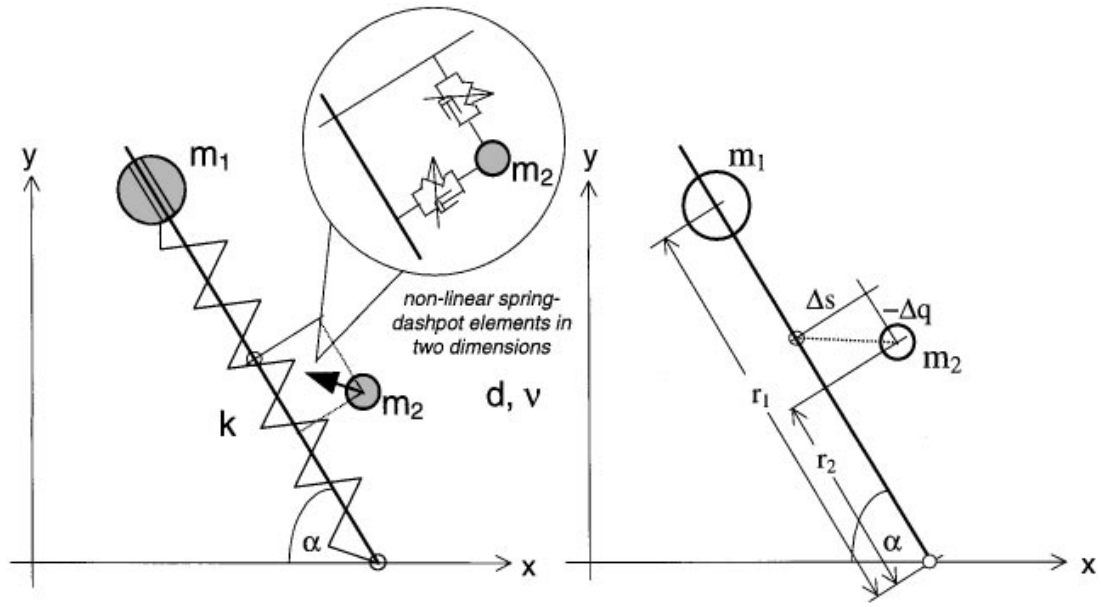

Figure 3.1 Representation of the model of Seyfarth et al. (1999) (adapted from Seyfarth et al., 1999)

As with Linthorne and Kemble (1998), Seyfarth et al. (2000) also adapted Alexander's (1990) model in order to investigate the action of the knee extensor muscles during the long jump take-off. Seyfarth et al. (2000) increased the complexity of Alexander's (1990) representation of the muscle-tendon complex in order to demonstrate the advantages of eccentric force production and non-linear tendon properties. The model showed that the angle of attack was insensitive to running speeds above 6 m/s and to muscle design. Seyfarth et al. (2000) noted that jumping distance was more sensitive to relative muscle fibre length than the ratio of tendon to muscle fibre cross-sectional areas and that good jumpers benefit from short muscles and long tendons. Maximum velocity of shortening of the muscle was not very important in the performance during take-off, but is probably important in attaining high approach speeds.

Seyfarth et al. (online) adapted the four-segment model of van Soest et al. (1993) (Section 3.2.2) to investigate the spring-like behaviour of the leg in long jumping. They incorporated the free leg into the head-arms-trunk segment of van Soest et al. (1993) to produce a rigid head-arms-trunk-leg segment in addition to stance thigh, shank, and foot segments. They assumed the stance leg would have 65 % of the maximal isometric force values van Soest et al. (1993) used for two legs in vertical jumping. They optimised the performance of the model by varying muscle activation timings which led to a jump of

5.72 m. They found that the predicted GRFs were similar to experimental findings but that the contact time was 115 ms which they stated was 17% shorter than experimental values. This discrepancy may have been due to the lack of swinging leg and arms which would act to maintain ground contact. The maximum vertical depression at the foot-ground interface was approximately 7 cm which is much larger than was observed experimentally, and may partly have been a consequence of the model not incorporating wobbling masses. Seyfarth et al. (online) then attempted to decompose the force trace into active and passive traces. They found that the passive peak was largely (80%) due to the deceleration of distal segments and the active peak was almost solely due to muscle activity. They concluded that the leg displayed spring-like behaviour in the optimised performance. They stated that the leg stiffness was a behaviour of the whole body and that muscle-tendon complexes displayed quasi-elastic behaviour at high loading rates due to inherent force / length / velocity properties and activation dynamics.

Ridka-Drdacka (1986) produced a simple model of the long jump take-off where the athlete was represented as a point mass. A constant force was then applied to the mass, representing the GRF. This force had two values, one representing the value up to the impact peak and the other the value beyond the impact peak. Various parameters such as the location of the COM, approach velocity, and magnitude of the post-impact peak GRF were varied in order to ascertain their effects on performance. They used their results to comment on the preparatory and take-off phases of long jumping. The former being used to secure a low COM position and nonnegative vertical velocity and the quality of the latter being dependent on the magnitude of the GRF.

There have also been a number of more complex models developed in an attempt to produce a more faithful representation of the human body performing a long jump (Hatze, 1981; Sorensen et al., 1999; Wilson et al., 2006). The most complex of these was the model of Hatze (1981), which comprised 17 segments driven by 46 myoactuators representing the major muscle groups of the body. Each myoactuator was driven by individual neural controls, motor unit recruitment and stimulation rate. The simulations did not model the impact of the foot at touchdown - instead simulations were initiated 0.019 s after the foot contacted the ground and also did not include wobbling masses. Hatze (1981) used this model to simulate a long jump take-off. The model displayed a very close match to experimental GRFs despite not including wobbling masses, which

might be considered surprising. However, despite the complexity of the model, or perhaps due to the complexity of the model, no attempt was made to speculate on matters of technique. This discussion was promised in a subsequent paper, however this paper could not be found in order that it might be included in this review.

Sorensen et al. (1999) produced a two-dimensional, six-segment model comprising a trunk, thighs, shanks, and a right foot, with all segments, apart from the foot, having rigid and wobbling portions connected by damped springs. The model was driven by eight major muscle groups in the take-off leg, which were represented by three-component Hill-type models (Hill, 1938). The foot-ground interface was modelled vertically by a damped spring and horizontally by a dry friction force element as described by Gerritsen et al. (1995). In order to account for the model's lack of damping in the shoe, heel pad, bones and joints and its inability to evert during take-off, Sorensen et al. (1999) reduced the spring stiffness from that used by Gerritsen et al. (1995). Two optimisation procedures were performed using an algorithm: tracking; and performance. The tracking algorithm matched performance GRFs measured from a long jumper, however there was no mention of any model parameters that were specific to the subject. As with Hatze (1981) no conclusions were drawn from the model's performance regarding optimum technique.

Wilson et al. (2004) used an eight-segment, planar model to investigate performance in high and long jumping (Figure 3.2). The segments represented the foot, calf, and thigh of the take-off leg, shank and thigh of the free leg, and a trunk, upper arm, and lower arm (representing both arms). The model had ten torque generators, each comprising a contractile component and a series elastic component. These were situated at the ankle, knee, and hip of the take-off leg, the hip joint of the free leg, and the shoulder joint. The torque generators were on both sides of each joint, allowing the model to co-contract. Joint torques were governed by a nine-parameter function incorporating the joint torque / angle / angular velocity, and angular velocity / differential activation relationships of human joint torque generation (Yeadon et al., 2006). Wobbling masses were situated at the shank, thigh, and trunk and were attached to the rigid elements representing the skeleton by non-linear damped springs. The foot-ground interface was also modelled by non-linear spring-damper systems at the toe and heel. Spring stiffness and damping parameters were determined using an angle-driven optimisation procedure. The simulations of jumps for height and distance were matched to actual performances with

errors of 1.6% and 8% respectively. The performance of the model was then optimised for height and distance and produced increases of 11% and 6% respectively. A number of other papers employed this model to investigate various features of simulation modelling and performance in running jumps (Wilson et al., 2006; King et al., 2006; Wilson et al., 2007).

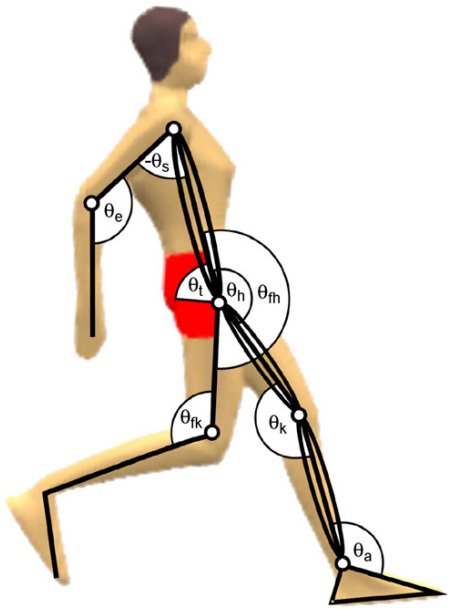

Figure 3.2 Representation of the model of Wilson et al. (2007) (adapted from Wilson et al., 2007).

Wilson et al. (2006) described the determination of subject-specific viscoelastic parameters of the foot-ground interface and wobbling masses using this model. They used a simulated annealing algorithm to vary the stiffness and damping coefficients of viscoelastic elements in order to minimise the difference between a kinematically-driven model and performance data. The six-component objective function comprised: (1) the absolute difference in trunk orientation at take-off; (2) the root mean square (RMS) difference in joint angles at take-off; (3) the percentage difference in absolute time of contact; (4) the percentage difference in vertical and horizontal momentum at take-off; (5) the percentage difference in absolute angular momentum at take-off; and (6) the overall RMS difference in the horizontal and vertical GRFs during the take-off phase as a percentage of peak force. Angles were measured in degrees and 1° was considered equal to 1%. Whole-body angular momentum was small so the weighting of component (5) was adjusted so a 1% difference in angular momentum was equivalent to a 1° difference in landing orientation. The optimisation process achieved differences of 6% and 9% between simulation and performance in jumps

for height and distance respectively. Wilson et al. (2006) showed that these parameters led to poor agreement between simulation and performance when those from the jump for height were used in simulations of a jump for distance and vice versa. They therefore produced a common set of parameters which led to a mean difference of 8% (made up of 7% and 10%) over the two phases. They concluded that subject-specific viscoelastic parameters should be obtained using more than one performance in order to obtain a robust set of parameters that can be used in different simulations.

King et al. (2006) described the evaluation of this model against performance data in a jump for height. Torque generator activation timings were varied using a simulated annealing algorithm in order to minimise the difference between simulation and performance. The objective function was similar to the one used by Wilson et al. (2006) with the addition of minimum joint angles reached by the ankle, knee, and hip to component (2). A 6.6% difference between simulation and performance was achieved. The performance of the model in terms of the maximum height achieved by the mass centre was then optimised in the same fashion and resulted in a 9 cm increase in jump height compared to the matched simulation. They concluded that the model was sufficiently complex and had appropriate strength parameters to give realistic simulations of running jumps for height.

Wilson et al. (2007) investigated various considerations that affect the optimum peak height in a running jump. The model was matched to performance data using the same method as King et al. (2006). This resulted in a performance of 1.99 m compared to the measured performance of 2.01 m. Simulation jump height was maximised by varying torque generator activation timings whilst using the same initial conditions as the matched simulation. Optimisations were run with no constraints, with constraints on angular momentum at take-off, with further constraints on joint angles, and with an additional requirement that the technique be robust to perturbations of torque generator activation timings. These optimisations resulted in performances of 2.37 m, 2.21 m, 2.14 m, and 1.99 m respectively. They concluded that the peak height achieved in the simulation with all three constraints was similar to that of the matched simulation and therefore these constraints have a substantial influence on technique and should be included in future simulation studies.

3.2.2 Models of two-legged jumps

Pandy et al. (1990) investigated maximum height human jumping with a four-segment planar model driven by eight musculotendon actuators. The musculotendon actuators were driven by Hill-type contractile components (Hill, 1938) containing a series elastic component and a parallel elastic component. The tendon properties were defined by a stress-strain curve and the musculotendon actuators were driven by a first-order representation of excitation-contraction coupling. The performance of the model was optimised using an optimisation algorithm, however the model was not evaluated against experimental data. The results showed that there were shortcomings in the model as it did not follow experimental results. Pandy et al. (1990) were unable to speculate on the features of optimum technique, noting that it was, 'at least qualitatively similar to experimental data reported for jumping', but not similar enough to be considered a reasonable optimum technique to be employed by humans. They investigated the effects of muscle timings on performance, noting that the performance of the model was particularly sensitive to the activation timings of the vastii muscles and suggesting that the model will allow an investigation into the effects of the manipulation of various physiological factors on standing jump performance.

Pandy and Zajac (1991) used this model to investigate optimal muscular control strategies for squat jumping. The optimal control strategy comprised a proximal-to-distal sequence of muscle activation from hip to ankle. They found that the vasti and gluteus maximus muscles were the major energy producers of the lower extremity, dominating the angular acceleration of the hip and instantaneous power of the trunk. However the ankle plantarflexors dominated the total energy of the thigh. They investigated the effects of the biarticular gastrocnemius by replacing it with a monoarticular muscle and found jumping performance to be similar in both conditions.

Anderson and Pandy (1999) produced a three-dimensional model of vertical jumping. The model comprised 10 segments: a head, arms, and torso (HAT) segment; a pelvis; two thighs; two shanks; two hindfeet; and two forefeet. The model was actuated by 54 muscles; 24 in each leg and six in the upper body. The foot-ground interface was modelled using a series of five spring-damper units placed under the sole of each foot. The muscles comprised three-elements: a series elastic element; a contractile element; and a parallel

elastic element, all in series with a tendon (Figure 3.3). Ligament torques were modelled using exponential terms. A first order differential equation governed the excitation-contraction dynamics. Musculoskeletal geometry and properties were taken from the literature, and maximal isometric strength was scaled to the average of the subjects in the study. Anthropometric measurements were taken from each subject, and mass and inertia properties were calculated for each segment by averaging this data. The height jumped by the model was then optimised using a computational algorithm. Anderson and Pandy (1999) noted that there was quantitative agreement between the model and the performance of the five subjects. With the peak vertical acceleration, velocity at take-off, and height jumped, all being within the range of those achieved by the subjects. They did also note however that the ground contact time was considerably shorter in the simulation than the measured performance and that the joints of the legs extended more. They hypothesised that this may be due to the short rise time of the muscle activation (20 ms), which was based on results from a single muscle fibre.

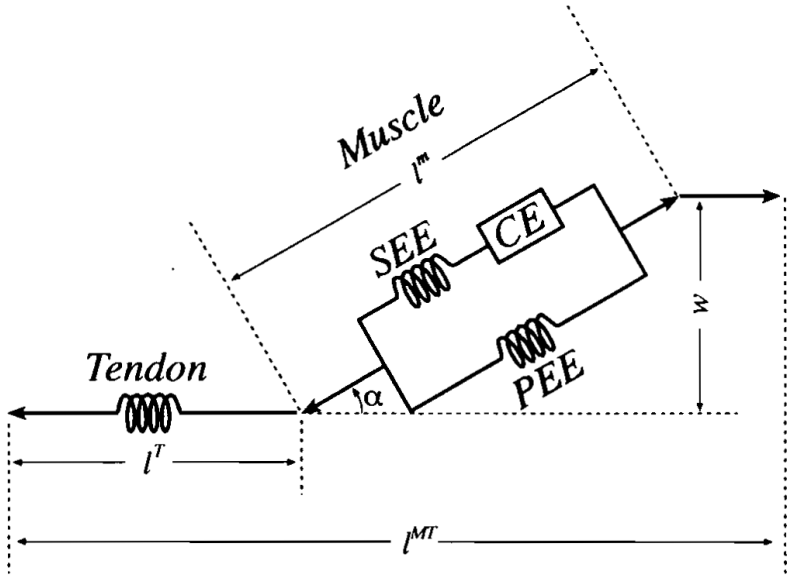

Figure 3.3 Representation of the muscle model of Anderson and Pandy (1999) (adapted from Anderson and Pandy, 1999).

Van Soest et al. (1993) used a four-segment planar model of vertical jumping to investigate the influence of the biarticularity of the gastrocnemius muscle on performance. The model comprised four rigid segments representing the feet, lower legs, upper legs, and head and trunk (Figure 3.4). These were connected by three frictionless hinge joints representing the

hip, knee, and ankle, and were connected to the floor at the toe by another frictionless hinge joint. The model was driven by Hill-type muscle models consisting of a series elastic component, a parallel elastic component, and a contractile component. Muscle groups incorporated were the glutei, hamstrings, vasti, rectus femoris, soleus, and gastrocnemius. Vertical jump performance was optimised by varying muscle stimulation patterns, with the model alternatively equipped with a biarticular gasctrocnemius, and a monoarticular gasctrocnemius. They found jump height decreased by 10 mm when the gastrocnemius was converted to a monoarticular muscle. This was in contrast to the results of Pandy and Zajac (1991). Van Soest et al. (1993) explained this as being an effect of the moment arm of the biarticular gastrocnemius in the study of Pandy and Zajac (1991) approaching zero when the knee approached full extension. This meant the biarticular gastrocnemius essentially acted as a monoarticular muscle during this range.

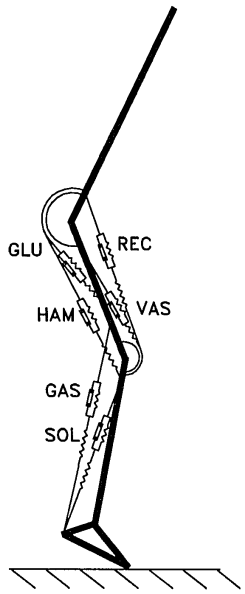

Figure 3.4 Schematic representation of the model of van Soest et al. (1993) (adapted from Bobbert and van Soest, 1994).

This model was subsequently employed in a number of studies (van Soest and Bobbert, 1993; Bobbert and van Soest, 1994; Bobbert et al., 1996; Bobbert and van Zandwijk, 1999; Bobbert, 2001; Bobbert and van Soest, 2001; Bobbert and Casius, 2005, Vanrenterghem et al., 2008; Bobbert et al., 2008). Those studies considered directly relevant to the current one are reviewed below. Van Soest and Bobbert (1993) investigated how the force / length / velocity relationships inherent in skeletal muscle affect the control of movements. They

found that, when compared to the moments directly applied to joints, moments under muscular control led to performances that were less sensitive to perturbations to initial joint angles. They concluded that the muscle properties, specifically the force / length / velocity relationship, act as a feedback mechanism with no time delay which allow humans to maintain movement patterns in the face of minor levels of disturbance.

Bobbert and van Soest (1994) investigated the effect of strengthening muscles on vertical jump performance. They found that strengthening muscles alone without a re-optimisation of muscle stimulation timings invariably resulted in a decrement in performance. However, a subsequent re-optimisation of muscle stimulation timings invariably led to an increase in jump height, with the magnitude of improvement increasing with strength increases.

Bobbert et al. (1996) investigated the reasons why countermovement jump height is greater than squat jump height. They used joint kinematics and EMG from performances as input, and calculated muscle states and forces, and net joint moments. They attributed the majority of the increase in jump height in the countermovement condition to the fact that muscles were able to build up a greater active state and level of force prior to shortening than in the squat jump. They used a single joint model to demonstrate that stored elastic energy did not contribute to increased force development. They stated that spinal reflexes could contribute to an increased active state of the muscle but that muscular potentiation was unlikely to enhance countermovement performance due to the delay between muscular stretch and maximal power production.

Bobbert and van Zandwijk (1999) investigated the sensitivity of jump performance to muscle stimulation onset times with different stimulation rise times (the time it took for the activation level of the muscle to increase from 10% to 90%). They found that vertical jump height decreased with increasing rise times; however the performance of the model was more robust. The explanation they gave for this was that the slow rise time let to slower development of errors in comparison to faster rise times. They stated that this effect was likely to be larger in activities in which the musculoskeletal chain behaves like an inverted pendulum, because of the destabilising effect of gravity. They speculated that humans may vary the rise times of their muscles depending on the accuracy and response time requirements of the task.

Bobbert (2001) investigated the dependence of squat jump performance on the elastic compliance of the triceps surae. He varied the strain of the series elastic element at maximum isometric force and optimised squat jump performance by varying muscle activation timings. This was done for various strain values as a percentage of the muscle-tendon complex length: 1%; 4%; 10%; 15%; and 20%. Concentrating on the differences between the reference 4% series elastic element strain, and the increased 10% series elastic element strain, he noted that it facilitated an increase of 4 cm in jump height. He stated that the increase in jump performance with increasing series elastic element strain was due to extra work being done due to elastic recoil of the series elastic element putting the contractile component into slower concentric conditions, and also an increased efficacy of this work due to a redistribution of the segmental contributions to the vertical velocity of the COM. He concluded that long, compliant tendons in the triceps surae are an elegant solution to the problem of maximising jump performance. This result is in agreement with the results of Seyfarth at al. (2000) in simulations of the long jump, who observed that good jumpers benefit from long tendons and short muscles.

Bobbert and Casius (2005) again investigated the differences between countermovement and squat jumps, this time using muscle stimulation timings as inputs to the simulation model in order to reproduce the two types of jump. In line with Bobbert et al. (1996) they found that the greater jump height in countermovement jumps could be explained by the fact that the active state of the muscle increased during the countermovement, whereas in the squat jump it inevitably increased during the propulsive phase. This meant that the muscles in the countermovement jump could do more work over the initial 30% of the propulsive phase in comparison with the squat jump.

Selbie and Caldwell (1996) investigated how initial jumping posture affected vertical jump performance using a four-segment planar model driven by three torque actuators. The torque actuators incorporated torque / angle / angular velocity relationships and an activation parameter controlling the rate of torque onset. The distal point of the foot was connected to the floor by a frictionless hinge and the contact of the heel with the ground was modelled using a rotational spring damper (Figure 3.5). They optimised vertical jump performance by varying torque actuator onset timings from 125 different starting postures. They found that jump performance was relatively insensitive to initial posture but that there was large variability in the torque actuator onset times employed to achieve these

performances. They did not find the proximal-to-distal sequence of joint coordination that had been found in previous studies of vertical jumping (Bobbert and van Ingen Schenau, 1988; Pandy and Zajac, 1991). They explained that this may have been due to the model not incorporating antagonist or biarticular muscles.

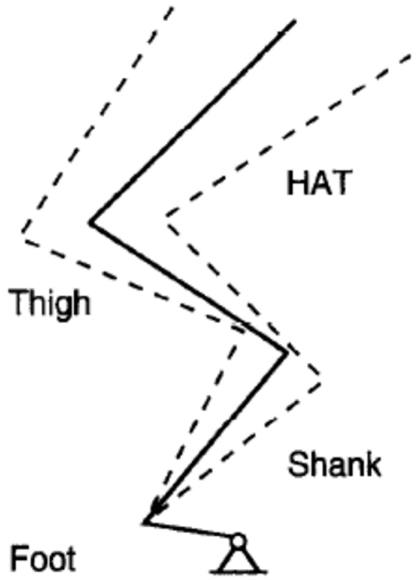

Figure 3.5 Representation of the model of Selbie and Caldwell (1996) in reference (solid lines) and most extreme starting postures (adapted from Selbie and Caldwell, 1996).

Dapena (1999) adapted the model used by Alexander (1990), with the addition of a piston-like ring to represent the arms, in order to explain the effects of arm actions on a vertical jump. The initial and final velocities of the arms were then manipulated in order to ascertain their effects on vertical jump height. Dapena (1999) found that a constant velocity of 3 m/s produced the largest vertical velocity of the COM, whereas initial and final arm velocities of –3 m/s and 3 m/s respectively produced the lowest vertical velocity, despite producing the most downward acceleration on the trunk. This led Dapena (1999) to state that the maximum velocity of the COM depended more on the average vertical velocity of the arms than on the change in this velocity during the take-off phase. He then hypothesised that a constant arm velocity of 3 m/s applied a force that led to the take-off leg musculature being put in slower and more advantageous concentric conditions. However, if the arms are moving at a constant velocity, the only force being applied to them is equivalent to the weight of the arms, which is comparable to the arms being static. Therefore during this simulation the arms could transfer no more force to the torque

generator than if they were static. Dapena (1999) set the initial velocity of the system to zero; therefore the largest positive initial arm velocity would result in the largest negative velocity of the trunk and thus eccentric conditions in the knee extensor torque generator. Therefore the effect of the positive velocity of the arms was not to apply a force to the trunk but to put the knee extensors in the most favourable conditions for torque generation at the start of the simulation.

Ashby and Delp (2006) also investigated the mechanisms by which arm movement improves jump performance, this time in the standing long jump. They developed a two-dimensional, five-segment model comprising: a foot; shank; thigh; head-neck-trunk; and arm (Figure 3.6). The ankle, knee, hip, and shoulder were actuated by torque generators incorporating torque / angle / angular velocity relationships. Ligamentous torques were also included to prevent hyperextension or hyperflexion at the extremes of joint range. Torque generator activations were determined by nodes at 50 ms intervals that could take any value between -1 and 1 (the signs denoting flexion and extension). These activations were varied throughout the ground contact and airborne phases in an optimisation process using a simulated annealing algorithm in order to maximise jump distance. Initial kinematic conditions were taken from experimental studies, and inertia and torque parameters were taken from the literature. Penalties were implemented for ligamentous torques in all simulations. Optimisations were then run with free and restricted arm movements. One set of these was run with no consideration for landing configuration, and one with penalties for landing positions where the COM was too low or too far behind the toe. Simulated jump distance was found to be 40 cm further when arm movement was free (2.00 m) than when it was restricted (1.60 m). They found that three mechanisms contributed to this improved performance: (1) airborne motions of the arms allowed a re-orientation of the body in the air and, as such, less consideration had to be taken of angular momentum constraints during take-off than when arms were restricted; (2) joint torques were augmented by the arm swing (Dapena, 1999) and produced 27 J more work; and (3) the shoulder joint torque generator did 80 J of work. They concluded that the most significant contributor to the increased take-off velocity was the work done directly by the shoulder joint.

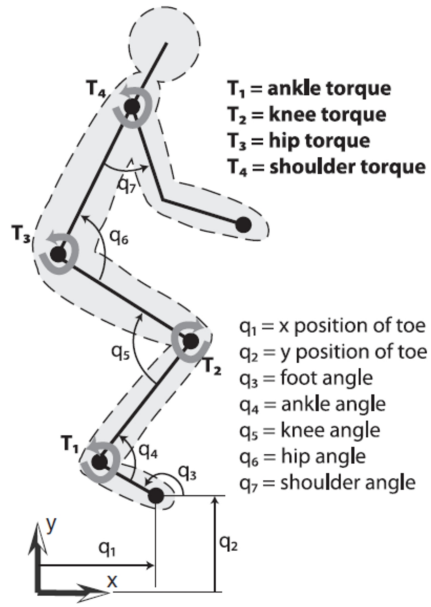

Figure 3.6 Diagram describing the model of Ashby and Delp (2006) (adapted from Ashby and Delp, 2006).

3.3 LITERATURE ON MODELLING SOFT TISSUE MOTION

Pain and Challis (2004) attempted to ascertain how sensitive a wobbling mass model of drop landings was to variations in certain parameters. The model consisted of three segments: a head-arms-trunk segment; an upper leg; and a shank-and-foot. Each comprised a wobbling and rigid element attached by non-linear spring-dampers. Actuators produced torques at each joint. Joint torque profiles, anthropometric data, and initial body configuration were taken from Gruber et al. (1998). Pain and Challis (2004) found that the model output was not sensitive to most model parameters but was sensitive to joint torque activation timings. They found that varying the stiffness of the heel pad had the most influence on peak vertical GRFs and that the simulations were relatively insensitive to the parameters governing the connections between the wobbling masses and rigid elements. They concluded that to produce an accurate model of a drop landing the correct properties for the foot-ground interface, accurate mass distribution, effective joint stiffnesses, and joint torque activation timings must all be calculated.

Pain and Challis (2006) investigated the effects of soft tissue motion on GRFs, joint torques, and joint forces during drop landings. Using a four-segment computer simulation model consisting of: a head-arms-trunk segment; an upper leg; a shank; and a foot, they compared a model including wobbling masses with a similar rigid body model. The model

was actuated by revolute spring-dampers and had subject-specific anthropometric, mass, and moment of inertia parameters. They found that the model including wobbling masses had a reduction in joint forces and torques of up to 50% and matched empirical GRFs from a subject performing drop jumps (Figure 3.7). This is in line with the findings of Gruber et al. (1998) who advocated the use of wobbling masses in inverse dynamics calculations from motions involving impacts.

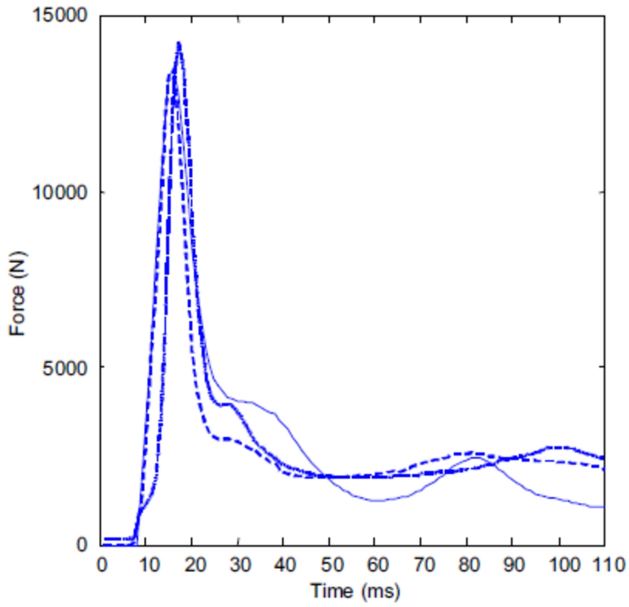

Figure 3.7 Simulated (solid line) and empirical (dotted and dashed lines) GRFs during drop landings (adapted from Pain and Challis, 2006).

Pain and Challis (2001) investigated the effect of the heel pad and soft tissue of the shank on shock attenuation during heel impacts. They found that both had an important role to play in the dissipation of energy during impacts. In light of this, computer models of impacts should include wobbling masses and account for the force attenuating properties of the heel pad.

3.4 SUMMARY OF LITERATURE

There have been a number of relatively simple models of jumping described in this chapter (Ridka-Drdacka, 1986; Alexander, 1990, 1992; Seyfarth, 1999; Chow and Hay, 2005). While these models were suited to investigating general trends in jumping, they were not suited to providing specific information on individual features of technique, since they

often require unrealistic simplifications and input parameters in order to reproduce realistic performances. In order to investigate specific technical issues more complexity is required. Simulations such as the model of the long jump take-off developed by Hatze (1981) and the model of vertical jumping constructed by Anderson and Pandy (1999) attempted to provide this complexity. However, whilst these models were valuable academic exercises, their complexity meant they were not ideally suited to the optimisation and manipulation of technique. For this, models with a balance of sufficient complexity and suitable simplifications seem better suited (Ashby and Delp, 2006; van Soest et al., 1993; Wilson et al., 2004). These models attempted to use realistic parameters (strength, anthropometric etc.) in order to capture the main features of the activity they were attempting to measure, whilst maintaining enough simplicity to allow optimisation and investigation of technique. It was also shown that models of human jumping should include wobbling masses if they include impacts (Pain and Challis, 2006), and have suitable constraints in order to reproduce realistic performances (Wilson et al., 2007; Chow and Hay, 2005). Wilson et al., (2006) demonstrated that viscoelastic parameters determined from kinematically driven simulations should be derived from a number of performances in order to obtain a set that is robust enough to be used in different simulations.

3.5 COMPUTER SIMULATION MODEL OF TRIPLE JUMPING

Simple models such as those of Alexander (1990, 1992) provided very eloquent additions to the knowledge base of human jumping activities. Occam's razor states that 'entities should not be multiplied beyond necessity' and in this vein Alexander (1992) stated:

'The simpler the model, the easier it is to discover which of its features are essential to the observed effect'

However, Alexander (1992) also noted that a model should be adapted to its function, and if the function requires additional complexity then this should be included. Therefore the computer simulation model in this study was created in line with Alexander's (1990) premise that models should be as simple as possible, whilst being complex enough to reproduce realistic performances.

3.5.1 Structure of the computer simulation model

Since a triple jump requires alternating ground contacts using both legs, the model required two legs. The relative importance of the muscles spanning the ankle, knee and hip joints to the performance in jumping activities (Stefanyshyn and Nigg, 1998) indicated the model should include feet, shanks, legs, and a trunk segment to properly represent a human jumping activity. The feet comprised two segments, thus allowing three contact points with the ground (Figure 3.8). Were the feet represented by just one segment the COP would be forced to remain in one place once the heel left the ground. Arms contribute to angular momentum and velocity changes during the airborne and ground contact phases of a triple jump (Yu and Hay, 1998) and the elbow joint is likely to have an effect on the nature of this contribution; hence two, two-segment arms were included. Hands were not considered essential as they were likely to have a negligible effect on the performance of the model and therefore were included in a forearm and hand segment. The head was likewise included in a head and trunk segment since its individual contribution to the performance of the model was likely to be limited.

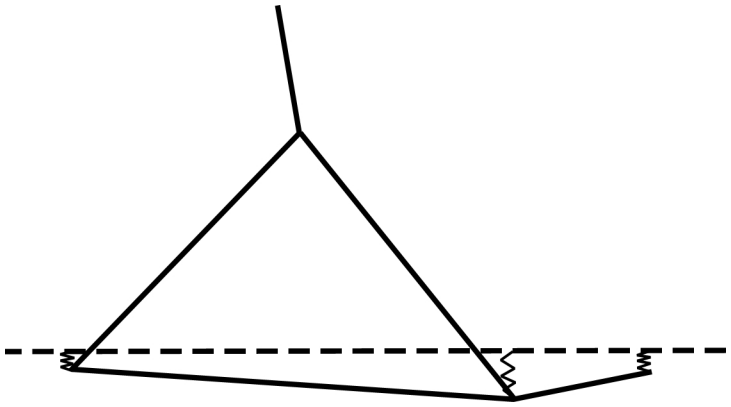

Figure 3.8 Representation of the foot-ground interface.

Wobbling masses were included at the shank, thigh, and trunk, and attached to the rigid elements at each end by spring-dampers (Pain and Challis, 2006) (Figure 3.9). The foot-ground interface was also modelled by three spring-dampers, situated at the heel, ball, and toe of each foot (Figure 3.8). Torque generators were located at the shoulder, hip, knee, ankle, and ball joints. These torque generators had flexion and extension profiles allowing co-contraction. The torque generators included contractile components and series elastic components, and followed the force / length / velocity relationships of skeletal muscle

(Hill, 1938; Gordon et al. 1966) and also allowed for differential activation (Westing et al., 1988) (Section 4.7.4).

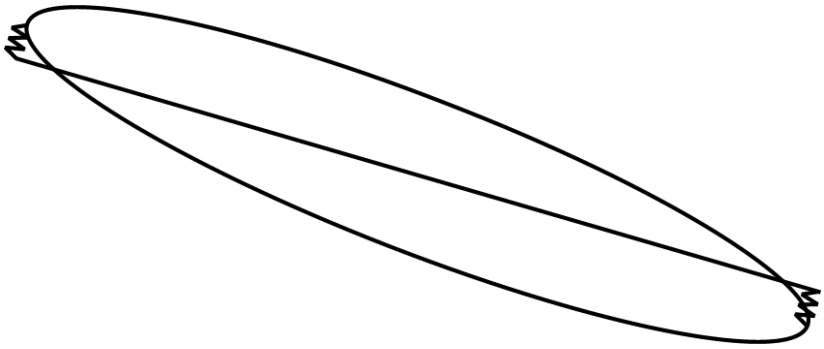

Figure 3.9 Representation of the attachment of a wobbling mass to a rigid element.

In summary the model was made up of 13 rigid elements with five additional wobbling masses (Figure 3.10). These segments represented: head and trunk; two upper arms; two forearms and hands; two legs; two shanks; two two-segment feet; wobbling masses on shanks, legs, and torso.

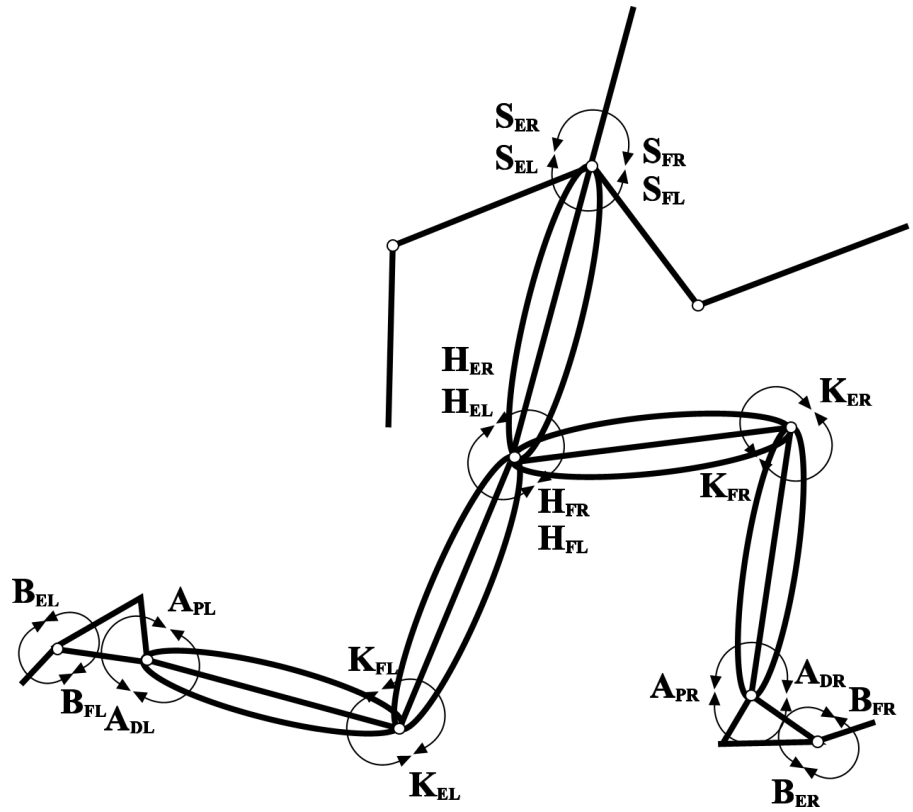

Figure 3.10 Structure of the computer simulation model of triple jumping (subscript definitions in text below).

3.5.2 Torque generators

Active torque generators

Torque generators employing contractile components (CON) and series elastic components (SEC) (Figure 3.11) were employed to flex (F) and extend (E) the right (R) and left (L) shoulder (S), hip (H), knee (K), ankle (A) and ball (B) joints (Figure 3.10). The elbow joints were angle-driven since it was assumed they would have little effect on performance.

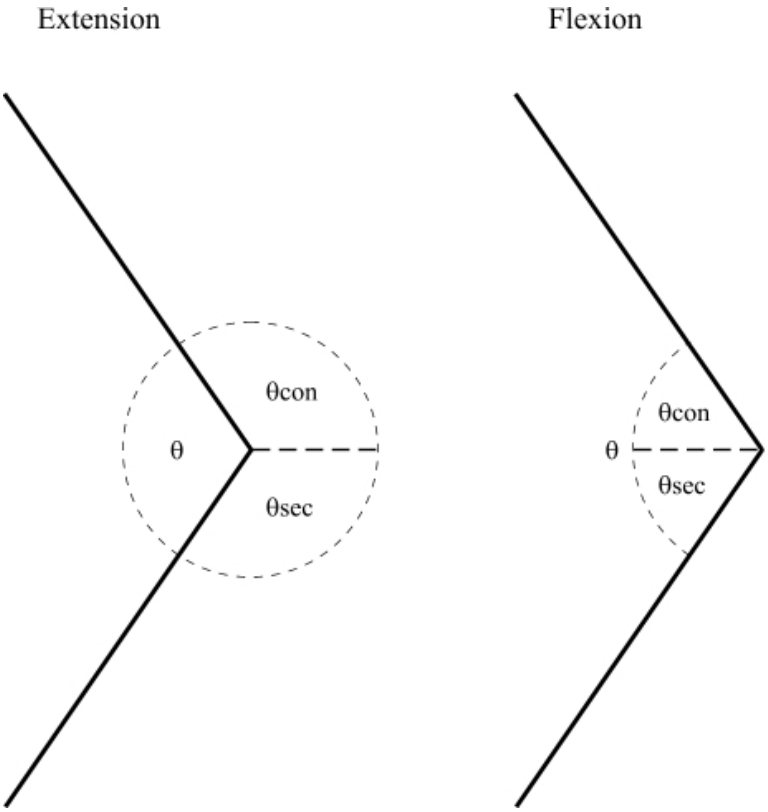

Figure 3.11 Diagram of the muscle-tendon complex in extension and flexion.

Figure 3.11 represents the muscle-tendon complex. In each case the muscle is active; therefore the SEC has a non-zero length.

Where:

θ = joint angle.

θ_{con} = contractile component angle.

$\theta_{\sec}$ = series elastic component angle.

As can be seen from Figure 3.11:

In extension: $$\theta = 2 \cdot \pi - \theta_{con} - \theta_{\sec} . \quad (3.1)$$

In flexion: $$\theta = \theta_{con} + \theta_{\sec} . \quad (3.2)$$

The contractile component torque (T_{con}) was calculated using the nine-parameter fit described in Section 4.7.5 combined with the torque generator activation level. It was assumed that, at the beginning of the simulation ($t = 0$), the angular velocity of the contractile component was equal to the angular velocity of the joint, and that T_{con} was equal to the series elastic component torque ($T_{\sec}$):

When $t = 0$,

$$\dot{\theta} = \dot{\theta}_{con} . \quad (3.3)$$

$$T_{con} = T_{\sec} . \quad (3.4)$$

Having calculated this, it was possible to calculate $\theta_{\sec}$ using the following equation:

$$T_{\sec} = k_{\sec} \cdot \theta_{\sec} , \quad (3.5)$$

where $k_{\sec}$ is the stiffness of the SEC calculated from the literature.

Calculating SEC lengths

The SEC was modelled as a linear torsional spring with a resting length of zero. The stiffness of each SEC was calculated using data from the literature (Pierrynowski, 1995; Jacobs et al., 1996; Duda et al., 1996; Rugg, et al., 1990) (Appendix 1).

With reference to Figure 3.12, the SEC length was calculated as follows:

$$l_{\sec} = l_t + l_b - l_f \cdot \cos\alpha , \quad (3.6)$$

where $l_{\sec}$ is the length of the SEC, l_t is the length of the tendon, l_b is the length of the muscle belly, l_f is the muscle fibre length, and α is the pennation angle of the muscle.

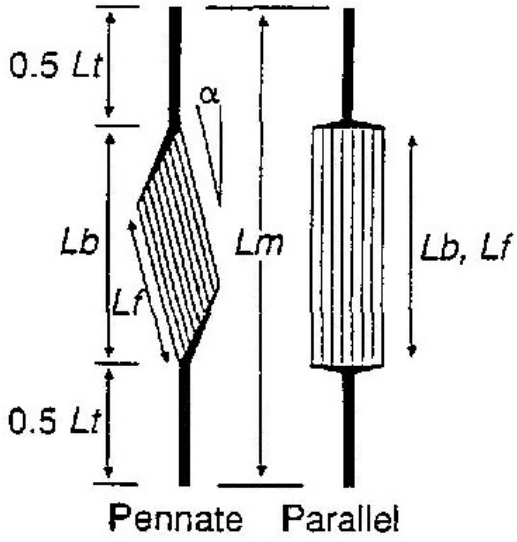

Figure 3.12 Diagram representing muscles with pennate and parallel muscle fibres (adapted from Pierrynowski, 1995)

The SEC lengths of the subject ($l_{\sec sub}$) were calculated using the ratio of the standing height of the subject in this study (h_{sub}) and height (h_{lit}) and SEC lengths ($l_{\sec lit}$) from the literature:

$$l_{\sec sub} = l_{\sec lit} \cdot \frac{h_{sub}}{h_{lit}}. \qquad (3.7)$$

Scaling moment arms

A ratio of the radii of the body segments of the subject in this study and those in the literature was calculated by considering the body as being proportional to a cylinder:

letting $m \alpha r^2 \cdot h$ (since mass α volume),

therefore $r \alpha \sqrt{\frac{m}{h}}$, (3.8)

where r is a theoretical radius, m is body mass, and h is standing height.

The moment arms were then scaled to the subject in this study by multiplying moment arms from the literature by the ratio of the theoretical radii from Equation 3.8:

$$d_{sub} = d_{lit} \cdot \frac{r_{sub}}{r_{lit}}, \qquad (3.9)$$

where d is the moment arm, and the subscripts sub and lit represent the subject and values from the literature.

Calculating SEC stiffness

The contribution of each muscle to the maximum isometric torque was calculated as follows:

$$T_i = T_{iso} \cdot \frac{PCSA_i \cdot d_i}{\sum_j^n PCSA_j \cdot d_j}, \tag{3.10}$$

where n is the total number of muscles considered, T_i is the torque associated with an individual muscle, T_{iso} is the maximum isometric torque measured at the joint, $PCSA_i$ is the physiological cross sectional area of the muscle, and d_i is the moment arm of the muscle.

The change in length of the SEC (Δl_{sec}) was assumed to be 5% of its total length during maximum isometric contractions (Finni and Komi, 2002).

$$\Delta l_{\text{sec}} = 0.05 \cdot l_{\text{sec}}. \tag{3.11}$$

The associated change in SEC angle ($\Delta\theta_{\text{sec}}$) was calculated as follows:

$$\Delta\theta_{\text{sec}} = \frac{\Delta l_{\text{sec}}}{d}. \tag{3.12}$$

The stiffness (k_m) of the SEC of an individual muscle was then calculated by dividing the maximum isometric torque by the associated angle change:

$$k_m = \frac{T_{iso}}{\Delta\theta_{\text{sec}}}. \tag{3.13}$$

The total stiffness k_{tot} of the SEC for a joint was the sum of the stiffness values for the i muscles spanning the joint:

$$k_{tot} = \sum_{i}^{n} k_i \ . \tag{3.14}$$

Due to the lack of data on the muscles spanning the shoulder joint the stiffnesses of the SEC for shoulder flexion and extension were set at 1500 Nm/rad based on the literature (King, 1998).

Passive torque generators

Although the measured joint torques (Section 4.4.4) may have some passive torques incorporated in them, this was assumed to be small due to the limited comfortable range over which the subject could be tested. Also due to the acceleration of the crank the angle range at which isovelocity data were obtained would be smaller still (Chow et al., 1997). This could lead to an underestimation of the width of the joint torque / joint angle relationship, since it was unlikely that joint torque measurements were obtained for joint angle ranges in which passive torques have a large influence. Therefore, in addition to active torque generators, the ankle, knee, and hip had passive elements which produced restorative torques at the extremes of range. These acted to stop the limb exceeding anatomical limits, since initial kinematic conditions could put torque generators at angles outside the range of their torque / angle curves (Section 4.7.5). These torques were described by a simple mathematical model of a 'generic subject' generated by measuring passive torques from ten males of a comparable age, mass, and height to the subject in this study, over a range of angles at the ankle, knee, and hip joints (Riener and Edrich, 1999). This model related the measured passive torque at a joint to the angle of the joint in question and also the angle of adjacent joints, in order to account for the effect of biarticular muscles spanning these joints. The equations for the passive torques at each joint are displayed below:

$$T_A = \exp(2.1016 - 0.0843\theta_A - 0.0176\theta_K) - \exp(-7.9763 + 0.01949\theta_A + 0.0008\theta_K) - 1.792, \tag{3.15}$$

$$T_K = \exp(1.800 - 0.0460\theta_A - 0.0352\theta_K + 0.0217\theta_H) - \exp(-3.971 - 0.0004\theta_A + 0.0495\theta_K - 0.0128\theta_H) - 4.820 + M_K, \tag{3.16}$$

$$T_H = \exp(1.4655 - 0.0034\theta_K - 0.0750\theta_H) - \exp(-1.3404 - 0.0226\theta_K + 0.0305\theta_H) + 8.072, \quad (3.17)$$

where T_A, T_K, T_H and $\theta_A, \theta_K, \theta_H$ are the ankle, knee, and hip torques and angles respectively.

Torque generator activation timings

At any given time during a simulation the activation level of each torque generator was governed by the following quintic function which has zero accelerations and velocities at the endpoints (Yeadon and Hiley, 2000):

$$a = t^3 \cdot \left(6 \cdot \left(\frac{t - t_0}{t_1 - t_0} \right)^2 - 15 \cdot \left(\frac{t - t_0}{t_1 - t_0} \right) + 10 \right), \quad (3.18)$$

where a is the activation level, t is the time, t_0 is the initial time at which the activation level is equal to zero, and t_1 is the final time at which the activation level is equal to one.

Figure 3.13 shows an example activation curve representing a torque generator ramping up and down during a simulation. The bold line indicates the activation of the torque generator. The first quintic function begins at time ts_1 whereupon it ramps up over a time period tr_1. The activation level is initially set to a_0 and remains at this level until such time that the value of the quintic function exceeds a_0. The torque generator activation level then follows that of the quintic function until its value exceeds a_1. The activation level then plateaus at a_1 for a period of time governed by the start time and duration of the second quintic function, which ramps down over a time period tr_2. When the value of the second quintic function is less than a_1 the activation again follows the quintic function until it reaches a_2 whereupon it plateaus again at this value until the end of the simulation. The time it would take for the activation level to go from zero to one, or vice versa, is represented by tr_1 and tr_2. The first ramp was allowed to initiate prior to the start of the simulation provided this did not cause the initial activation level to be above its upper bound.

These total ramp times were given a lower limit of 70 ms (Freund and Budingen, 1978) and no upper limit.

Figure 3.13 shows a two ramp profile where the torque generator ramps up and down, but the torque generators were also able to take a ramp down-ramp up profile or simply ramp up or ramp down, allowing four possibilities in total (Table 5.4).

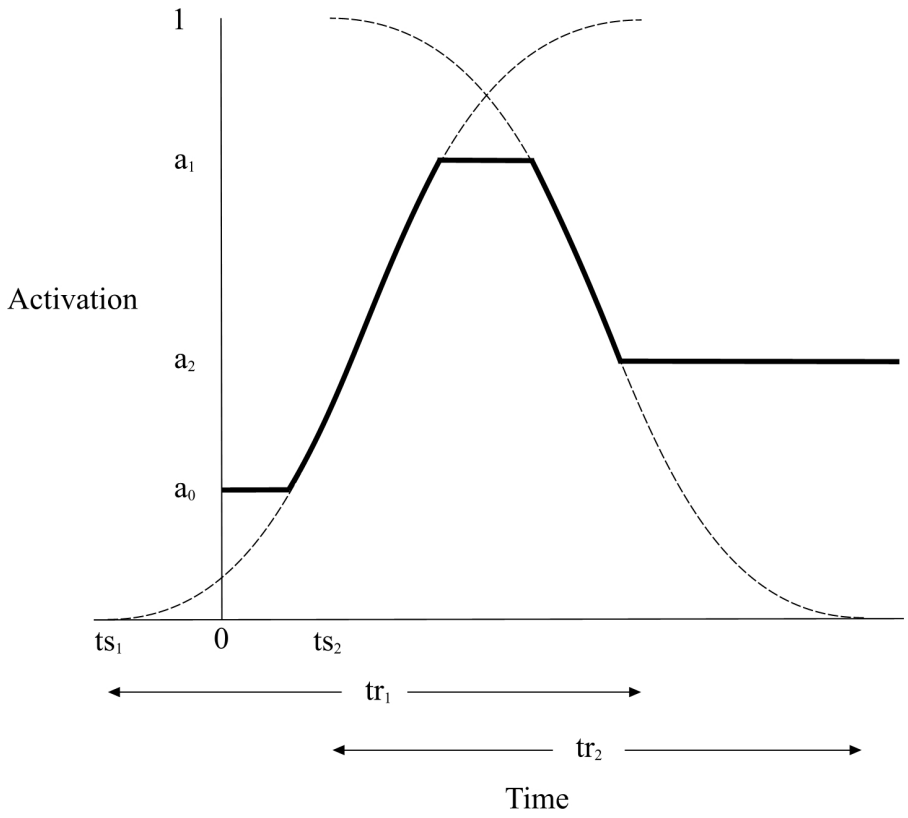

Figure 3.13 Diagram showing a torque generator activation curve.

This activation level was multiplied by a nine-parameter function defining maximal torque production (Section 4.7.5) in order to calculate the joint torque at any given point in time.

3.5.3 Formulating equations of motion

The computer simulation model was developed using Autolev^{TM} Professional Version 3.4 (Kane and Levinson, 1996) (Appendix 2). This is a software package that facilitates the construction of multibody simulations, using Kane's method (Kane and Levinson, 1996) in order to formulate the equations of motion. The simulation is constructed using generalised coordinates that are required to define the position and orientation of a segment

with respect to one that has already been defined, or to a global origin, generalised speeds, which are linear combinations of the time derivatives of the generalised coordinates (Kane and Levinson, 1985), along with inertia parameters and all the internal and external forces and torques acting upon the system. Expressions are then developed for generalised active forces and generalised inertia forces, and the simulation is advanced over a prescribed time period using a Kutta-Merson numerical integration algorithm with a variable step size Runge-Kutta integration method. Autolev^{TM} outputs code in the FORTRAN programming language. When an Autolev^{TM} file is executed, three files are produced, one containing FORTRAN code describing the simulation, one containing input values for the simulation, and another containing a list of output files and their contents, produced when a simulation is run.

3.5.4 Spring-dampers

Wobbling masses

The connection between wobbling and rigid elements was defined by a non-linear spring-damper (Pain and Challis, 2001) (Figure 3.9):

$$R = (-k_1 \cdot |v|^3 - k_2 \cdot |\dot{v}|) \cdot i, \tag{3.19}$$

where v is a vector defining the position of one point from another, i is a unit vector in the direction of v, $|v|$ is the magnitude of v, $|\dot{v}|$ is the first time differential of $|v|$, k_1 and k_2 are stiffness and damping coefficients respectively, and R is a force vector.

The wobbling masses of the torso, thigh, and shank each had different k_1 and k_2 coefficients, but the coefficients were consistent across both legs and both attachments of the wobbling mass.

Foot-ground interface

The horizontal and vertical forces at the foot were both modelled as modified linear spring-dampers situated at the heel, ball, and toe of each foot (Figure 3.8). The damping term in the vertical spring was multiplied by the magnitude of the displacement in order to ensure the force was zero at touchdown and take-off (Equation 3.20).

$$R_{yi} = -k_{1i} \cdot y_i - k_{2i} \cdot \dot{y}_i \cdot |y_i| \qquad \text{(for i=1,3)}, \qquad (3.20)$$

where R_y is the vertical force, y is the vertical displacement with respect to the floor, $\dot{y}$ is the first differential of y, k_1 and k_2 are stiffness and damping coefficients respectively, and i represents the three points of contact on the foot.

The equation for the horizontal spring-damper was multiplied by the vertical force, ensuring the force was zero at touchdown and take-off (Equation 3.21).

$$R_{xi} = (-k_{3i} \cdot x_i - k_{4i} \cdot \dot{x}_i) \cdot R_{yi} \qquad \text{(for i=1,3)}, \qquad (3.21)$$

where R_x is the horizontal force, R_y is the vertical force, x is the horizontal displacement from the initial ground contact point, $\dot{x}$ is the first differential of x, k_3 and k_4 are stiffness and damping coefficients respectively, and i represents the three points of contact on the foot.

The total horizontal and vertical GRFs on each foot were the sum of these values:

$$\begin{aligned} R_x &= \sum_{i=1}^{3} R_{xi} \\ R_y &= \sum_{i=1}^{3} R_{yi} \end{aligned} \quad . \qquad (3.22)$$

The stiffness and damping coefficients were consistent across both feet.

3.6 CHAPTER SUMMARY

In this chapter literature on analytical models of jumping and modelling soft tissue movement was reviewed. The structure of the computer simulation model of triple jumping was outlined and justified, and the individual aspects of the model were described. The next chapter will cover the collection of triple jump performance data and methods for subject-specific parameter determination.

CHAPTER 4

DATA COLLECTION AND PARAMETER DETERMINATION

4.1 CHAPTER OVERVIEW

In this chapter the experimental protocol and equipment used to collect kinematic, kinetic and anthropometric data from a triple jumper of national standard is described. Where required, relevant literature is reviewed. Procedures used to interpolate, rotate and translate kinematic data are outlined. Experimental and theoretical procedures allowing the calculation of viscoelastic parameters and maximal voluntary torque profiles are also described.

4.2 DATA COLLECTION SUMMARY

The testing procedures were explained to the subject, a male triple and long jumper of national standard (age: 22 yr, mass: 72.6 kg, height: 1.82 m; personal bests: triple jump: 14.35 m, long jump: 7.10 m). In accordance with the Loughborough University ethical guidelines, a pre-selection medical questionnaire was filled in, and an informed consent form was signed (Appendix 3). Kinematic and force data were gathered at the Loughborough University High Performance Athletics Centre (HiPAC). Force data were collected from a single force platform. In order that force data could be collected from each ground contact phase of the triple jump the subject performed a number of trials from his full approach run where the take-off of the hop, step, and jump respectively was from the force platform. The subject also performed a number of long jumps from the force platform. Kinematic data were collected for all trials using a Vicon MX motion capture system. High-speed and digital video were also captured and anthropometric measurements taken. In a subsequent session, maximal voluntary joint torque data were obtained using an isovelocity dynamometer.

4.3 COLLECTION OF KINEMATIC DATA

4.3.1 Literature on motion capture

Motion capture systems

Previously, cinematographic analysis was the main technique used in the collection of kinematic data in order to identify positions, velocities, and accelerations of joint centres. This necessitated the use of manual digitization which is tedious and time consuming (Clayton, 1991). These drawbacks are partially overcome by semi-automated systems, which use point prediction to estimate the location of markers. Fully automated systems rely on the use of contrasting markers attached to the skin of the subject overlying the anatomical landmarks (Clayton, 1991).

There are two categories of commercial instrumentation commonly used to measure whole-body motion: Those that provide a visual record of body segment positions, and those that utilise magnetic sensors to determine the position and orientation of segments in space (Richards, 1999).

Image-based devices can be further divided into the categories of passive and active systems, depending on the type of markers each system utilises. Passive systems use markers that reflect light back to the sensor, while active systems use markers that emit the light for the sensors (Richards, 1999). Passive systems have the advantage that no wires or batteries are required, and markers are inexpensive to replace (Yeadon and Challis, 1994). Active systems have good resolution at high sampling rates with the disadvantage of the subject having to carry a power supply and wires for the light emitting diodes (LEDs) (Yeadon and Challis, 1994). Magnetic tracking systems have the disadvantages of the active marker systems with the additional disadvantage of interference from metal in the capture volume (Richards, 1999).

Richards (1999) reviewed seven optical-based (Ariel, CODA, Elite, Motion, Peak, Qualisys, and Vicon) and one electromagnetic-based measurement systems (Skill Technologies). Five of the optical-based systems produced RMS errors of less than 2 mm when measuring fully visible moving markers and less than 1 mm RMS errors when

measuring a stationary marker. The Vicon system consistently had the lowest RMS errors amongst the optical-based systems in measurement of moving markers and angles based on marker positions. Richards (1999) also noted that the tracking and editing time for the Vicon system was low.

All the systems discussed above necessitate the placement of markers or sensors on the skin, which are typically used to calculate the positions of joint centres and model the subject as a system of rigid bodies. This method can produce artefacts due to skin movement over the underlying bony landmarks and changes in technique by the subject caused by the markers or sensors on the skin. Mundermann et al. (2006) discussed the use of markerless motion capture for biomechanics. They described a method using an articulated iterative closest point (ICP) algorithm to track human body segments in visual hull sequences. They stated that the biomechanical applications of the current methods for markerless motion capture have been limited by their accuracy. However, they predicted markerless tracking will become a feasible and practical alternative to marker-based systems, minimising patient preparation time and reducing experimental error.

Currently, the good accuracy of the passive optical-based systems (Richards, 1999), combined with the lack of requirement for the subject to carry a power supply and wires, make them a suitable option for the measurement of dynamic human jumping activities.

Soft tissue motion

It has been shown that soft tissue movement can lead to skin markers not exactly representing underlying joint motion during activities involving impacts. Minetti and Belli (1994) investigated the movement of the visceral mass during periodic movements; they found a maximum displacement of 0.1 m during hopping tasks. Lafortune et al. (1992) found external markers moved 4.3 cm and 7.5 cm with respect to the tibia and femur respectively, during loaded and unloaded knee flexion / extension. Reinschmidt et al. (1997a) investigated the effect of this skin movement on the calculation of knee joint motion during running. They demonstrated average errors relative to the range of motion of 21%, 63%, and 70% in flexion / extension, internal / external rotation, and abduction / adduction respectively between skin markers and markers attached directly to the tibia and femur. Reinschmidt et al. (1997b) showed that knee flexion / extension angles calculated from skin markers showed good agreement with underlying bone movement (mean 2.1°

difference) during walking. This is in contrast to abduction / adduction and internal / external rotation which, on occasions, produced errors larger than the true bone movement. This suggests that only flexion / extension angles should be calculated at the knee using external markers and, even then, with caution.

4.3.2 Vicon MX

Vicon MX is a suite of networked Vicon MX cameras and devices that provide real-time and offline digital-optical motion capture data. Each camera has a strobe unit that emits flashes of near infrared light (Figure 4.1), illuminating retroreflective markers located at key locations on the subject (Figure 4.2). The camera then captures and electronically converts the pattern of reflected light from the markers into data that represents the position and radius of each marker in the image.

Figure 4.1 A view of the experimental setup from behind.

Details of marker positions

Forty-five 25 mm retroreflective markers were positioned at locations on the subject's body in order that the positions of joint centres could subsequently be estimated (Figure 4.2 and Appendix 4).

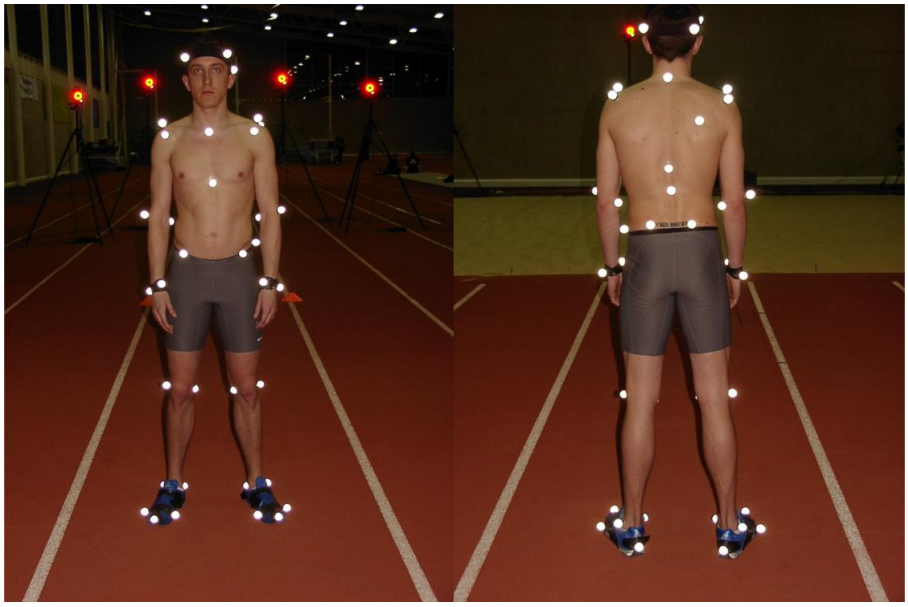

Figure 4.2 Positioning of retroreflective markers on the subject.

Camera setup

Eighteen Vicon MX cameras were situated around the capture volume in order that a ~18m x 2m x 2.5m volume was covered (Figures 4.1 and 4.3). This volume included the full triple jump and the last stride of the approach run. Data were captured from a number of whole triple jumps at 240 Hz. In addition to this a number of hop and step take-offs from the force platform, and two additional complete triple jumps, were also captured at 480 Hz.

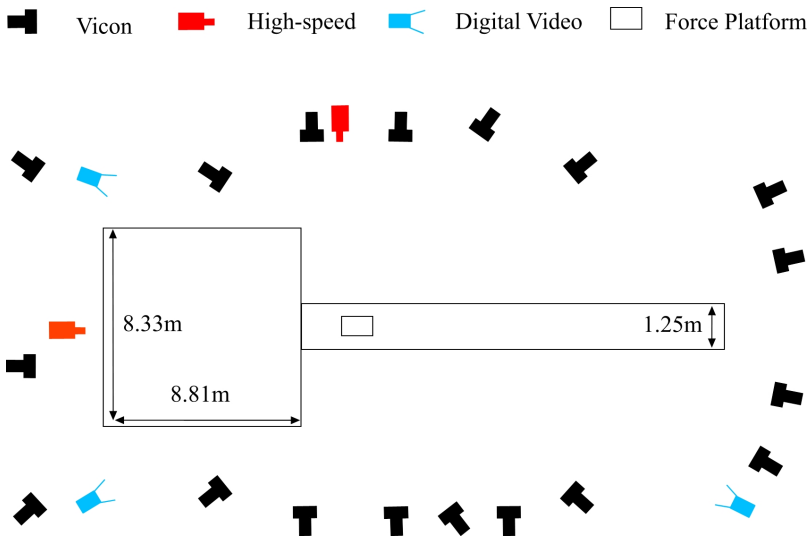

Figure 4.3 Diagram of the experimental setup.

Vicon calibration

In order to calibrate the Vicon cameras it was necessary to identify internal (focal length and distortion) and external (camera position and orientation) camera parameters. Vicon accomplished this using a dynamic calibration procedure which calculated these parameters through two processes:

- Linearisation:
    - Distortion in the camera lenses and other non-linearities were measured and a correction matrix was then applied to the data.
- Photogrammetric Calibration:
    - The physical location and orientation of the cameras were calculated.

Prior to this dynamic calibration, a static calibration was performed in order to define the global coordinate system in the capture volume using a calibration frame. The calibration frame had four 25 mm markers located in a plane with three markers defining the x axis and another marker which combined with the x axis to define the origin and y axis. The z axis is then obtained by taking the cross product of the x and y axes.

The dynamic calibration was performed with three collinear 25 mm retroreflective markers situated at known distances from each other on a wand. Due to the large capture volume the wand was placed on the end of an extension pole in order that a much larger volume could be covered by the wand. This allowed more cameras to recognise the markers and lower camera residuals to be achieved.

Camera residuals

The quality of the calibration was determined by camera 'residuals' representing the RMS of the distance between the light ray emitted from the camera to the retroreflective marker and the ray reflected back to the camera from the marker. The 'mean residual' is the mathematical mean of all the camera residuals and the 'residual range' indicates the difference between the highest and lowest camera residuals.

According to Vicon, the individual camera residuals should not be more than 0.1 % of the distance from the camera to the centre of the capture volume. This would indicate that a

residual of less than 1 mm would be acceptable for a distance of 1 m from the centre of the capture volume. Since all cameras were a number of metres from the centre of the volume, the measured residuals (mean 0.609 mm) were more than adequate (Appendix 5).

Static reproducibility

The static reproducibility is a measure of the RMS error of the calculated relative positions of markers on the static calibration object with respect to the known relative coordinates of the markers. Vicon recommends that this value be less than 1%, hence on this occasion the value of 0.944% was just acceptable. However, the accuracy of the static calibration object was not an issue in this case as the data subsequently underwent a rotation and translation. This was based on a matrix determined from markers placed on the floor throughout the capture volume in order to define a global coordinate system (Appendix 6).

Rotation and translation of the coordinate data

Due to the relatively large capture volume, some of the cameras could not detect the static calibration frame, which caused problems when calibrating the equipment. The calibration frame was elevated and rotated until the maximum number of cameras could detect it. This led to a global coordinate system that did not relate well to the activity being measured and therefore required a rotation and translation to be performed on the data to bring the origin and coordinate system in line with the running track before it could be analysed (Appendix 6).

Vicon reconstruction parameters

Vicon automatically tracks markers and reconstructs their position. This reconstruction is dependent on various parameters, namely:

- Maximum acceleration;
- Maximum noise factor;
- Intersection limit;
- Residual factor;
- Predictor radius;
- Minimum cameras to start trajectories.

In order to optimise the number of markers that were tracked, and the accuracy of this tracking, these values were varied. Each one was manipulated away from the default values whilst holding the other values constant. It was assumed the effect of each parameter was independent, unless indicated otherwise in Vicon literature. One way of assessing the quality of the reconstruction is to observe the number of segments created; if all trajectories are unbroken there will be one segment per marker. In all cases there were a number of broken trajectories and therefore a much higher segment number than there were markers, so minimising this number was an indicator of less broken trajectories. This is just an indicator and it was important to visually inspect the data too, as some trajectories were more important to the analysis than others. Therefore, parameter values that also optimised the tracking of these trajectories were chosen. For parameter values and explanations see Appendix 7.

4.3.3 Video

In addition to Vicon data, high-speed video of the ground contact phases on the force platform was captured from the front and side using Phantom high-speed cameras (Figure 4.3). These were used as a visual reference to aid the analysis and processing of the kinetic and kinematic data. Digital video was captured at 50 Hz using three Sony digital Handycam VX1000E video cameras, two situated diagonally in front of the jumper and one diagonally behind (Figure 4.3). In addition to acting as a visual reference, this was treated as a contingency plan had there been problems with the kinematic data from Vicon necessitating manual digitising.

4.3.4 Analysis of kinematic data

Marker files

Once the kinematic data had undergone the rotation and translation it was necessary to assign each tracked marker with a name in order that segments could be defined and angles between segments calculated. In order to do this Vicon required a marker file containing all the relevant marker labels. A list of these names is displayed in Appendix 4. This file also defined segments using marker positions and subsequently defined the sequence in which these segments were attached to each other. The order in which lines between markers were drawn was also defined for display purposes.

For each trial it was necessary to label each marker with the correct name. Since trajectories were often broken, some markers were labelled multiple times over the time period of the trial.

Filling gaps in marker trajectories

Where marker trajectories were broken, gaps of up to 10 frames were filled automatically by Vicon, since it is relatively easy to predict a trajectory over a small time period where information is known about the trajectory at either side of the gap. In this case trajectories were then visually checked to ensure the interpolation was sensible. Where the gaps were larger than 10 frames the pattern of movement of proximal markers was used to predict the trajectory of the marker in question. Discretion was used in order to pick suitable markers, i.e. the trajectory of one knee, ankle, or elbow marker can be used with some confidence to predict the trajectory of the other marker on the same joint since they are on hinge joints and therefore bound to follow similar trajectories. This technique was used mainly in airborne phases and not very close to impacts where marker movement is more erratic. Where a portion of a trajectory was clearly spurious this portion was deleted and the gap filled in one of the ways described above.

Model files

Once all the markers in the trials had been labelled it was possible to obtain joint centres and relevant joint angles for input into the simulation model from Vicon using a model written in Vicon BodyLanguage (Appendix 8). Since the data were collected in three dimensions and the simulation model was restricted to the sagittal plane, it was necessary to convert the angles into two dimensions. As most of the activity occurred in the sagittal plane, angles could be read in directly from Vicon if the axes defined within Vicon were in line with those of the simulation model. Two potential operations were possible: projection of the angle onto the sagittal plane; or rotation of the coordinate system of the limb in order to obtain the angle in the sagittal plane.

Projection of the limb angle

The angle of the limb (θ) was calculated by simply using the coordinates in the axes describing the sagittal plane (x and z) and disregarding the coordinate in the third axis (y) (Figure 4.4).

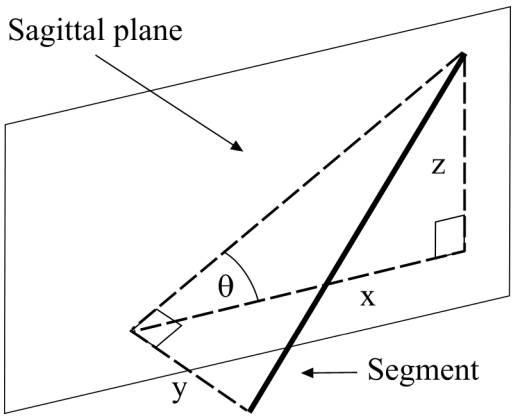

Figure 4.4 Illustration of the projection of a segment onto the sagittal plane.

Rotation of the arm coordinate system

The other option was that the angle of a 'child' segment could be calculated with respect to the coordinate system of the 'parent' segment that it was attached or the global coordinate system (Figure 4.5).

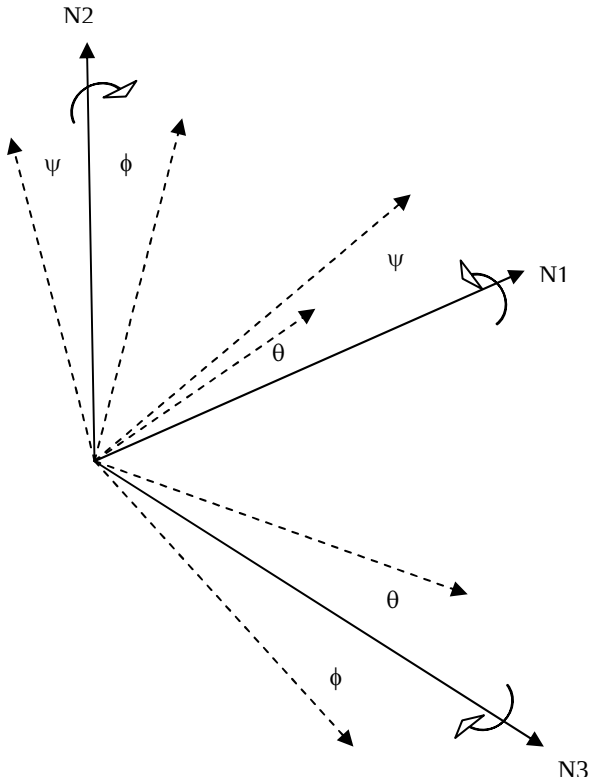

Figure 4.5 Diagram showing clockwise rotations about three axes (indicated by arrows around the axes) in a right hand coordinate system.

A directional cosine matrix can be derived which performs rotations on data points about three axes:

$$\begin{bmatrix} \cos\theta & 0 & -\sin\theta \\ \sin\phi\cdot\sin\theta & \cos\phi & \sin\phi\cdot\cos\theta \\ \cos\phi\cdot\sin\theta & -\sin\phi & \cos\phi\cdot\cos\theta \end{bmatrix}. \qquad (4.1)$$

With reference to Figure 4.5, the directional cosine matrix described in Equation 4.1 represents clockwise rotations about three axes: N1; N2; and N3. Through angles: θ; ϕ; and ψ.

The order of rotation chosen was based on the likely range of motion about each of the axes during common human motions such as walking and running (Tupling and Pierrynowski, 1987); with internal / external rotation being the smallest, followed by adduction / abduction, and then flexion / extension. Each segment was therefore rotated first about the flexion / extension axis, followed by the adduction / abduction axis, and lastly the internal / external rotation axis.

Both methods were trialled in the angle-driven model and it was found that the projection angles allowed the model to match performance data better, since they represented motion in the sagittal plane better than the rotated angles, so that method was preferred.

4.4 COLLECTION OF KINETIC DATA

4.4.1 Literature on force measurement

Force is generally measured using the deformation of transducer elements to generate a voltage proportional to the applied force (Yeadon and Challis, 1994). Kinetic data of foot-ground contacts is typically collected using force platforms. According to Yeadon and Challis (1994) the key design features of a force platform are that it should be large enough to accommodate the contact area within the movement of interest and that it should have a natural frequency high enough to eliminate interference of vibrations in the plate with the signal of interest.

4.4.2 Force data collection protocol

Force data were obtained using an AMTI BP600900 force platform with a 4000 lb (17800 N) vertical force capacity. This force platform uses strain gauges mounted on four precision strain elements to measure forces and moments, producing a total of six voltage outputs: three force; and three moment channels. The raw voltage outputs from the strain gauges were amplified and converted to a digital signal by an AMTI Miniamp using a gain of 1000, and a 12 bit analog-to-digital converter. The excitation voltage was set to 10 V and the voltage range was ±10 V. The force data were captured at 1000 Hz and synchronised with the kinematic data using a remote trigger. This trigger initiated the capture of force data, using a 50% pre-trigger with 2 s of capture time, and applied a voltage to an external patch panel eliciting a square wave in an analogue channel within the Vicon MX system.

The force platform had a covering of synthetic track. Initially no corrections were made for this since it was assumed this would only slightly affect the transferred forces, as the mass of the deformed surface was small (Nigg and Yeadon, 1987).

4.4.3 Literature on isovelocity dynamometry

In torque-driven models of sporting activities it is necessary to ascertain joint torque parameters for the subject in order that joint torques in the model remain within realistic boundaries. These joint torques may be measured using an isovelocity dynamometer (e.g. Cybex, Isocom). These dynamometers have a powered crank which rotates back and forth through a pre-defined angle range, varying resistance in order to maintain a set velocity, whilst the subject exerts maximal torque on the crank, both concentrically and eccentrically. This torque is measured by a strain gauge in the crank.

Chow (2001) highlighted several issues concerning the use of isovelocity dynamometers: torque ‘overshoot’ and ‘oscillation’ can occur before constant angular velocity is attained and deceleration occurs towards the end of the contraction (Osternig et al., 1982); the period of constant angular velocity decreases as the pre-set angular velocity increases due to the greater angular distance through which the limb has to travel before reaching

constant angular velocity (Chow et al., 1997); errors in torque measurement occur when gravitational and inertial effects are not considered (Chow et al., 1997), although Chow (2001) stated that most modern machines have a gravity correction feature; and mixed results on within-day, inter-day, and inter-machine reliability of strength data have been reported for different exercises (Madsen, 1996). Despite these concerns Chow (2001) emphasised that recognising the limitations of these machines does not detract from the valuable contribution they make to the understanding of muscular function.

4.4.4 Joint torque measurement protocol

An Isocom isovelocity dynamometer was used to gather data for the ankle plantar and dorsi flexion and for flexion and extension of the knee, hip, and shoulder on the right side of the body (Figures 4.6-4.7).

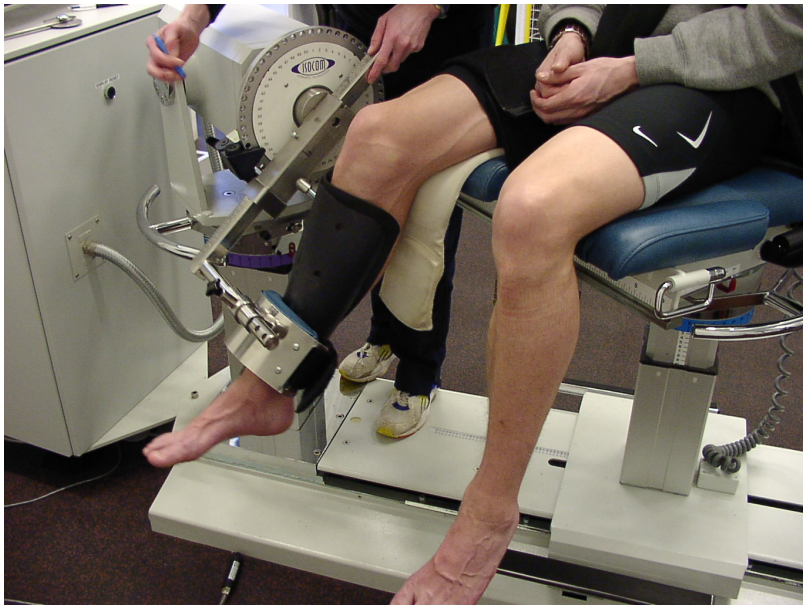

Figure 4.6 Position of subject and dynamometer for knee extension.

Bilateral symmetry was assumed. Measurements were taken at angular velocities ranging from 0°/s (isometric) to 400°/s at 50º/s intervals, using a sampling frequency of 1000 Hz. These data subsequently allowed torque / angle and torque / angular velocity profiles to be calculated for the subject and joints in question.

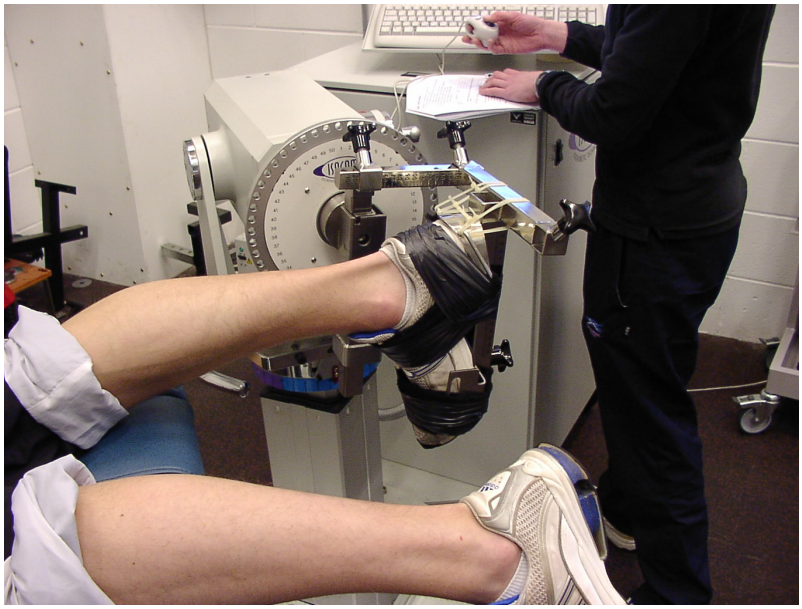

Figure 4.7 Position of subject and dynamometer for ankle plantar flexion.

When setting up the apparatus it was important to ensure that the centre of rotation of the crank arm was as close to that of the relevant joint as possible. In order to do this, the subject was instructed to apply torque to the crank arm whilst the centre of rotation of the crank was aligned with that of the joint, as the joint centre moves when torque is applied.

Calculation of inertial properties

Inertial properties for the system were obtained automatically by the machine. The crank and limb were allowed to fall under gravity at a prescribed angular velocity and the applied torque was measured. Once this had been calculated, the torque due to gravitational acceleration of the limb could be accounted for to give the gross torque produced around the joint.

Conversion of crank angle to joint angle

The crank angle and joint angle differ due to the way the subject's limb is attached to the crank arm. In order to get joint angle data from the crank angles measured by the dynamometer, a mechanical goniometer was used to measure joint angles statically throughout the range of crank angles used by the dynamometer, whilst the subject applied a torque to the crank arm. A line was then fitted to the data relating joint angles to crank angles. This allowed joint angles and angular velocities to be calculated from the crank data.

4.4.5 Maximum joint velocity measurements

In addition to the isovelocity data, maximum velocity data were also taken for the knee, hip, and shoulder joints with the limb unloaded. The ankle was omitted as it was deemed impractical because maximum voluntary velocity was unlikely to exceed that measured by the isovelocity dynamometer. These data were gathered using Vicon MX; retroreflective markers were placed on the ankle, knee, hip, shoulder, and elbow joints and the subject was instructed to flex and extend at each joint as quickly as possible, with flexion and extension being two separate movements.

These data allowed a realistic maximum achievable velocity to be measured, which could then be used as a lower bound for ω_{max} in the optimisation procedure, during which a surface was fitted to the torque / angular velocity and torque / angle data gathered using the isovelocity dynamometer (Section 4.7.5). A more accurate torque / angular velocity relationship for input to the simulation model of triple jumping could then be calculated.

4.5 DATA PROCESSING

4.5.1 Filtering force data

Upon visual inspection it became apparent that the experimental force data might be noisy. This was especially marked in the horizontal force traces. The simulation model determined forces at the foot using equations based on the movement of the foot and shoe relative to the ground. If a portion of the force trace was governed by factors other than this, e.g. movement of the force plate or the force plate covering, the model could not be expected to reproduce this portion. In order to determine whether this was the case, similar jumps were performed from the force plate in the laboratory, and the force plate in the HiPAC where the experimental data was collected. These jumps were performed using the same footwear and approach run length. The HiPAC data displayed a high frequency component which was absent from the laboratory data (Figures 4.8 and 4.9).

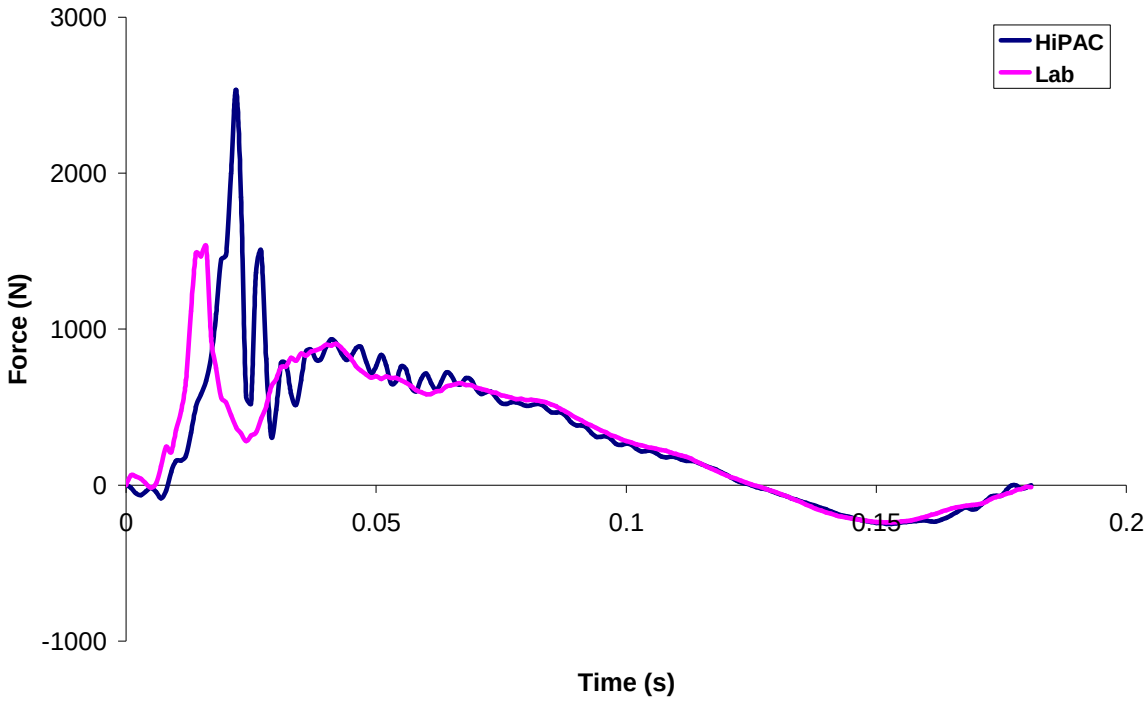

Figure 4.8 Horizontal force traces for similar jumps in the laboratory and HiPAC.

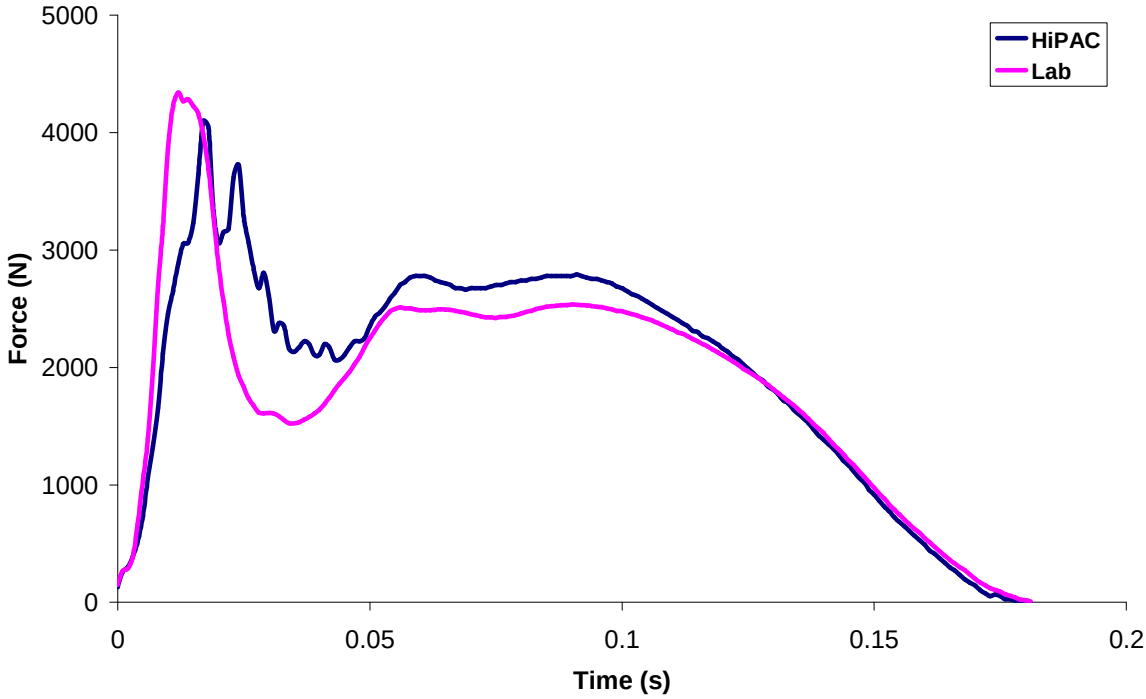

Figure 4.9 Vertical force traces for similar jumps in the laboratory and HiPAC.

A spectral analysis was then performed on both sets of data in order to ascertain which frequencies were common to both sets and which were not, and hence could be filtered out of the HiPAC data. It can been seen that there was a marked increase in the spectral density of the HiPAC data signal above 100 Hz, peaking at around 200 Hz (Figure 4.10). There was no such increase in the laboratory data, with the signal continuing to die away to near zero (Figure 4.11). Since the spectral density graphs differ in form after approximately 100 Hz for the two jumps, a low pass Butterworth filter was used to remove frequencies above 100 Hz from the HiPAC data. This resulted in a total change in horizontal and vertical impulse of only 0.1188 % and -0.0245 % respectively, but quite a marked change in the form of the horizontal force trace (Figure 4.12) and a less marked change in the vertical force trace (Figure 4.13).

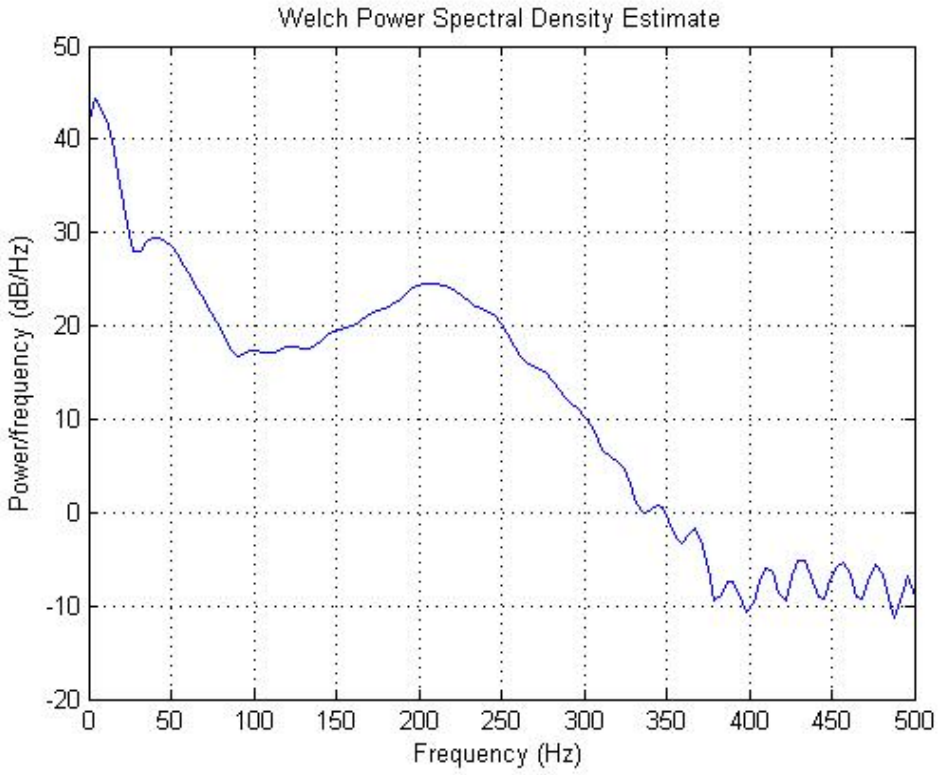

Figure 4.10 Spectral analysis of force data from HiPAC.

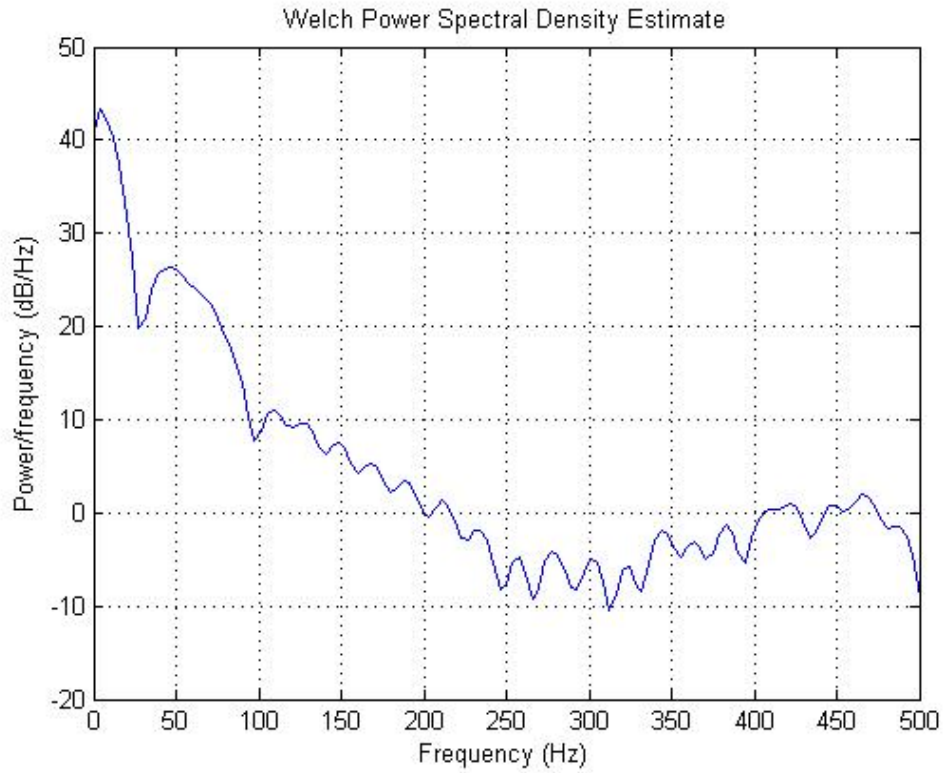

Figure 4.11 Spectral analysis of force data from the laboratory.

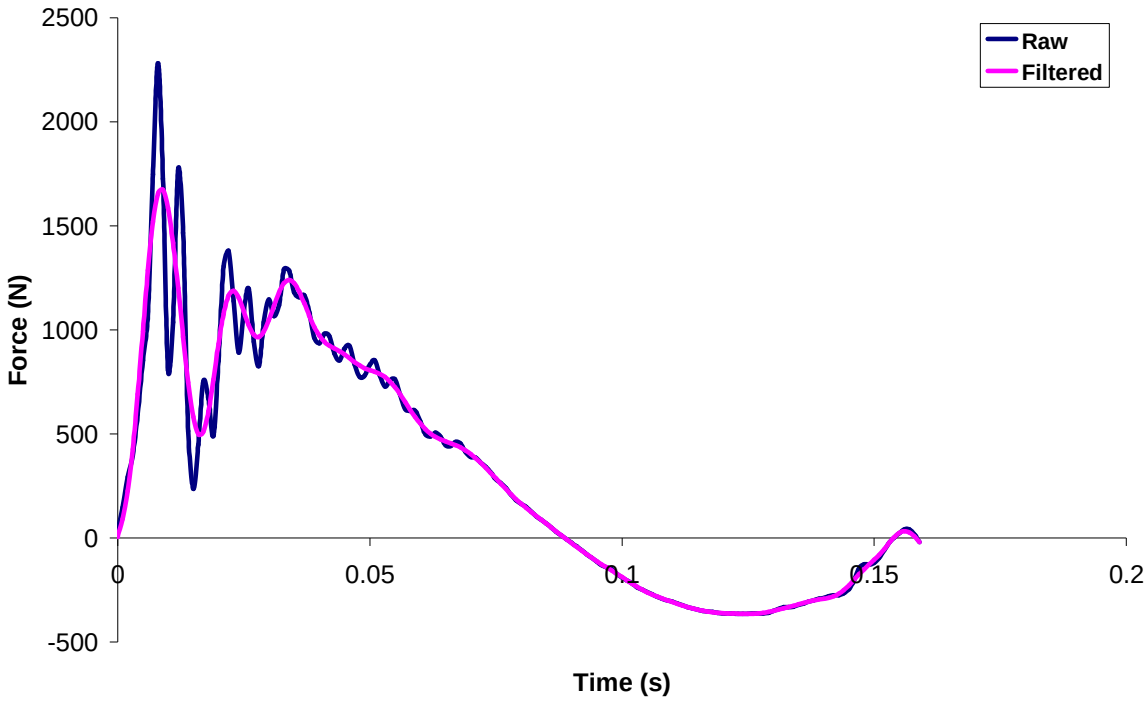

Figure 4.12 Filtered and raw horizontal force traces from HiPAC data.

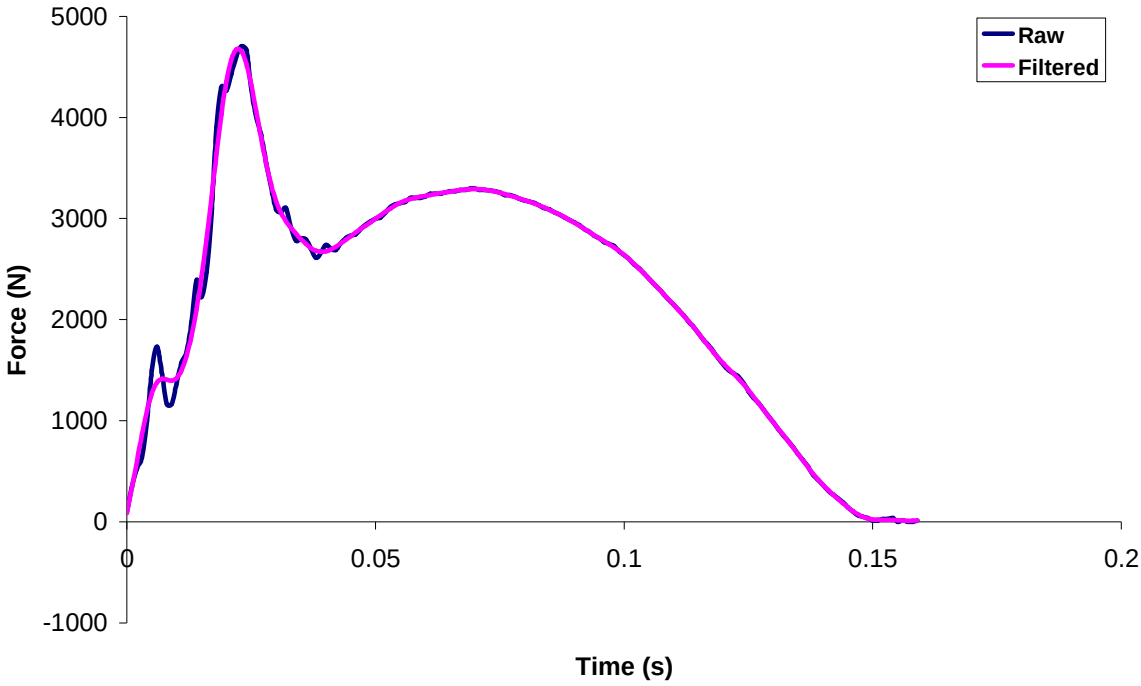

Figure 4.13 Filtered and raw vertical force traces from HiPAC data.

4.5.2 Calculating COM velocities

It was necessary to obtain accurate COM velocities at touchdown and take-off for each phase of the triple jump. These were used as initial conditions and in the objective function to evaluate the accuracy of the model. Whole-body COM positions were obtained using an inertia model (Yeadon 1990a) (Figure 4.14).

Figure 4.14 Graphical representation of the inertia model for trial 05.

Touchdown and take-off velocities were calculated from the COM positions at the beginning and end of the flight phases preceding and following the ground contact using equations of motion (Table 4.1).

Table 4.1 Calculated COM velocities

Phase	Trial	Direction	Touchdown velocity (m/s)	Take-off velocity (m/s)
07	Jump	Horizontal	6.81	5.52
		Vertical	-2.22	2.28
09	Hop	Horizontal	7.73	7.00
		Vertical	-0.95	2.35
10	Step	Horizontal	7.07	6.30
		Vertical	-2.71	1.64

In order to quantify the accuracy of this data the impulses calculated from the difference between touchdown and take-off velocities were compared to those measured from the force plate, and implied differences in velocities were calculated (Table 4.2).

Table 4.2 Comparison of calculated and measured impulses

Phase	Trial	Direction	Calculated impulses (N.s)	Measured impulses (N.s)	Implied difference in velocity (m/s)
07	Jump	Horizontal	-93.81	-90.98	0.04
		Vertical	467.92	473.71	0.08
09	Hop	Horizontal	-53.19	-46.94	0.09
		Vertical	339.64	342.59	0.05
10	Step	Horizontal	-56.13	-55.89	0.00
		Vertical	456.52	462.35	0.08
Average			176.83	180.81	0.05

These implied differences in velocities were used as a number by which the initial COM velocities were allowed to vary in simulations to account for inaccuracies in the coordinate data.

4.5.3 Splining angle data

Joint angle time histories from the performance obtained using Vicon were used as input to an angle-driven simulation model. In order to drive the simulation model using different time-steps it is necessary to fit quintic splines (Wood and Jennings, 1979) to the joint angle time histories to ensure that angles could be calculated for input to the simulation model at any time interval during the simulations. Six spline coefficients were calculated for each time step. The simulation model could then read in these six spline coefficients and use them to interpolate between time-steps, calculating the angles and their first and second time derivatives to obtain angular velocity and acceleration for the requisite points in time.

In addition to interpolation, quintic splines were also used to smooth the angle data, removing noise due to marker movement or errors in the tracking of markers. In order to estimate errors a pseudo data set was calculated by averaging the points before and after each original data point; the difference between this pseudo data point and the original data point gave an estimate of the error in this point (Yeadon and King, 2002).

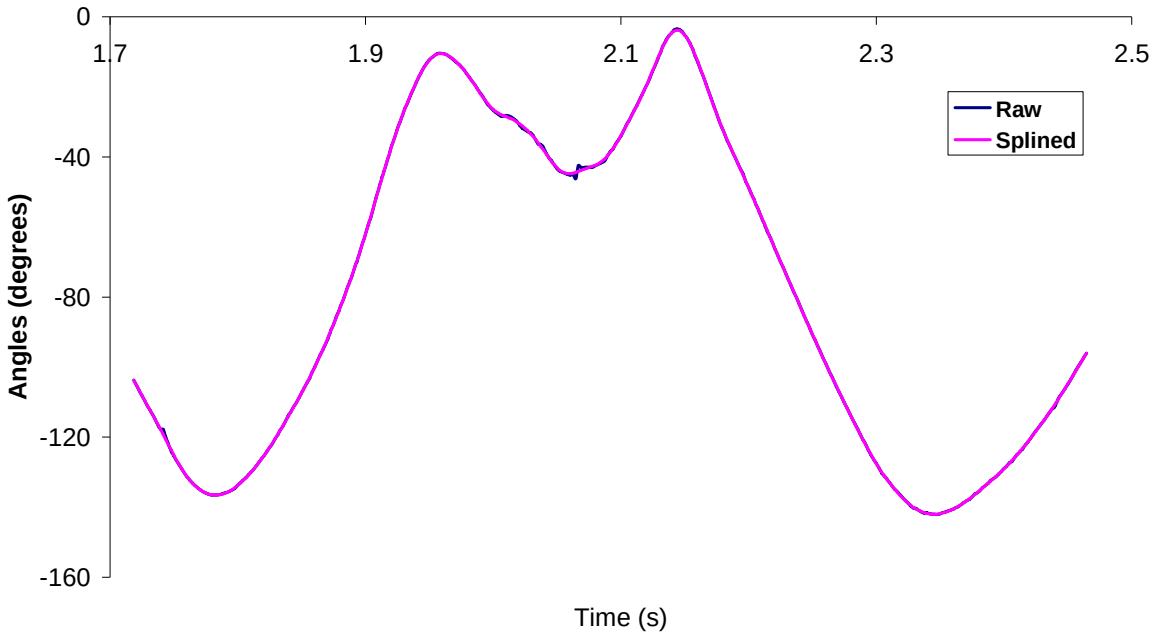

Figure 4.15 A comparison of raw and splined knee angles.

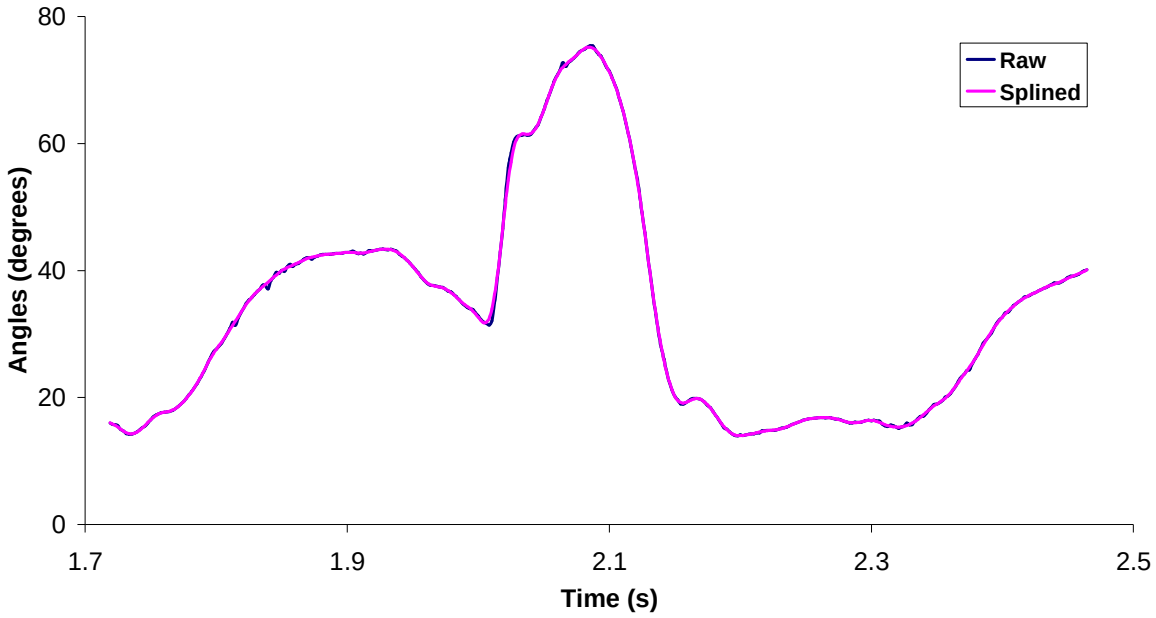

Figure 4.16 A comparison of raw and splined ankle angles.

The level of smoothing was important in order to remove noise whilst keeping as much of the genuine signal as possible. This level was determined by the weighting of local and global errors on the overall level of smoothing. This was particularly important around impacts since large angular accelerations would have occurred and should not have been removed due to over-smoothing. In order to obtain a balance between removing noise and over-smoothing, local and global errors were each given a weighting of 50%. Average errors were less than 0.5° for angles at all joints. Selected raw and splined angle time histories are displayed in Figures 4.15-4.16 and it can be seen that genuine angle peaks have been largely maintained, whilst high frequency noise has been removed.

4.6 ANALYSIS OF TRIPLE JUMP DATA

4.6.1 Phase ratios

During the data collection the subject performed a number of complete triple jumps, the total distances, phase distances and phase ratios for these jumps are displayed in Table 4.3. A diagram showing how each phase distance is calculated is shown in Figure 2.7.

Table 4.3 Distance of jumps and individual phase ratios for complete trials

Trial	Hop (m)	Step (m)	Jump (m)	Total (m)	Hop %	Step %	Jump %
1	4.32	4.26	4.17	12.75	33.88	33.41	32.71
3	4.80	4.04	4.34	13.18	36.42	30.65	32.93
5	4.59	3.96	4.53	13.08	35.09	30.28	34.63
6	4.44	3.98	4.37	12.79	34.71	31.12	34.17
7	4.51	3.96	4.28	12.75	35.37	31.06	33.57
Mean	4.59	4.03	4.34	12.91	35.10	31.30	33.60
Range	0.48	0.30	0.36	0.43	2.54	3.14	1.93

It can be seen in Table 4.3 that, on average, the subject employed a balanced technique; one where neither the hop nor the jump was more than two percent greater than the other (Hay, 1999). Only in trial number three, which resulted in the greatest distance, did the subject exhibit another, hop-dominated, technique (Hay, 1999). The phase ratios displayed in Table 4.3 are all within those percentages reported for Olympic triple jumpers by Hay (1999).

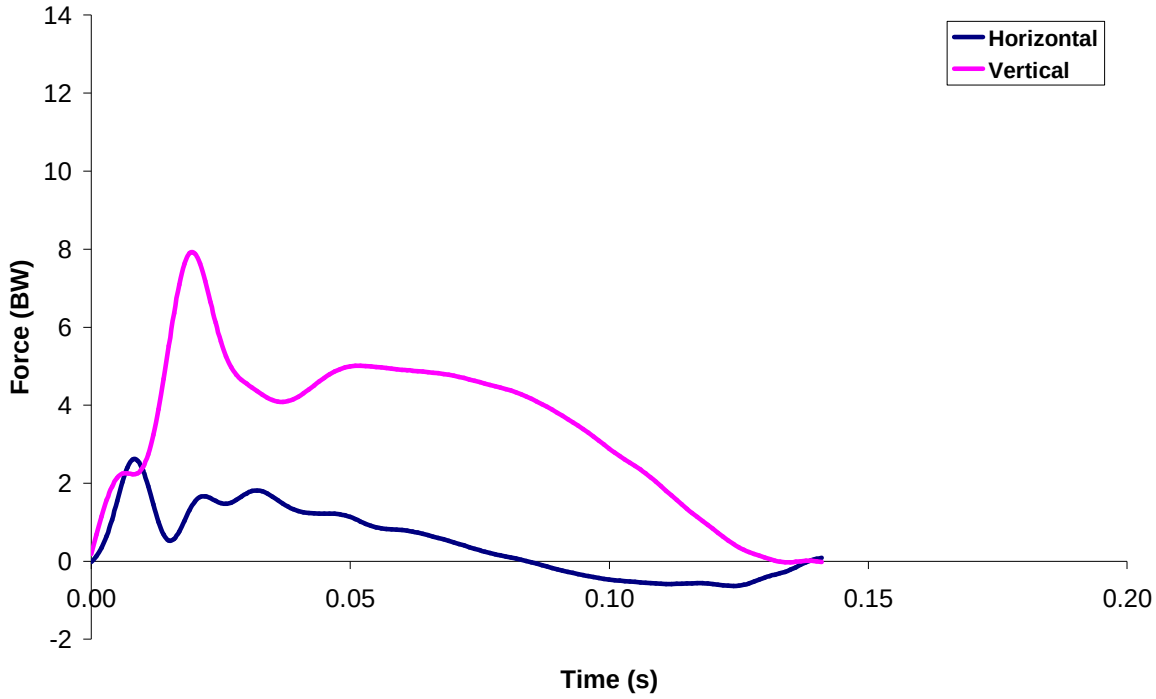

Figure 4.17 Horizontal and vertical forces for the hop phase (Trial 09).

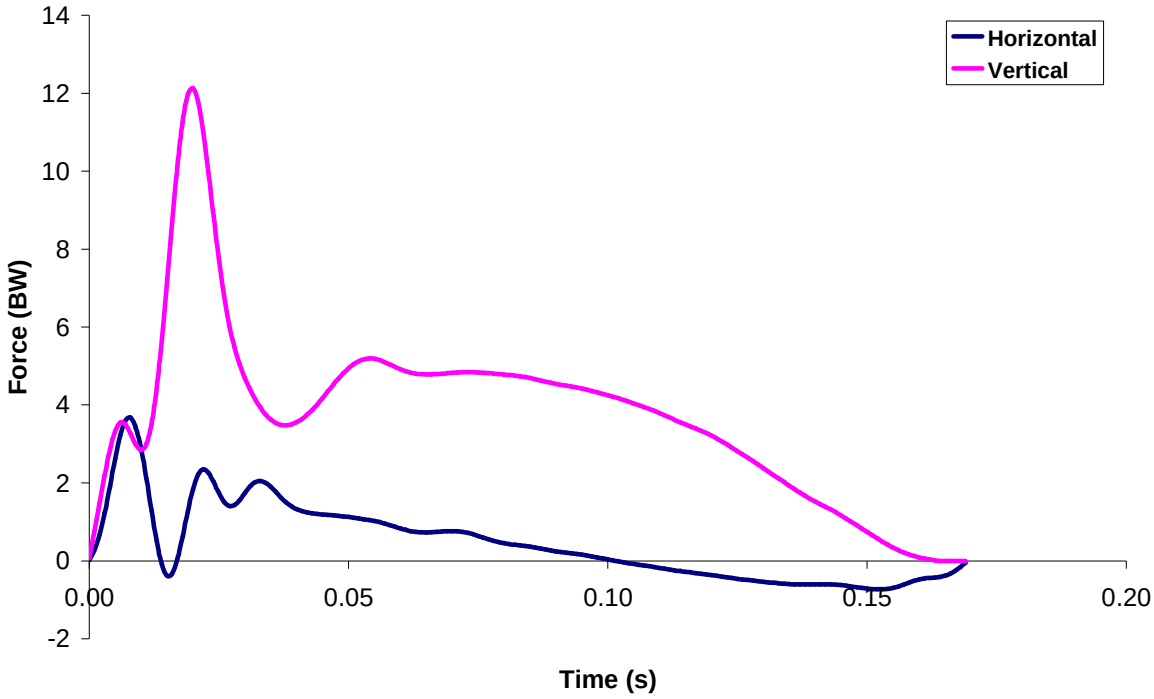

Figure 4.18 Horizontal and vertical forces for the step phase (Trial 11).

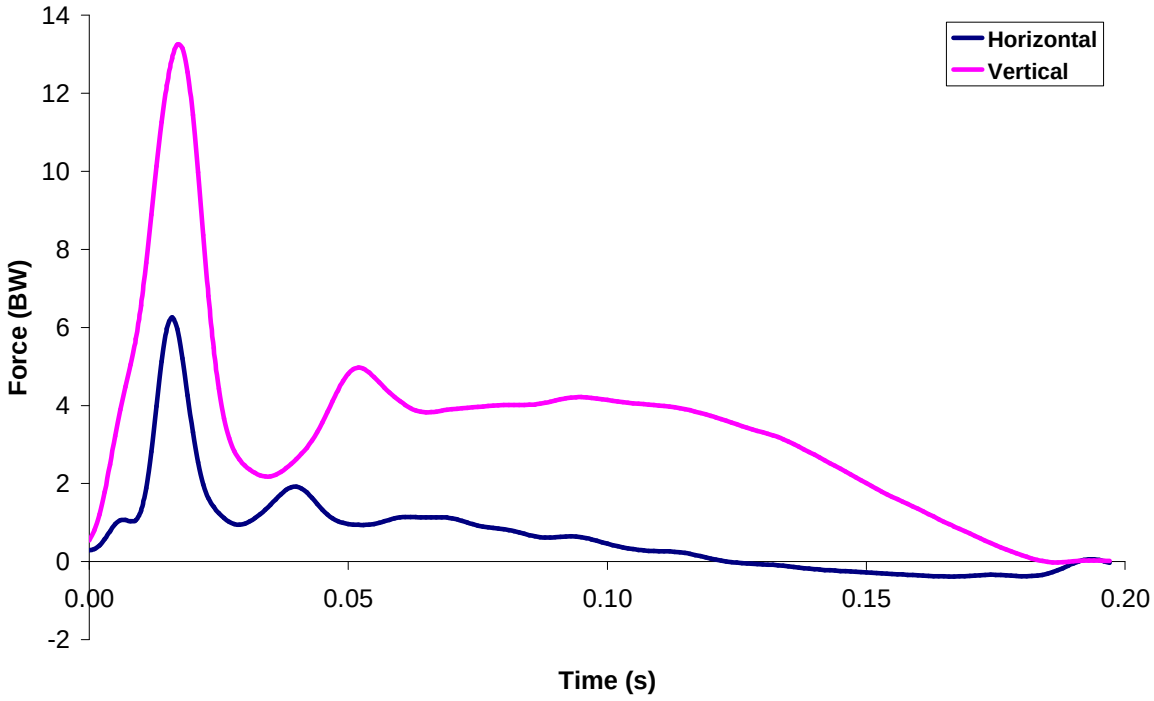

Figure 4.19 Horizontal and vertical forces for the jump phase (Trial 07).

Figures 4.17 to 4.19 show filtered forces measured in BWs for the hop, step, and jump phases respectively. These forces are in line with values in the literature, in that the magnitude of the vertical force peak in the hop landing is around 12 body weights (Ramey and Williams, 1985). However, surprisingly the highest peak force was recorded in the

step landing (> 13 BWs); this was perhaps due to the subject having a bruised heel which he tried to protect from high forces in the hop landing by contacting the ground first with his toe. This was not apparent in the step landing.

4.7 PARAMETER DETERMINATION

4.7.1 Literature on anthropometric measurement

Yeadon and Challis (1994) stated that experimental techniques for determining body segment inertia parameters such as water immersion (Plagenhoef et al., 1983), reaction board measurements for mass centre locations (Drillis et al., 1964) and oscillation techniques for moments of inertia (Hatze, 1975) are time consuming and not suitable for determining inertia properties of central segments such as the pelvis. Yeadon and Challis (1994) list a number of methods which allow calculation of body segment inertia parameters. These include geometric models (Hatze, 1980; Yeadon, 1990a), regression equations (Hinrichs, 1985), non-linear regression equations (Yeadon and Morlock, 1989) and the scaling of cadaver inertia values (Forwood et al., 1985). They claim that regression equations based purely on cadaver data should be viewed with caution and that techniques based to a lesser extent on cadaver data, i.e. geometric models, are preferable.

Yeadon and Challis (1994) predicted that the use of computer aided tomography (CAT) (Huang and Wu, 1976) and magnetic resonance imaging (MRI) (Martin et al., 1989) may circumvent the reliance on cadaver data or at least allow an evaluation of models using these data.

Geometric models

Yeadon (1990a) evaluated his geometric model against those of Jensen (1978) and Hatze (1980). The maximum errors of the total body mass estimates of these models were 2.3%, 1.8%, and 0.5% respectively. However Yeadon (1990a) stated that the accuracy with which the model estimates total body mass is not a good indicator of the accuracy of predicted segmental masses and inertias. Instead Yeadon (1990a) proposed that, since the model was developed for the calculation of personalised inertia parameters for input into a simulation model, the agreement of the simulation model with performance data would

give an indication of the accuracy of the model. Yeadon (1990b) performed this evaluation using a computer simulation of aerial movement; he found maximum deviations between simulation and film of 0.04 revolutions for somersault, 7° for tilt, and 0.12 revolutions for twist. The model of Hatze (1980) requires 242 measurements, taking over an hour of the subject's time, whereas the model of Yeadon (1990a) requires only 95 measurements, taking between 20 and 30 minutes.

4.7.2 Anthropometric measurements

Ninety-five anthropometric measurements were taken to be used as input to the inertia model of Yeadon (1990a). Measurements were taken using anthropometric callipers and a measuring tape (Figure 4.20). These comprised 34 lengths, 41 perimeters, 17 widths, and three depths (Appendix 9).

Figure 4.20 Anthropometric measurement of the subject.

The subject was weighed without shoes and the shoes were weighed separately in order to obtain inertia properties for the foot and shoe segment. Density values for individual segments were taken from Chandler et al. (1975) and allied with the measured volumes of the segments to calculate the inertia values. After initial estimation these values were adjusted in order that the total mass of the body exactly matched the measured value.

The inertia model of Yeadon (1990a) has 16 segments and for each segment the mass, location of the mass centre, principal moments of inertia about the mass centre, and distance between joint centres are calculated. The simulation model of triple jumping requires 11 segments, therefore the forearm and hand, and the head, chest, torso and pelvis were considered together using the Parallel Axis Theorem.

4.7.3 Determining rigid and wobbling element mass and inertia parameters

Determining mass parameters

In order to determine the mass of the rigid and wobbling elements, values for the percentage bone, muscle, and fat mass of individual limbs were taken from Clarys and Marfell-Jones (1986).

The ratios of the rigid and wobbling element masses were calculated from this data using a method adapted from Pain (1999). Since body fat percentages reported in literature are much higher than that of the subject in this study, excess fat could simply be re-distributed as muscle, or the muscle-to-bone ratio could be kept constant.

Table 4.4 Segment mass compositions (Clarys and Marfell-Jones, 1986)

	Thigh	Shank	Trunk
Mass of segment (kg)	7.78	2.14	37.36
Bone mass of segment (kg)	0.70	0.46	4.88
Fat mass of segment (kg)	3.32	0.61	12.2
% mass of bone	9.03	21.69	13.06
% mass of fat	42.63	28.78	32.65
% mass of muscle	48.34	49.52	54.28

Using the segmental masses and compositions from Table 4.4 it was possible to ascertain the relative fat percentage of the segment with respect to the whole body.

According to Clarys et al. (1984):
Percentage of body mass due to fat = 34.6%.
Percentage of body mass due to bone = 13.4%.

The subject's body fat percentage was assumed to be 8% since this has been shown to be typical of elite male jumpers (Houtkooper et al. 2007).

Re-distributing fat as muscle

Using the thigh as an example:

Mass of subject's thigh from inertia model (Yeadon, 1990a) = 9.743 kg.

Fat mass percentage of thigh from literature = $\frac{3.3161}{7.7785} \cdot 100 = 42.63\%$.

Ratio of segment fat to total fat from literature = $\frac{42.63}{34.6} = 1.23$.

Fat mass percentage of subject's thigh = $8 \cdot 1.23 = 9.86\%$.

Therefore percentage fat left to re-distribute as muscle = $42.63 - 9.86 = 32.77\%$.

Percentage mass of wobbling element = $9.86 + 48.34 + 32.77 = 90.97\%$.

Mass of rigid element = $\frac{9.03}{100} \cdot 9.743 = 0.88$ kg.

Mass of wobbling element = $\frac{90.97}{100} \cdot 9.743 = 8.86$ kg.

Maintaining muscle to bone ratio

Using the thigh as an example:

Percentage fat-free mass of subject's thigh = $100 - 9.86 = 90.14\%$.

Percentage of fat-free mass made up of bone = $\frac{9.03}{9.03 + 48.34} \cdot 90.14 = 14.19\%$.

Percentage of fat-free mass made up of muscle = $90.14 - 14.19 = 75.95\%$.

Percentage mass of wobbling element = $75.95 + 9.86 = 85.81\%$.

Mass of rigid element = $\frac{14.19}{100} \cdot 9.743 = 1.38$ kg.

Mass of wobbling element = $\frac{85.81}{100} \cdot 9.743 = 8.36$ kg.

Average value

The two methods described above were considered to yield an upper and lower limit for the masses of each segment, thus the input to the simulation model was taken as an average of the two:

Mass of rigid element = $\frac{0.88+1.38}{2} = 1.13$ kg.

Mass of wobbling element = $\frac{8.86+8.36}{2} = 8.61$ kg.

Determining inertia parameters

Having determined the mass and inertia parameters of the segment and calculated the masses of the wobbling and rigid elements (Table 4.5), inertia parameters of the wobbling and rigid elements could be calculated. It was assumed that the rigid elements were cylinders of uniform density, with knowledge of their length and mass their radii could be calculated using bone densities reported in the literature (Table 4.6).

Table 4.5 Subject data from inertia program (Yeadon, 1990a)

	Thigh
Segment length (m)	0.45
Rigid segment COM position (m)	0.23
COM position of segment from proximal joint (m)	0.19
MOI of whole segment (kg.m^2)	0.17
Mass of segment (kg)	9.74
Mass of rigid element (kg)	1.13
Mass of wobbling element (kg)	8.61

Table 4.6 Bone densities in different body segments

	Thigh	**Shank**	**Trunk**
Bone density (kg/m^3)	1218	1207.5	1100
	Clarys and Marfell-Jones (1986)		Dempster (1955)

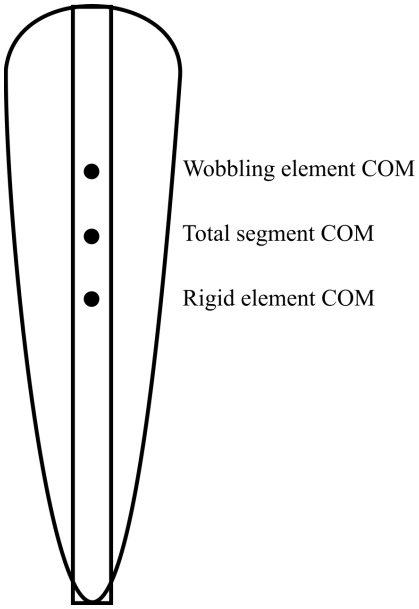

Figure 4.21 Diagram showing wobbling element, rigid element and total segment COMs.

Again the thigh is used as an example.

Using the equation for the volume of a cylinder: $v = \pi r^2 h$. (4.2)

The radius of the cylinder can be calculated: $\sqrt{\frac{1.13}{\pi \cdot 0.451 \cdot 1218}} = 0.0256$ m.

Since the cylinder is of uniform density, the distance of COM from proximal joint equals half the length:

$$\frac{L}{2} = \frac{0.451}{2} = 0.2255 \text{ m.}$$

Taking moments from the proximal joint, the COM position of the wobbling element can be determined:

$$M_{seg} g d_{seg} = M_{rig} g d_{rig} + M_{wob} g d_{wob}. \quad (4.3)$$

Rearranging equation 4.3:

$$\frac{M_{seg} \cdot d_{seg} - M_{rig} \cdot d_{rig}}{M_{wob}} = d_{wob}. \quad (4.4)$$

The radius of the wobbling element can then be calculated:

$$\frac{9.743 \cdot 0.191 - 1.131 \cdot 0.2255}{8.612} = 0.186 \text{ m.}$$

Using the equation for the moment of inertia (MOI) about the transverse axis of a cylinder of uniform density:

$$MOI = \frac{L^2 \cdot M}{12} + \frac{r^2 \cdot M}{4}. \quad (4.5)$$

The MOI of the rigid element was therefore:

$$\frac{0.451^2 \cdot 1.13}{12} + \frac{0.0256^2 \cdot 1.13}{4} = 0.019 \text{ kg} \cdot \text{m}^2.$$

The parallel axis theorem dictates: $I_o = I_g + Md^2$. (4.6)

With reference to Equation 4.6, the MOI of the whole segment is the sum of the MOIs of the wobbling (*wob*) and rigid (*rig*) elements (Figure 4.21):

$$I_{gseg} + M_{seg} d_{seg}^2 = I_{gwob} + M_{wob} d_{wob}^2 + I_{grig} + M_{rig} d_{rig}^2. \quad (4.7)$$

Equation 4.7 can be rearranged to obtain the MOI of the wobbling element (I_{gwob}):

$$I_{gseg} - I_{grig} + M_{seg} d_{seg}^2 - M_{wob} d_{wob}^2 - M_{rig} d_{rig}^2 = I_{gwob}. \quad (4.8)$$

The MOI of the wobbling element is therefore:

$$0.171 - 0.019 + (9.743 \cdot 0.191^2) - (8.612 \cdot 0.186^2) - (1.131 \cdot 0.2255^2) = 0.150 \text{ kg} \cdot \text{m}^2.$$

The same methods were used for the shank and trunk segments.

4.7.4 Literature on modelling muscular function

Muscle models in the literature can be broadly split into two sections: macroscopic (Hill, 1938); and microscopic (Huxley, 1957).

The sliding filament theory (Huxley, 1957) is a complicated model involving molecular interactions at a microscopic level and, as such, has limited application in whole-body simulation models of human movement. Therefore typically Hill-type models are employed (Alexander 1990, 1992; Pandy et al., 1990; van Soest et al., 1993; Wilson et al., 2006).

Force / velocity relationship in muscle

Hill (1938) produced a model of muscle function determining the effect of load on the speed of shortening, comprising what he termed the 'dynamic constants' of muscle:

- P, the isometric tension of the muscle;
- a, the shortening heat per centimetre of shortening;
- b, the increase of energy rate per gram decrease in load.

From this he produced a 'characteristic equation' for the speed of shortening, v, under a load P:

$$(P + a)(v + b) = constant.$$

He stated that this equation also applies to lengthening.

Yeadon et al. (2006) produced a four-parameter function that represented this force / velocity relationship as a joint torque / angular velocity relationship for use in simulation models of human movement.

Differential activation of muscle in eccentric contractions

It has been shown above that, in muscle fibres in vitro, tetanic muscle force decreases hyperbolically with increasing speed of shortening in the concentric phase to approach zero at the maximum rate of shortening (Hill, 1938). In the eccentric phase muscle force

quickly reaches 1.5 times the maximum isometric value with increasing speeds of lengthening and then plateaus for values above 0.5 times the maximum rate of shortening (Harry et al., 1990). However in maximum voluntary eccentric contractions in human skeletal muscle there is little increase in force above the isometric level (Westing et al., 1988). This indicates full activation cannot be achieved in maximum voluntary eccentric contractions. Westing et al. (1990) found that force was increased by 21-24% during eccentric contractions when electrical stimulation was applied to the muscle, where no corresponding increase was seen for isometric and concentric conditions. This led them to hypothesise that a neural mechanism inhibits activation levels during maximum voluntary eccentric contractions in order to reduce the risk of injury due to the extreme muscle tension that would otherwise be generated. Yeadon et al. (2006) attempted to mimic this 'differential activation' of muscle using a three-parameter function; this was used in addition to a four-parameter function modelling the theoretical tetanic torque / angular velocity relationship to produce a seven-parameter function. This seven-parameter function was then used to fit a line to two sets of experimental joint torque / angular velocity data giving unbiased root mean squared differences of 1.9% and 3.3% of the maximum torques achieved. They stated that failure to include differential activation considerations when modelling maximal movements will lead to errors in the estimation of joint torque in the eccentric phase and low-velocity concentric phase.

Force / length relationship in muscle

The force / length relationship of muscle in isolated fibres was initially thought to be of a polygonal form (Gordon et al., 1966) but more recently has been shown to approximate more closely to a bell-shaped pattern (Edman and Regianni, 1987). King et al. (2006) added two parameters to the seven-parameter function of Yeadon et al. (2006) describing the maximum torque as a quadratic function of contractile element angle. This produced a nine-parameter function defining the torque / angle / angular velocity relationship in maximum voluntary human joint movement which they employed in a torque-driven model of jumping for height. In future simulations it may be beneficial to model the torque / angle relationship as a bell-shaped pattern in line with the findings of Edman and Regianni (1987).

The nine-parameter fit of King et al., (2006) accounts for the contractile mechanisms involved in torque production around joints. In addition to these contractile mechanisms,

passive structures in the form of parallel and series elastic components also modify torques produced.

4.7.5 Torque / angle / angular velocity profiles

Once the torque / angle / angular velocity data had been measured using the isovelocity dynamometer and the maximum voluntary angular velocity tests, a seven-parameter function was fitted to the data. This was done using the method described by Yeadon et al. (2006). In the concentric phase of the action the curve is represented by the classic Hill hyperbola (Hill, 1938) (Appendix 10):

$$T = \frac{C}{(\omega_c + \omega)} - T_c \qquad (\text{if } \omega \geq 0), \tag{4.9}$$

where $T_c = \frac{T_0 \omega_c}{\omega_{\max}}$, $C = T_c(\omega_{\max} + \omega_c)$.

In the eccentric phase the relationship between T and ω is given by the rectangular hyperbola (Appendix 10):

$$T = \frac{E}{(\omega_e - \omega)} + T_{\max} \qquad (\text{if } \omega \leq 0), \tag{4.10}$$

where $\omega_e = \frac{(T_{\max} - T_0)}{kT_0} \frac{\omega_{\max} \omega_c}{(\omega_{\max} + \omega_c)}$, $E = -(T_{\max} - T_0)\omega_e$.

In addition to the four-parameter function defining the concentric and eccentric phase, there was a three-parameter function used to define the differential activation of the muscles during concentric and eccentric actions (Appendix 10):

$$\omega - \omega_1 = \frac{+ m(a - 0.5(a_{\min} + a_{\max}))}{(a_{\max} - a)(a - a_{\min})}. \tag{4.11}$$

Having defined the three-parameter and four-parameter functions (see Appendix 10 for symbol definitions) they were subsequently multiplied to give a seven-parameter function describing the maximum torque and differential activation. An additional two-parameter function describing the dependence of the torque production on joint angle variation was added to the seven-parameter function to produce a nine-parameter function (King et al.,

2006). This two parameter function differed from the quadratic function used by King et al. (2006). Instead it was represented by a bell curve (Edman and Regianni, 1987).

$$t_a = e^{-(\theta-\theta_{opt})^2/(2k_2^2)}, \tag{4.12}$$

where θ_{opt} is the angle at which maximum torque is produced and k_2 represents the width of the curve.

Fitting the nine-parameter function

For each joint and joint motion tested, a nine-parameter function was used to fit a surface to the experimental data using a simulated annealing algorithm. Experimental torque data were restricted to those obtained from the constant angular velocity period of the crank motion (Section 4.4.3). Contractile component angles were obtained using calculated SEC stiffnesses (Section 3.5.2), and it was assumed that during the period of isovelocity the contractile component velocity was equal to the velocity of the joint. Figure 4.22 shows a 3D surface fit to measured data for knee flexion, where the open circles represent measured joint torques. This surface describes how much torque can be produced at any combination of angle and angular velocity within the specified range. Appendix 11 gives values for each of the nine parameters for each of the joints and joint actions and associated absolute and percentage RMS error values.

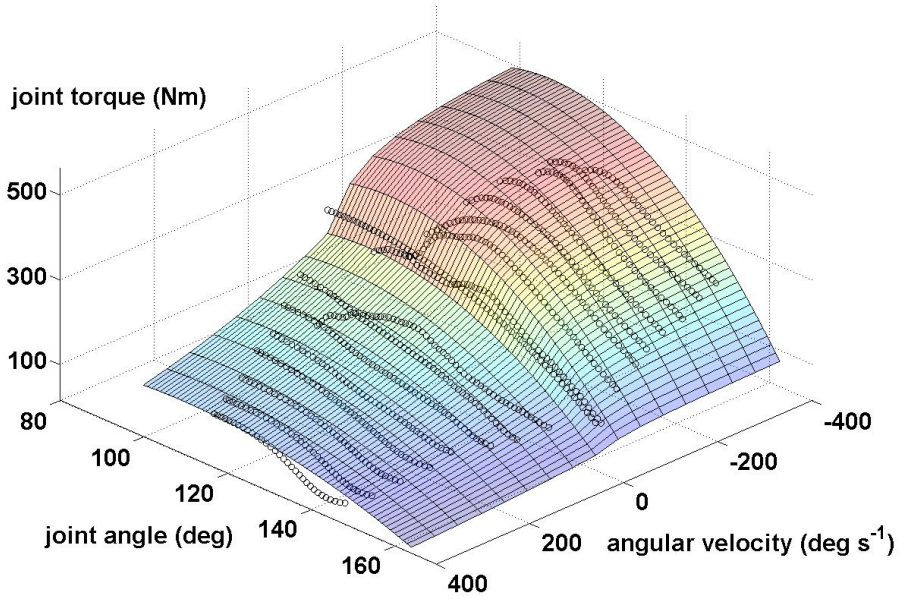

Figure 4.22 Example surface fit to torque data for knee flexion.

The metatarsophalangeal joints

Since no data were collected for the MTP joint, the torque parameters were estimated using the method described below.

With reference to Figure 4.23, imagine a person is balancing on 'tiptoes' causing a large reaction force towards the end of their toes. Taking moments about the point of force application, O, where B is the MTP joint and A the ankle joint:

$$T_A = d_A \cdot R\,. \tag{4.13}$$

It was estimated that d_B is one third of the length of d_A therefore:

$$T_B = T_A / 3\,. \tag{4.14}$$

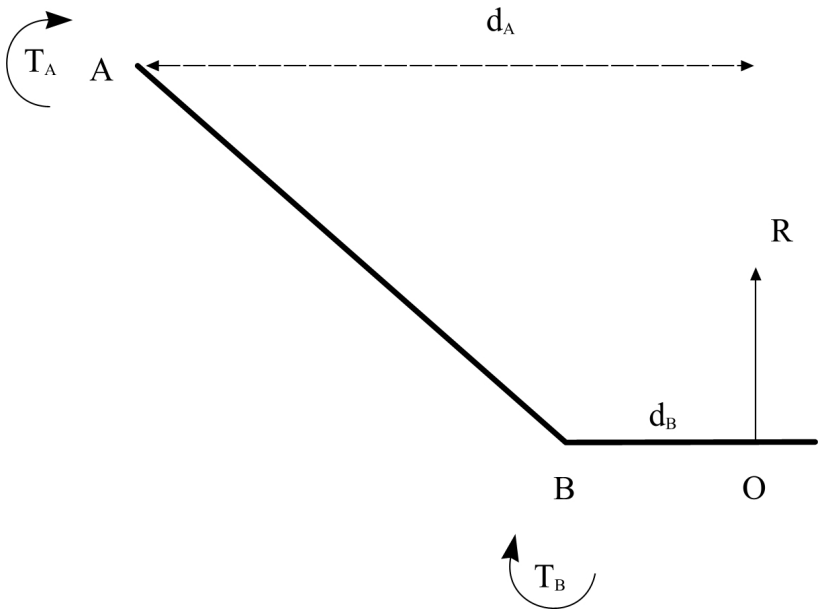

Figure 4.23 Diagram of MTP joint torque.

So the MTP joint was considered to have the same torque / angular velocity parameters as the ankle joint with one third of the maximum isometric torque. The torque / angle relationship from the ankle was not included in order to avoid projecting the same optimum angle onto the MTP joint; therefore a seven-parameter function was used for the MTP joint.

The shoulder joints

The subject was only able to complete three isometric trials in the shoulder flexion protocol due to injury. The torque / angle relationship and maximum isometric torque were therefore calculated from these trials and this was then combined with the seven-parameter torque / angular velocity relationship calculated from the shoulder extension protocol to form the nine-parameter fit.

Increased T_0 values

The nine-parameter fits were calculated with the intention of 90% of the measured values lying below the surface and 10% lying above the surface. It was decided not to calculate fits with 100% of values below the surface, since this made it difficult for the algorithm to accurately match the shape of the data. However since the subject had achieved all the measured values it was decided that the fits should subsequently be raised based on the number and position of the points above the surface. Therefore the average distances of the measured points above the surfaces were calculated, with isometric and dynamic points weighted such that each accounted for half of the calculated mean values. The T_0 and Tmax values were then increased accordingly by these average values, with all other measures remaining the same.

4.8 CHAPTER SUMMARY

In this chapter the collection of kinetic and kinematic performance data from a triple jump has been described. Considerations for the processing of kinematic data have been discussed and experimental and theoretical techniques for subject-specific parameter determination have been outlined. The next chapter will contain an evaluation of the computer simulation model of triple jumping.

CHAPTER 5

MODEL EVALUATION

5.1 CHAPTER OVERVIEW

In this the chapter the method for the determination of subject-specific viscoelastic parameters using an angle-driven model is described. Issues regarding matching angular momentum and limiting depression at the foot-ground interface are discussed. The results from the determination of subject-specific viscoelastic parameters are detailed. The methods for the evaluation of a torque-driven model are then described and results of this evaluation are reported.

5.2 EVALUATION OF JUMPING MODELS IN THE LITERATURE

This review will consider the methods of evaluation used in those studies involving analytical models of jumping reviewed in Section 3.2. Where a model is employed by more than one study, the method of evaluation used in the study where the model was introduced will be described.

5.2.1 Models of one-legged jumps

Alexander (1990, 1992), in his simple models of jumping, did not quantitatively evaluate his models as such; he did however discuss features of the simulation results with respect to those from the literature. Sorensen at al. (1999) matched their model to performance using GRFs measured from a long jump. The only quantitative measure of how closely the simulation matched performance data they offered was that the stance knee angle deviated maximally from the performance knee angle by 4°. Seyfarth et al. (1999) matched their simulation force data to measured force data. They provided parameter values from the model and the respective performance values which gave an indication of how well the model matched performance, without performing an evaluation per se. Seyfarth et al. (2000) also did not provide an explicit evaluation of their model, but they did provide

experimental force data for comparison with simulated force data, and stated that the angle of attack at touchdown agreed with experimental observations within a range of 5°. They stated that the model did not reproduce the magnitude of the first GRF peak and, as such, the model's jumps were shorter (-9%) and had a flatter take-off angle (-7°) than experimental data. These are the only quantitative attempts at evaluation that they made. Seyfarth at al. (online) used the results from the best of 30 long jumps (6.90 m) in order to compare the results of their optimised model to actual performance. The distance jumped by the model (5.72 m) was quite considerably less than this best performance, so comparisons may not necessarily have been as valid as with a jump of a similar distance. Linthorne and Kemble (1998) in their adaptation of the model of Alexander (1990) stated that the model accurately predicted the differences in optimum take-off technique between males and females, and the changes in jump performance as an athlete uses a faster approach. However they made no attempt to quantitatively evaluate their results. Ridka-Drdacka (1986) did not provide a quantitative evaluation of their model. Ranges of input parameters were reported but their origin was not specified. Some mention was made of estimating the influence of some of the simplifications of their model using experimental measures but there was only a qualitative description of these effects. Hatze (1981) showed experimental and theoretical GRFs which appeared to show a very close match, stating that the good agreement between theoretical and experimental results was apparent. However he did not provide any quantitative measure of this agreement, or mention how well the model matched performance data in any other way. Chow and Hay (2005) used kinematic and kinetic data from a long jump from the literature in order to calculate a 'reference jump' which best matched this data. They did not provide a quantitative evaluation of the jump; however they did give values for the parameters used in order to produce the reference jump, alongside those from the literature. Wilson et al. (2006) and King et al. (2006) explicitly evaluated their subject-specific models against a performance by that subject. Wilson et al. (2006) used a kinematically-driven model to determine viscoelastic parameters, using a six-component objective function (Section 3.2.1) to evaluate how closely the model matched performance data in a jump for height, and a jump for distance. They found that parameters derived from either one of the types of jump did not reproduce the performance well in the other type of jump. They therefore produced a common set of parameters for a jump for height and a jump for distance which led to a mean difference between simulation and performance of 8% (made up of 7% and 10%)

over the two simulations. King et al. (2006) also used a six-component objective function (Section 3.2.1) to determine how closely a torque-driven model matched performance data, achieving a difference of 6.6%.

5.2.2 Models of two-legged jumps

Pandy et al. (1990) made some mention of how well their musculotendon model matched experimental data; providing graphs and mentioning that the model's torque / angle curve was offset by up to 20° from experimental data. They stated that their jumping model qualitatively matched experimental results and provided a quantitative comparison of ground contact time, jump height, peak GRF, and rotation of the trunk with respect to data from the literature. Anderson and Pandy (1999) provided a quantitative comparison of model and experiment, as their model was based on subject-specific data. They compared peak GRFs, peak vertical acceleration of the body, vertical velocity of the COM at take-off, and jump height, noting that they were all in the range of those achieved by the subjects in their study. They did state however that the ground contact time in the model was considerably shorter than the average of their subjects. Van Soest et al. (1993) evaluated their model against experimental data. They stated that it corresponds well qualitatively with the proximo-distal sequence of muscle activations observed in vertical jumping. They compared joint angular velocity time histories and joint moments with experimental data graphically. They also quantified a number of differences in: work done at each joint; maximal jump height; and vertical velocity at take-off. Overall they acknowledged a few areas of concern, but stated that the degree of correspondence between experiment and simulation was highly encouraging. Selbie and Caldwell (1996) compared the COM and joint kinematics of their model to experimental results from the literature. They stated that several model COM kinematics are within the range of those seen in actual human jumps and that the model joint ranges of motion also compared well with experimental results. They also stated that the segmental patterns and COM displacement and velocity patterns resembled those found in the literature. Overall they claimed that their model captured many of the important characteristics of human jumping. Dapena (1999) made no mention of any sort of evaluation of his model, either quantitative or qualitative, in what was only a very brief paper. Ashby and Delp (2006) whose model's anthropometric and mass / inertia characteristic were taken from subjects who performed

standing long jumps, included a table comparing kinematic results at take-off between their simulation and these experimental results in jumps with and without restricted arms. They found that the experimental jump distances were 9-12 cm further than the simulated ones, attributing this difference mainly to a lack of toe segment in the model. They stated that the COM velocities at take-off were within 3% of experimental results in both arm conditions.

5.2.3 Summary of literature on the evaluation of models

The reviewed studies displayed various levels of evaluation; these ranged from those that either did not perform any evaluation, or only qualitatively compared their models to data from the literature (Ridka-Drdacka, 1986; Alexander, 1990, 1992; Dapena, 1999; Linthorne and Kemble, 1998), through those that performed some quantitative comparison between their models and performance data (Hatze, 1981; Pandy et al, 1990, Selbie and Caldwell, 1996, Seyfarth et al., 1999, 2000, online) to those that evaluated their partially subject-specific models against various aspects of performance data (van Soest et al., 1993, Anderson and Pandy (1999); Ashby and Delp, 2006). However, only Wilson et al. (2006) and King et al. (2006) provided an explicit quantitative evaluation of their subject-specific models against performance data. In order to have confidence in the results of optimisations of technique using simulation models, it is essential that an evaluation is first performed. Furthermore subject-specificity in models allows a direct evaluation of the model against performance data from that subject, in order to ensure that the model is an accurate representation of the system it is attempting to simulate.

5.3 LITERATURE ON OPTIMISATION ALGORITHMS

Van Soest and Casius (2003) evaluated the performance of four different algorithms in solving ‘hard’ optimisations problems. They defined these problems as sharing the following characteristics: (1) the objective function typically has many local optima and is non-smooth or even discontinuous; (2) the objective function is available in implicit form only, necessitating time consuming simulations be performed for every evaluation of the objective function; and (3) even for relatively simple models the dimensions of the optimisation parameter space cannot be kept very low.

The algorithms they evaluated were:

- Downhill Simplex Algorithm (DS);
- Sequential Quadratic Programming (SQP);
- Genetic Algorithm (GA);
- Simulated Annealing Algorithm (SAA).

They evaluated each algorithm in five separate problems for a range of starting values. Two of these problems were musculoskeletal performance optimisation problems which are of particular relevance to this study. They found that all algorithms managed to converge to a reasonable optimum in a vertical jumping problem involving six parameters, however the DS and SQP performed poorly in a higher-dimensional sprint cycling problem with 16 parameters, which were increased to 32 parameters by including initial conditions. GA typically converged on values close to the global optimum and SAA did not fully converge due to the initial temperature being too high to do so within the permitted number of function evaluations. However results indicated that it had not been trapped in a local optimum; this suggested that it may have achieved results closer to the global optimum with a lower initial temperature or more function evaluations. Van Soest and Casius (2003) concluded that it is essential that the initial temperature is tuned to the problem at hand when using SAA. These results suggest that both SAA and GA are capable of finding global optima in hard optimisation problems; however GA was the most easily parallelised of the algorithms studied which allowed a considerable reduction in processing time.

5.3.1 Simulated annealing algorithms

Simulated annealing algorithms (Kirkpatrick et al., 1983) are based on an analogy with a physical property: while at high temperatures the molecules of a liquid metal move freely, if the temperature of the liquid is slowly decreased the thermal mobility of the liquid is lost and they form a pure crystal which also corresponds to a state of minimum energy (Locatelli et al., 2000). If the temperature is decreased too quickly the liquid metal ends up in a polycrystalline or amorphous state with a high energy and not in a pure crystal. Simulated annealing algorithms were developed in order to find solutions for

combinatorial optimisation problems and the approach has later been extended to continuous global optimisation problems (Locatelli, 2000). Simulated annealing algorithms randomly generate a candidate point at each iteration and, through a random mechanism controlled by a parameter known as temperature, they decide whether to move the candidate point or to stay in the current one at the next iteration (Locatelli, 2000). Corana et al., (1987) found that simulated annealing can provide very high reliability in the minimisation of multimodal functions but that this comes at a high computational cost which increases linearly with the number of dimensions of the problem.

5.3.2 Genetic algorithms

Genetic algorithms (Holland, 1975) are models of machine learning that derive their mechanisms from the Darwinian principle of 'survival of the fittest' (Yang et al., 1998). An initial population of size *n*, representing a generation, is created by randomly selecting parameters within the parameter space. Each parameter set represents the individual's chromosomes (Yang et al., 1998). Each individual is assigned a fitness based on an objective function. Three operations then occur in order to create the next generation: (1) selection; (2) crossover; and (3) mutation. Fit individuals are selected for mating while weak individuals die off (Yang et al., 1998). Mated parents create a child with a chromosome set that is some mix of the parent's chromosomes. This process is continued until an entirely new population of size *n* is generated. The fitness of this generation is determined and the process is repeated. Successive generations are created until a global optimum is found.

5.4 DETERMINATION OF VISCOELASTIC PARAMETERS

Subject-specific viscoelastic parameters were determined using the method outlined by Wilson et al. (2006) (Section 3.2.1). The simulation model of triple jumping was angle-driven using performance data. Stiffness and damping characteristics, and initial conditions of the model were varied using a simulated annealing algorithm (Kirkpatrick et al., 1983) in order to minimise the difference between simulation and performance, since it has been shown to converge to a global optimum in 'hard' optimisation problems such as the one considered here (van Soest and Casius, 2003) (Section 5.3). In order to obtain a

common set of viscoelastic parameters that was robust to changes between the three contact phases of the triple jump, these three phases were simulated consecutively with the same set of viscoelastic parameters and a total average difference calculated. Therefore the same 18 stiffness and damping parameters comprising: three horizontal and three vertical stiffness values at the feet; three horizontal and three vertical damping values at the feet; and one stiffness and one damping value at each of the torso, thigh, and shank wobbling masses (Section 3.5.4), were evaluated for each phase. In addition to these viscoelastic values, three kinematic parameters specific to each phase (Section 5.4.2) were included, making a total of 21 parameters per simulation, and 27 parameters included in the optimisation process in total.

5.4.1 Objective function

Each simulation was given a score comprising four components adapted from the protocol of Wilson et al. (2006):

- S_1 - Percentage difference in horizontal velocity of COM at take-off;
- S_2 - Percentage difference in vertical velocity of COM at take-off;
- S_3 - Overall RMS difference in trunk orientation in degrees in the contact and airborne phases;
- S_4 - Percentage absolute difference in time of contact.

The score was calculated by taking the overall RMS of these components in order to reduce the chance of any one component being neglected during the optimisation process. Components were equally weighted, where one degree was considered comparable to a 1% difference in other measures (Wilson et al., 2006):

$$F = \sqrt{\left(\frac{S_1^{\,2} + S_2^{\,2} + S_3^{\,2} + S_4^{\,2}}{4} \right)}. \qquad (5.1)$$

The overall difference for the simulation was therefore the average of the scores for the three phases:

$$\overline{F} = \frac{F_1 + F_2 + F_3}{3}. \qquad (5.2)$$

Penalties

Penalties were implemented to limit foot movement to 2 cm vertically, and 2 cm horizontally, relative to the initial horizontal position of the point on the foot when it first contacted the ground. Wobbling mass movement was also limited to a maximum of 4.5 cm at the shank, 7 cm at the thigh, and 10 cm at the trunk (Section 4.3.1).

Changes to the objective function of Wilson et al. (2006)

One change to the protocol of Wilson et al. (2006) (Section 3.2.1) was to match the whole-body orientation into flight, rather than match whole-body angular momentum at take-off (Component S_3). This was because it was found that the orientation of the model in the air was sensitive to movement of the wobbling masses. The wobbling masses accounted for the majority of the mass of the limbs and torso, and hence their angular momenta accounted for the majority of the whole-body angular momentum. Thus it was impossible to prescribe an angular momentum of the entire system at take-off that would lead to a particular orientation at a point later in flight, since, although the joint angles were prescribed, the wobbling masses were free to move independently.

Another change was the decision not to attempt to match horizontal or vertical GRFs, resulting in a four-component and not a six-component objective function. Initial optimisations where foot depression was not penalised showed excessive vertical depression at the foot (> 4cm). It was hypothesised that this was due to the pin joints in the model not accounting for compressions that occur in the joints of the stance leg and the spine. Thus the model required unrealistically low stiffness and damping parameters in order to match force traces. Table 5.1 and Figure 5.1 show the scores for the simulation and the associated GRFs respectively, and Appendix 12 contains the optimised stiffness and damping parameters.

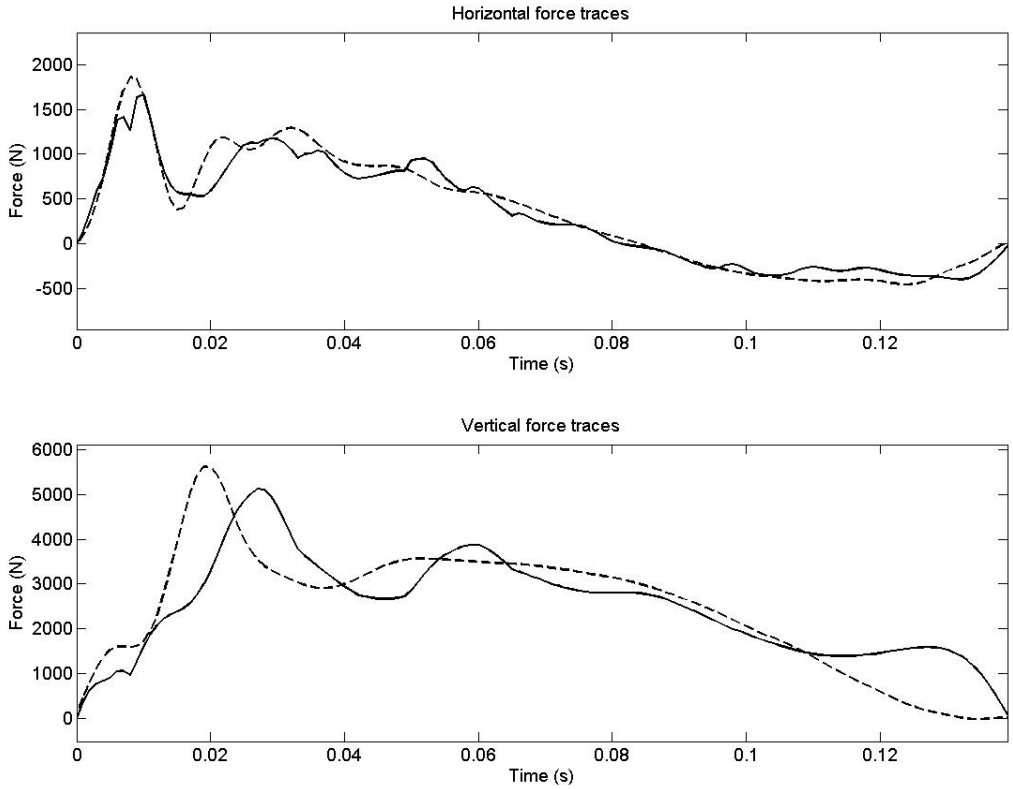

Figure 5.1 Horizontal and vertical GRFs for a simulation of the hop phase with no penalties for foot depression (solid line) compared to performance (dashed line).

Table 5.1 Score for simulation of the hop phase with no penalties for foot depression

Score Component	Value
RMS Vertical Force (%)	7.6
RMS Horizontal Force (%)	14.6
Horizontal Velocity (%)	1.4
Vertical Velocity (%)	0.0
RMS Orientation (°)	1.0
Contact Time (%)	1.1
Overall Score	7.2

When the springs representing the foot-ground interface depressed by a large amount (> 4 cm) it led to a delayed impact force peak and an unrealistic time history of the path of the centre of pressure along the foot. This in turn led to excessively high torques at the MTP joint when the springs recoiled towards the end of the ground contact, since the toe was the only point in contact with the ground at this time. The torque-driven model would not be

able to reproduce these torques at the MTP joint. Therefore it was decided that foot depression should be limited to a maximum of 2 cm, since this was slightly greater than the maximum level of depression observed in the performance data. This depression was measured as the distance moved vertically by the ankle joint centre after the heel had contacted the ground. Limiting the depression of the foot led to the overall modelled system being stiffer and more highly damped than the actual system. It was decided that, since the main function of the model was to optimise performance, it was most important that the viscoelastic parameters allowed the torque-driven model to accurately match the kinematics of the performance. Hence force data were removed from the objective function. Due to this, the simulation force data did not match the performance force data as closely, however impulses and other measures were well matched (Table 5.2 and Figure 5.2).

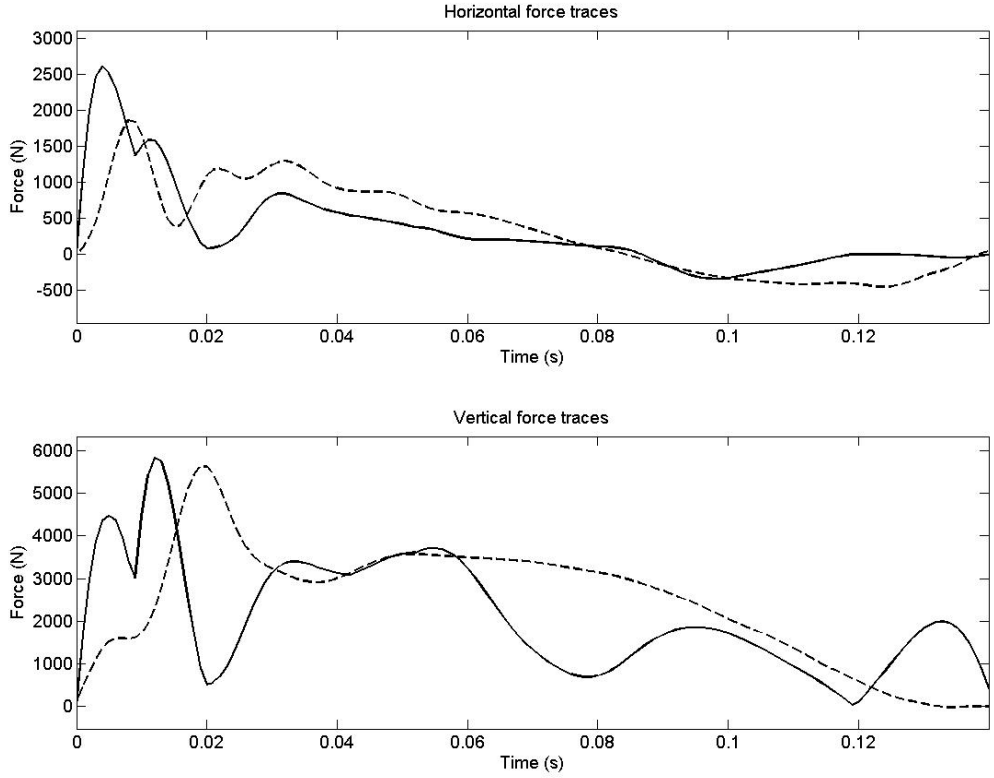

Figure 5.2 Horizontal and vertical GRFs for a simulation of the hop phase with depression of the foot limited to 2 cm (solid line) compared to performance (dashed line).

5.4.2 Initial conditions

In addition to the angles and angular velocities driving the simulation, the other initial conditions required to define the system were the horizontal and vertical velocity of the

COM, and the angular velocity of the torso segment, which determined the angular momentum of the whole body.

Errors in COM velocities were calculated (see Section 4.5.2) in order to determine the levels by which these initial conditions were allowed to vary from the measured values. The initial horizontal and vertical velocities were allowed to vary by ± 0.05 m/s. The angular velocity of the trunk was allowed to vary by ± 1 rad/s to account for errors in the kinematic data (King et al., 2006) (Section 4.3.1).

5.4.3 Optimisation results

Simulation results indicated that these viscoelastic parameters led to accurate model kinematics and were therefore acceptable for use in further simulations of the triple jump (Table 5.2). Each phase was well matched, with a combined average difference of 1.8%. Optimised parameters obtained from all three phases of the triple jump are shown in Appendix 13.

Table 5.2 Individual and combined scores for angle-driven simulations of all three phases of the triple jump

Component	Hop	Step	Jump	Combined
Horizontal Velocity (%)	2.1	0.1	2.2	1.6
Vertical Velocity (%)	1.6	0.4	0.5	0.8
RMS Orientation (Degs)	2.0	1.5	1.7	1.7
Contact Time (%)	2.8	1.2	4.0	2.7
Overall Difference (%)	2.2	1.0	2.4	1.8

5.5 EVALUATION OF THE TORQUE-DRIVEN MODEL

5.5.1 Optimisation method

Having obtained the viscoelastic parameters from the angle-driven model, these parameters could then be used in an evaluation of the torque-driven model. The model was driven by flexion-extension torques at all joints except the elbows, which were angle-driven. A

genetic algorithm (Carroll, 1996) (Section 5.3) was employed to minimise an objective function by varying 77 torque generator activation timings in addition to seven kinematic initial conditions (Section 5.5.4), making a total of 84 parameters per phase. A genetic algorithm was used in preference to the simulated annealing algorithm used in the optimisation of viscoelastic parameters, since it was found that the simulated annealing algorithm took much longer to converge on an optimal value than the genetic algorithm with such a large number of parameters, despite the fact that the genetic algorithm was not parallelised (van Soest and Casius, 2003). The genetic algorithm was run with a population of 200 using input parameters described by Carroll (1996). This typically led to convergence within 150 generations. Bounds on the torque generator activation timings were estimated using torques from the kinematically driven simulation and from observation of the movement in order to estimate which torque generators were active and when. If the bounds were subsequently hit in the optimisations then they were increased, unless they were at a limit of activation level or ramp time (Section 3.5.2).

5.5.2 Determining the objective function

The objective function used to evaluate the torque-driven model was similar to that used in the angle-driven model, with some alterations. Body configuration was added to the objective function, this comprised the RMS difference in angles between simulation and performance in those joints that were being matched. RMS configuration and orientation were only matched during ground contact, not into the airborne phase as with the angle-driven model. This would have necessitated a considerable increase in the number of torque generator activation timings in order to match the joint angles.

Angular momentum

Since the torque-driven model only simulated the contact phases, and not the airborne phases, it was necessary to calculate whether it would be possible for it to achieve the requisite landing orientation and configuration for the subsequent phase.

In order that angular momentum could be included in the objective function on a comparable basis to the other measures, the error in landing orientation associated with the simulation angular momentum value at take-off was calculated. Using a percentage

measure for the angular momentum value itself would have penalised phases with low angular momenta disproportionately.

So as to ascertain the effect of angular momentum on the orientation of the body during flight, an angle-driven simulation of each airborne phase was run using performance data, with the whole-body angular momentum set to zero. From this the average MOI of the whole body ($\bar{I}$) was calculated by summing the MOIs at each timestep:

$$\bar{I} = \frac{\sum_{i=0}^{n} I(t_i)}{n}, \tag{5.3}$$

where n is the number of data points, and $I(t_i)$ is the MOI at time t_i.

Since the angular momentum was zero, the change in orientation angle solely due to changes in body configuration measured from performance data ($\Delta\theta_{cfperf}$) could then easily be calculated:

$$\Delta\theta_{cfperf} = \theta_{final} - \theta_{init}, \tag{5.4}$$

where θ_{init} and θ_{final} are the orientation angles at the times representing touchdown and take-off from performance data respectively.

In simulations of ground contact, the theoretical time of flight of the model (Δt_{sim}) was calculated using equations of motion. This was done using the simulation COM take-off height (h_{tosim}), and vertical take-off velocity (v_{tosim}), and the performance COM height (h_{tdperf}) at the touchdown of the subsequent phase:

$$\Delta t_{sim} = \frac{-v_{tosim} - \sqrt{v_{tosim}^2 + 2 \cdot g \cdot (h_{tdperf} - h_{tosim})}}{g}, \tag{5.5}$$

It was assumed that the model would undergo the same configuration changes irrespective of flight time, and therefore the orientation change due to these configuration changes would be the same regardless of variations in flight time.

Using these values the simulation landing orientation (θ_{tdsim}) was calculated in the following fashion:

$$\theta_{tdsim} = \theta_{tosim} + \Delta\theta_{cfperf} + ((H_{sim} \cdot \Delta t_{sim}) / \bar{I}), \quad (5.6)$$

where H_{sim} is the whole-body angular momentum of the simulation at take-off, and θ_{tosim} is the orientation of the simulation at take-off.

The absolute difference between the simulation landing orientation and the performance landing orientation (Equation 5.7) was the component included in the objective function (Equation 5.8):

$$S_6 = \left|\theta_{tdsim} - \theta_{tdperf}\right|, \quad (5.7)$$

where S_6 is the score component, and θ_{tdperf} is the performance orientation.

Objective function

The objective function contained the following components:

- S_1 - Percentage difference in horizontal velocity of COM at take-off;
- S_2 - Percentage difference in vertical velocity of COM at take-off;
- S_3 - Overall RMS difference in trunk orientation in degrees during ground contact;
- S_4 - Overall RMS difference in whole-body configuration in degrees during ground contact;
- S_5 - Percentage absolute difference in time of contact;
- S_6 - Absolute difference in orientation at touchdown of the subsequent phase in degrees (Equation 5.7).

As with the angle-driven model the score was calculated by taking the overall RMS of these components, with each one equally weighted.

The score was calculated as follows:

$$F = \sqrt{\left(\frac{S_1^2 + S_2^2 + S_3^2 + S_4^2 + S_5^2 + S_6^2}{6}\right)}. \quad (5.8)$$

Penalties

Where necessary, the model incurred penalties if the joint angles exceeded what were considered normal ranges of motion (Luttgens and Hamilton, 1997) at the equivalent of one percentage point per degree. These limits were only in place if the model was likely to violate them, this was not considered to be the case at the shoulders. Also where passive non-ligament torques were already present (Section 3.5.2), these penalties were not considered necessary. The ball joint was assumed only to flex and not to extend with respect to the neutral position, due to the structure of the shoe prohibiting extension. Penalties were therefore implemented in extension at the knee, ankle, and ball joints (Table 5.3).

Table 5.3 Limits on the range of motion of the joints of the leg

Joint	Flexion Limit (Degs)	Extension Limit (Degs)
Knee	n/a	0
Ankle	n/a	85
Ball	n/a	0

5.5.3 Activation profiles

The levels of torques driving the model were determined by the activation timings of the various torque generators (Section 3.5.2). These profiles were either ramp up, ramp up-ramp down, or ramp down-ramp up and were consistent across the three phases. The ankle and ball joints in the free leg had fixed activation profiles since they were only expected to have a negligible influence on the performance of the model, so were not included in the matching process. The ball joint of the stance leg was assumed only to extend, so did not have a flexion profile included in the optimisation process. The elbows were also not included since they were angle-driven. Levels of activation at touchdown were limited to 0.5 times maximum in all joints except the free hip flexor, these were similar to levels reported in the literature (Perttunen et al., 2000). The activation level of the free hip was allowed to take any value up to maximum, since the limb did not have to undergo an impact and the flexion movement could be initiated some time prior to impact. The type of profile of each torque generator was estimated using joint torques calculated using inverse

dynamics from the angle-driven model, and muscle activations reported in the literature for triple jumping (Perttunen et al., 2000).

Muscular co-contraction

The ankle and knee joints of the leg in contact with the ground were assumed to have some level of co-contraction at the start of the simulation, as has been shown in drop jumping and drop landing (Viitasalo, 1998; Minetti, 1998; Kellis et al., 2003; Yeadon et al., accepted for publication). And hence flexors in these joints were assigned ramp down-ramp up profiles. In drop jumping angular velocities around these joints are small immediately prior to touchdown, allowing simulations to assume that net joint torques are zero (Yeadon et al., accepted for publication). However in this study joint angular velocities were non-zero at the instant of impact, therefore it was not assumed that net joint torques were zero. Initial activations at the ankle and knee of the stance leg were therefore forced to vary between 0.3-0.5.

Ramp up-ramp down, or ramp down-ramp up profiles had the ability to only ramp up, or only ramp down, respectively by delaying the initiation of the second quintic function (Section 3.5.2).

Ramp types for each joint action are given in Table 5.4 and are decribed in terms of the stance and free legs, and the right and left shoulders.

Table 5.4 Activation profile types for each joint action

Joint Action	Activation profile
Stance Hip Extension	Ramp up – Ramp down
Free Hip Extension	Ramp up
Stance Knee Extension	Ramp up – Ramp down
Free Knee Extension	Ramp up – Ramp down
Stance Ankle Plantar Flexion	Ramp up – Ramp down
Free Ankle Plantar Flexion	Fixed
Stance Ball Extension	Ramp up
Free Ball Extension	Fixed

Right Shoulder Flexion	Ramp up – Ramp down
Left Shoulder Flexion	Ramp up – Ramp down
Stance Hip Flexion	Ramp up
Free Hip Flexion	Ramp up – Ramp down
Stance Knee Flexion	Ramp down – Ramp up
Free Knee Flexion	Ramp up
Stance Ankle Dorsi Flexion	Ramp down
Free Ankle Dorsi Flexion	Fixed
Stance Ball Flexion	Fixed
Free Ball Flexion	Fixed
Right Shoulder Extension	Ramp up
Left Shoulder Extension	Ramp up

5.5.4 Initial conditions

As in the angle-driven model initial horizontal and vertical COM velocities and torso angular velocities were varied. The torque-driven model was also allowed some freedom in the initial joint angles. It is inevitable that discrepancies exist between calculated and actual joint centre positions. Likely reasons for this include: inherent error in the measurement system; skin motion artefacts; and joint centres calculated from accurate marker positions not representing joint centre locations throughout measured angle ranges.

Measured marker locations using Vicon motion analysis systems have been shown to be accurate to within 2 mm of actual locations (Richards, 1999), therefore it was assumed measured marker positions were representative of the actual motion of the markers.

With respect to the skin motion artefacts, Reinschmidt (1997b) showed mean errors of 2° due to soft tissue motion in knee flexion / extension angles during walking calculated from skin markers (Section 4.3.1). Therefore it was decided each initial angle in the stance leg should be allowed to vary by a minimum of $\pm 2°$ due to this.

Marker positions may not have represented joint centre locations due to various factors. Where the model represents joints as rigid and pin-linked, some joints, especially distal

joints in the limb in contact with the ground, will actually undergo deformation to the joint structures and changes in joint contact area and location due to changes in joint angle and loading (Kimizuka et al., 1980; Nisell et al., 1986; Millington et al. 2007b). This could lead to changes in the point of application of forces with respect to the joint centres of rotation. Nisell at al. (1986) found that the centre of the tibio-femoral contact area shifted by more than 20 mm when the knee was extended from 120° to straight. At the ankle Millington et al. (2007a) found a change in talo-tibia contact area between ankle plantar flexion ($4.39 \pm 1.41\,cm^2$) and dorsiflexion ($7.34 \pm 1.69\,cm^2$) and Kimizuka et al. (1980) found an increase in contact area with increasing load (2.29 cm^2 at 200 N to 4.83 cm^2 at 1500 N), both of which would likely result in a shift in the notional point of application of force with respect to the centre of rotation. Since the point of application of force in the model is always through the centre of rotation of the joint, this centre of rotation would have to be moved in order to account for this effect. A shift of 20 mm would account for a change in angle of $> 5°$ at the knee. This, in addition to the skin motion mentioned above, introduced a level of error in every calculated joint angle, irrespective of the joint architecture, especially in the stance leg.

In an attempt to account for these effects in simulations, initial joint angles in the stance leg were allowed to vary. The ankle was allowed to vary by $\pm 3°$, the knee by $\pm 5°$, and the hip and orientation angles by $\pm 2°$. With the exception of these four, the initial angular kinematics were taken from the performance. As with the angle-driven simulations the initial COM horizontal and vertical velocities were allowed to vary by ± 0.05 m/s and the angular velocity of the trunk by ± 1 rad/s (Section 5.4.2).

5.5.5 Evaluation results

Each of the three phases matched well with performance data, with overall differences of 3.8%, 2.7% and 3.1% for the hop, step, and jump phases respectively (Table 5.5). Appendix 14 shows the optimised torque generator activation timings associated with each phase.

Each phase distance (d_{phase}) comprises three components (Figure 5.3): The take-off distance is the horizontal distance from the toe of the stance leg to the COM at take-off

($d_{take\text{-}off}$); the flight phase is the distance travelled by the COM whilst the athlete is airborne; and the landing distance is the horizontal distance from the COM to the toe of the stance leg at touchdown, or in the case of the jump, the most posterior of the two heels at landing ($d_{landing}$). Table 5.6 gives a breakdown of the component distances for each phase. The step had the largest take-off and landing distances. This was a function of the low COM at take-off which led to a shorter flight distance than the other two phases.

Table 5.5 Differences between performance and simulation of individual phases

Score Component	Hop	Step	Jump
RMS Configuration (Degs)	7.26	6.48	7.03
RMS Orientation (Degs)	1.77	1.19	1.08
Contact Time (%)	0.14	0.16	2.45
Horizontal Velocity (%)	4.66	0.27	0.07
Vertical Velocity (%)	2.55	0.37	0.46
Landing orientation (Degs)	1.78	1.16	0.80
Overall Score (%)	3.81	2.74	3.10

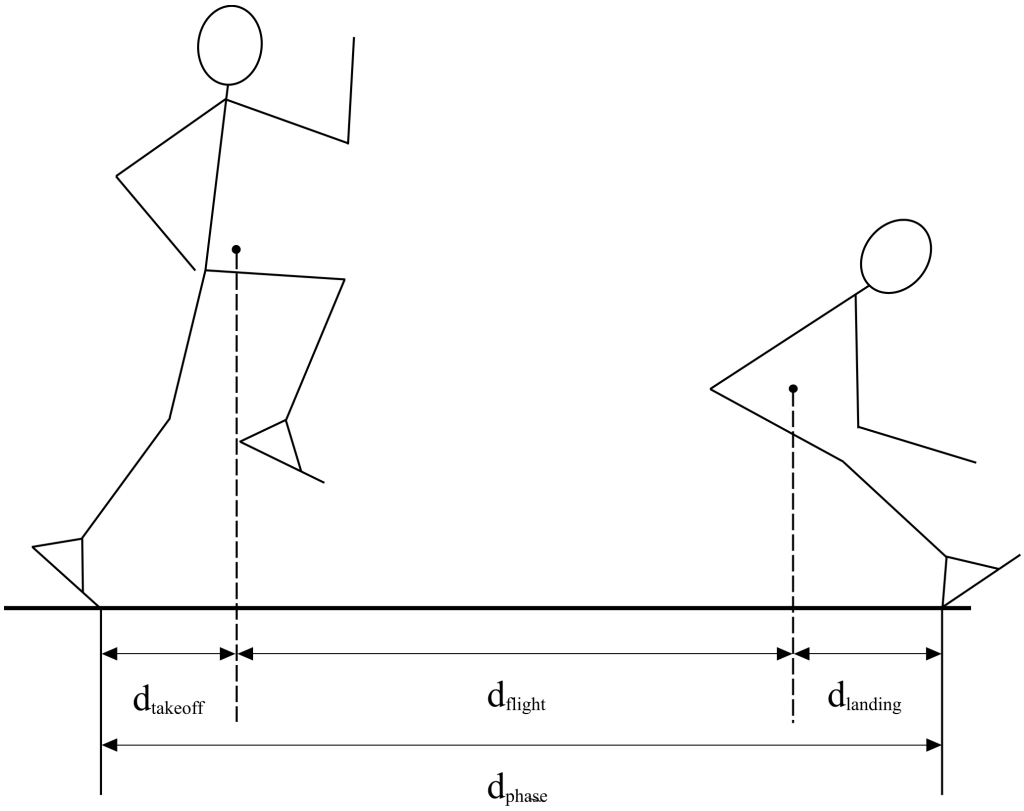

Figure 5.3 The three component distances for an individual phase.

Table 5.6 Component distances of individual phases

Phase	Take-off Distance (m)	Flight Distance (m)	Landing Distance (m)	Total Distance (m)
Hop	0.43	3.21	0.65	4.29
Step	0.58	2.59	0.72	3.89
Jump	0.47	3.37	0.44	4.28

5.5.6 Joint angles

Figures 5.4-5.6 show visual representations of the performance and matched simulations for each of the three phases. Individual joint angle RMS differences between performance and matched simulations are shown in Table 5.7 for each of the joints considered in the matching process (Section 5.5.3). Figures 5.7-5.9 show comparisons of individual joint angles between performance and matched simulations. There was no clear trend for simulation joint angles to match performance joint angles more closely at one joint than another. This indicates that no individual torque generator was consistently incapable of providing the requisite torques for the simulation to match performance data. The overall close agreement between performance and simulation joint angles indicates that the simulation torque generators were consistently strong enough to match performance torques.

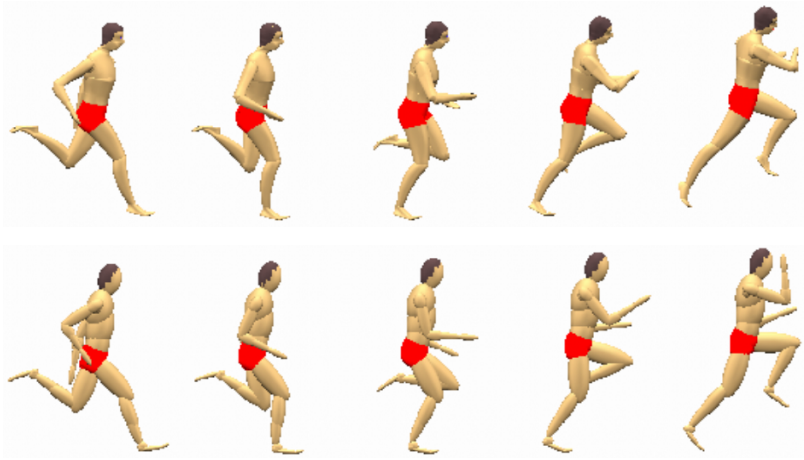

Figure 5.4 Performance (top) and matched simulation (bottom) of the hop phase.

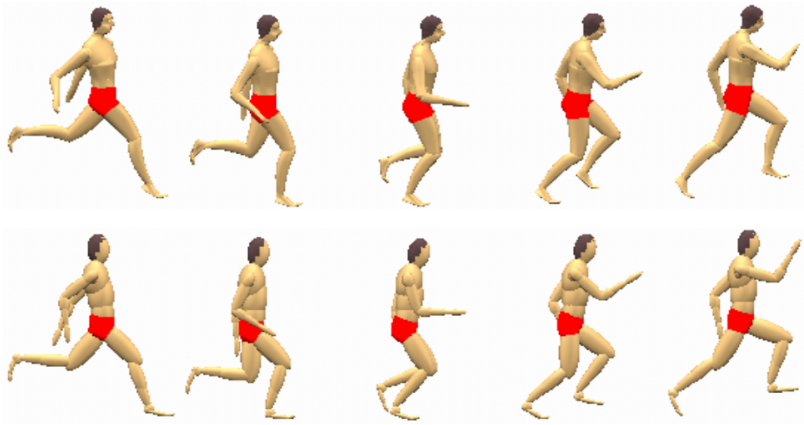

Figure 5.5 Performance (top) and matched simulation (bottom) of the step phase.

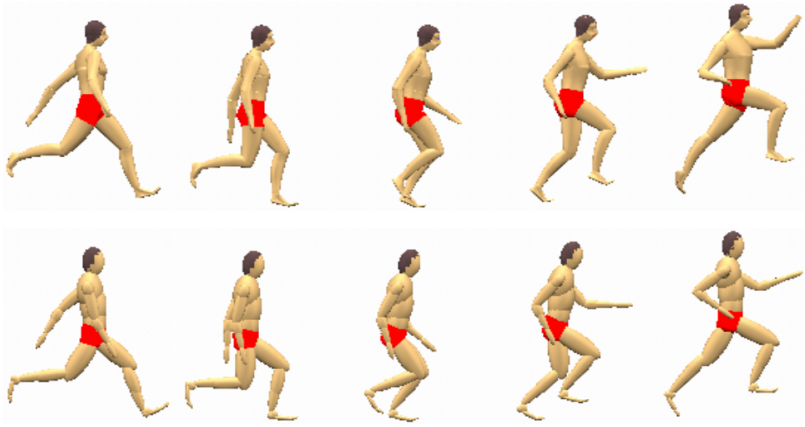

Figure 5.6 Performance (top) and matched simulation (bottom) of the jump phase.

Table 5.7 RMS angle differences between performance and matched simulation for individual joints in each phase

Score Component	Hop	Step	Jump
RMS Difference Right Shoulder	6.72	3.26	3.16
RMS Difference Left Shoulder	2.03	6.48	9.07
RMS Difference Right Hip	8.95	8.69	6.03
RMS Difference Left Hip	10.39	5.99	5.17
RMS Difference Right Knee	7.71	7.52	7.14
RMS Difference Left Knee	4.43	3.84	5.36
RMS Difference Stance Ankle*	8.33	7.89	8.55
RMS Difference Stance Ball*	5.91	6.16	9.34

*the ankle and ball joints of the free leg were angle-driven, stance leg is the right leg for the hop and step phase and the left for the jump phase.

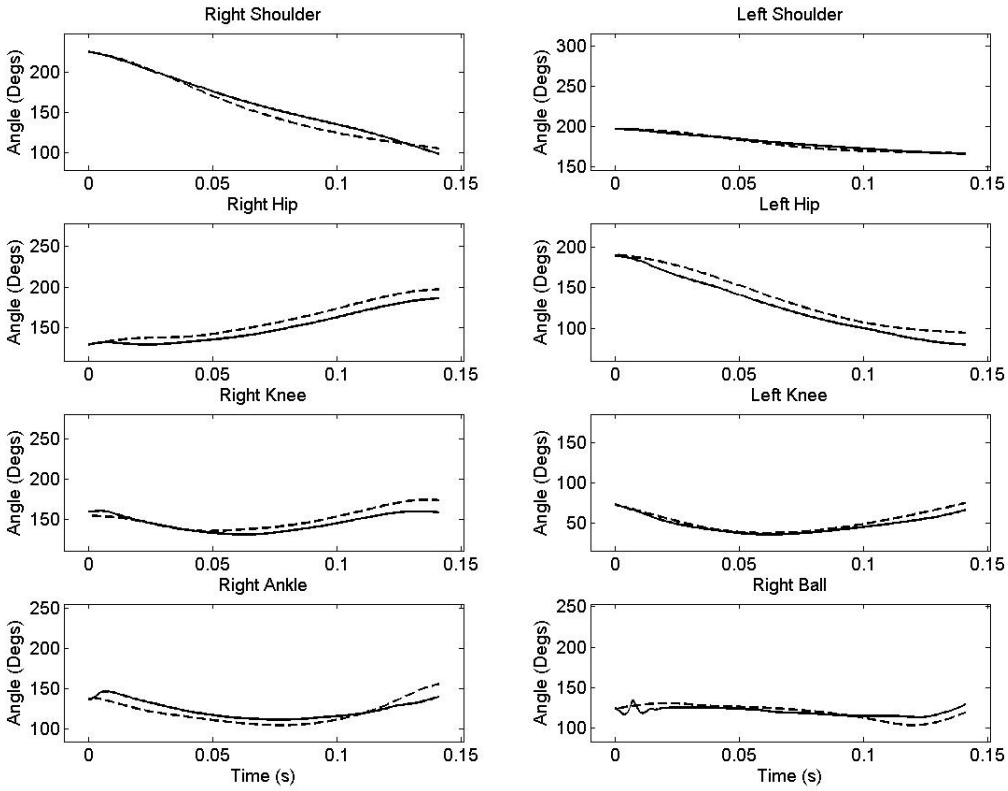

Figure 5.7 Joint angle time histories from performance (dashed lines) and matched simulation (solid lines) of the hop phase.

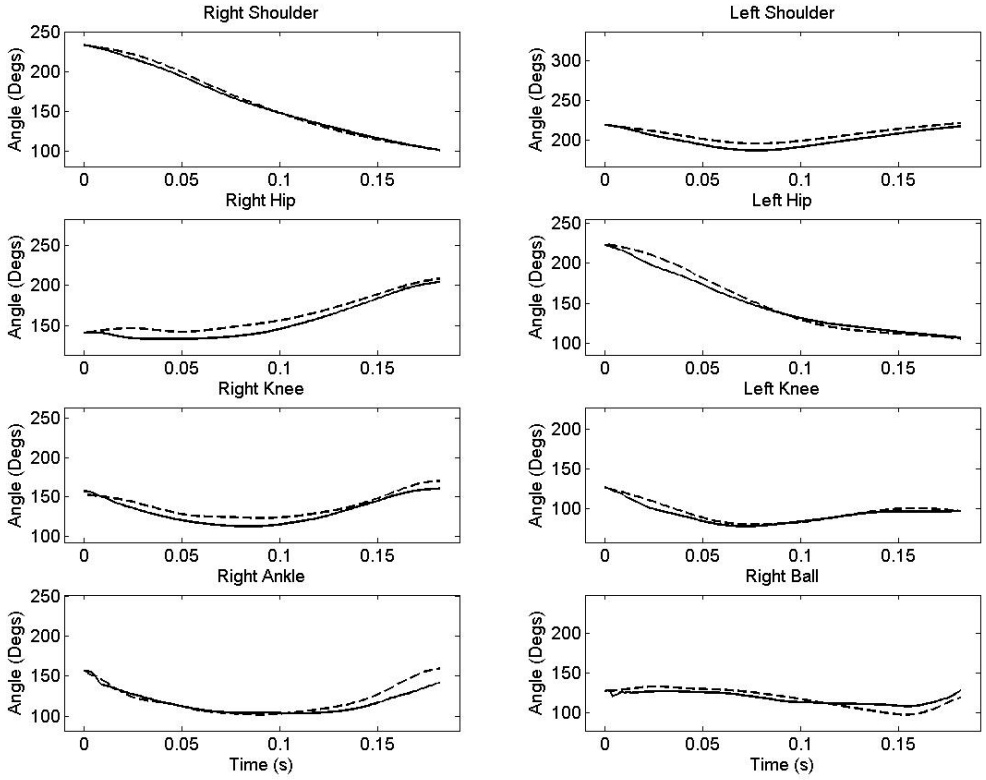

Figure 5.8 Joint angle time histories from performance (dashed lines) and matched simulation (solid lines) of the step phase.

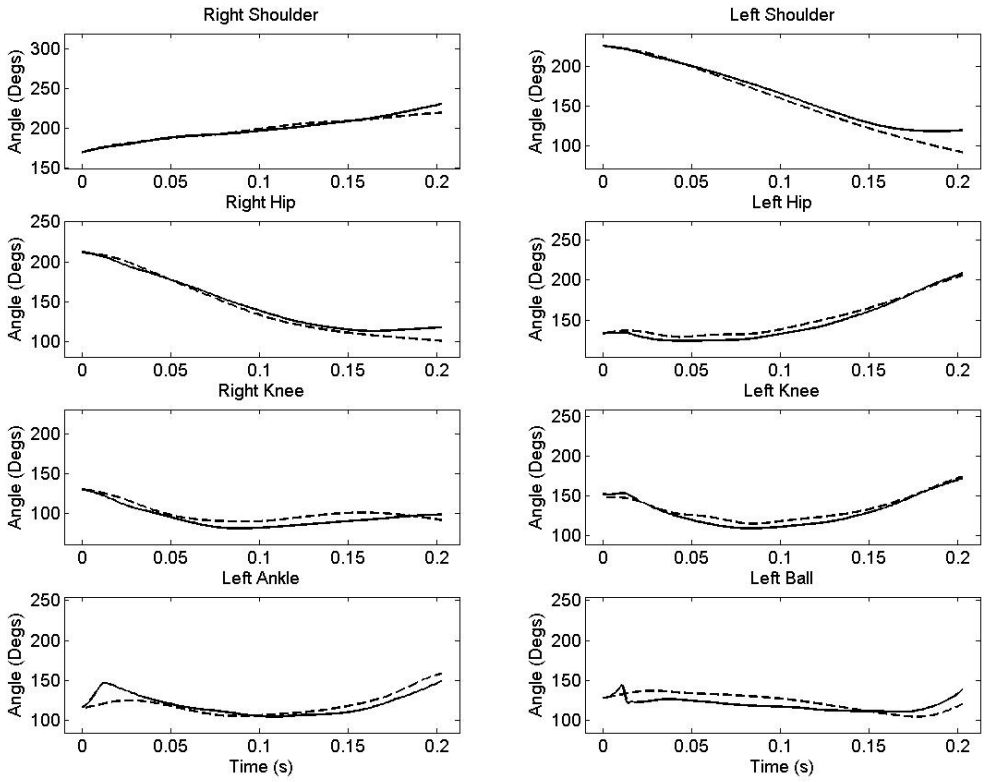

Figure 5.9 Joint angle time histories from performance (dashed lines) and matched simulation (solid lines) of the jump phase.

5.5.7 Joint torques

Joint torques in each phase showed a similar pattern, with a general trend of increasing torques from phase to phase (Table 5.8) and consistently large extension torques at the hip, knee, and ankle of the stance leg (Figures 5.10-5.12). All three of these joints reached the maximum activation level in each of the three phases of the triple jump (Figures 5.13-5.15). This underlines the importance of strength at these joints in jumping performance.

Table 5.8 Maximum extension torques at main joints of the stance leg for matched simulations

	Hop	Step	Jump
Maximum hip extension torque (Nm)	317	374	410
Maximum knee extension torque (Nm)	351	433	454
Maximum ankle extension torque (Nm)	269	307	304

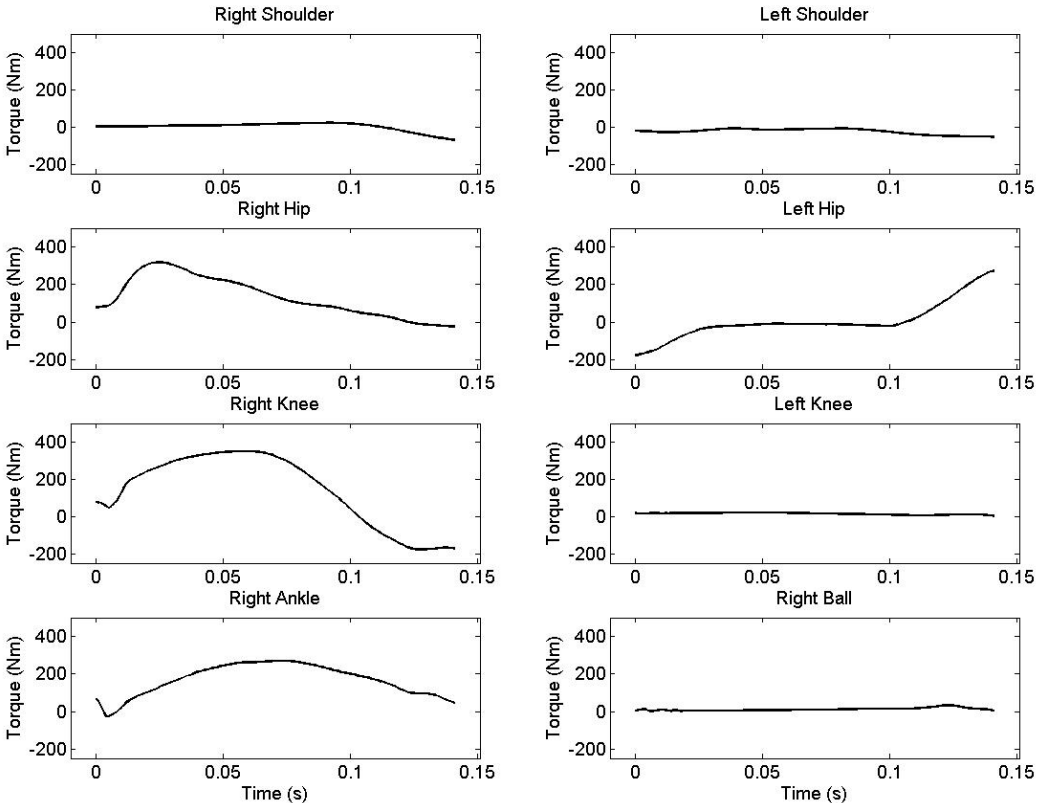

Figure 5.10 Joint torque time histories from the matched simulation of the hop phase (extension is positive except at shoulder joints).

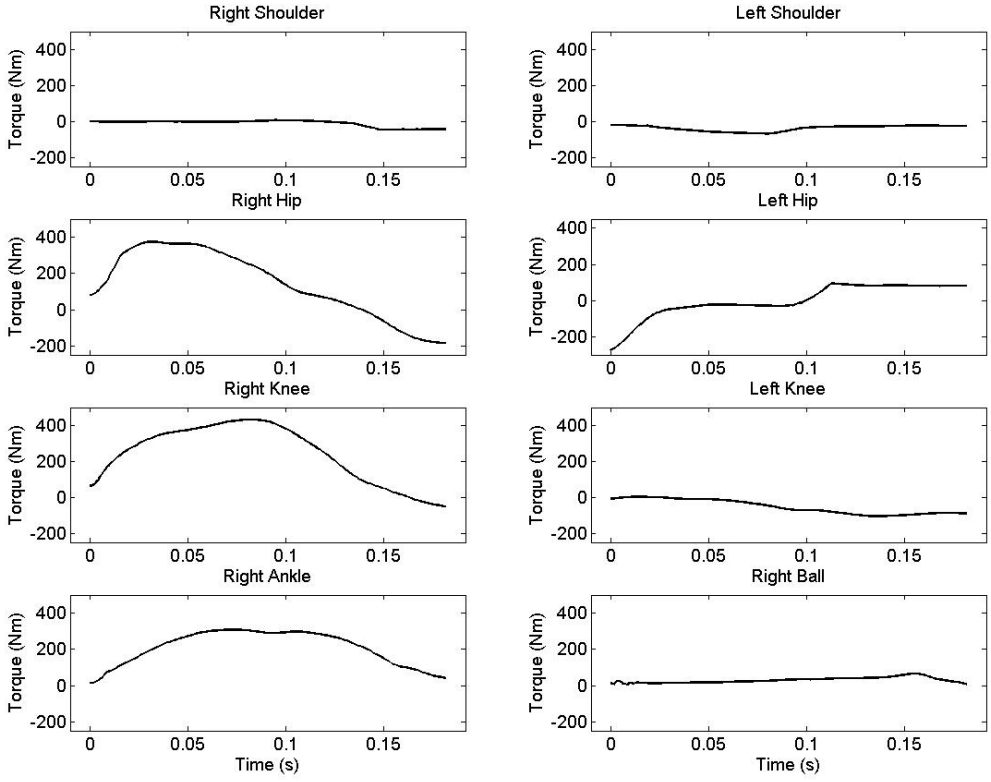

Figure 5.11 Joint torque time histories from the matched simulation of the step phase (extension is positive except at shoulder joints).

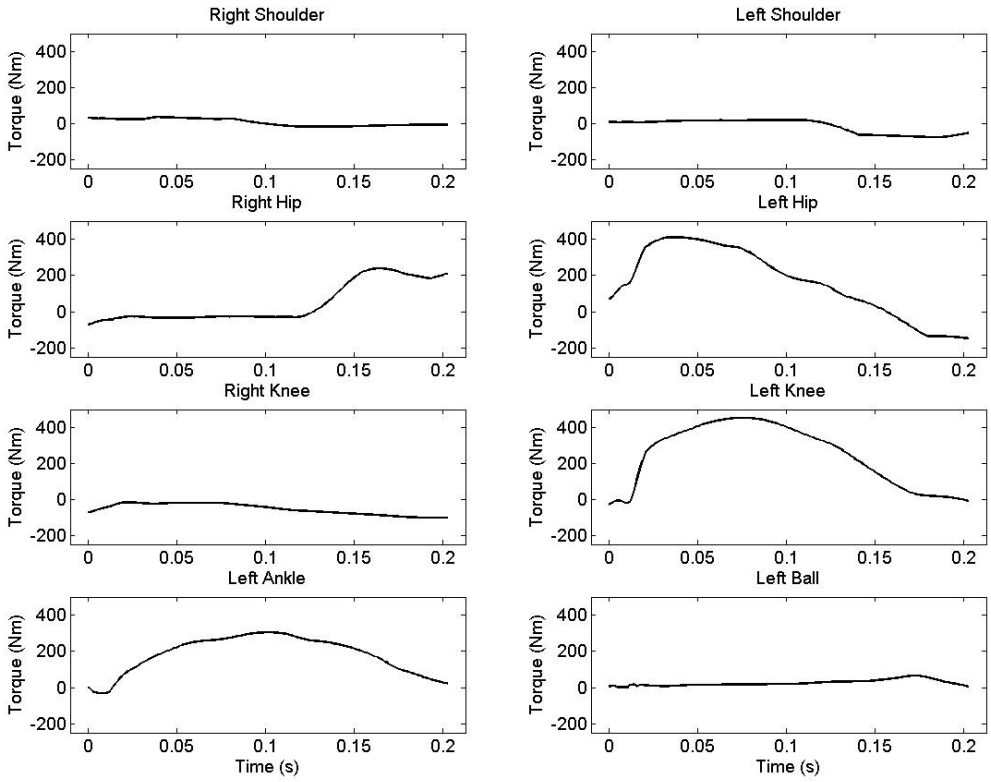

Figure 5.12 Joint torque time histories from matched simulation of the jump phase (extension is positive except at shoulder joints).

5.5.8 Torque generator activation timings

The activation time histories show flexion torques in the stance leg towards the end of the contact phase which acted to prevent the joint hyperextending. Levels of flexor activity in the knee and ankle of the stance leg at touchdown indicate co-contraction is necessary towards the end of the airborne phase to hold the joint in the correct configuration for landing whilst keeping the activation level of the extensor muscles high (Figures 5.13-5.15). Initial flexion torques in these joints were maintained for up to 50 ms after touchdown which indicates that maximum torques at these joints were not required until after this point in time. This is evident in the torque time histories of these joints (Figures 5.10-5.12). In contrast peak torques in the stance hip occurred before 50 ms in each phase. In general both the torque and activation time histories indicate that the joints in the stance leg followed a proximal-to-distal hip-knee-ankle extension sequence (Figures 5.10-5.15). This was similar to that which has previously been observed in vertical jumping (Bobbert and van Ingen Schenau, 1988; Pandy and Zajac, 1991).

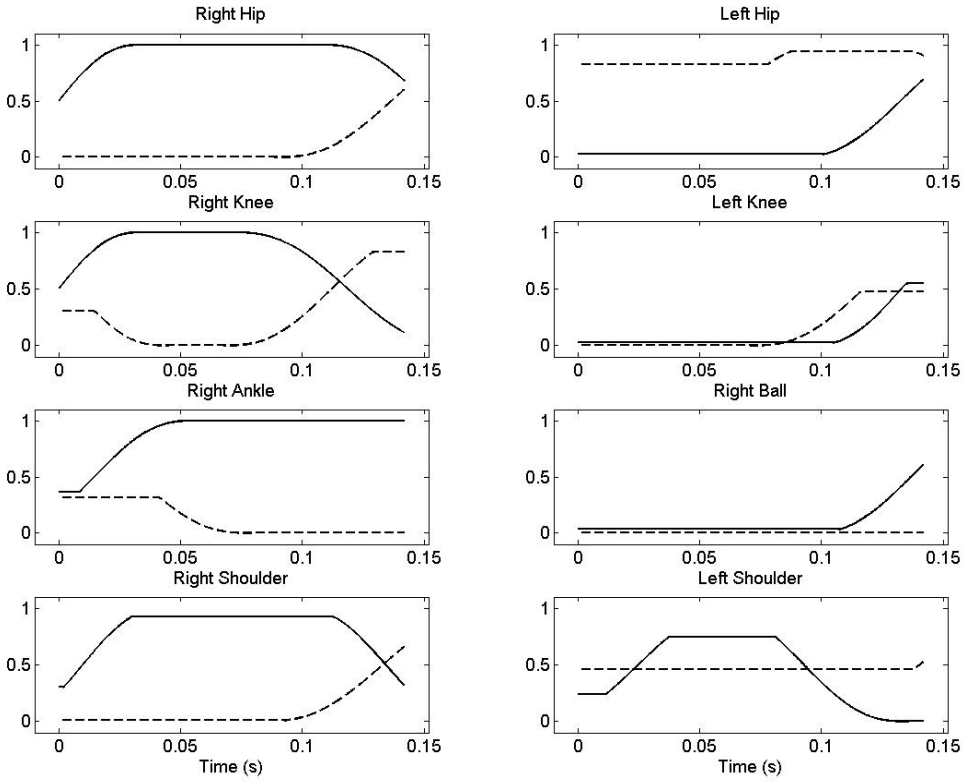

Figure 5.13 Extensor* (solid lines) and flexor* (dashed lines) torque generator activation levels for matched simulation of the hop phase. *Shoulder joints are opposite.

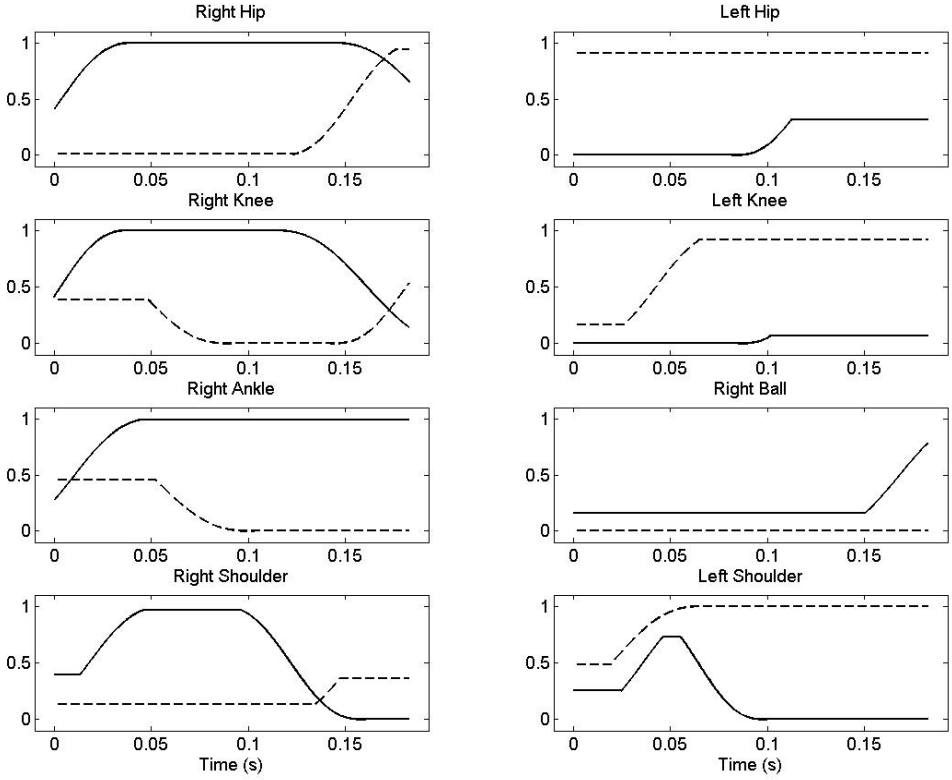

Figure 5.14 Extensor* (solid lines) and flexor* (dashed lines) torque generator activation levels for matched simulation of the step phase. *Shoulder joints are opposite.

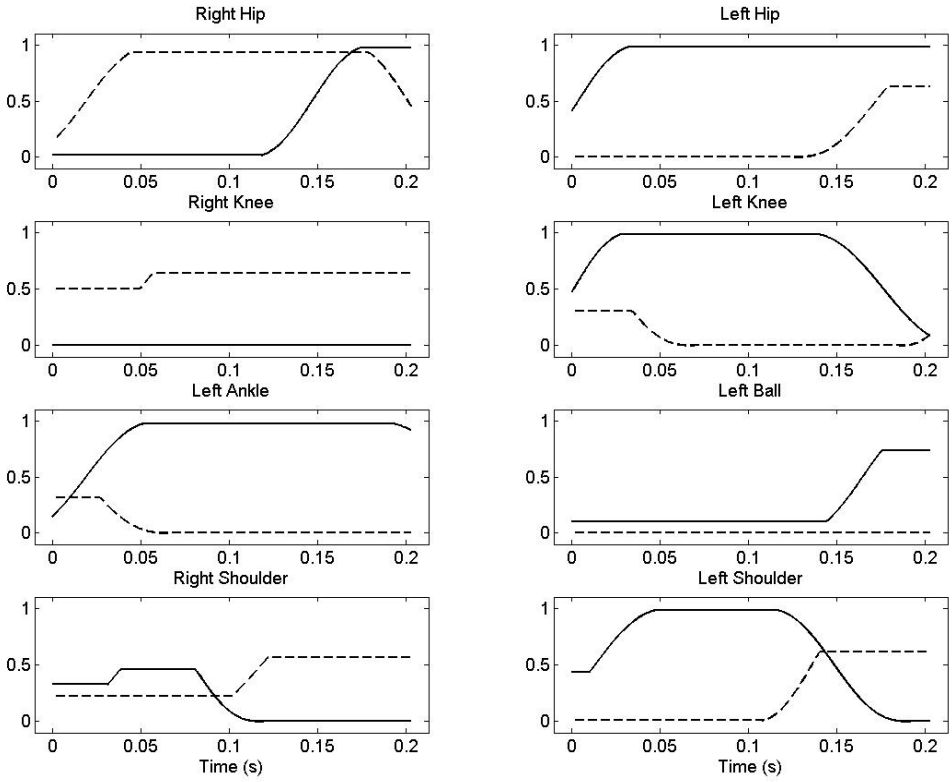

Figure 5.15 Extensor* (solid lines) and flexor* (dashed lines) torque generator activation levels for matched simulation of the jump phase. *Shoulder joints are opposite.

5.5.9 Passive torques

Since the passive torques implemented in the programme were not subject-specific, it was important to ensure that they were behaving sensibly. These torques were included in the model primarily to provide realistic restorative torques when the joints began to approach the end of their anatomical range. This was found to be necessary when the initial kinematic conditions put a joint outside the joint angle range at which the torque generator could exert a suitable restorative torque, potentially due to an underestimation of the width of the joint torque / joint angle relationship (Section 3.5.2). They were not intended to have a large influence on the optimal performance of the model. Figure 5.16 shows the passive torques for the matched simulation of the hop phase. It can be seen that the maximal torques are relatively small (<20 Nm) and therefore should not have an excessive effect on the performance of the model.

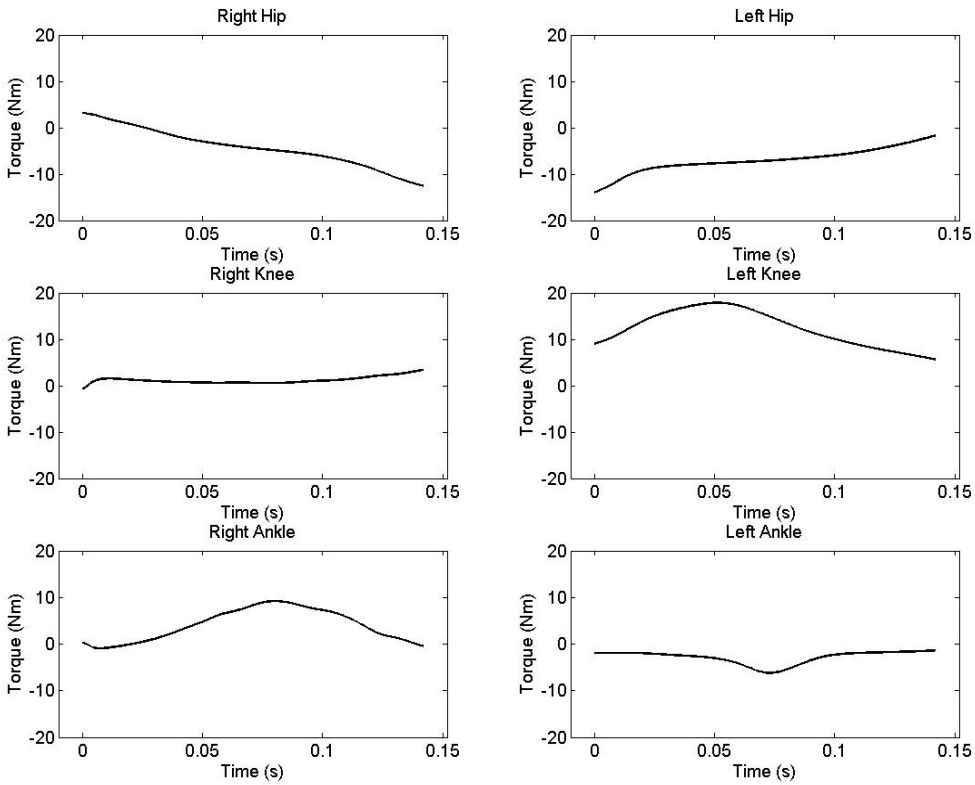

Figure 5.16 Passive torques for matched simulation of the hop phase (extension is positive).

5.6 CHAPTER SUMMARY

In this chapter the method of determining viscoelastic parameters using an angle-driven model of the stance and airborne phases of a triple jump has been described. The evaluation of a torque-driven model has also been outlined. This model showed close agreement with performance data and was shown to be accurate enough for simulation of the triple jump. The next chapter will describe the technique optimisation process.

CHAPTER 6

OPTIMISATION OF TECHNIQUE

6.1 CHAPTER OVERVIEW

In this chapter procedures employed to optimise the performance of simulation models of jumping in the literature is described. The method for optimisation of performance of the simulation model of triple jumping in this study is then described. Results from the optimisation of each phase of the triple jump are outlined and analysed. A demonstration of how the model can be applied to investigate issues concerned with the optimisation of technique and simulation modelling is then given.

6.2 OPTIMISATION OF JUMPING MODELS IN THE LITERATURE

This review considers the methods of optimisation employed by those analytical models of jumping reviewed in Section 3.2. Where a model is employed by more than one study, the method of optimisation used in the study where the model was introduced will be considered.

6.2.1 Models of one-legged jumps

Alexander (1990, 1992) did not optimise the performance of his model computationally, rather he ran his model with ranges of different input parameters in order to obtain results within these ranges, from which he could then obtain the best performances. Linthorne and Kemble (1998) used a similar method, running their model with a range of initial kinematic conditions and obtaining the optimum performance from these results. Chow and Hay (2005) used a search process to obtain a reference jump by evaluating their model using a range of initial conditions. They then performed sensitivity analyses by varying one parameter at a time and calculating results from a range of input parameters in order to obtain the longest jump. Seyfarth et al. (1999) calculated a parameter set which filled the least-square criterion between measured and calculated GRFs. They then used a genetic

algorithm in order to calculate the optimum jump attained by varying individual parameters. Seyfarth et al. (2000) did not specify an optimisation process, seemingly evaluating their model for a range of input parameters in order to obtain optimum performance for a given parameter. Ridka-Drdacka (1986) used a similar approach, evaluating the model over a range of input parameters in order to obtain optimum performance. Seyfarth et al. (online) used a similar optimisation process to van Soest et al. (1993), optimising muscle activation timings. However since this was a model of long jumping and not vertical jumping the activation of muscles prior to touchdown was included in the optimisation process by allowing muscles to have a negative activation time. Hatze (1981) used an optimisation process in order to maximise an objective function governing the distance jumped by varying the initial kinematics and the muscle stimulation timings. He stated that the technique and problems associated with the optimisation of the long jump were rather involved and hence he would report on them in a subsequent paper. Sorensen et al. (1999) used an optimisation algorithm in order to track measured GRFs by varying muscle stimulation timings, initial kinematics and viscoelastic parameters in their simulation model. They subsequently optimised performance by varying muscle stimulation timings and initial kinematics, using the viscoelastic parameters calculated from the tracking procedure. Wilson et al. (2007) used a simulated annealing algorithm to maximise jump height by varying torque-generator activation timings subject to various constraints. Optimisations without constraints, with constraints on angular momentum at take-off, with further constraints on joint angles, and with an additional requirement that the technique be robust to perturbations of torque generator activation timings, resulted in performances of 2.37 m, 2.21 m, 2.14 m, and 1.99 m respectively. The latter result closely matched performance data, indicating that optimisations of jumping should include these constraints in order to accurately represent jumping performance.

6.2.2 Models of two-legged jumps

Pandy et al. (1990) used an algorithm to estimate initial muscle forces by minimising an objective function representing the sum of the squares of the muscle forces at each joint. They were then able to calculate muscle activation levels. The height attained by the mass centre was then maximised by varying muscle activation timings using an optimisation algorithm. Anderson and Pandy (1999) used a similar optimisation procedure to Pandy et

al. (1990) in order to calculate their initial muscle activations by first minimising the sum of the squares of the joint torques, and then the sum of the squares of the muscle forces, from which they could calculate muscle activations. They then used a computational algorithm to optimise their muscle activation timings in order to maximise jump height. They stated that the algorithm allowed each perturbation of muscle activation timings to be performed independently and was thus suited to the architecture of a parallel computer. Van Soest et al. (1993) used an optimisation procedure partly based on that of Pandy et al. (1990). Like Pandy et al. (1990) they used an optimisation algorithm to maximise jump height by varying muscle activation timings, however they imposed constraints on the muscle activation timings, allowing them to switch to their maximal value only once and thereafter remain at that level. They evaluated this approach by running an optimisation without constraints and found only a 2 mm difference in jump height, indicating that imposing the constraints had little effect on the ability of the algorithm to find an optimal jump height. Selbie and Caldwell (1996) used the same technique as Pandy et al. (1990) to optimise their initial muscle activations. They then used a multidimensional downhill simplex method to maximise the vertical displacement of the COM in the airborne phase of the jump by varying torque generator activation timings. They found optimal solutions for a range of 125 different starting positions. They tested the optimality of their solution by restarting the algorithm using the previously obtained optimal torque generator activation timings, and also by widely varying the onset times to ensure a global, rather than a local, maximum was reached. Dapena (1999) evaluated the performance of his model for a range of input values for arm velocity, obtaining the optimum value from these results. Ashby and Delp (2006) used a simulated annealing algorithm to vary the activation levels of the torque generators in order to minimise an objective function comprising: jump performance; a penalty for activations that did not improve jump distance; and a penalty for passive ligament torques.

6.2.3 Summary of literature on the optimisation of jumping models

The studies described above can be broadly split into those that manually optimised their models (Alexander, 1990, 1992; Linthorne and Kemble, 1998; Chow and Hay, 2005; Seyfarth et al., 2000; Ridka-Drdacka, 1986; Dapena, 1999) and those that used optimisation algorithms (Seyfarth et al., 1999; Seyfarth et al., online; Hatze, 1981; Sorensen et al., 1999; Wilson et al., 2007; Pandy et al., 1990; Anderson and Pandy, 1999;

van Soest et al., 1993; Selbie and Caldwell, 1996; Ashby and Delp, 2006). Those studies that used manual optimisation processes typically used simple models with few variables which made this feasible. It would be virtually impossible to manually optimise the more complex models in the studies described above, therefore a suitable optimisation algorithm should be chosen in order to minimise an objective function that incorporates all the main features of the activity being modelled. A description of these algorithms was given in Section 5.3. It is possible to reduce the search space by applying sensible constraints on input parameters; van Soest et al. (1993) limited their search space by using constraints on muscle activation timings, which they showed did not appreciably affect the ability of the algorithm to find an optimal solution, but reduced processing time. Wilson et al. (2007) demonstrated the importance of using realistic constraints in order to obtain results that were consistent with performance data.

6.3 OPTIMISATION METHODS

The model was optimised for jump distance. The initial conditions outlined in Section 5.5.4 were maintained from the matched simulations for each phase. Therefore the method of optimisation was the same as in the matched simulations, but with only the 77 torque generator activation timings being varied using a genetic algorithm. The activation timings from the matched simulations were used as a starting point around which tight bounds were set (van Soest et al., 1993), since it was assumed that optimal technique would not differ too much from that employed in the performance. Therefore the genetic algorithm population size was reduced from 200 in the matched simulations to 100, because the search space was reduced and it was found that a population size higher than this did not result in an improved result. This indicated that the genetic algorithm was likely to have converged on a global optimum and considerably reduced the calculation time required. The bounds were increased if they were hit during optimisations. In this case an objective function which simply comprised the jump distance was maximised.

6.3.1 Penalties

As with the matched simulations, penalties were imposed if the joints exceeded anatomical limits (Section 5.5.2). Penalties were also imposed if the model was more than 5° from the

measured orientation at touchdown of the subsequent phase in the hop and step phases. It was assumed additional configuration changes to those in the measured performance could be made in the air, partly due to an altered body configuration at take-off, which could offset this 5° change in orientation. For the jump phase it was hypothesised that the opportunity for rotational motions of the limbs to counteract whole-body rotation were smaller, so the model was penalised if it was over 2° from the orientation in the measured trial.

For the first two phases, the model was penalised in order that it remained within this 5° range. For the jump phase the penalties were calculated differently; penalties were implemented based on the amount of distance this change in orientation would have cost the performance. For the purposes of this calculation it was assumed the performance landing orientation and configuration were optimal and any deviation would result in either a maintenance or a decrement in performance. If the simulation was under-rotated (rotated anti-clockwise as viewed from the performer's right) it was assumed the performer would have had to open their hip angle by an equivalent amount in order to maintain the distance of the heels from the COM hence maintaining the same performance. If the simulation was over-rotated (rotated clockwise as viewed from the performer's right) the performer would maintain the same configuration and suffer a decrement in performance. The decrement in performance, P_x and P_y, due to the altered horizontal and vertical positions of the heels, was calculated using the following equations based on the length of a chord of a circle (Figure 6.1):

$$P_x = r \cdot 2 \cdot \sin\left(\frac{\theta}{2}\right) \cdot \sin(\theta - r) - r \cdot 2 \cdot \sin\left(\frac{\theta - \alpha}{2}\right) \cdot \sin(\theta - \alpha); \qquad (6.1)$$

$$P_y = \left(r \cdot 2 \cdot \sin\left(\frac{\theta}{2}\right) \cdot \cos(\theta - r) - r \cdot 2 \cdot \sin\left(\frac{\theta - \alpha}{2}\right) \cdot \cos(\theta - \alpha) \right) \cdot \left| \frac{v_x}{v_y} \right|, \qquad (6.2)$$

where r represents the radial distance from the COM to the heel at touchdown, θ and α represent the orientation of the body at touchdown in the performance and the change in this orientation in the simulation respectively, and v_x and v_y represent the horizontal and vertical components of the COM velocity (Figure 6.1).

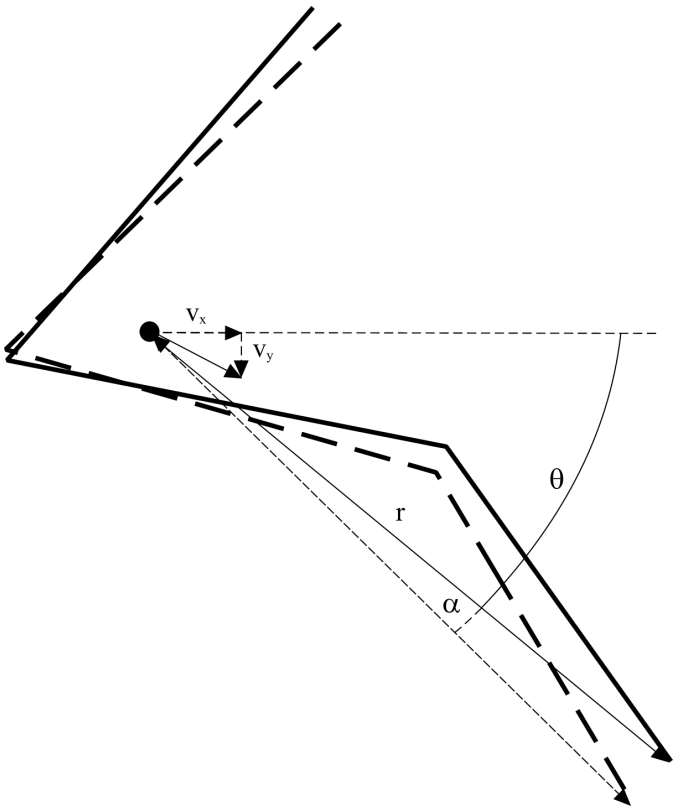

Figure 6.1 A visual representation of a performance (solid line) and simulation (dashed line) landing orientation.

This is an approximation since the amount of rotation and the landing velocity are calculated using the flight time associated with the performance COM position at landing, whereas the COM position of the simulation will be different due to the altered rotation. The effects of the rotation and the landing velocity on the performance decrement were in opposite directions so this was considered an acceptable approximation. In practice none of the optimised simulations incurred penalties for altered rotation.

6.4 OPTIMISATION RESULTS AND DISCUSSION

6.4.1 Hop phase

Components of phase distance

Table 6.1 shows the differences between the take-off, flight, and landing distances (Figure 5.3) between matched and optimised simulations of the hop phase. The landing distance was fixed for all simulations so improvements could only come from the take-off and flight distances. Table 6.1 shows that the majority of the improvement in the hop phase from the

matched simulation to the optimised simulation came from an increase in take-off distance of 0.12 m, in comparison to an increased flight distance of only 0.02 m. This led to a total increase of 0.14 m (3.3%) in phase distance.

Table 6.1 Differences in each component of phase distance between matched and optimised simulations of the hop phase

Simulation Type	Take-off Distance (m)	Flight Distance (m)	Landing Distance (m)	Total Distance (m)
Matched	0.43	3.21	0.65	4.29
Optimised	0.55	3.23	0.65	4.43
Difference	0.12	0.02	0.00	0.14

Joint angles

Figure 6.2 gives a visual representation of the matched and optimised simulations of the hop phase and Figure 6.3 shows the corresponding joint angles for each of the torque-driven joints included in the optimisation process.

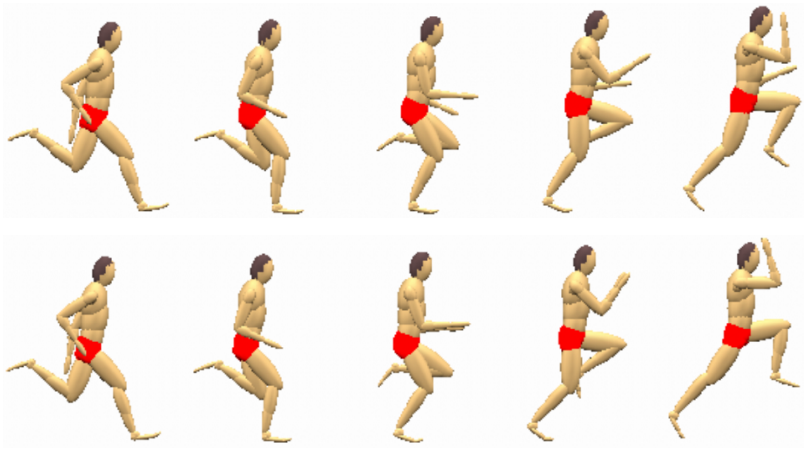

Figure 6.2 Matched (top) and optimised (bottom) simulations of the hop phase.

The most marked difference between the matched and optimised simulations can be seen in the shoulder angles. The left shoulder joint angle in the optimised simulation deviates considerably from the matched simulation angle. The joint angles in the optimised simulation show a symmetric flexion of both shoulder joints, whereas the matched joint angles show a plateau of the left shoulder joint angle, indicating an asymmetric arm movement (Figure 6.3). For the duration of the ground contact time of the matched

simulation the hip extension angle in the stance (right) leg in the optimised simulation is similar to that of the matched simulation, but after this time the hip continues to extend and has a greater degree of extension at take-off (Figure 6.3) leading to an increased ground contact time (Table 6.2). The other angles of the stance leg, and the free (left) hip, are similar in form to the stance hip; showing a greater degree of flexion / extension at take-off, leading to an increased ground contact time. One other notable difference in the joint angle histories is that the stance knee flexes more in the optimised simulation than in the matched simulation. The knee joint angles of the stance leg are the same in matched and optimised simulations at the time of take-off of the matched simulation (Figure 6.3) so this should not have affected the ground contact time geometrically. The increase in take-off distance (Table 6.1), which comprises the majority of the total phase length increase, is largely due to the increased hip extension angle in the stance leg and the increased flexion of the left shoulder joint. The increased extension of the stance hip would also act to lower the COM of the body, however due to the increased flexion of the shoulder joints and the free hip, and the increased extension of the knee, ankle, and ball joints of the stance leg, the optimised simulation showed a slight increase in COM height at take-off of 0.01 m (Table 6.3).

Table 6.2 Ground contact times in matched and optimised simulationso of the hop phase

Simulation Type	Contact Time (ms)
Matched	142
Optimised	160
Difference	18

Table 6.3 COM height at take-off in matched and optimised simulations of the hop phase

Simulation Type	COM Height (m)
Matched	1.14
Optimised	1.15
Difference	0.01

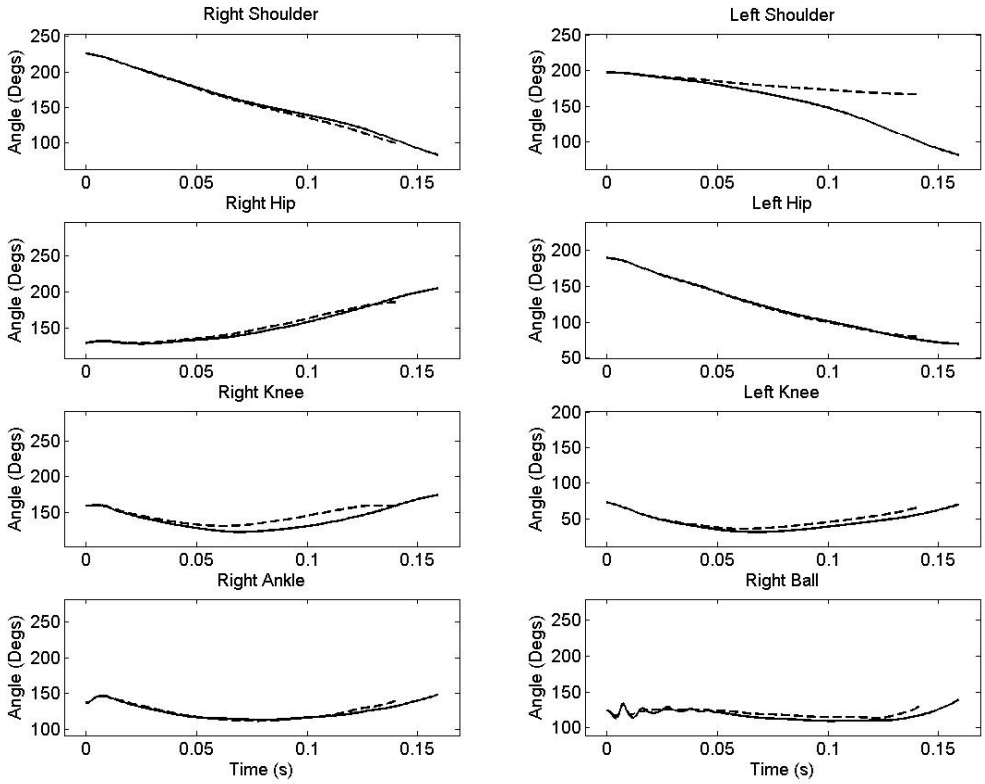

Figure 6.3 Joint angle time histories from matched (dashed lines) and optimised (solid lines) simulations of the hop phase.

Joint torques

Figure 6.4 shows the net joint torque time histories at each torque-driven joint in the optimised and matched simulations, Figures 6.5-6.6 show the flexor and extensor torque generator activation time histories and Appendix 15 shows the optimised torque generator activation timings. The reason for the increased flexion of the stance knee can be seen in Figure 6.4 where the optimised simulation initially showed a reduced torque relative to the matched simulation and then a larger torque in the latter portion of the ground contact. Interestingly, Figures 6.5-6.6 show that the increased extensor torque at the stance knee joint was not due to an increased activation of the extensors, but was instead a feature of the kinematics of the joint. The torque generator activation timings in the optimised simulation initially showed reduced extensor activation (Figure 6.5), and increased flexor activation (Figure 6.6), with respect to the matched simulation. This allowed the knee to flex more initially and put it in more advantageous conditions for torque production later in the stance phase. Towards the end of the stance phase the optimised simulation showed reduced flexor activity with respect to the matched simulation, allowing the stance knee to extend more. With the exception of the knee, the general trend in the torque generators of

the stance leg was for the extensors to ramp up earlier in the optimised simulation than in the matched simulation, with the flexors then ramping up later (Figures 6.5-6.6). The extra extension of the other joints of the stance leg in the optimised simulation was probably the main factor in increasing the ground contact time (Table 6.2). The extra flexion of the free hip can be explained primarily by the increased ground contact time, combined with the delayed initiation of the extensor ramp (Figure 6.5). Whereas the increased flexion of the left shoulder joint was due to a higher and more sustained activation of the flexor torque generator and a decreased extensor activation (Figures 6.5-6.6).

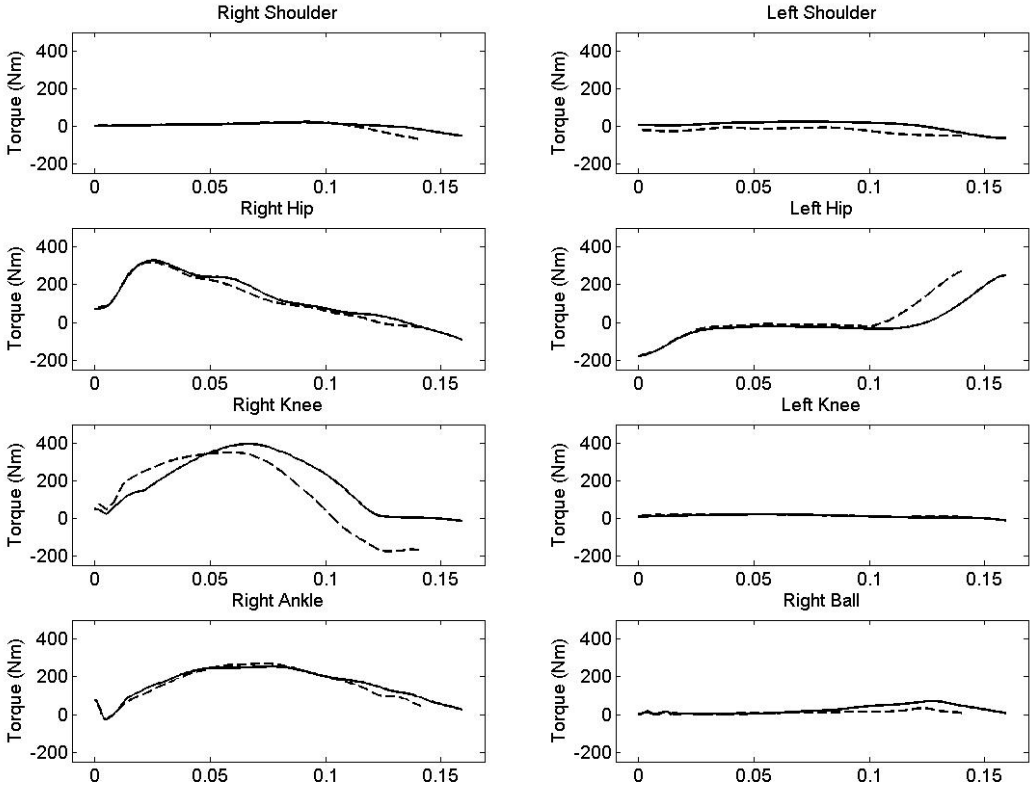

Figure 6.4 Joint torque time histories from matched (dashed lines) and optimised (solid lines) simulations of the hop phase (extension is positive except at shoulder joints).

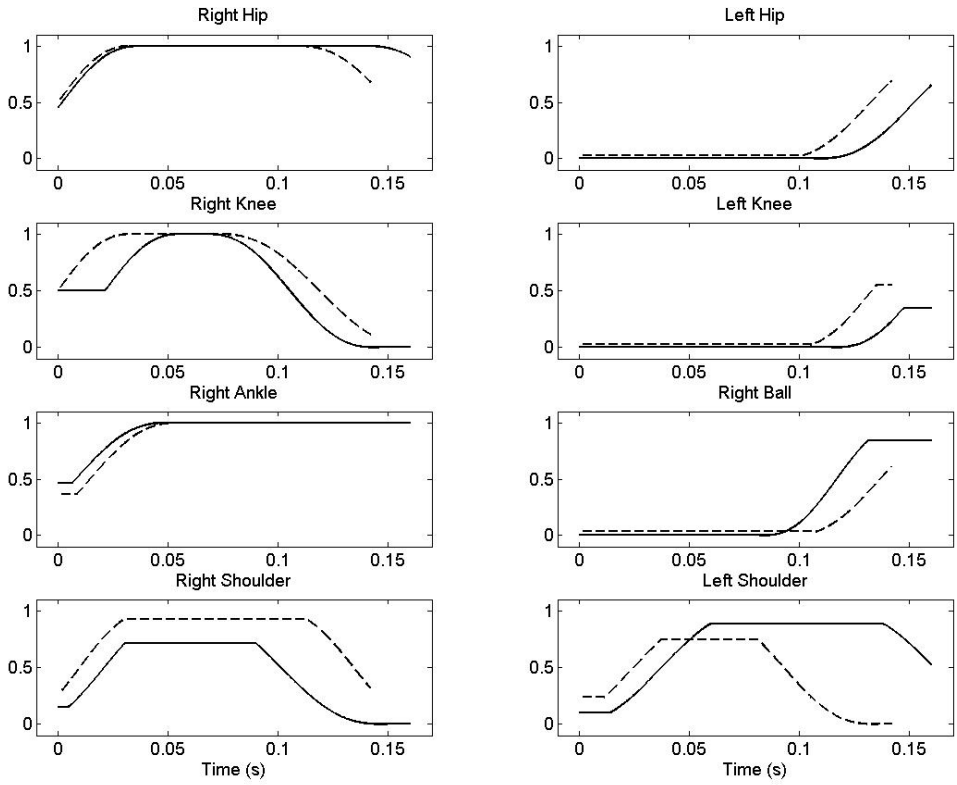

Figure 6.5 Activation time histories for joint extensors* in optimised (solid lines) and matched (dashed lines) simulations of the hop phase. *Shoulders show flexors.

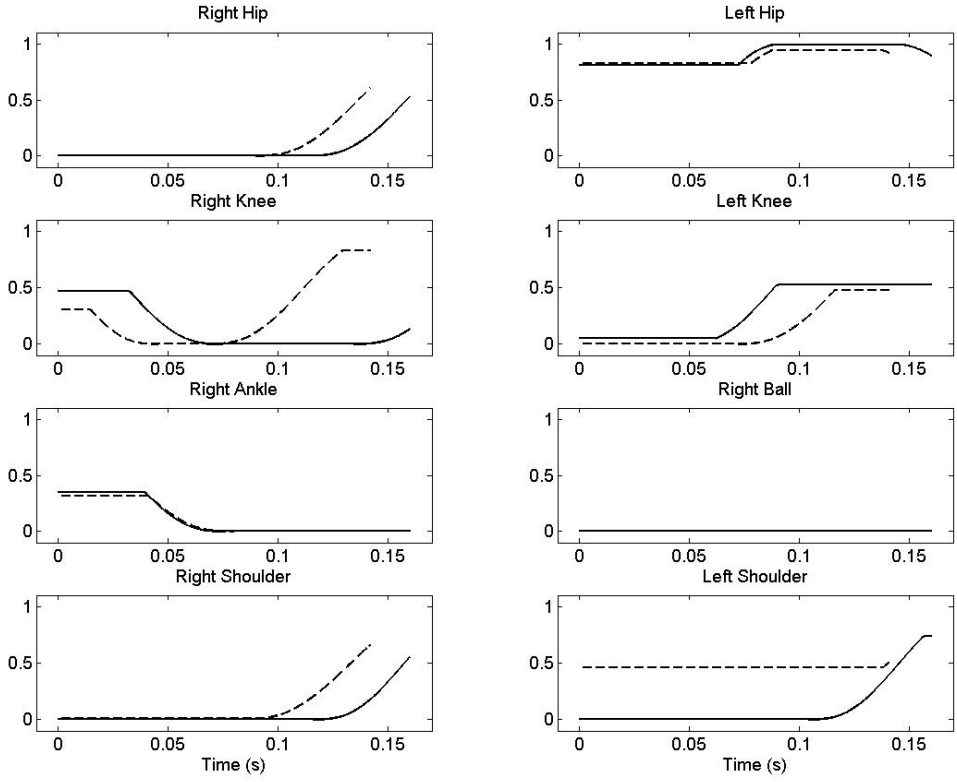

Figure 6.6 Activation time histories for joint flexors* in optimised (solid lines) and matched (dashed lines) simulations of the hop phase. *Shoulders show extensors.

Work done and angular impulses

Tables 6.4-6.5 show the work done and angular impulses at each torque-driven joint included in the optimisation process in the matched and optimised simulations. There was an overall increase in energy of 70 J contributed by these joints in the optimised simulation. It can be seen that the largest increases in the optimised simulation in both work (31 J) and angular impulse (9.6 Nms) came from the stance knee. Other notable increases in work came from the free hip (25 J) and in impulse from the left shoulder (3.9 Nms). There is a general trend towards increased impulses in the optimised simulation, with larger extension impulses in all joints of the stance leg, and larger (more negative) flexion impulses in the free hip, and shoulder joints (Table 6.5).

Table 6.4 Work done at different joints in matched and optimised simulations of the hop phase

	Right Hip (J)	Left Hip (J)	Right Knee (J)	Left Knee (J)	Right Ankle (J)	Right Ball (J)	Right Shoulder (J)	Left Shoulder (J)
Optimised	77	59	-68	-8	-21	13	1	-6
Matched	86	34	-98	-7	-28	0	0	-12
Difference	-9	25	31	-2	7	13	0	5

Negative sign indicates eccentric work

Table 6.5 Angular impulses at different joints in matched and optimised simulations of the hop phase

	Right Hip (Nms)	Left Hip (Nms)	Right Knee (Nms)	Left Knee (Nms)	Right Ankle (Nms)	Right Ball (Nms)	Right Shoulder (Nms)	Left Shoulder (Nms)
Optimised	20.0	-1.2	29.4	1.7	26.0	3.9	0.4	0.4
Matched	18.7	0.7	19.8	2.1	23.8	1.5	0.2	-3.4
Difference	1.3	-1.9	9.6	-0.4	2.2	2.4	0.2	3.9

Negative sign indicates flexion impulse, except in shoulder joints which are opposite

Ground reaction forces

Figure 6.7 shows the horizontal and vertical GRFs for the matched and optimised simulations for each phase of the triple jump. Table 6.6 shows the horizontal impulse, and the vertical impulses including (gross) and excluding (net) the body weight impulses for the matched and optimised simulations. The signs of the horizontal impulses are positive

but they were opposite to the direction of motion (i.e. braking impulses). The vertical velocity at take-off was lower in the optimised simulation than the matched simulation (Table 6.7) due to the decreased net vertical impulse (208 Ns vs 212 Ns). However the decreased horizontal impulse led to an increased horizontal (7.33 m/s vs 7.20 m/s), and resultant (7.58 m/s vs 7.46 m/s), take-off velocity, and a lower take-off angle (15.2° vs 15.9°). These changes did not alter the flight distance appreciably (Table 6.1). A difference can be seen in the form of the force traces, with the optimised simulation showing a depressed vertical force after the main impact peak, in comparison to the matched simulation (Figure 6.7). This was due to the greater extension of the joints of the stance leg (Figure 6.3) which facilitated a longer ground contact time and greater take-off distance, increasing the phase distance (Table 6.1).

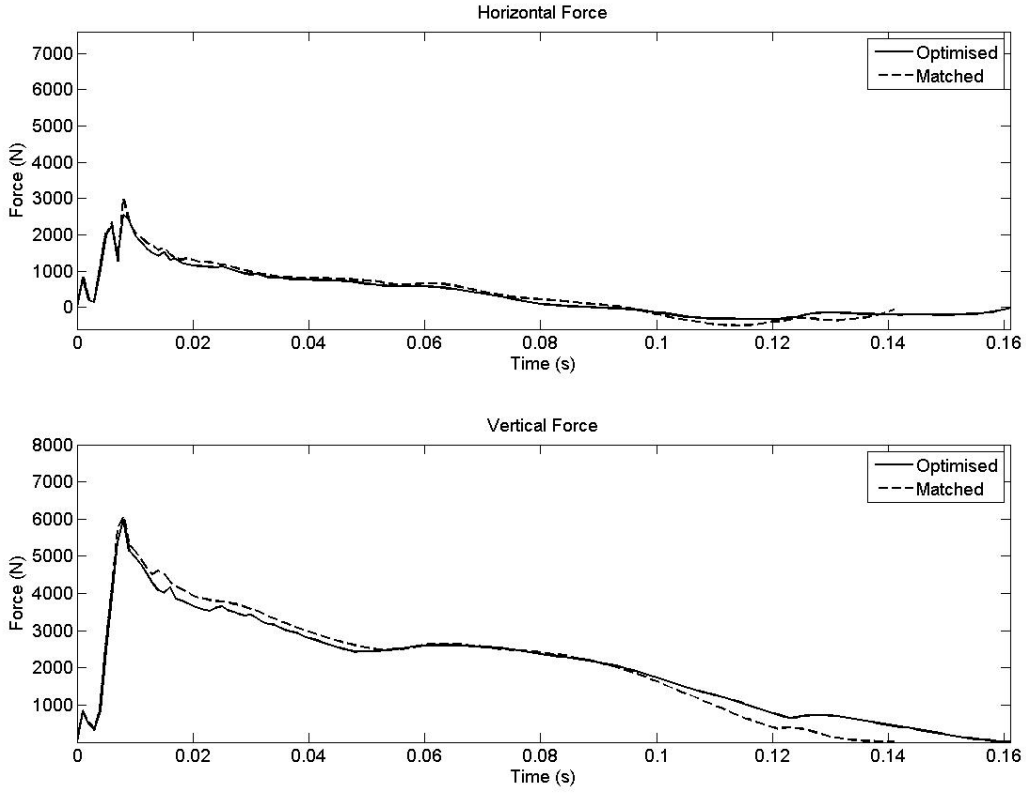

Figure 6.7 GRFs for optimised (solid lines) and matched (dashed lines) simulations of the hop phase.

Table 6.6 Horizontal and vertical impulses in matched and optimised simulations of the hop phase

Direction	Matched Impulse (Ns)	Optimised Impulse (Ns)
Horizontal	60	50
Vertical (Gross)	313	322
Vertical (Net)	212	208

Table 6.7 Take-off velocities and projection angle in matched and optimised simulations of the hop phase

Direction	Matched Velocity (m/s)	Optimised Velocity (m/s)
Horizontal	7.20	7.33
Vertical	1.97	1.92
Resultant	7.46	7.58
Projection Angle	15.9	15.2

6.4.2 Step phase

Components of phase distance

In contrast to the hop phase, the improvement in the step phase distance came mainly from the flight component, with a difference of 0.39 m. The improvement in the take-off distance was 0.04 m, leading to a total increase in phase distance of 0.43 m (11.1%) (Table 6.8).

Table 6.8 Differences in each component of phase distance between matched and optimised simulations of the step phase

Simulation Type	Take-off Distance (m)	Flight Distance (m)	Landing Distance (m)	Total Distance (m)
Matched	0.58	2.59	0.72	3.89
Optimised	0.62	2.98	0.72	4.32
Difference	0.04	0.39	0.00	0.43

Joint angles

As with the hop phase, the main difference in technique between the matched and optimised simulations came in the left shoulder angle (Figures 6.8-6.9); the shoulder angle in the optimised simulation continued to flex throughout the ground contact phase whereas the left shoulder angle in the matched simulation flexed initially then extended. The right shoulder also flexed more in the optimised simulation, showing the same symmetrical flexion of the shoulder joints as the optimised simulation in the hop phase. The joint angles in the stance leg did not differ appreciably between the matched and optimised simulations. As with the hop phase, the ground contact time was increased in the optimised simulation (Table 6.9) and this was in part due to the increased extension of the stance knee and stance hip towards the end of the ground contact. Again, as with the hop phase, the free hip had a greater degree of flexion at take-off in the optimised simulation than the matched simulation. This flexion of the free hip, coupled with the increased flexion of the shoulders and increased extension of the stance hip and knee, led to an increase in the take-off distance and the COM height at take-off in the optimised simulation (Tables 6.8 and 6.10).

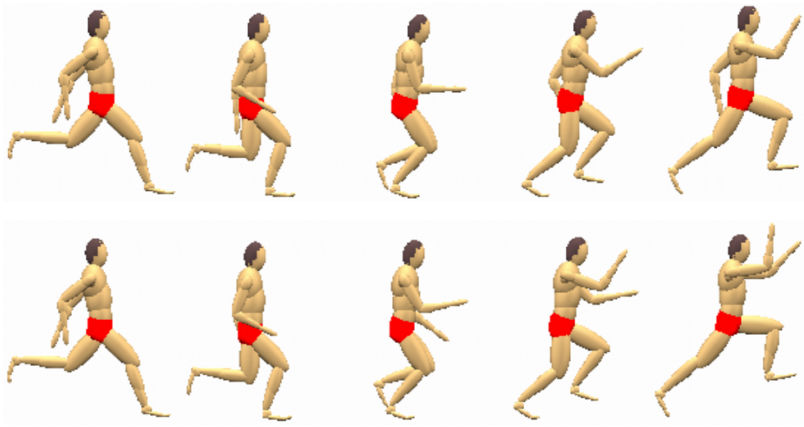

Figure 6.8 Matched (top) and optimised (bottom) simulations of the step phase.

Table 6.9 Ground contact times in matched and optimised simulations of the step phase

Simulation Type	Contact Time (ms)
Matched	183
Optimised	191
Difference	8

Table 6.10 COM heights at take-off in matched and optimised simulations of the step phase

Simulation Type	COM Height (m)
Matched	1.06
Optimised	1.10
Difference	0.04

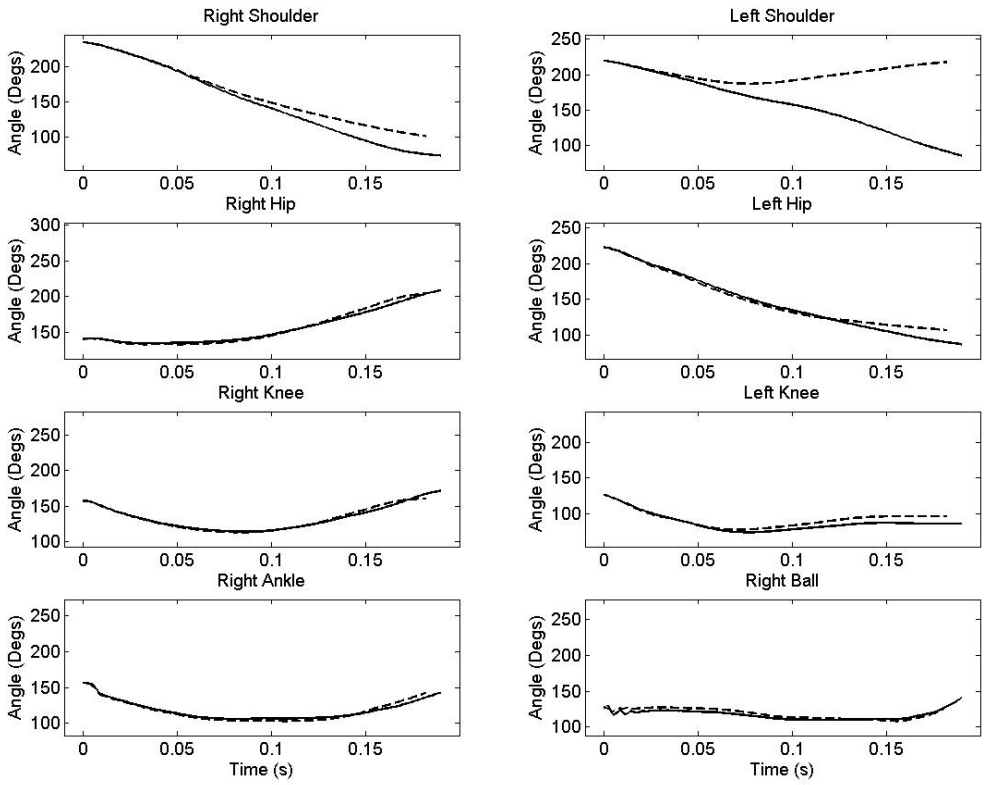

Figure 6.9 Joint angle time histories from matched (dashed lines) and optimised (solid lines) simulations of the step phase.

Joint torques

The main differences in the joint torque time histories between the matched and optimised simulations (Figure 6.10) were in the left shoulder, stance and free hips. The left shoulder produced a flexion torque for the majority of the stance phase, whereas the matched simulation showed an extensor torque for the same period, resulting in the increased flexion angle of the left shoulder joint (Figure 6.9). The cause of this can be seen in the torque generator activation time histories (Figures 6.11-6.12) where the optimised simulation showed an increased flexor activation and decreased extensor activation in

comparison to the matched simulation. The stance (right) hip torque in the optimised simulation deviated from the matched simulation towards the end of the stance phase and shows what was initially an increased extension torque and latterly a decreased flexion torque. This was achieved via a decreased flexor activation towards the end of the stance phase in the optimised simulation when compared to the matched simulation, since the extensor activation actually ramps off marginally earlier in the optimised simulation. The free (left) hip in the optimised simulation showed a decreased extensor torque in the latter half of the stance phase when compared to the matched simulation. This can be attributed to a delayed onset of the extensor activation ramp in the optimised simulation (Figure 6.11 and Appendix 15). The other joint torques did not show a large difference between the matched and optimised simulations.

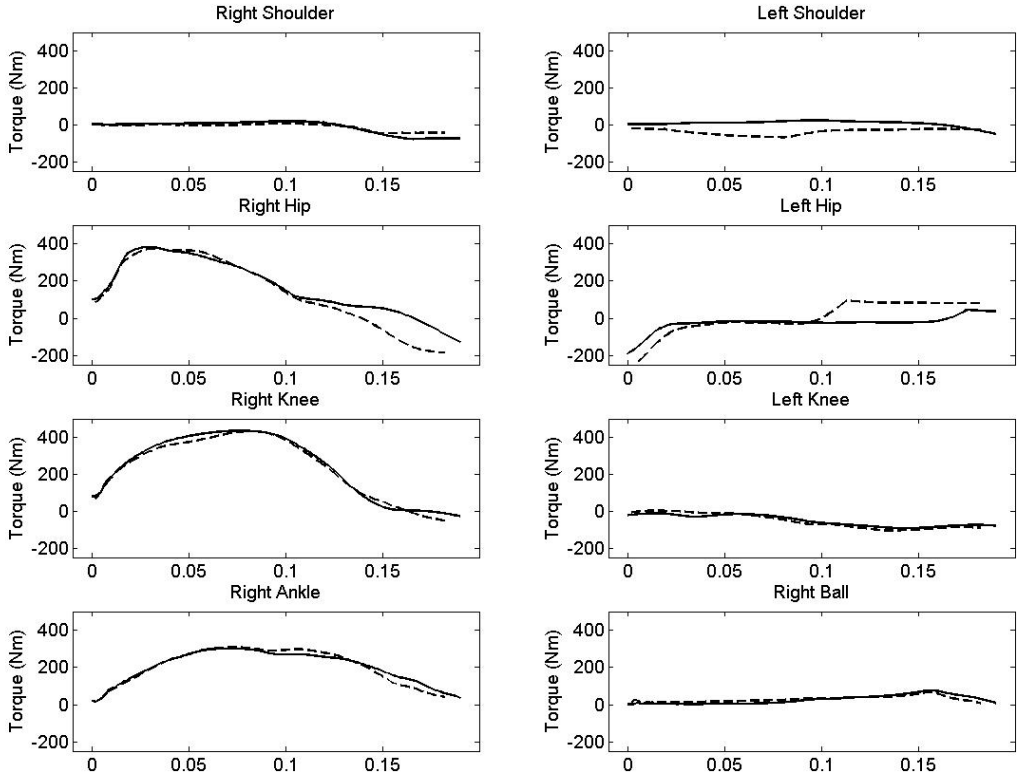

Figure 6.10 Joint torque time histories from matched (dashed lines) and optimised (solid lines) simulations of the step phase (extension is positive except at shoulder joints).

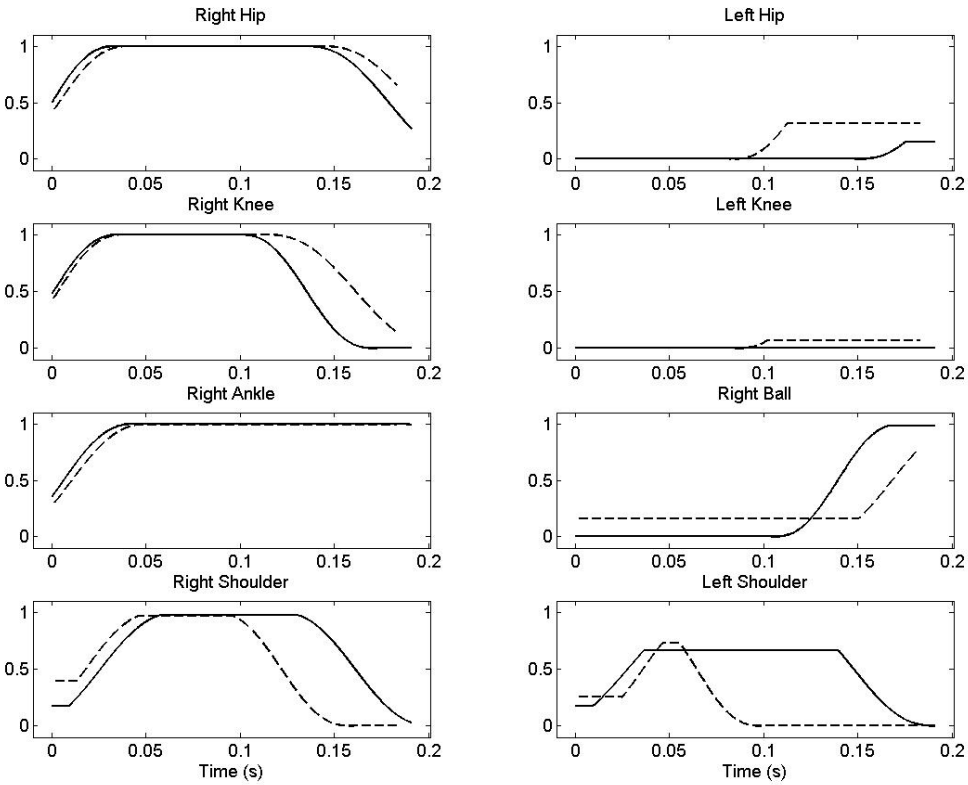

Figure 6.11 Activation time histories for joint extensors* from matched (dashed lines) and optimised (solid lines) simulations of the step phase. *Shoulders show flexors.

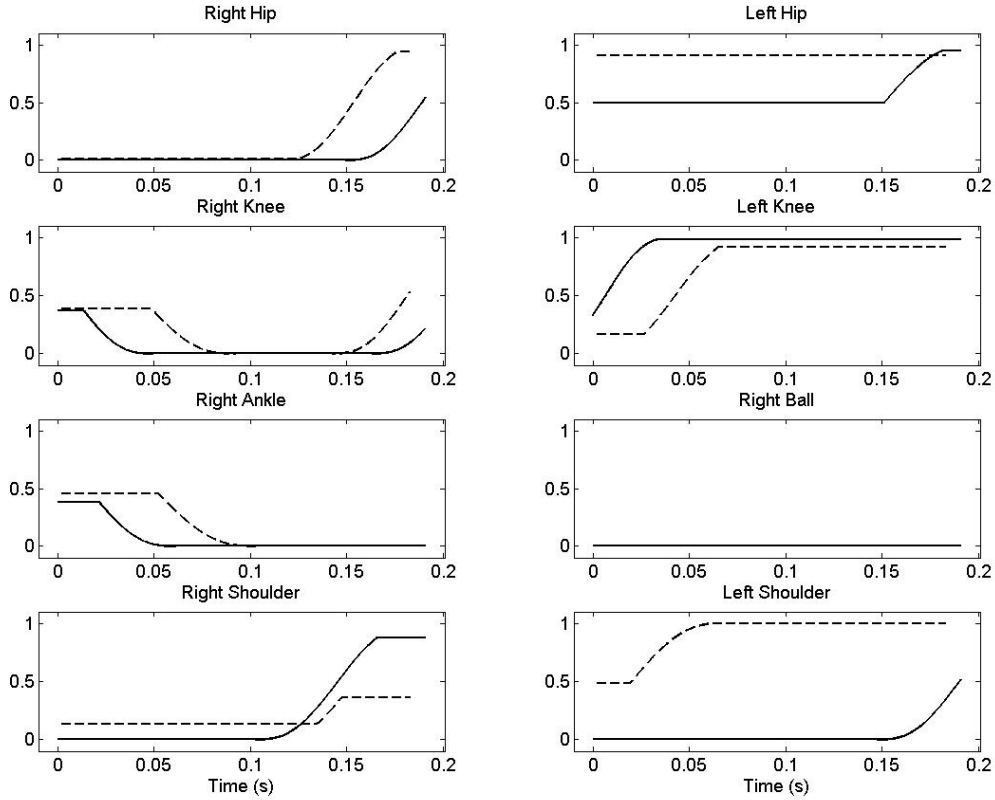

Figure 6.12 Activation time histories for joint flexors* from matched (dashed lines) and optimised (solid lines) simulations of the step phase. *Shoulders show extensors.

Work done and angular impulses

Tables 6.11-6.12 show the work done and angular impulses at each torque-driven joint included in the optimisation process in the matched and optimised simulations. There was an overall increase in work done of 103 J by these joints from the matched to the optimised simulations. The largest difference in work was in the stance hip (64 J); this joint also showed an increased angular impulse (5.8 Nms), which was indicated by the torque time history (Figure 6.10). There was an increased angular impulse in the stance knee (1.9 Nms) which led to more negative (eccentric) work being done in the optimised simulation (-28 J). Despite this negative work decreasing the kinetic energy of the model, it may have in some way facilitated the large increase in work achieved at the hip joint. The left shoulder joint displayed a large increase in angular impulse (8.2 Nms) which was evident from the torque time histories (Figure 6.10) and also an increase in work done (21 J). The free knee also showed an increase in work done (26 J), despite showing a slightly reduced angular impulse (-0.2 Nms). The flexor torque generator in this joint initiated its ramp earlier in the optimised simulation, but showed little difference in either joint angle time history (Figure 6.9) or torque time history (Figure 6.10 and Table 6.12) from the matched simulation. The ball joint of the stance leg also showed an increase in work done (19 J) in the optimised simulation, but as with the left knee, showed a slight decrease in angular impulse (-0.3 Nms). As with the left knee, the ball joint extensor torque generator time history showed an earlier initiation of its ramp and achieved a higher activation in the optimised simulation, although the matched simulation did show a higher initial level of activation (Figure 6.11). Despite this, there is little difference in the form of either the joint angle time histories (Figure 6.9) or the joint torque time histories at the ball joint (Figure 6.10).

Table 6.11 Work done at different joints in matched and optimised simulations of the step phase

	Right Hip (J)	Left Hip (J)	Right Knee (J)	Left Knee (J)	Right Ankle (J)	Right Ball (J)	Right Shoulder (J)	Left Shoulder (J)
Optimised	50	69	-135	2	-53	17	-16	14
Matched	-15	71	-108	-23	-54	-2	-18	-7
Difference	64	-2	-28	26	1	19	2	21

Negative sign indicates eccentric work

Table 6.12 Angular impulses at different joints in matched and optimised simulations of the step phase

	Right Hip (Nms)	Left Hip (Nms)	Right Knee (Nms)	Left Knee (Nms)	Right Ankle (Nms)	Right Ball (Nms)	Right Shoulder (Nms)	Left Shoulder (Nms)
Optimised	31.6	-4.7	45.8	-10.0	38.8	4.9	-2.4	1.3
Matched	25.8	0.0	43.9	-9.8	38.0	5.2	-2.0	-6.9
Difference	5.8	-4.7	1.9	-0.2	0.8	-0.3	-0.4	8.2

Negative sign indicates flexion impulse, except in shoulder joints which are opposite

Ground reaction forces

The GRFs show an increased vertical force in the optimised simulation with respect to the matched simulation (Figure 6.13). This was manifested in increases in both the gross and net vertical impulses (441 Ns vs 421 Ns and 305 Ns vs 291 Ns). The horizontal force traces were similar, displaying only a slightly increased braking impulse in the optimised simulation (43 Ns vs 41 Ns) (Table 6.13), and leading to similar horizontal take-off velocities (6.94 m/s vs 6.93 m/s) (Table 6.14). The change in net vertical impulse led to an increased vertical and resultant take-off velocity in the optimised simulation (1.78 m/s vs 1.56 m/s and 7.15 m/s vs 7.11 m/s), which in turn increased the projection angle (14.9° vs 13°) (Table 6.14). This led to a large increase in flight distance of 0.39 m (Table 6.8).

Table 6.13 Impulses in matched and optimised simulations of the step phase

Direction	Matched Impulse (Ns)	Optimised Impulse (Ns)
Horizontal	41	43
Vertical (Gross)	421	441
Vertical (Net)	291	305

Table 6.14 Take-off velocities and projection angle in matched and optimised simulations of the step phase

Direction	Matched Velocity (m/s)	Optimised Velocity (m/s)
Horizontal	6.94	6.93
Vertical	1.56	1.78
Resultant	7.11	7.15
Projection Angle	13.0	14.9

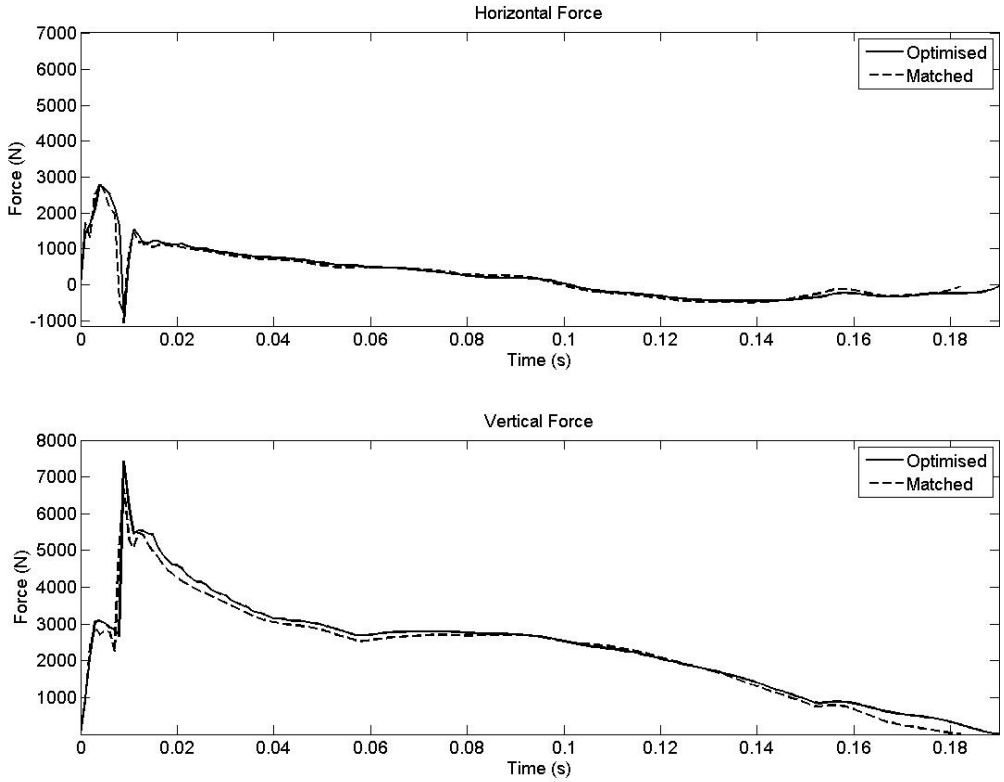

Figure 6.13 GRFs from matched (dashed lines) and optimised (solid lines) simulations of the step phase.

6.4.3 Jump phase

Components of phase distance

As with the step phase, but contrary to the hop phase, improvement in the jump phase distance came mainly from the flight component, with a difference of 0.27 m. There was an increase in the take-off distance, as there was in the previous two phases, of 0.08 m, leading to a total improvement in phase distance of 0.35 m (8.2%) (Table 6.15).

Table 6.15 Differences in each component of phase distance between matched and optimised simulations of the jump phase

Simulation Type	Take-off Distance (m)	Flight Distance (m)	Landing Distance (m)	Total Distance (m)
Matched	0.47	3.37	0.44	4.28
Optimised	0.55	3.64	0.44	4.63
Difference	0.08	0.27	0.00	0.35

Joint angles

As with the hop and step phases there is a large difference in the joint angle time history of the shoulder joint contralateral to the stance leg, in this case the right one (Figures 6.14-6.15). The shoulder flexion at take-off was not as great as in the hop and step phases but was still noticeably different between the optimised and matched simulations. Again, as is seen in the previous two phases, the free (right) hip flexed more in the optimised simulation (Figure 6.15). However, in contrast to the two previous phases, the joints of the stance (left) leg did not extend further in the optimised simulation than the matched simulation (Figure 6.15). Therefore the increase in take-off distance (Table 6.15) was due to the increased flexion of the shoulder joints and the free hip. This increased flexion also led to an 0.02 m increase in COM height at take-off of the optimised simulation compared to the matched simulation, as was seen in the previous two phases (Table 6.16). The same trend was seen in the ground contact time as in the previous phases, with an increase in the optimised simulation (Table 6.17). The increase in the ground contact time in the jump phase must have been due to the increased flexion of the free limbs, since there was not an increased extension of the joints of the stance leg as there was in the previous two phases. The torques leading to the increased flexion of the free limbs would give rise to an upward acceleration of the mass of the limbs which would in turn have imparted downward accelerations, via the shoulder and hip joints, on the remainder of the mass of the body. Assuming the stance leg did not fully resist these downward accelerations this would have caused the model to maintain contact with the ground for longer.

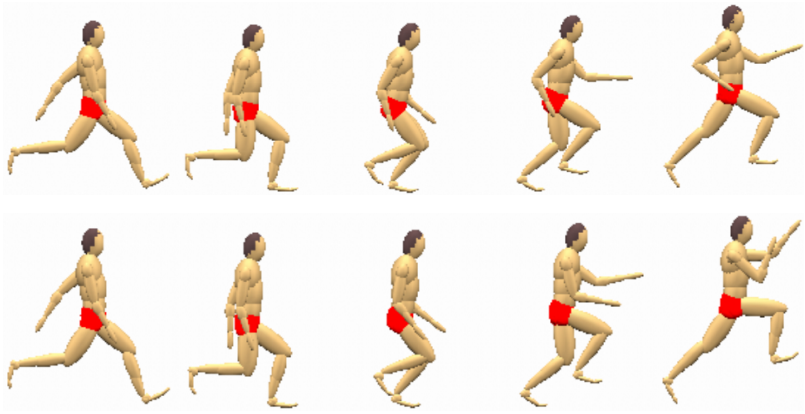

Figure 6.14 Matched (top) and optimised (bottom) simulations of the jump phase.

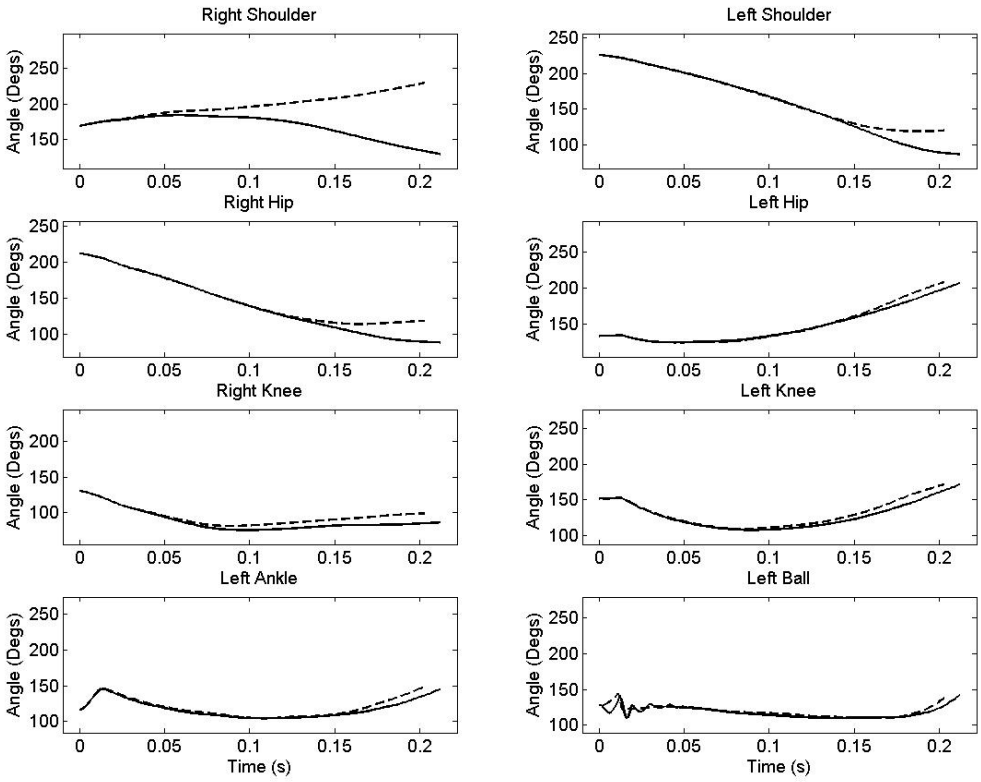

Figure 6.15 Joint angle time histories from matched (dashed lines) and optimised (solid lines) simulations of the jump phase.

Table 6.16 COM height at take-off in matched and optimised simulations of the jump phase

Simulation Type	COM Height (m)
Matched	1.07
Optimised	1.09
Difference	0.02

Table 6.17 Ground contact times in matched and optimised simulations of the jump phase

Simulation Type	Contact Time (ms)
Matched	203
Optimised	212
Difference	9

Joint torques

The main differences in the joint torque time histories between the optimised and matched simulations of the jump phase were in the shoulder and hip joints (Figure 6.16). The difference between hip joint torques of the stance (left) hip between the optimised and matched simulations occurred towards the end of the stance phase, with what was initially an increased extension torque and later a decreased flexion torque. The torque generator activation timings show that the model achieved these larger extension torques / decreased flexion torques in the stance hip by activating the flexors later in the optimised simulation (Figures 6.17-6.18 and Appendix 15). The free hip also showed a reduced extension torque in the optimised simulations towards the end of the stance phase (Figure 6.16) which was due to a delayed initiation of the flexor ramp (Figure 6.18). This manifested itself in the increased flexion angle of the free hip at take-off (Figure 6.15). The jump phase also showed an increased knee extension torque in the stance leg of the optimised simulation during the latter half of the stance phase. An inspection of Figures 6.17-6.18 shows that there was neither increased extensor or decreased flexor activation at this joint, so the increase in extensor torque must have come about as a result of changes in angular velocity arising from the action of torques at other joints (Dapena, 1999). The stance ankle torque generator in the jump phase showed extensor and flexor profiles (Figures 6.17-6.18) in the optimised simulation that ramped up and down respectively later than the matched simulation. These timings account for the initial depression of the torque time history in the optimised simulation with respect to the matched simulation, but they do not explain the increased torques later in the stance phase, since the extensor and flexor torque generators were fully active and fully inactive respectively in the matched and optimised simulations. Therefore the increase in torque must have come about due to the changed kinematic conditions of the joint putting the torque generators in more advantageous angle / angular velocity conditions for torque generation.

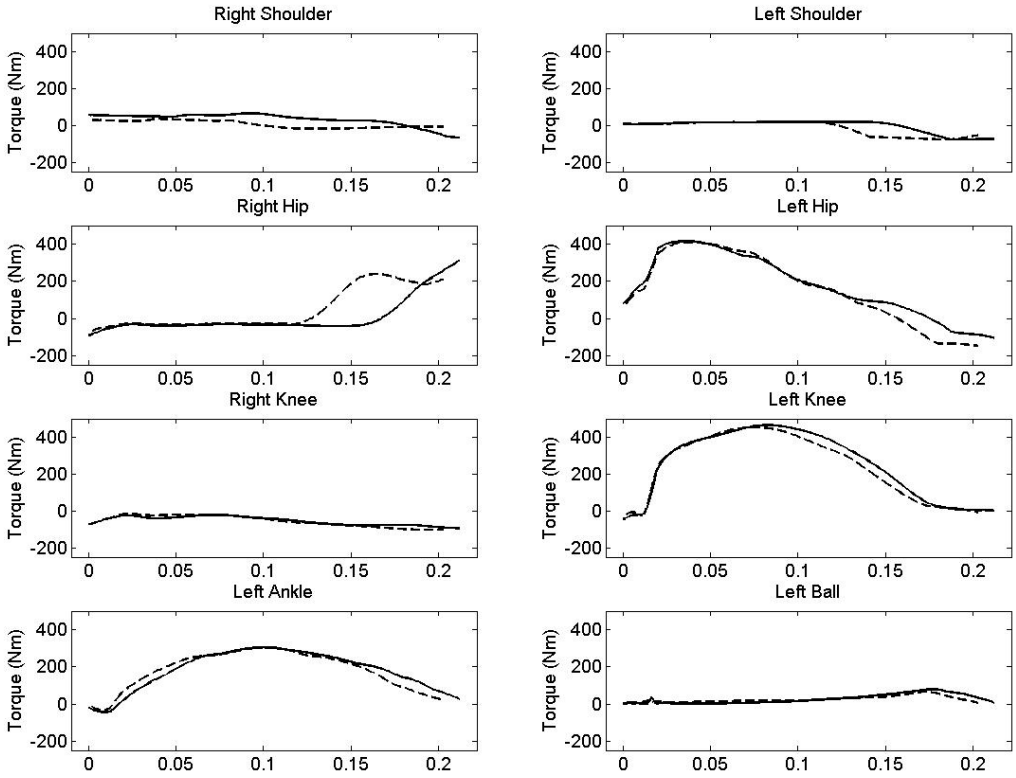

Figure 6.16 Joint torque time histories from matched (dashed lines) and optimised (solid lines) simulations of the jump phase (extension is positive except at shoulder joints).

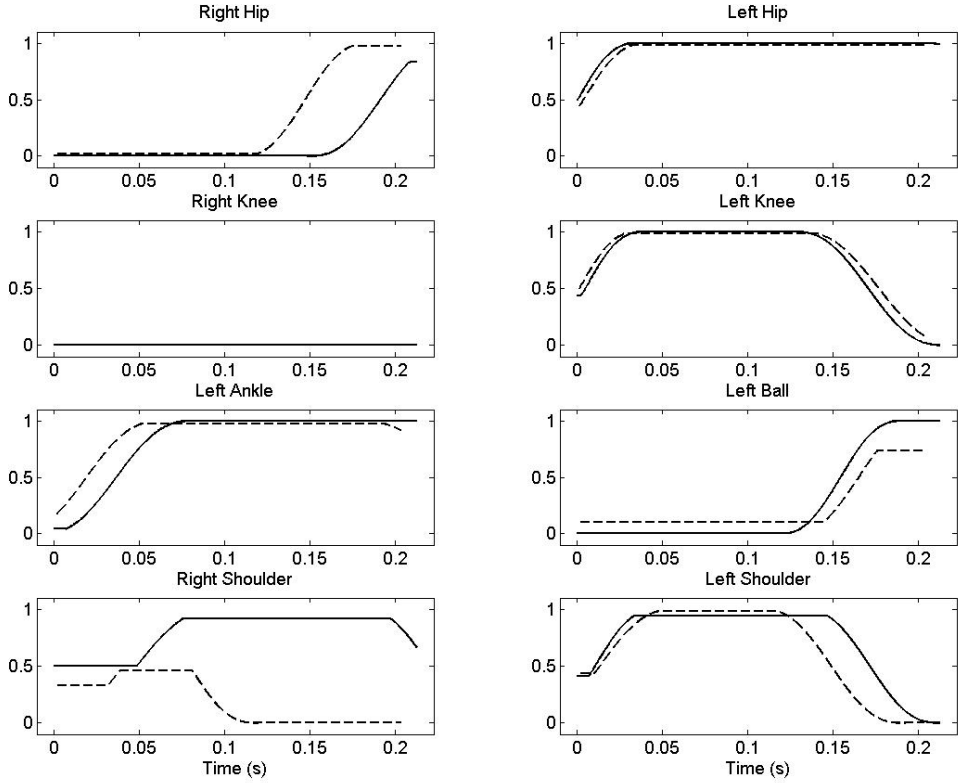

Figure 6.17 Activation time histories for joint extensors* in matched (dashed lines) and optimised (solid lines) simulations of the jump phase. *Shoulders show flexors.

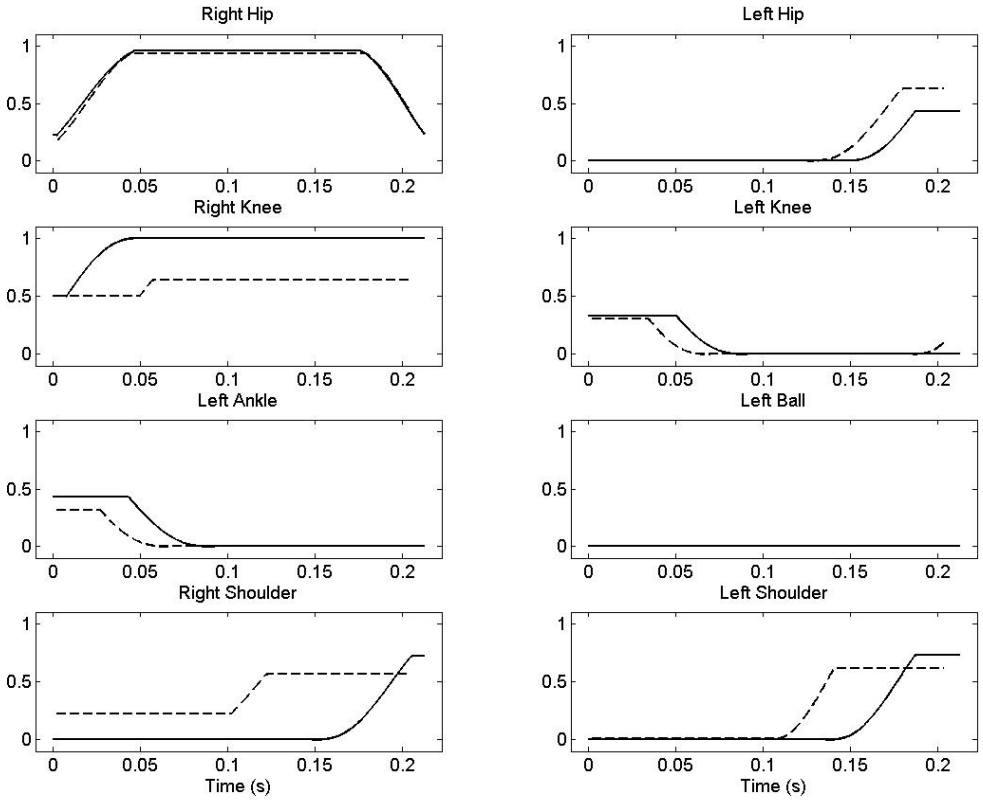

Figure 6.18 Activation time histories for joint flexors* in matched (dashed lines) and optimised (solid lines) simulations of the jump phase. *Shoulders show extensors.

Work done and angular impulses

Tables 6.18-6.19 show the work done and angular impulses at each torque-driven joint included in the optimisation process in the matched and optimised simulations. There was a total increase in work of 130 J done by the joints included in the optimisation procedure (Table 6.18). The largest increase in work done was in the stance (left) hip - as with the step phase but in contrast to the hop phase - with a contribution of 59 J. As in the step phase, the stance knee had an increased angular impulse (3.7 Nms) but was a net absorber of energy, although less in the jump phase than the step phase (-6 J vs -28 J). The stance ankle and ball also performed more work in the optimised simulation than the matched simulation (28 J and 15 J). The largest change in impulse was seen in the free hip (-8.1 Nms) but there was very little difference in work done between the optimised and matched simulations (52 J vs 50 J). This was due to the fact that the free hip in the matched simulation started to flex towards the end of the stance phase, allowing the extensors to perform positive work, whereas the hip continued to flex in the optimised simulation therefore the extensors were performing negative work (Figure 6.15). Likewise the right shoulder joint showed a large increase in impulse in the optimised simulation (5.6 Nms)

but performed a similar amount of work (-3 J vs -5 J) with respect to the matched simulation. An inspection of Figure 6.15 shows that the joint angle extended then flexed, so the flexion torque produced at the joint (Figure 6.16) did negative work followed by positive work, leading to a small net amount of work done, but a large impulse and consequently a large change in joint angle and the COM position and velocity of the arm.

Table 6.18 Work done by different joints in matched and optimised simulations of the jump phase

	Right Hip (J)	Left Hip (J)	Right Knee (J)	Left Knee (J)	Left Ankle (J)	Left Ball (J)	Right Shoulder (J)	Left Shoulder (J)
Optimised	52	20	20	-123	-29	17	-3	4
Matched	50	-39	0	-117	-57	3	-5	-5
Difference	3	59	20	-6	28	15	2	9

Negative sign indicates eccentric work

Table 6.19 Angular impulses at different joints in matched and optimised simulations of the jump phase

	Right Hip (Nms)	Left Hip (Nms)	Right Knee (Nms)	Left Knee (Nms)	Left Ankle (Nms)	Left Ball (Nms)	Right Shoulder (Nms)	Left Shoulder (Nms)
Optimised	0.9	37.1	-11.5	53.6	38.1	5.5	6.7	-0.7
Matched	9.0	32.8	-11.1	49.9	37.0	5.0	1.2	-3.1
Difference	-8.1	4.4	-0.4	3.7	1.1	0.5	5.6	2.5

Negative sign indicates flexion impulse, except in shoulder joints which are opposite

Ground reaction forces

The horizontal force trace shows a slightly reduced horizontal braking force followed by a slightly increased propulsive force in the optimised simulation in comparison to the matched simulation (Figure 6.19). This initial reduced braking force was likely to have been due to the lower extensor torque in the stance ankle and the increased flexor torque in the right shoulder (Figure 6.16). There was an associated depression in the vertical force over the same time period in the optimised simulation, due to the same factors. The decreased horizontal and increased vertical forces in the latter half of the ground contact phase were due to the increased torques of the stance leg during this period (Figure 6.16). This led to a decreased braking impulse (62 Ns vs 78 Ns) and an increased net vertical impulse (471 Ns vs 456 Ns) in the optimised simulation compared to the matched

simulation (Table 6.20). This led to an increased horizontal (6.06 m/s vs 5.84 m/s) and vertical (2.23 m/s vs 2.12 m/s) take-off velocity in the optimised simulation and an increased projection angle (21.6° vs 21.3°) which led to an increase in the flight component of the phase distance (3.64 m vs 3.37 m) (Table 6.21).

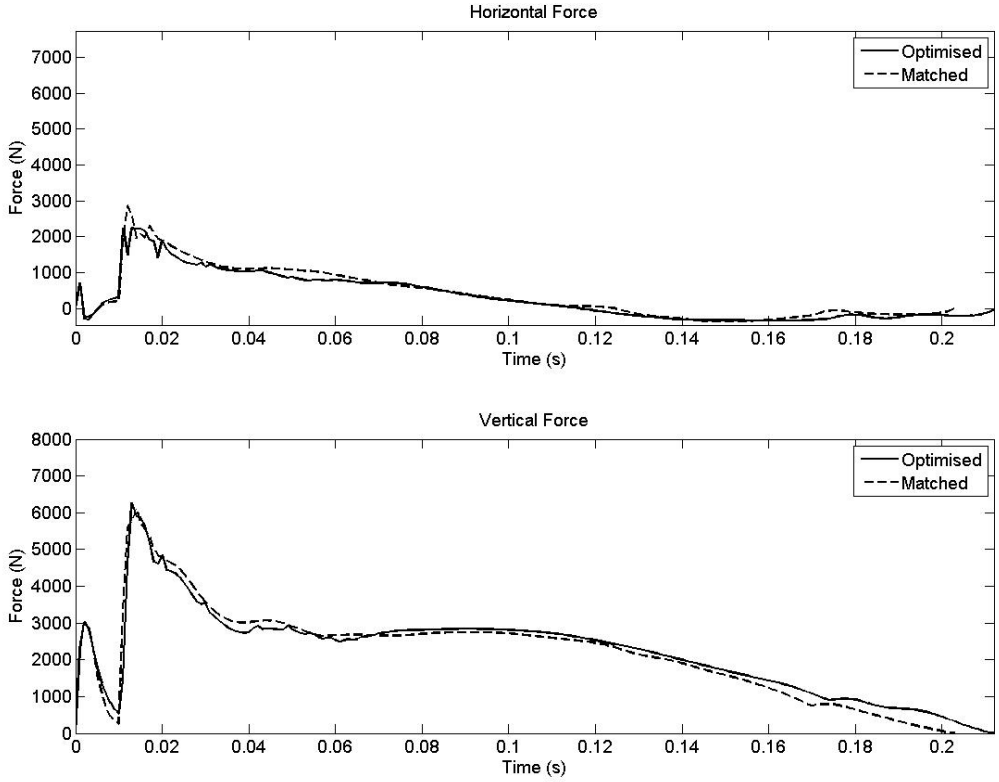

Figure 6.19 GRFs from matched (dashed lines) and optimised (solid lines) simulations of the jump phase.

Table 6.20 Impulses at take-off in matched and optimised simulations of the jump phase

Direction	Matched Impulse (Ns)	Optimised Impulse (Ns)
Horizontal	78	62
Vertical (Gross)	456	471
Vertical (Net)	311	320

Table 6.21 Take-off velocities and projection angle for matched and optimised simulations of the jump phase

Direction	Matched Velocity (m/s)	Optimised Velocity (m/s)
Horizontal	5.84	6.06
Vertical	2.12	2.23
Resultant	6.21	6.47
Projection Angle	21.3	21.6

6.4.4 Increased strength

In order to investigate the effects of increasing strength on triple jump performance, maximum isometric and eccentric torques were increased by 5% from the measured values displayed in Appendix 11. The model was optimised for jump distance in the hop phase using the method described in Section 6.3.

Components of phase distance

Table 6.22 shows that the model with increased strength jumped 0.15 m (3.4%) further than the optimised simulation with measured torques. A slight decrease in take-off distance (-0.01 m) was outweighed by an increased flight distance (0.16 m).

Table 6.22 Differences in each component of phase distance between optimised simulations of the hop phase with and without increased strength

Torques	Take-off Distance (m)	Flight Distance (m)	Landing Distance (m)	Total Distance (m)
Measured	0.55	3.23	0.65	4.43
Increased	0.54	3.39	0.65	4.58
Difference	-0.01	0.16	0.00	0.15

Figure 6.20 gives a visual representation of the optimised simulations with and without increased strength; the techniques employed in both simulations were visually very similar. There is also very little difference between the joint angle time histories (Figure 6.21). The hip angles in the increased torque conditions showed a slight increase in extension in the stance hip and an increase in flexion in the free hip, with respect to the measured torque

condition. The stance knee was more extended at take-off in the increased torque condition, having flexed slightly more, earlier in the stance phase. Also the right shoulder is slightly more flexed at take-off in the increased strength condition.

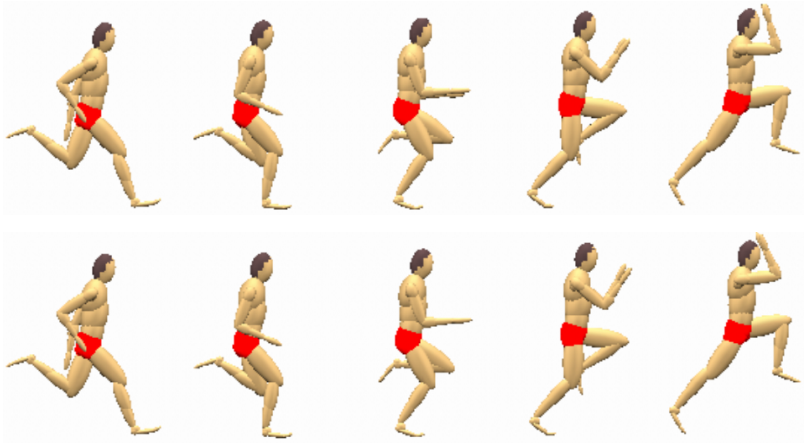

Figure 6.20 Optimised simulations of the hop phase with measured (top) and increased (bottom) strengths.

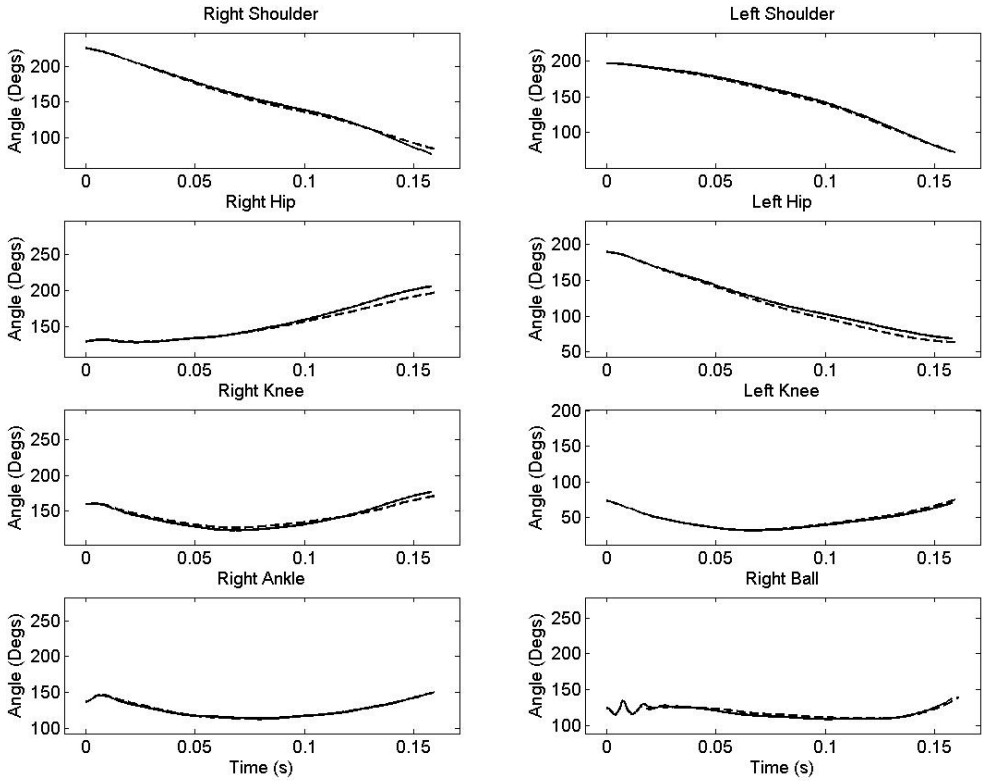

Figure 6.21 Joint angle time histories from simulations of the hop phase with measured (dashed lines) and increased (solid lines) strengths.

The joint torque time histories show that the only major difference in the increased strength condition was at the stance knee, where the torque ramps up later and is markedly higher then the optimisation with measured torques (Figure 6.22). This gives an initial indication that the stance knee is an important joint in which to increase strength in order to improve performance in the hop phase of the triple jump.

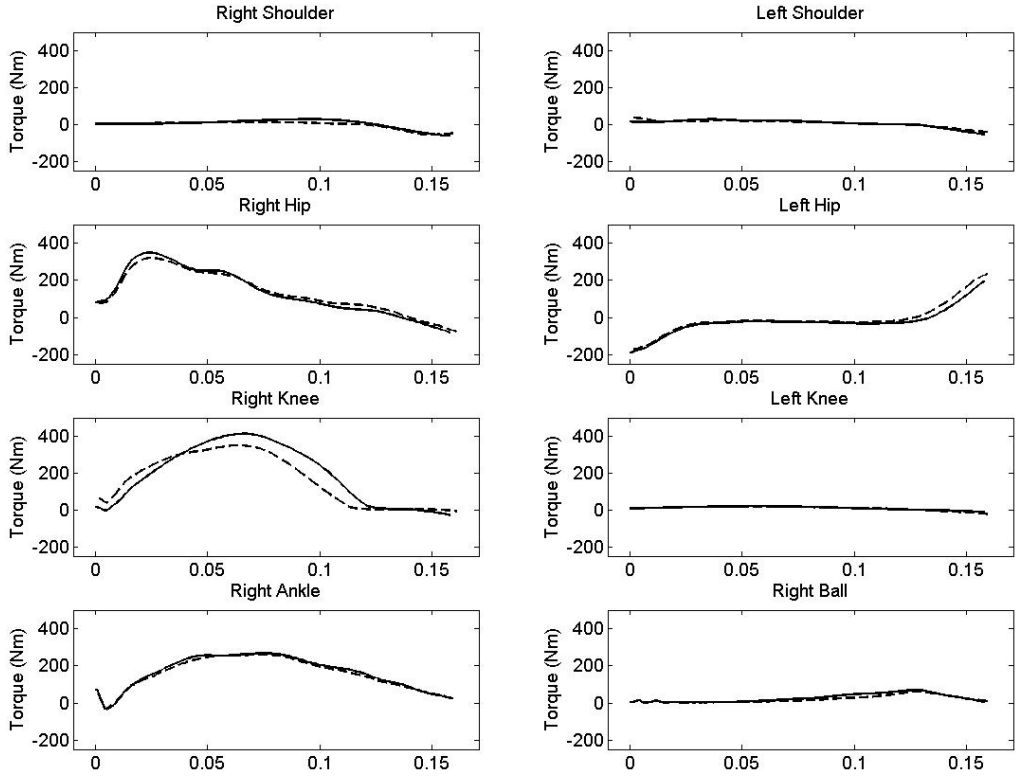

Figure 6.22 Joint torque time histories from simulations of the hop phase with measured (dashed lines) and increased (solid lines) strengths (extension is positive except at shoulder joints).

6.4.5 No angular momentum constraints

Angular momentum constraints were removed (Section 6.3.1) in order to ascertain how important they were to the performance of the model. The model was optimised for jump distance in the hop phase using the method described in Section 6.3.

Components of phase distance

Table 6.23 shows that the model without angular momentum constraints jumped 0.30 m (6.8%) further than the optimised simulation with angular momentum constraints. As with

the increased strength condition a slight decrease in take-off distance (-0.01 m) was outweighed by an increased flight distance (0.31 m).

Table 6.23 Differences in each component of phase distance between optimised simulations of the hop phase with and without constraints on angular momentum

Angular Momentum	Take-off Distance (m)	Flight Distance (m)	Landing Distance (m)	Total Distance (m)
Constrained	0.55	3.23	0.65	4.43
Unconstrained	0.54	3.54	0.65	4.73
Difference	-0.01	0.31	0.00	0.30

Figure 6.23 shows that the optimised technique without constraints on angular momentum differs markedly from that with constraints, whereas the joint angles do not show any great differences (Figure 6.24). The optimisation without constraints shows a much greater 'forward lean' of the body at take-off, whereas the optimisation with constraints has a vertically oriented torso. The free limbs also show a greater degree of flexion in the simulation without constraints. Despite this the take-off distance is slightly reduced due to the hip being less extended. The simulation without constraints exhibited a landing orientation error of 47° compared to performance kinematics (Section 5.5.2). This further demonstrates the importance of including angular momentum constraints in simulation models of human jumping. (Wilson et al., 2007).

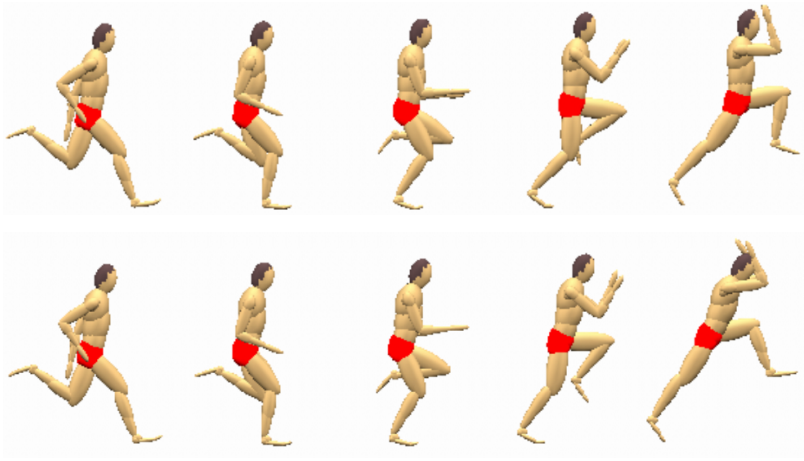

Figure 6.23 Optimised simulations of the hop phase with (top) and without (bottom) constraints on angular momentum.

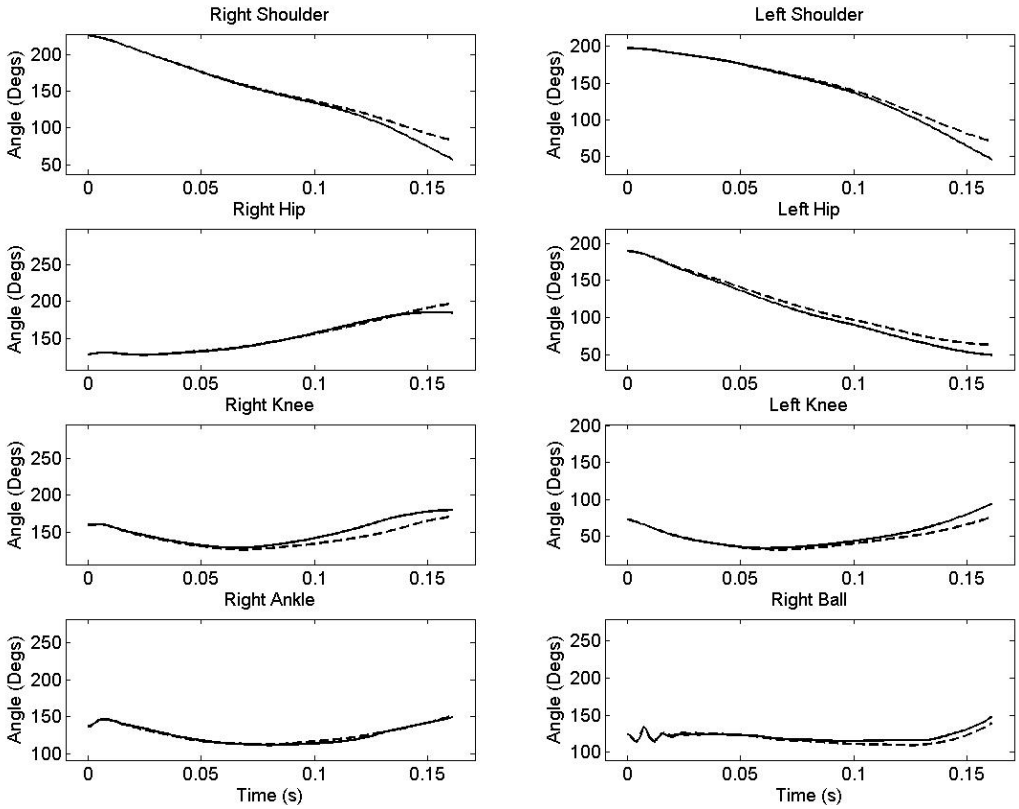

Figure 6.24 Joint angle time histories for simulations of the hop phase with (dashed lines) and without (solid lines) constraints on angular momentum.

Joint torque time histories show that the largest difference between the simulations with and without angular momentum constraints is at the hip joint of the stance leg (Figure 6.25). The simulation without constraints showed a strong hip flexion towards the end of the ground contact phase where this was not apparent in the simulation with constraints. Other than this, joint torques were broadly similar across the joints, with slight increases in knee and ankle torques of the stance leg being the other most influential differences.

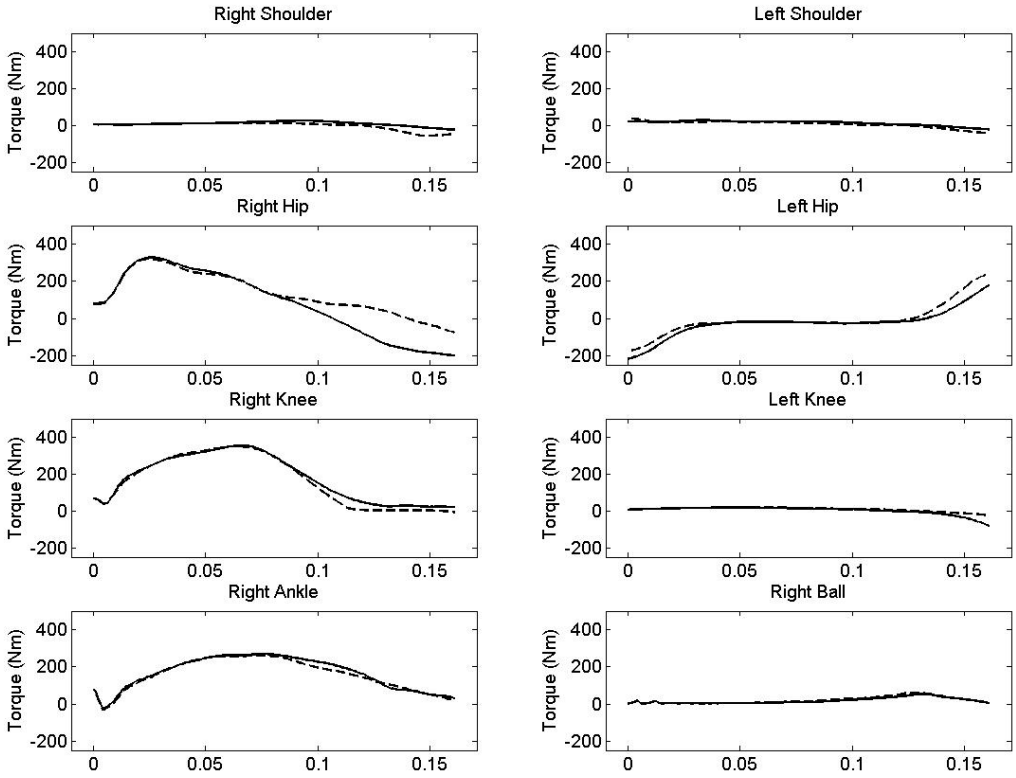

Figure 6.25 Joint torque time histories for simulations of the hop phase with (dashed lines) and without (solid lines) constraints on angular momentum (extension is positive except at shoulder joints).

6.5 CHAPTER SUMMARY

In this chapter literature on the methods of optimisation of simulation models of human jumping was reviewed. The method for optimisation of technique in the simulation model of triple jump was described. The components of the objective function were outlined and the penalties the model could incur were explained. The results of the optimisation process were discussed with reference to the differences in the kinematic and kinetic features of the model between the matched and optimised simulations. The effects of increasing strength, and neglecting angular momentum constraints on the simulation were investigated. The next chapter will provide a summary of this thesis with a discussion of methods used, areas for improvement, implications, applications, and future directions of the study.

CHAPTER 7

SUMMARY AND DISCUSSION

7.1 CHAPTER OVERVIEW

The purposes of this study were:

1. To develop a full-body torque-driven computer simulation model of triple jumping;
2. To gather anthropometric, strength, and performance data, and derive viscoelastic parameters, in order that the model would be subject-specific;
3. To evaluate the model against performance data to ensure that it was a good representation of the activity being modelled;
4. To optimise the technique of the model in order to maximise the distance jumped in each phase individually;
5. To draw conclusions on the components of optimal technique.

In this chapter the extent to which these aims have been achieved is considered. The methodologies are summarised, and limitations and potential improvements are highlighted. The results of the model are discussed with respect to the research questions posed in Chapter 1. Future applications of the model are then outlined.

7.2 DISCUSSION AND LIMITATIONS

7.2.1 Computer simulation model of triple jumping

A whole-body torque-driven model of triple jumping was developed in Autolev^{TM} comprising thirteen segments, of which five had both rigid and wobbling elements. The model was two-dimensional so only represented motion in the sagittal plane. Torque generators with flexion and extension profiles were included at each of the joints of the leg and at the shoulders. Elbow joints were angle-driven.

During a triple jump motion occurs outside the sagittal plane which cannot be represented in the model. For instance the hip and shoulder joints on either side of the body move independently of each other and were modelled as single joints. However the results of the model evaluation indicate that the model accurately represents the important features of triple jumping (Chapter 5). This indicated that these motions only had a minimal effect on performance. It was assumed that the action of the elbow joints would have only a small effect on performance and therefore simulations used angles derived from performance data in order to angle-drive these joints. However if more accuracy were required, torque profiles could be included at the elbow joints in order to simulate the effect of the arms on performance. Joints were modelled as rigid and pin-linked and did not incorporate compressions seen in real joints. The effects of this are discussed in Section 7.2.3.

7.2.2 Methodology

Anthropometric, strength, and performance data were gathered from a triple jumper of national standard (Chapter 4).

Kinematic data

Kinematic data were collected individually from each phase of a triple jump and also from a whole triple jump (Section 4.3). Forty-five retroreflective markers were tracked using an 18 camera Vicon automatic motion capture system at 480 Hz for the individual phases from the force plate in order that the kinematic data could be combined with force data. The sampling frequency was reduced to 240 Hz for the whole jump, since the large capture volume (~18 m x 2 m x 2.5 m) necessitated an increased resolution and there is a trade off between sampling frequency and resolution. Joint centres were determined from the positions of these markers and flexion / extension joint angles were calculated by 'projecting' them onto the sagittal plane.

Due to the large capture volume the system sometimes failed to track markers for the entire period. Thus in future studies using such large capture volumes more cameras should be used, if available, in order to increase the resolution and frequency, and thus the chances of tracking markers throughout the duration of the activity.

Since the triple jump involves large GRFs, skin mounted markers were sometimes lost during impacts. Skin mounted markers should be adhered as securely as possible in an attempt to limit these losses.

Obtaining kinematics that accurately represent underlying joint motions using skin-mounted markers is very difficult (Section 4.3.1). It is not practical to use bone-mounted markers or imaging techniques (dynamic MRI) during dynamic movements, so it is unlikely these errors can be removed altogether.

Force data

Force data were collected from a force platform for individual phases of the triple jump at 1000 Hz (Section 4.4.2). The force data demonstrated a high frequency component that was not representative of the motion being measured and was therefore removed using a filtering process (Section 4.5.1). Although this altered the horizontal and vertical impulses very little, this filtering process may have inadvertently removed a small portion of the actual signal. Therefore in future studies researchers should ensure that the force plate is properly housed and that the material covering it is securely attached in order to minimise any signal not representative of the activity being measured.

Torque data

Torque data were collected from an isovelocity dynamometer for the shoulder, hip, knee, and ankle at 1000 Hz (Section 4.4.4). Angular velocities ranged from -400°/s to 400°/s at 50°/s intervals. A correction was applied in order to convert crank angles to joint angles by using a mechanical goniometer to obtain joint angles at various crank angles isometrically. This correction might not properly represent this relationship during dynamic contractions. Therefore in future studies joint angles should be obtained using an automatic motion capture system during the movement thus allowing a more accurate correction to be made.

Another limitation of the protocol used was that the effects of biarticular muscles were not completely included. The inclusion of biarticular muscles in simulation models has been shown to have only a minor effect on jumping performance (van Soest et al., 1993). In this protocol angles at joints proximal and / or distal to the joint being measure were not varied

in order to ascertain the effects of any biarticular muscles crossing these joint on the measured torques. Future studies could therefore incorporate this in their joint torque data collection protocol in order that they can more accurately model the torque / angle / angular velocity relationship.

The subject could not complete the dynamic shoulder flexion protocol due to injury, therefore the seven-parameter torque / angular velocity function calculated from the shoulder extension data was also used for shoulder flexion (Section 4.7.5). It is unlikely that this will have greatly affected the data, since the peak isometric torque and torque / angle relationship were obtained for shoulder flexion and the torque / angular velocity relationship is unlikely to differ markedly between shoulder flexion and extension.

Bilateral symmetry was assumed, if increased accuracy were desired then the protocol could incorporate limbs on both sides of the body. This would greatly increase the duration of the data collection and it is unlikely any great asymmetry exists in able-bodied athletes whose performance depends on the generation of large torques on both sides of the body.

The torque parameters for the ball joint were estimated due to the difficulties in measuring torques at this joint on an isovelocity dynamometer (Section 4.7.5). It would be beneficial to develop a method of measuring torques at this joint in order to obtain accurate parameters for future models.

Anthropometric data

Anthropometric data were obtained using a geometric model (Yeadon, 1990a). Simulations of aerial movement using data from this model have been shown to reproduce realistic performances, especially for movements in the sagittal plane (Yeadon, 1990b). The distribution of mass between the rigid and wobbling elements was calculated using values from the literature (Clarys and Marfell-Jones, 1986; Clarys et al, 1984). Although attempts were made to account for the likely difference in body composition of the subject in this study and those in the literature (Section 4.7.3) there were inevitably inaccuracies. The use of imaging techniques such as CAT (Huang and Wu, 1976) or MRI (Martin et al., 1989) would allow a more accurate estimation of segmental composition and inertia parameters and should be used in future if available.

7.2.3 Viscoelastic parameter determination

The viscoelastic parameters were determined by an optimisation process (Section 5.4). The viscoelastic parameters that led to the model best matching force traces also led to an excessive depression of the foot (> 4 cm). Due to this force traces were removed from the objective function. It was hypothesised that this excessive depression was due to the rest of the system being too stiff; not accounting for compressions in the joints of the stance leg and the spine (Seyfarth et al., online). If future models are to match force traces well, the joints of the stance leg and the spine should include springs to model these compressions.

Once force traces were removed from the objective function the model matched performance data closely, with differences of 2.2%, 1.0%, and 2.4% for the hop, step, and jump phases respectively, giving an overall difference of 1.8%.

7.2.4 Evaluation and optimisation of the torque-driven model

Model evaluation

The torque-driven model was matched to performance data by varying 77 torque generator activation timings using a genetic algorithm. The initial joint angles in the stance leg were included in the optimisation process, this was in an attempt to account for errors in the kinematic data, and deformations in the joints which were not represented in the pin-linked joints of the model. A model with springs at these joints could go some way to account for these deformations (Section 7.2.3).

Each of the three phases showed a close match to performance data, with overall differences of 3.8%, 2.7%, and 3.1% for the hop, step, and jump phases respectively. This indicated the model was a good representation of the activity in question and suitable for simulation of the triple jump.

Model optimisation

The technique of the model was optimised in order to maximise distance jumped at each phase. As with the model evaluation this was achieved by varying 77 torque generator activation timings. Initial kinematics were maintained from the matched simulations.

These optimisations resulted in performance increases of 3.3%, 11.1%, and 8.2% respectively for the hop, step, and jump phases.

The most marked difference in technique between the optimised and matched simulations was at the shoulder joints. In each phase the optimised simulations demonstrated a symmetrical flexion at both shoulders, whereas the matched simulations showed an asymmetrical technique (Figures 6.3, 6.9 and 6.15). Encouragingly this symmetrical shoulder flexion is a feature of elite triple jump technique which further indicates that the model is a good representation of the system it is simulating.

In addition to this symmetrical shoulder flexion, optimised simulations showed a greater extension of the stance knee and hip and a more flexed free hip. This technique resulted in an increased ground contact time in all phases with respect to matched simulations and facilitated an increased vertical impulse (Tables 6.6, 6.13 and 6.20).

The effects of increasing strength and neglecting angular momentum constraints on the performance of the model were also investigated. These led to increases in jump distance of 3.4% and 6.8% respectively. These results indicated that strength increases could be beneficial to a triple jumper and that angular momentum constraints were necessary in simulations of jumping.

A genetic algorithm was used in order to vary torque generator activation timings in order to maximise jump distance. These optimisations typically took 24-48 hours. This time period was acceptable, but the structure of the genetic algorithm is such that it lends itself to parallel processing (van Soest and Casius, 2003). This was not employed in this case and could reduce total processing time. In future optimisations, especially those attempting to optimise three phases sequentially, this is something that should be investigated.

7.3 RESEARCH QUESTIONS

Q1. How close to optimum was the performance of the subject in this study?

The optimisation of technique revealed that the athlete was operating sub-optimally at each phase. In the hop and step phases the performances might have been limited due to requirements of the subsequent take-off. However, the fact that the jump take-off, where there was no such requirement, showed a substantial improvement in performance when optimised, might indicate that this was not the case. The optimisation of the hop phase showed an improvement of 0.14 m, from 4.29 m to 4.43 m, the majority of this being made up by an increase in take-off distance of 0.12 m. The step phase showed the largest increase of 0.43 m, from 3.89 m to 4.32 m, this improvement consisted mainly of a 0.39 m increase in flight distance. The jump phase showed an improvement of 0.35 m, from 4.28 m to 4.63 m, the majority of which was made up by an increased flight distance of 0.27 m. These changes represented percentage improvements at each phase of 3.3%, 11.1%, and 8.2% giving an overall theoretical increase of 7.4%. This is a measure of how close to optimum the technique of the subject was post-touchdown during each take-off phase. Other improvements could likely be obtained by altering initial conditions.

Q2. What is the optimum arm technique for triple jump performance?

In each optimisation of technique the results showed a symmetrical flexion of the shoulders throughout the take-off phase, this was in contrast the asymmetrical technique employed by the subject. This symmetrical flexion is referred to as the double-arm technique in the literature (Hay, 1992). An analysis of angular impulses created at the shoulder joints in the matched and optimised simulations indicated that the shoulder joint contralateral to the stance leg showed some of the largest increases in impulse of all joints in the optimised simulations (Tables 6.5, 6.12, and 6.19). However, with the exception of the left shoulder joint in the step phase, there was little difference in the work done at the shoulder joints between matched and optimised simulations. These angular impulses could act to improve performance in more than one way. Initially during the period when the shoulders are flexing from a hyperextended position it has been shown that they act to cushion the impact on the stance leg in a high jump take-off employing a double-arm

technique (Dapena and Chung, 1988). This was due to the flexion of the arms reducing the radial distance of the COM from the hip joint during the period when this distance was decreasing. This cushioning could be of major benefit in triple jumping due to the exceptionally high GRFs (Section 2.2.3). The cushioning effect would be reduced or non-existent in the asymmetrical single-arm technique, since the combined COM of the arms relative to the hip joint should not change appreciably. During the subsequent period in the same high jump take-off when the radial distance of the COM to the hip joint was increasing, the arms were shown to act to increase this distance (Dapena and Chung, 1988). The increased flexion at the shoulder joints in the optimised simulations manifested itself in increases in both the take-off distance and the COM height at take-off (Table 6.). All the optimised simulations showed an increased impulse and ground contact time (Table 6.). The symmetrical flexion of the shoulder joints could have contributed to these increases; this would accelerate the mass of the arms forwards and upwards, thus applying a reaction force though the shoulder joints, accelerating the mass of the rest of the body in the opposite direction. This could act to put the torque generators of the leg into slower concentric conditions, facilitating an increased torque production (Dapena, 1999) and / or increase the ground contact time which would also allow a larger propulsive impulse.

Q3. How would an increase in strength affect triple jump performance?

In an attempt to ascertain how an increase in strength would affect performance in the triple jump maximal isometric and eccentric torques were increased by 5% and torque generator activation timings were subsequently optimised to maximise distance jumped in the hop phase. This optimisation led to an increase in performance of 0.15 m with respect to the optimised simulation with measured torques which represented a 3.4% improvement. This improvement was wholly due to an increase in flight distance of 0.16 m as the take-off distance was reduced by -0.01 m. The technique in the increased strength simulation did not differ visually from that of the optimised simulation with measured torques. However an inspection of the torque time histories (Figure 6.22) shows that, whilst there is little difference in most joints between the two optimisations, the optimisation with increased strength shows a marked difference in knee torque, ramping up later and reaching a higher level for longer than the simulation with measured torques. This gives the impression that the most beneficial joint around which to increase strength in order to improve performance in the hop phase would be the stance knee. A wider

investigation involving each phase and variations in the maximal torques at individual joints is needed to properly assess the benefits of an increase in strength on triple jump performance.

Q4. What influence do angular momentum constraints have on simulations of the triple jump?

In order to gauge what effect angular momentum constraints have on triple jump performance, a simulation without these constraints was optimised to maximise the distance jumped. The optimisation without angular momentum constraints jumped 0.30 m further than the optimisation with constraints, representing an improvement of 6.8%. This was entirely due to an increased flight distance of 0.31 m as there was a decrease in take-off distance of -0.01 m (Table 6.23). Visually it can be seen that there is a marked difference in orientation of the trunk in the two optimisations (Figure 6.23). The optimisation without angular momentum constraints displays a large 'forward lean' which is not a feature of horizontal jumps in athletics. The orientation of the body at the landing of the next phase in this simulation was estimated to have been 47° away from the measured orientation. This lends further weight to the findings of Wilson et al. (2007) who stated that models of jumping should include constraints on angular momentum.

7.4 CONCLUSION

With respect to the purposes of this study outlined at the beginning of this chapter, a subject-specific torque-driven model of the triple jump was successfully developed, evaluated and optimised. Anthropometric, strength, and performance data were obtained from a triple jumper and viscoelastic parameters were derived using an angle-driven model, ensuring subject-specificity. A torque-driven model was then evaluated against performance data and showed a close match for each phase of the triple jump, indicating that it is a good representation of the system it was simulating. The components of optimum technique were described, quantified, and discussed. The technique employed by the model in the performance optimisations showed features that are consistent with current elite triple jump technique which is encouraging and is a further indication of the

accuracy of the model. Finally the effects of increasing strength and neglecting angular momentum constraints on simulations were also quantified.

7.5 FUTURE RESEARCH

The immediate continuation of this project will be to use the model to simulate each phase of the triple jump sequentially, rather than individually as was done in this study. In order to do this the flight phases will be included in the simulation. A spline will be used to merge the take-off angles from the simulation into the angles from the performance over the initial portion of the flight phase (~100 ms), the remainder of the flight phase will then be angle-driven. This will allow a more accurate determination of the landing orientation for the subsequent phase. The initial kinematic conditions of the subsequent phase will then be directly related to the take-off conditions from the previous phase. Simulating the whole jump in this fashion will provide information on the interdependence of the phases and what the phase ratios for optimum performance in the triple jump are. More generally, the model has been shown to accurately simulate human motion in the sagittal plane with alternating foot-ground contacts. Consequently it can be used in future to answer questions relating to any activity of this type with confidence. Research questions that will be addressed in the future include:

- What is the contribution of approach velocity to triple jump performance?
- How sensitive is triple jump performance to variations in initial conditions?
- How is triple jump performance affected in each phase by variations in strength parameters at individual joints?
- How sensitive is triple jump performance to variations in muscle activation timings?
- How do altered anthropometric and mass/inertia characteristics affect triple jump performance?
- Is a symmetrical arm technique suitable for use in long jumping?
- What are the limitations on maximum sprinting speed?

REFERENCES

AAGAARD, P., HAVROK, M., SIMONSEN, E.B., ARIEL, G. and DAHLBERG, L.,online, A kinematic analysis of the world championships triple jump final. Available: http://www.elitetrack.com/articles/triple.pdf [05/22, 2006].

ALEXANDER, R.M., 1992. Simple models of walking and jumping. *Human Movement Science,* **11**(1-2), 3-9.

ALEXANDER, R.M., 1990. Optimum take-off techniques for high and long jumps. *Philosophical Transactions of the Royal Society of London: Series B,* **329**, 3-10.

AMADIO, A.C., 1985. *Biomechanische analyse des dreisprungs*, Deutsche Sporthochschule, Koln.

ANDERSON, F.C. and PANDY, M.G., 1999. A dynamic optimization solution for vertical jumping in three dimensions. *Computer Methods in Biomechanics and Biomedical Engineering,* **2**, 201-231.

ASHBY, B.M. and DELP, S.L., 2006. Optimal control simulations reveal mechanisms by which arm movement improves standing long jump performance. *Journal of Biomechanics,* **39**(9), 1726-1734.

BALLREICH, R. and BRUGGEMANN, P., 1986. Biomechanik des weitsprungs. In: R. BALLREICH and A. KUHLOW, eds, *Biomechanik der sportarten 1. Biomechanik der Leichtathletik.* Stuttgart: Enke, pp. 28-47.

BOBBERT, M.F., 2001. Dependence of human squat jump performance on the series elastic compliance of the triceps surae: a simulation study. *Journal of Experimental Biology*, **204**, 533-542.

BOBBERT, M.F. and CASIUS, L.J.R., 2005. Is the effect of a countermovement on jump height due to active state development? *Medicine and Science in Sports and Exercise,* **37**, 440-446.

BOBBERT, M.F., CASIUS, L.J.R., SIJPKENS, I.W.T. and JASPERS, R.T., 2008. Humans adjust control to initial squat depth in vertical squat jumping. *Journal of Applied Physiology,* **105**, 1428-1440.

BOBBERT, M.F., GERRITSEN, K.G., LITJENS, M.C. and VAN SOEST, A.J., 1996. Why is countermovement jump height greater than squat jump height? *Medicine and Science in Sports and Exercise*, **28**, 1402-1412.

BOBBERT, M.F., HUIJING, P.A. and VAN INGEN SCHENAU, G. J., 1987a. Drop jumping. I. The influence of jumping technique on the biomechanics of jumping. *Medicine and Science in Sports and Exercise,* **19**(4), 332-338.

BOBBERT, M.F., HUIJING, P.A. and VAN INGEN SCHENAU, G. J., 1987b. Drop jumping. II. The influence of dropping height on the biomechanics of drop jumping. *Medicine and Science in Sports and Exercise,* **19**(4), 339-346.

BOBBERT, M.F., HUIJING, P.A. and VAN INGEN SCHENAU, G. J., 1986. An estimation of power output and work done by the human triceps surae muscle-tendon complex in jumping. *Journal of Biomechanics,* **19**(11), 899-906.

BOBBERT, M.F. and VAN INGEN SCHENAU, G. J., 1988. Coordination in vertical jumping. *Journal of Biomechanics,* **21**(3), 249-262.

BOBBERT, M.F. and VAN SOEST, A.J., 2001. Why do people jump the way they do? *Exercise and sports sciences reviews,* **29**(3), 95-102.

BOBBERT, M.F. and VAN SOEST, A.J., 1994. Effects of muscle strengthening on vertical jump height: A simulation study. *Medicine and Science in Sports and Exercise,* **26**(8), 1012-1020.

BOBBERT, M.F. and VAN ZANDWIJK, J.P., 1999. Sensitivity of vertical jumping performance to changes in muscle stimulation onset times: a simulation study. *Biological cybernetics,* **81**, 101-108.

BOSCO, C. and AND KOMI, P.V., 1979. Mechanical characteristics and fiber composition of human leg extensor muscles. *European Journal of Applied Physiology,* **24**, 21-32.

BRIDGETT, L.A. and AND LINTHORNE, N.P., 2006. Changes in long jump take-off technique with increasing run-up speed. *Journal of Sports Sciences,* , 1-9.

BRUGGEMANN, P., NIXDORF, E. and ERNST, H., 1982. Biomechanische untersuchungen beim weitsprung. *Die Lehre der Leichtathletik,* **4**, 36-40.

CARROLL, D.L., 1996. Genetic algorithms and optimizing chemical oxygen-iodine lasers. In: H. WILSON, R. BATRA, C. BERT, A. DAVIS, R. SCHAPERY, D. STEWART and F. SWINSON, eds, *Developments in theoretical and applied mechanics.* Tuscaloosa, AL: School of Engineering, The University of Alabama, pp. 411-424.

CHANDLER, R.F., CLAUSER, C.E., MCCONVILLE, J.T., REYNOLDS, H.M. and YOUNG, J.W., 1975. *Investigation of inertial properties of the human body.*

ADA016485. AIR FORCE AEROSPACE MEDICAL RESEARCH LAB WRIGHT-PATTERSON AFB OH.

CHALLIS, J.H., 1995. A procedure for determining rigid body transformation parameters. *Journal of Biomechanics,* **28**(6), 733-737.

CHOW, J.W., 2001. Isokinetic exercise and knee joint forces during isokinetic knee extensions, *Proceedings of the 25th Annual Meeting of the American Society of Biomechanics,* 2001, pp127-128.

CHOW, J.W., DARLING, W.G. and HAY, J.G., 1997. Mechanical characteristics of knee extension exercise performed on an isokinetic dynamometer. *Medicine and Science in Sports and Exercise,* **29**, 794-803.

CHOW, J.W. and HAY, J.G., 2005. Computer simulation of the last support phase of the long jump. *Medicine and Science in Sports and Exercise,* **37**, 115-123.

CLARYS, J.P. and MARFELL-JONES, M.J., 1986. Anthropometric prediction of component tissue masses in the minor limb segments of the human body. *Human Biology,* **58**(5), 761-769.

CLARYS, J.P., MARTIN, A.D. and DRINKWATER, D.T., 1984. Gross tissue weights in the human body by cadaver dissection. *Human Biology,* **54**, 459-473.

CLAYTON, H.M., 1991. Advances in motion analysis. in: veterinary clinics of north america. *Equine Practice,* **7**, 365-382.

CORANA, A., MARCHESI, M., MARTINI, C. and RIDELLA, S., 1987. Minimising multimodal functions of continuous variables with the "Simulated Annealing" algorithm. *ACM Transactions on Mathematical Software,* **12**, 262-280.

COSTA, K.E. and MCNITT-GRAY, J.L., 1999. Lower extremity power generation strategies used by elite athletes during the take-off of the long jump, *23rd Annual Meeting of the American Society of Biomechanics,* October 21-23 1999, .

DAPENA, J., 1999. A biomechanical explanation of the effect of arm actions on the vertical velocity of a standing vertical jump, *Proceedings of the XVIIth Congress of the International Society of Biomechanics,* 1999, .

DAPENA, J. and CHUNG, C.S., 1988. Vertical and radial motions of the body during the take-off phase of high jumping. *Medicine and Science in Sports and Exercise,* **20**(3), 290-302.

DEMPSTER, W.T., 1955. *Space requirements of the seated operator.* Rpt-55-159. Wright-Patterson Air Force Base: WADC.

DRILLIS, R., CONTINI, R. and BLUESTEIN, M., 1964. Body segment parameters: a survey of measurement techniques. *Artificial Limbs*, **8**, 44-66.

DUDA, G.N., BRAND, D., FREITAG, S., LIERSE, W. and SCHNEIDER, E., 1996. Variability of femoral muscle attachments. *Journal of Biomechanics,* **29**, 1185-1190.

EDMAN, K.A.P. and REGGIANI, C., 1987. The sarcomere length-tension relation determined in short segments of intact muscle fibres of the frog. *Journal of Physiology*, **385**, 709-732.

FINNI, T. and KOMI, P.V., 2002. Two methods to estimate tendinous tissue elongation during human movement. *Journal of Applied Biomechanics,* **18**, 180-188.

FORWOOD, M.R., NEAL, R.J. and WILSON, B.D., 1985. Scaling segmental moments of inertia for individual subjects. *Journal of Biomechanics,* **18**, 755-761.

FREUND, H.J. and BUDINGEN, H.J., 1978. The relationship between speed and amplitude of the fastest voluntary contractions of human arm muscles. *Experimental Brain Research,* **31**, 1-12.

FUKASHIRO, S., ILMOTO, Y., KOBAYASHI, H. and MIYASHITA, M., 1981. A biomechanical study of the triple jump. *Medicine and Science in Sports and Exercise,* **13**(4), 233-237.

GERRITSEN, K.G.M., VAN DEN BOGERT, A. J. and NIGG, B.M., 1995. Direct dynamics simulation of the impact phase in heel-toe running. *Journal of Biomechanics,* **28**(6), 661-668.

GOLDBERG, D.E., 1989. Genetic algorithms in search, optimization and machine learning. First edn. Boston, MA: Addison-Wesley.

GORDON, A.M., HUXLEY, A.F. and JULIAN, F.J., 1966. The variation in isometric tension with sarcomere length in vertebrate muscle fibers. *Journal of Physiology,* **184**, 170-192.

GRAHAM-SMITH, P. and LEES, A., 2005. A three-dimensional kinematics analysis of the long jump takeoff. *Journal of Sports Sciences,* **23**(9), 891-903.

GREIG, M.P. and YEADON, M.R., 2000. The influence of touchdown parameters on the performance of a high jumper. *Journal of Applied Biomechanics,* **16**, 367-378.

GRUBER, K., RUDER, H., DENOTH, J. and SCHNEIDER, K., 1998. A comparative study of impact dynamics: wobbling mass model versus rigid body models. *Journal of Biomechanics,* **31**(5), 439-444.

HARRY, J.D., WARD, A.W., HEGLUND, N.C., MORGAN, D.L. and MCMAHON, T.A., 1990. Cross-bridge cycling theories cannot explain high-speed lengthening behaviour in frog muscle. *Biophysical Journal,* **57**, 201-208.

HATZE, H., 1981. A comprehensive model for human motion simulation and its application to the take-off phase of the long jump. *Journal of Biomechanics*, **14**(3), 135-142.

HATZE, H., 1980. A mathematical model for the computational determination of parameter values of anthropomorphic segments. *Journal of Biomechanics,* **13**(10), 833-843.

HATZE, H., 1975. A new method for the simultaneous measurement of the moment of inertia, the damping coefficient and the location of the centre of mass of a body segment *in situ*. *European Journal of Applied Physiology,* **34**, 217-226.

HAY, J.G., 1999. Effort distribution and performance of Olympic triple jumpers. *Journal of Applied Biomechanics,* **15**, 36-51.

HAY, J.G., 1997. Phase distances, percentages, and techniques in the men's triple jump at the 1996 U.S. Olympic trials. *Track Coach,* **139**, 4435-4442.

HAY, J.G., 1995. The case for a jump dominated technique in the triple jump. *Track Coach,* **132**, 4214-4219.

HAY, J.G., 1993. Citius, altius, longius (faster, higher, longer): the biomechanics of jumping for distance. *Journal of Biomechanics,* **26**, 7-21.

HAY, J.G., 1992. The biomechanics of the triple jump: a review. *Journal of Sports Sciences,* **10**, 343-378.

HAY, J.G., 1987. Biomechanics of the long jump - and some wider implications. In: R.C. NELSON and C.A. MOREHOUSE, eds, *Biomechanics IV.* First edn. Human Kinetics, pp. 1193-1203.

HAY, J.G., 1986. The biomechanics of the long jump. *Exercise and sports science reviews,* **14**, 401-446.

HAY, J.G., THORSON, E.M. and KIPPENHAN, B.C., 1999. Changes in muscle-tendon length during the take-off of a running long jump. *Journal of Sports Sciences,* **17**, 159-172.

HERZOG, W., 1986. Maintenance of body orientation in the flight phase of long jumping. *Medicine and science in sports and exercise,* **18**(2), 231-241.

HILEY, M.J. and YEADON, M.R., 2001. Swinging around the high bar. *Physics Education,* **36**(1), 14-17.

HILL, A.V., 1938. The heat of shortening and the dynamic constants of muscle. *Proceedings of the Royal Society of London. Series B, Biological Sciences*, **126**(843), 136-195.

HINRICHS, R.N., 1985. Regression equations to predict segmental moments of inertia from anthropometric measurements: An extension of the data of Chandler et al. (1975). *Journal of Biomechanics*, **18**(8), 621-624.

HOLLAND, J.H., 1975. Adaptation in natural and artificial systems. First edn. Ann Arbor: University of Michigan Press.

HOUTKOOPER, L., MAURER ABBOT, J. and NIMMO, M., 2007. Nutrition for throwers, jumpers and combined events athletes. *Journal of Sports Sciences*, **25**(1), S39-S47.

HUANG, H.K. and WU, S.C., 1976. The evaluation of mass densities of human body in vivo from CT scans. *Computers in Biology and Medicine*, **6**, 337-343.

HUDSON, J.L., 1986. Coordination of segments in the vertical jump. *Medicine and Science in Sports and Exercise*, **18**, 242-251.

HUXLEY, A.F., 1957. Muscle structure and theories of contraction. *Progress in Biophysics and Biophysical Chemistry*, **7**, 255-318.

JACOBS, R., BOBBERT, M.F. and VAN INGEN SCHENAU, G. J., 1996. Mechanical output from individual muscles during explosive leg extensions: The role of biarticular muscles. *Journal of Biomechanics*, **29**(4), 513-523.

JENSEN, R.K., 1978. Estimation of the biomechanical properties of three body types using a photogrammetric method. *Journal of Biomechanics*, **11**, 349-358.

KAKIHANA, W. and SUZUKI, S., 2001. The EMG activity and mechanics of the running jump as a function of take-off angle. *Journal of Electromyography and Kinesiology*, **11**, 365-372.

KANE, T.R. and LEVINSON, D.A., 1996. Dynamics online: theory and implementations with AUTOLEV. First edn. Sunnyvale: Online Dynamics Inc.

KANE, T.R. and LEVINSON, D.A., 1985. Dynamics: theory and applications. First edn. New York: McGraw-Hill Book Co.

KELLIS, E., ARAMBATZI, F. and PAPADOPOULOS, C., 2003. Muscle co-activation around the knee in drop jumping using the co-contraction index. *Journal of Electromyography and Kinesiology*, **13**(3), 229-238.

KIMIZUKA, M., KUROSAWA, H. and FUKUBAYASHI, T., 1980. Load-bearing pattern of the ankle joint contact area and pressure distribution. *Archives of Orthopaedic and Traumatic Surgery,* **96**, 45-49.

KING, M.A., 1998. *Contributions to performance in dynamic jumps,* Loughborough University.

KING, M.A., YEADON, M.R. and WILSON, C., 2006. Evaluation of a torque-driven computer simulation model of jumping. *Journal of Applied Biomechanics,* **22**, 264-274.

KIRKPATRICK, S., GELATT, C.D. and VECCHI, M.P., 1983. Optimization by simulated annealing. *Science,* **220**(4598), 671-680.

KOH, T.J. and HAY, J.G., 1990a. Landing leg motions and performance in the horizontal jumps I: the long jump. *International Journal of Sports Biomechanics,* **6**, 343-360.

KOH, T.J. and HAY, J.G., 1990b. Landing leg motions and performance in the horizontal jumps II: the triple jump. *International Journal of Sports Biomechanics,* **6**, 361-373.

KOMI, P.V. and BOSCO, C., 1978. Utilization of stored elastic energy in men and women. *Medicine and Science in Sports and Exercise,* **10**, 261-265.

KUTSAR, K., 1988. An overview of common injuries in track and field events. *Modern Athlete and Coach (Australia),* **26**, 3-6.

LAFORTUNE, M.A., CAVANAGH, P.R., SOMMER III, H.J. and KALENAK, A., 1992. Three-dimensional kinematics of the human knee during walking. *Journal of Biomechanics,* **25**(4), 347-357.

LEES, A., FOWLER, N. and DERBY, D., 1993. A biomechanical analysis of the last stride, touch-down and take-off characteristics of the women's long jump. *Journal of Sports Sciences,* **11**(4), 303-314.

LEES, A., GRAHAM-SMITH, P. and FOWLER, N., 1994. A biomechanical analysis of the last stride, touchdown, and takeoff characteristics of the men's long jump. *Journal of Applied Biomechanics,* **10**, 61-78.

LINTHORNE, N.P., 2001. Analysis of standing vertical jumps using a force platform. *American Journal of Physics,* **69**, 1198-1204.

LINTHORNE, N.P., GUZMAN, M.S. and BRIDGETT, L.A., 2005. Optimum take-off angle in the long jump. *Journal of Sports Sciences,* **23**, 703-712.

LINTHORNE, N.P. and KEMBLE, B.A., 1998. Take-off technique in the high jump, *Proceedings I of the XVI International Symposium on Biomechanics in Sports,* July 21-25 1998, pp356-359.

LOCATELLI, M., 2000. Simulated annealing algorithms for continuous global optimization: convergence conditions. *Journal of Optimization Theory and Applications,* **104**, 121-133.

LUTTGENS, K. and HAMILTON, N., 1997. Kinesiology: scientific basis of human motion. Ninth edn. Madison, WI: Brown & Benchmark.

MADSEN, O.R., 1996. Trunk extensor and flexor strength measured by the Cybex 6000 dynamometer. Assessment of short-term and long-term reproducibility of several strength variables. *Spine,* **21**, 2770-2776.

MARTIN, P., MUNGIOLE, M., MARZKE, M. and LONGHILL, J., 1989. The use. of magnetic resonance imaging for measuring segment inertial properties. *Journal of Biomechanics,* **22**, 367-376.

MATVEYEV, A.E., 1985. Analysis of the push-off technique of the running triple jump. *Theory and Practice and Physical Education,* **12**, 5-6.

MCINTOSH, P. and HAYLEY, H.W.B., 1952. An investigation into the running long jump. *Journal of Physical Education,* **54**, 105-108.

MILLER, J.A. and HAY, J.G., 1986. Kinematics of a world record and other world-class performances in the triple jump. *International Journal of Sports Biomechanics,* **2**, 272-288.

MILLINGTON, S.A., LI, B., TANG, J., TRATTNIG, S., CRANDALL, J.R., HURWITZ, S.R. and ACTON, S.T., 2007a. Quantitative and topographical evaluation of ankle articular cartilage using high resolution MRI. *Journal of Orthopaedic Research,* **25**(2), 143-151.

MILLINGTON, S.A., GRABNER, M., WOZELKA, R., HURWITZ, S.R. and CRANDALL, J.R., 2007b. A stereophotographic study of ankle joint contact area. *Journal of Orthopaedic Research,* **25**, 1465-1473.

MINETTI, A.E., ARDIGO, L.P., SUSTA, D. and COTELLI, F., 1998. Using leg muscles as shock absorbers: theoretical predictions and experimental results of drop landing. *Ergonomics,* **41**(12), 1771-1791.

MINETTI, A.E. and BELLI, G., 1994. A model for the estimation of visceral mass displacement in periodic movements. *Journal of Biomechanics,* **27**(1), 97-101.

MÜNDERMANN, L., CORAZZA, S. and ANDRIACCHI, T.P., 2006. The evolution of methods for the capture of human movement leading to markerless motion capture for biomechanical applications. *Journal of NeuroEngineering and Rehabilitation,* **3**, 6.

NIGG, B.M. and YEADON, M.R., 1987. Biomechanical aspects of playing surfaces. *Journal of Sports Sciences,* **18**(5), 117-145.

NISELL, R., NEMETH, G. and OHLSEN, H., 1986. Joint forces in extension of the knee: Analysis of a mechanical model. *Acta Orthopaedica Scandinavica,* **57**, 41-46.

OSTERNIG, L.R., SAWHILL, J.A., BATES, B.T. and HAMILL, J., 1982. A method for rapid collection and processing of isokinetic data. *Research Quarterly for Exercise and Sport,* **53**, 252-256.

PAIN, M.T.G., 1999. *An analysis of human soft tissue,* Penn State University.

PAIN, M.T.G. and CHALLIS, J.H., 2006. The influence of soft tissue movement on ground reaction forces, joint torques and joint reaction forces in drop landings. *Journal of Biomechanics,* **39**(1), 119-124.

PAIN, M.T.G. and CHALLIS, J.H., 2004. Wobbling mass influence on impact ground reaction forces: a simulation model sensitivity analysis. *Journal of Applied Biomechanics,* **20**(3), 309-316.

PAIN, M.T.G. and CHALLIS, J.H., 2001. The role of the heel pad and shank soft tissue during impacts: a further resolution of a paradox. *Journal of Biomechanics,* **34**(3), 327-333.

PANDY, M.G. and ZAJAC, F.E., 1991. Optimal muscular coordination strategies for jumping. *Journal of Biomechanics,* **24**(1), 1-10.

PANDY, M.G., ZAJAC, F.E., SIM, E. and LEVINE, W.S., 1990. An optimal control model for maximum-height human jumping. *Journal of Biomechanics,* **23**(12), 1185-1198.

PERTTUNEN, J., 2000. Biomechanical loading in the triple jump. *Journal of Sports Sciences,* **18**, 363-370.

PIERRYNOWSKI, M.R., 1995. Analytic representation of muscle line of action and geometry. In: P. ALLARD, I.A.F. STOKES and J. BLANCHI, eds, *Three-Dimensional Analysis of Human Movement.* Champaign, IL: Human Kinetics, pp. 215-256.

PLAGENHOEF, S., EVANS, F.G. and ABDELNOUR, T., 1983. Anatomical data for analyzing human motion. *Research Quarterly for Exercise and Sport,* **54**, 169-178.

RAMEY, M.R., 1973. Use of force plates for long jump studies. *Medicine and Sport,* **8**.

RAMEY, M.R. and WILLIAMS, K.R., 1985. Ground reaction forces in the triple jump. *International Journal of Sports Sciences,* **1**, 233-239.

REINSCHMIDT, C., VAN DEN BOGERT, A. J., LUNDBERG, A., NIGG, B.M., MURPHY, N., STACOFF, A. and STANO, A., 1997b. Tibiofemoral and tibiocalcaneal motion during walking: external vs skeletal markers. *Gait & Posture,* **6**, 98-109.

REINSCHMIDT, C., VAN DEN BOGERT, A. J., NIGG, B.M., LUNDBERG, A. and MURPHY, N., 1997a. Effect of skin movement on the analysis of skeletal knee joint motion during running. *Journal of Biomechanics,* **30**(7), 729-732.

RICHARDS, J.G., 1999. The measurement of human motion: a comparison of commercially available systems. *Human Movement Science,* **18**, 589-602.

RIDKA-DRDACKA, E., 1986. A mechanical model of the long jump and its application to a technique of preparatory and takeoff phases. *International Journal of Sports Biomechanics,* **2**, 289-300.

RIENER, R. and EDRICH, T., 1999. Identification of passive elastic joint moments in the lower extremities. *Journal of Biomechanics,* **32**(5), 539-544.

RUGG, S.G., GREGOR, R.J., MANDELBAUM, B.R. and CHIU, L., 1990. In vivo moment arm calculations at the ankle using magnetic resonance imaging (MRI). *Journal of Biomechanics,* **23**(5), 495-497, 499-501.

SELBIE, W.S. and CALDWELL, G.E., 1996. A simulation study of vertical jumping from different starting postures. *Journal of Biomechanics,* **29**(9), 1137-1146.

SEYFARTH, A., BLICKHAN, R. and VAN LEEUWEN, J.L., 2000. Optimum takeoff techniques and muscle design for long jump. *Journal of Experimental Biology,* **203**, 741-750.

SEYFARTH, A., BOBBERT, M.F. and BLICKHAN, R., 17/07/2000, 2000-last update, the origin of spring-like leg behaviour in long jump. Available: http://www2.uni-jena.de/bewsys/projects/pr_c1a.htm [03/24, 2006].

SEYFARTH, A., FRIEDRICHS, A., WANK, V. and BLICKHAN, R., 1999. Dynamics of the long jump. *Journal of Biomechanics,* **32**(12), 1259-1267.

SORENSEN, H., SIMONSEN, E.B. and VAN DEN BOGERT, A. J., 1999. A simulation model of the long jump takeoff, *Proceedings of the VIIth International Symposium on Computer Simulation in Biomechanics,* August 5-7 1999.

STEFANYSHYN, D.J. and NIGG, B.M., 1998. Contributions of the lower extremity joints to mechanical energy in running vertical jumps and running long jumps. *Journal of Sports Sciences*, **16**, 177-186.

TIUPA, V.V., ALESHINSKI, S.I., PRIMAKOV, I.N. and PEREVERZEV, A.P., 1982. The biomechanics of the movement of the body's centre of mass during the long jump. *Theory and Practise of Physical Culture,* , 11-14.

TUPLING, S.J. and PIERRYNOWSKI, M.R., 1987. Use of Cardan angles to locate rigid bodies in three-dimensional space. *Medical and Biological Engineering and Computing*, **25**, 527-532.

VANRENTERGHEM, J., BOBBERT, M.F., CASIUS, L.J.R. and DE CLERCQ, D., 2008. Is energy expenditure taken into account in human sub-maximal jumping? – A simulation study. *Journal of Electromyography and Kinesiology,* **18**(1), 108-115.

VAN SOEST, A.J. and BOBBERT, M.F., 1993. The contribution of muscle properties in the control of explosive movements. *Biological cybernetics,* **69**, 195-204.

VAN SOEST, A.J. and CASIUS, L.J.R., 2003. The merits of a parallel genetic algorithm in solving hard optimisation problems. *Journal of Biomechanical Engineering,* **125**, 141-146.

VAN SOEST, A.J., SCHWAB, A.L., BOBBERT, M.F. and VAN INGEN SCHENAU, G. J., 1993. The influence of the biarticularity of the gastrocnemius muscle on vertical-jumping achievement. *Journal of Biomechanics,* **26**(1), 1-8.

VIITASALO, J.T., SALO, A. and LAHTINEN, J., 1998. Neuromuscular functioning of athletes and non-athletes in the drop jump. *European Journal of Applied Physiology*, **78**, 432-440.

WAKAI, M. and LINTHORNE, N.P., 2005. Optimum take-off angle in the standing long jump. *Human Movement Science,* **24**(1), 81-96.

WAKAI, M. and LINTHORNE, N.P., 2002. Optimum takeoff angle in the standing long jump. In: S. UJIHASHI and S.J. HAAKE, eds, *The Engineering of Sport 4: Proceedings of the 4th International Conference on The Engineering of Sport, Kyoto, 3-6 September 2002.* Oxford: Blackwell Science, pp. 817-823.

WESTING, S.H., SEGER, J.Y., KARLSON, E. and EKBLOM, B., 1988. Eccentric and concentric torque-velocity characteristics of the quadriceps femoris in man. *European Journal of Applied Physiology,* **58**, 100-104.

WESTING, S.H., SEGER, J.Y. and THORSTENSSON, A., 1990. Effects of electrical stimulation on eccentric and concentric torque-velocity relationships during knee extension in man. *Acta Physiologica Scandinavica,* **140**, 17-22.

WILSON, C., KING, M.A. and YEADON, M.R., 2006. Determination of subject-specific model parameters for visco-elastic elements. *Journal of Biomechanics,* **39**(10), 1883-1890.

WILSON, C., YEADON, M.R. and KING, M.A., 2007. Considerations that affect optimised simulation in a running jump for height. *Journal of Biomechanics,* **40**(14), 3155-3161.

WILSON, C., YEADON, M.R. and KING, M.A., 2004. Optimisation of running jumps. *Journal of Sports Sciences,* **22**(3), 246-247.

WOOD, G.A. and JENNINGS, L.S., 1979. On the use of spline functions for data smoothing. *Journal of Biomechanics,* **12**, 477-479.

YANG, G., REINSTEIN, L.E., PAI, S., XU, Z. and CARROLL, D.L., 1998. A new genetic algorithm technique in optimization of permanent 125I prostate implants. *Medical Physics*, **25**(12), 2308-2315.

YEADON, M.R., 1990a. The simulation of aerial movement—II. A mathematical inertia model of the human body. *Journal of Biomechanics,* **23**(1), 67-74.

YEADON, M.R., 1990b. The simulation of aerial movement—IV. A computer simulation model. *Journal of Biomechanics,* **23**(1), 85-89.

YEADON, M.R. and CHALLIS, J.H., 1994. The future of performance-related sports biomechanics research. *Journal of Sports Sciences*, **12**, 3-32.

YEADON, M.R. and HILEY, M.J., 2000. The mechanics of the backward giant circle on the high bar. *Human Movement Science,* **19**(2), 153-173.

YEADON, M.R. and KING, M.A., 2002. Evaluation of a torque-driven simulation model of tumbling. *Journal of Applied Biomechanics,* **18**, 195-206.

YEADON, M.R., KING, M.A., FORRESTER, S.E., CALDWELL, G.E. and PAIN, M.T.G., Accepted for publication. The need for muscle co-contraction prior to a landing. *Journal of Biomechanics*.

YEADON, M.R., KING, M.A. and WILSON, C., 2006. Modelling the maximum voluntary joint torque/angular velocity relationship in human movement. *Journal of Biomechanics,* **39**(3), 476-482.

YEADON, M.R. and MORLOCK, M., 1989. The appropriate use of regression equations for the estimation of segmental inertia parameters. *Journal of Biomechanics,* **22**(6-7), 683-689.

YU, B., 1999. Horizontal-to-vertical velocity conversion in the triple jump. *Journal of Sports Sciences,* **17**, 221-229.

YU, B. and ANDREWS, J.G., 1998. The relationship between free limb motions and performance in the triple jump. *Journal of Applied Biomechanics,* **14**, 223-237.

YU, B. and HAY, J.G., 1996. Optimum phase ratio in the triple jump. *Journal of Biomechanics,* **29**(10), 1283-1289.

YU, B. and HAY, J.G., 1995. Angular momentum and performance in the triple jump. A cross-sectional analysis. *Journal of Applied Biomechanics,* **11**, 81-102.

APPENDIX 1

PARAMETERS FOR CALCULATION OF SEC STIFFNESS

Joint Action	Muscle	α (deg)	Lb (mm)	Lf (mm)	Lt (mm)
Ankle Dorsi	Tibialis Anterior	9	117	99	217
Ankle Plantar	Gastrocnemius	13.03	240.58	74.45	213.13
	Soleus	26	129	49	227
Knee Extension	Rectus Femoris	10	302	88	186
	Vastus Lateralis	11	273	110	138
	Vastus Medialis	10	360	112	49
	Vastus Intermedius	6	320	106	87
Knee Flexion	Biceps Femoris	15	152	146	96
	other Hamstrings	10.73	291.01	98.65	141.11
	Gastrocnemius	13.03	240.58	74.45	213.13
Hip Extension	Gluteus Maximus	1.43	172.43	162.91	232.83
	Hamstrings	10.73	291.01	98.65	141.11
Hip Flexion	Psoas Major	5	238	190	54
	Rectus Femoris	10	302	88	186

Joint Action	Muscle	Lsec (mm)	d (mm)	Height (cm)	PCSA (mm^2)	SEC Stiffness (Nm/rad)
Ankle Dorsi	Tibialis Anterior	241	40.3	168	2040	**195.03**
Ankle Plantar	Gastrocnemius	390	46	178	6167	**641.45**
	Soleus	319	46	178	11868	
Knee Extension	Rectus Femoris	410	42	178	3367	**981.99**
	Vastus Lateralis	310	42	178	6880	
	Vastus Medialis	305	42	178	4674	
	Vastus Intermedius	308	42	178	5368	
Knee Flexion	Biceps Femoris	109	26	178	1024	**508.27**
	other Hamstrings	343	26	178	7807	
	Gastrocnemius	390	17	178	6167	
Hip Extension	Gluteus Maximus	248	62	178	4171	**2274.73**
	Hamstrings	343	77	178	7807	
Hip Flexion	Psoas Major	105	4	178	1383	**300.60**
	Rectus Femoris	410	35	178	3367	

APPENDIX 2

AUTOLEV CODE FOR A COMPUTER SIMULATION MODEL OF THE TRIPLE JUMP

```
%TRIPLEJUMP.AL
%AUTOLEV CODE FOR 14 SEGMENT (HEAD ANGLE IS FIXED) COMPUTER
%SIMULATION MODEL OF TRIPLE JUMP

%--------------------------------------------------------------------------------------------
% PHYSICAL DECLARATIONS

NEWTONIAN N % WHERE N2 IS UP, N1 RIGHT AND N3 = N1 X N2
BODIES RF1,LF1,RF2,LF2
BODIES RS,LS,RTH,LTH,TR,HD,RUA,LUA,RFA,LFA
BODIES WRS,WLS,WRTH,WLTH,WTR
POINTS P{27},CM,O

%--------------------------------------------------------------------------------------------
% MATHEMATICAL DECLARATIONS

CONSTANTS LRF1,LLF1,LRF21,LRF22,LLF21,LLF22
CONSTANTS LRS,LLS,LRTH,LLTH,LTR,LHD,LRUA,LLUA,LRFA,LLFA
CONSTANTS LWRS,LWLS,LWRTH,LWLTH,LWTR
CONSTANTS LRSO,LLSO,LRTHO,LLTHO,LTRO,LHDO,LRUAO,LLUAO,
          LRFAO,LLFAO
CONSTANTS LRF2O1,LRF2O2,LLF2O1,LLF2O2,LRF1O,LLF1O
CONSTANTS LWRSO,LWLSO,LWRTHO,LWLTHO,LWTRO
CONSTANTS IRF1,ILF1,IRF2,ILF2
CONSTANTS IRS,ILS,IRTH,ILTH,ITR,IHD,IRUA,ILUA,IRFA,ILFA
CONSTANTS IWRS,IWLS,IWRTH,IWLTH,IWTR
CONSTANTS K{18},G,M,NANG
VARIABLES ARSHOE,ALSHOE,ARHIPE,ALHIPE,ARKNEE,ALKNEE,
          ARANKE,ALANKE,ARBALE,ALBALE
VARIABLES ARSHOF,ALSHOF,ARHIPF,ALHIPF,ARKNEF,ALKNEF,
          ARANKF,ALANKF,ARBALF,ALBALF
VARIABLES WRSHOE,WLSHOE,WRHIPE,WLHIPE,WRKNEE,WLKNEE,
          WRANKE,WLANKE,WRBALE,WLBALE
VARIABLES WRSHOF,WLSHOF,WRHIPF,WLHIPF,WRKNEF,WLKNEF,
          WRANKF,WLANKF,WRBALF,WLBALF
VARIABLES Q{30}',U{30}'
VARIABLES TQLUALFA,TQRUARFA

%--------------------------------------------------------------------------------------------
% SPECIFIED VARIABLES
```

```
SPECIFIED TQRSHOE,TQLSHOE,TQRHIPE,TQLHIPE,TQRKNEE,TQLKNEE,
          TQRANKE,TQLANKE,TQRBALE,TQLBALE
SPECIFIED TQRSHOF,TQLSHOF,TQRHIPF,TQLHIPF,TQRKNEF,
          TQLKNEF,TQRANKF,TQLANKF,TQRBALF,TQLBALF
SPECIFIED RFARUA",LFALUA"
SPECIFIED POP{1:27}X,POP{1:27}Y,POCMX',POCMY',VOCMX,VOCMY
SPECIFIED H,KE,PE,TE,SIMCOP
SPECIFIED STRETCH{1:10}'
SPECIFIED RXT, RYT,R{1:6}X,R{1:6}Y

%-----------------------------------------------------------------------------------------------
% SET TORQUES EQUAL TO T^3 TO OBTAIN TWO DERIVATIVES IN
% FORTRAN

TQTRRUA = T^3
TQTRLUA = T^3
TQTRRTH = T^3
TQTRLTH = T^3
TQRTHRS = T^3
TQLTHLS = T^3
TQRSRF2 = T^3
TQLSLF2 = T^3
TQRF2RF1 = T^3
TQLF2LF1 = T^3

%-----------------------------------------------------------------------------------------------
% SET ELBOW ANGLES EQUAL TO T^3 TO OBTAIN TWO DERIVATIVES IN
% FORTRAN

RFARUA = T^3
LFALUA = T^3

%-----------------------------------------------------------------------------------------------
% SIMPLIFY
AUTOZ OFF

%-----------------------------------------------------------------------------------------------
% MASS AND INERTIA

MASS RF1 = MRF1
MASS LF1 = MLF1
MASS RF2 = MRF2
MASS LF2 = MLF2
MASS RS = MRS
MASS LS = MLS
MASS RTH = MRTH
MASS LTH = MLTH
MASS TR = MTR
MASS HD = MHD
```

```
MASS RUA = MRUA
MASS LUA = MLUA
MASS RFA = MRFA
MASS LFA = MLFA
MASS WRS = MWRS
MASS WLS = MWLS
MASS WRTH = MWRTH
MASS WLTH = MWLTH
MASS WTR = MWTR

M = MRF1+MLF1+MRF2+MLF2+MRS+MLS+MRTH+MLTH+MTR+
&MRUA+MLUA+MRFA+MLFA+MWRS+MWLS+MWRTH+MWLTH+MWTR

INERTIA RF1,0,0,IRF1
INERTIA LF1,0,0,ILF1
INERTIA RF2,0,0,IRF2
INERTIA LF2,0,0,ILF2
INERTIA RS,0,0,IRS
INERTIA LS,0,0,ILS
INERTIA RTH,0,0,IRTH
INERTIA LTH,0,0,ILTH
INERTIA TR,0,0,ITR
INERTIA HD,0,0,IHD
INERTIA RUA,0,0,IRUA
INERTIA LUA,0,0,ILUA
INERTIA RFA,0,0,IRFA
INERTIA LFA,0,0,ILFA
INERTIA WRS,0,0,IWRS
INERTIA WLS,0,0,IWLS
INERTIA WRTH,0,0,IWRTH
INERTIA WLTH,0,0,IWLTH
INERTIA WTR,0,0,IWTR

%-----------------------------------------------------------------------------------------------
% SEGMENT ORIENTATION

SIMPROT (N,TR,3,Q1)
SIMPROT (TR,RUA,3,Q2)
SIMPROT (TR,LUA,3,Q3)
SIMPROT (RUA,RFA,3,RFARUA)
SIMPROT (LUA,LFA,3,LFALUA)
SIMPROT (TR,RTH,3,Q4)
SIMPROT (TR,LTH,3,Q5)
SIMPROT (RTH,RS,3,Q6)
SIMPROT (LTH,LS,3,Q7)
SIMPROT (RS,RF2,3,Q8)
SIMPROT (LS,LF2,3,Q9)
SIMPROT (RF2,RF1,3,Q10)
SIMPROT (LF2,LF1,3,Q11)
SIMPROT (RS,WRS,3,Q12)
```

```
SIMPROT (LS,WLS,3,Q13)
SIMPROT (RTH,WRTH,3,Q14)
SIMPROT (LTH,WLTH,3,Q15)
SIMPROT (TR,WTR,3,Q16)
SIMPROT (TR,HD,3,NANG)

%-----------------------------------------------------------------------------------------------
% POSITION VECTORS

P_O_P1> = Q17*N1>+Q18*N2>
P_P1_RF1O> = LRF1O*RF11>
P_P1_P2> = LRF1*RF11>
P_P2_RF2O> = LRF2O1*RF21>+LRF2O2*RF22>
P_P2_P3> = LRF21*RF21>
P_P3_P4> = LRF22*RF22>
P_P3_RSO> = LRSO*RS1>
P_P3_P5> = LRS*RS1>
P_P3_P17> = Q19*RS1>+Q20*RS2>
P_P17_WRSO> = LWRSO*WRS1>
P_P17_P18> = LWRS*WRS1>
P_P5_RTHO> = LRTHO*RTH1>
P_P5_P6> = LRTH*RTH1>
P_P5_P19> = Q21*RTH1>+Q22*RTH2>
P_P19_WRTHO> = LWRTHO*WRTH1>
P_P19_P20> = LWRTH*WRTH1>
P_P6_LTHO> = LLTHO*LTH1>
P_P6_P7> = LLTH*LTH1>
P_P6_P21> = Q23*LTH1>+Q24*LTH2>
P_P21_WLTHO> = LWLTHO*WLTH1>
P_P21_P22> = LWLTH*WLTH1>
P_P7_LSO> = LLSO*LS1>
P_P7_P8> = LLS*LS1>
P_P7_P23> = Q25*LS1>+Q26*LS2>
P_P23_WLSO> = LWLSO*WLS1>
P_P23_P24> = LWLS*WLS1>
P_P8_LF2O> = LLF2O1*LF21>+LLF2O2*LF22>
P_P8_P9> = LLF22*LF22>
P_P8_P10> = LLF21*LF21>
P_P10_LF1O> = LLF1O*LF11>
P_P10_P11> = LLF1*LF11>
P_P6_TRO> = LTRO*TR1>
P_P6_P12> = LTR*TR1>
P_P12_HDO> = LHDO*HD1>
P_P12_P27> = LHD*HD1>
P_P6_P25> = Q27*TR1>+Q28*TR2>
P_P25_WTRO> = LWTRO*WTR1>
P_P25_P26> = LWTR*WTR1>
P_P12_RUAO> = LRUAO*RUA1>
P_P12_P13> = LRUA*RUA1>
P_P13_RFAO> = LRFAO*RFA1>
```

```
P_P13_P14> = LRFA*RFA1>
P_P12_LUAO> = LLUAO*LUA1>
P_P12_P15> = LLUA*LUA1>
P_P15_LFAO> = LLFAO*LFA1>
P_P15_P16> = LLFA*LFA1>

%--------------------------------------------------------------------------------------------------
% POSITION OF POINTS WITH RESPECT TO O

P_O_P2> = P_O_P1> + P_P1_P2>
P_O_P3> = P_O_P2> + P_P2_P3>
P_O_P4> = P_O_P3> + P_P3_P4>
P_O_P5> = P_O_P3> + P_P3_P5>
P_O_P6> = P_O_P5> + P_P5_P6>
P_O_P7> = P_O_P6> + P_P6_P7>
P_O_P8> = P_O_P7> + P_P7_P8>
P_O_P9> = P_O_P8> + P_P8_P9>
P_O_P10> = P_O_P8> + P_P8_P10>
P_O_P11> = P_O_P10> + P_P10_P11>
P_O_P12> = P_O_P6> + P_P6_P12>
P_O_P13> = P_O_P12> + P_P12_P13>
P_O_P14> = P_O_P13> + P_P13_P14>
P_O_P15> = P_O_P12> + P_P12_P15>
P_O_P16> = P_O_P15> + P_P15_P16>
P_O_P17> = P_O_P3> + P_P3_P17>
P_O_P18> = P_O_P17> + P_P17_P18>
P_O_P19> = P_O_P5> + P_P5_P19>
P_O_P20> = P_O_P19> + P_P19_P20>
P_O_P21> = P_O_P6> + P_P6_P21>
P_O_P22> = P_O_P21> + P_P21_P22>
P_O_P23> = P_O_P7> + P_P7_P23>
P_O_P24> = P_O_P23> + P_P23_P24>
P_O_P25> = P_O_P6> + P_P6_P25>
P_O_P26> = P_O_P25> + P_P25_P26>
P_O_P27> = P_O_P12> + P_P12_P27>
P_O_CM> = CM(O)

%--------------------------------------------------------------------------------------------------
% X AND Y POSITION OF POINTS WITH RESPECT TO O

POP1X = DOT(P_O_P1>,N1>)
POP1Y = DOT(P_O_P1>,N2>)
POP2X = DOT(P_O_P2>,N1>)
POP2Y = DOT(P_O_P2>,N2>)
POP3X = DOT(P_O_P3>,N1>)
POP3Y = DOT(P_O_P3>,N2>)
POP4X = DOT(P_O_P4>,N1>)
POP4Y = DOT(P_O_P4>,N2>)
POP5X = DOT(P_O_P5>,N1>)
POP5Y = DOT(P_O_P5>,N2>)
```

```
POP6X = DOT(P_O_P6>,N1>)
POP6Y = DOT(P_O_P6>,N2>)
POP7X = DOT(P_O_P7>,N1>)
POP7Y = DOT(P_O_P7>,N2>)
POP8X = DOT(P_O_P8>,N1>)
POP8Y = DOT(P_O_P8>,N2>)
POP9X = DOT(P_O_P9>,N1>)
POP9Y = DOT(P_O_P9>,N2>)
POP10X = DOT(P_O_P10>,N1>)
POP10Y = DOT(P_O_P10>,N2>)
POP11X = DOT(P_O_P11>,N1>)
POP11Y = DOT(P_O_P11>,N2>)
POP12X = DOT(P_O_P12>,N1>)
POP12Y = DOT(P_O_P12>,N2>)
POP13X = DOT(P_O_P13>,N1>)
POP13Y = DOT(P_O_P13>,N2>)
POP14X = DOT(P_O_P14>,N1>)
POP14Y = DOT(P_O_P14>,N2>)
POP15X = DOT(P_O_P15>,N1>)
POP15Y = DOT(P_O_P15>,N2>)
POP16X = DOT(P_O_P16>,N1>)
POP16Y = DOT(P_O_P16>,N2>)
POP17X = DOT(P_O_P17>,N1>)
POP17Y = DOT(P_O_P17>,N2>)
POP18X = DOT(P_O_P18>,N1>)
POP18Y = DOT(P_O_P18>,N2>)
POP19X = DOT(P_O_P19>,N1>)
POP19Y = DOT(P_O_P19>,N2>)
POP20X = DOT(P_O_P20>,N1>)
POP20Y = DOT(P_O_P20>,N2>)
POP21X = DOT(P_O_P21>,N1>)
POP21Y = DOT(P_O_P21>,N2>)
POP22X = DOT(P_O_P22>,N1>)
POP22Y = DOT(P_O_P22>,N2>)
POP23X = DOT(P_O_P23>,N1>)
POP23Y = DOT(P_O_P23>,N2>)
POP24X = DOT(P_O_P24>,N1>)
POP24Y = DOT(P_O_P24>,N2>)
POP25X = DOT(P_O_P25>,N1>)
POP25Y = DOT(P_O_P25>,N2>)
POP26X = DOT(P_O_P26>,N1>)
POP26Y = DOT(P_O_P26>,N2>)
POP27X = DOT(P_O_P27>,N1>)
POP27Y = DOT(P_O_P27>,N2>)
POCMX = DOT(P_O_CM>,N1>)
POCMY = DOT(P_O_CM>,N2>)

%--------------------------------------------------------------------------------------------------
% KINEMATIC DIFFERENTIAL EQUATIONS
```

```
Q1' = U1
Q2' = U2
Q3' = U3
Q4' = U4
Q5' = U5
Q6' = U6
Q7' = U7
Q8' = U8
Q9' = U9
Q10' = U10
Q11' = U11
Q12' = U12
Q13' = U13
Q14' = U14
Q15' = U15
Q16' = U16
Q17' = U17
Q18' = U18
Q19' = U19
Q20' = U20
Q21' = U21
Q22' = U22
Q23' = U23
Q24' = U24
Q25' = U25
Q26' = U26
Q27' = U27
Q28' = U28
Q29' = U29
Q30' = U30

%-----------------------------------------------------------------------------------------------------
% ANGLES FOR TORQUE CALCULATION

% CONVERT AUTOLEV ANGLES TO JOINT ANGLES

ARSHOE = Q2-PI
ALSHOE = Q3-PI
ARHIPF = (2*PI)-Q4
ALHIPF = (2*PI)-Q5
ARKNEF = PI+Q6
ALKNEF = PI+Q7
ARANKF = PI-Q8
ALANKF = PI-Q9
ARBALF = PI-Q10
ALBALF = PI-Q11

% CALCULATE ANGLE FOR OPPOSITE JOINT ACTION

ARSHOF = (2*PI)-ARSHOE
```

```
ALSHOF = (2*PI)-ALSHOE
ARHIPE = (2*PI)-ARHIPF
ALHIPE = (2*PI)-ALHIPF
ARKNEE = (2*PI)-ARKNEF
ALKNEE = (2*PI)-ALKNEF
ARANKE = (2*PI)-ARANKF
ALANKE = (2*PI)-ALANKF
ARBALE = (2*PI)-ARBALF
ALBALE = (2*PI)-ALBALF

% CONVERT AUTOLEV ANGULAR VELOCITIES TO JOINT ANGULAR
% VELOCITIES

WRSHOE = -U2
WLSHOE = -U3
WRHIPF = U4
WLHIPF = U5
WRKNEF = -U6
WLKNEF = -U7
WRANKF = U8
WLANKF = U9
WRBALF = U10
WLBALF = U11

% CALCULATE ANGULAR VELOCITY FOR OPPOSITE JOINT ACTION

WRSHOF = -WRSHOE
WLSHOF = -WLSHOE
WRHIPE = -WRHIPF
WLHIPE = -WLHIPF
WRKNEE = -WRKNEF
WLKNEE = -WLKNEF
WRANKE = -WRANKF
WLANKE = -WLANKF
WRBALE = -WRBALF
WLBALE = -WLBALF

%-----------------------------------------------------------------------------------------------
% ANGULAR VELOCITIES

W_TR_N> = U1*TR3>
W_HD_TR> = 0>
W_RUA_TR> = U2*RUA3>
W_LUA_TR> = U3*LUA3>
W_RFA_RUA> = RFARUA'*RFA3> + U29*RFA3>
W_LFA_LUA> = LFALUA'*LFA3> + U30*LFA3>
W_RTH_TR> =  U4*RTH3>
W_LTH_TR> = U5*LTH3>
W_RS_RTH> = U6*RS3>
W_LS_LTH> = U7*LS3>
```

```
W_RF2_RS> = U8*RF23>
W_LF2_LS> = U9*LF23>
W_RF1_RF2> = U10*RF13>
W_LF1_LF2> = U11*LF13>
W_WRS_RS> = U12*WRS3>
W_WLS_LS> = U13*WLS3>
W_WRTH_RTH> = U14*WRTH3>
W_WLTH_LTH> = U15*WLTH3>
W_WTR_TR> = U16*WTR3>

%-----------------------------------------------------------------------------------------------
% ANGULAR ACCELERATIONS

ALF_TR_N> = DT(W_TR_N>,N)
ALF_HD_TR> = 0>
ALF_RUA_TR> = DT(W_RUA_TR>,TR)
ALF_LUA_TR> = DT(W_LUA_TR>,TR)
ALF_RFA_RUA> = DT(W_RFA_RUA>,RUA)
ALF_LFA_LUA> = DT(W_LFA_LUA>,LUA)
ALF_RTH_TR> = DT(W_RTH_TR>,TR)
ALF_LTH_TR> = DT(W_LTH_TR>,TR)
ALF_RS_RTH> = DT(W_RS_RTH>,RTH)
ALF_LS_LTH> = DT(W_LS_LTH>,LTH)
ALF_RF2_RS> = DT(W_RF2_RS>,RS)
ALF_LF2_LS> = DT(W_LF2_LS>,LS)
ALF_RF1_RF2> = DT(W_RF1_RF2>,RF2)
ALF_LF1_LF2> = DT(W_LF1_LF2>,LF2)
ALF_WRS_RS> = DT(W_WRS_RS>,RS)
ALF_WLS_LS> = DT(W_WLS_LS>,LS)
ALF_WRTH_RTH> = DT(W_WRTH_RTH>,RTH)
ALF_WLTH_LTH> = DT(W_WLTH_LTH>,LTH)
ALF_WTR_TR> = DT(W_WTR_TR>,TR)

%-----------------------------------------------------------------------------------------------
% LINEAR VELOCITIES

V_O_N> = 0>
V_P1_N> = DT(P_O_P1>,N)
V2PTS(N,RF1,P1,RF1O)
V2PTS(N,RF1,P1,P2)
V2PTS(N,RF2,P2,RF2O)
V2PTS(N,RF2,P2,P3)
V2PTS(N,RF2,P2,P4)
V2PTS(N,RS,P3,RSO)
V2PTS(N,RS,P3,P5)
V_P17_N> = DT(P_O_P17>,N)
V2PTS(N,WRS,P17,WRSO)
V2PTS(N,WRS,P17,P18)
V2PTS(N,RTH,P5,RTHO)
V2PTS(N,RTH,P5,P6)
```

```
V_P19_N> = DT(P_O_P19>,N)
V2PTS(N,WRTH,P19,WRTHO)
V2PTS(N,WRTH,P19,P20)
V2PTS(N,LTH,P6,LTHO)
V2PTS(N,LTH,P6,P7)
V_P21_N> = DT(P_O_P21>,N)
V2PTS(N,WLTH,P21,WLTHO)
V2PTS(N,WLTH,P21,P22)
V2PTS(N,LS,P7,LSO)
V2PTS(N,LS,P7,P8)
V_P23_N> = DT(P_O_P23>,N)
V2PTS(N,WLS,P23,WLSO)
V2PTS(N,WLS,P23,P24)
V2PTS(N,LF2,P8,LF2O)
V2PTS(N,LF2,P8,P9)
V2PTS(N,LF2,P8,P10)
V2PTS(N,LF1,P10,LF1O)
V2PTS(N,LF1,P10,P11)
V2PTS(N,TR,P6,TRO)
V2PTS(N,TR,P6,P12)
V_P25_N> = DT(P_O_P25>,N)
V2PTS(N,WTR,P25,WTRO)
V2PTS(N,WTR,P25,P26)
V2PTS(N,RUA,P12,RUAO)
V2PTS(N,RUA,P12,P13)
V2PTS(N,RFA,P13,RFAO)
V2PTS(N,RFA,P13,P14)
V2PTS(N,LUA,P12,LUAO)
V2PTS(N,LUA,P12,P15)
V2PTS(N,LFA,P15,LFAO)
V2PTS(N,LFA,P15,P16)
V2PTS(N,HD,P12,HDO)
V2PTS(N,HD,P12,P27)
V_CM_N> = DT(P_O_CM>,N)
VOCMX = DT(POCMX)
VOCMY = DT(POCMY)

%-----------------------------------------------------------------------------------------------
% LINEAR ACCELERATIONS

A_O_N> = 0>
A_P1_N> = DT(V_P1_N>,N)
A2PTS(N,RF1,P1,RF1O)
A2PTS(N,RF1,P1,P2)
A2PTS(N,RF2,P2,RF2O)
A2PTS(N,RF2,P2,P3)
A2PTS(N,RF2,P2,P4)
A2PTS(N,RS,P3,RSO)
A2PTS(N,RS,P3,P5)
A_P17_N> = DT(V_P17_N>,N)
```

```
A2PTS(N,WRS,P17,WRSO)
A2PTS(N,WRS,P17,P18)
A2PTS(N,RTH,P5,RTHO)
A2PTS(N,RTH,P5,P6)
A_P19_N> = DT(V_P19_N>,N)
A2PTS(N,WRTH,P19,WRTHO)
A2PTS(N,WRTH,P19,P20)
A2PTS(N,LTH,P6,LTHO)
A2PTS(N,LTH,P6,P7)
A_P21_N> = DT(V_P21_N>,N)
A2PTS(N,WLTH,P21,WLTHO)
A2PTS(N,WLTH,P21,P22)
A2PTS(N,LS,P7,LSO)
A2PTS(N,LS,P7,P8)
A_P23_N> = DT(V_P23_N>,N)
A2PTS(N,WLS,P23,WLSO)
A2PTS(N,WLS,P23,P24)
A2PTS(N,LF2,P8,LF2O)
A2PTS(N,LF2,P8,P9)
A2PTS(N,LF2,P8,P10)
A2PTS(N,LF1,P10,LF1O)
A2PTS(N,LF1,P10,P11)
A2PTS(N,TR,P6,TRO)
A2PTS(N,TR,P6,P12)
A_P25_N> = DT(V_P25_N>,N)
A2PTS(N,WTR,P25,WTRO)
A2PTS(N,WTR,P25,P26)
A2PTS(N,RUA,P12,RUAO)
A2PTS(N,RUA,P12,P13)
A2PTS(N,RFA,P13,RFAO)
A2PTS(N,RFA,P13,P14)
A2PTS(N,LUA,P12,LUAO)
A2PTS(N,LUA,P12,P15)
A2PTS(N,LFA,P15,LFAO)
A2PTS(N,LFA,P15,P16)
A2PTS(N,HD,P12,HDO)
A2PTS(N,HD,P12,P27)
A_CM_N> = DT(P_O_CM>,N)

%-----------------------------------------------------------------------------------------------
% SPRING POSITION VECTORS, AND VELOCITIES

STRETCH1 = MAG(P_P3_P17>)
STRETCH2 = MAG(P_P5_P18>)
STRETCH3 = MAG(P_P5_P19>)
STRETCH4 = MAG(P_P6_P20>)
STRETCH5 = MAG(P_P6_P21>)
STRETCH6 = MAG(P_P7_P22>)
STRETCH7 = MAG(P_P7_P23>)
STRETCH8 = MAG(P_P8_P24>)
```

```
STRETCH9 = MAG(P_P6_P25>)
STRETCH10 = MAG(P_P12_P26>)

UVEC1> = UNITVEC(P_P3_P17>)
UVEC2> = UNITVEC(P_P5_P18>)
UVEC3> = UNITVEC(P_P5_P19>)
UVEC4> = UNITVEC(P_P6_P20>)
UVEC5> = UNITVEC(P_P6_P21>)
UVEC6> = UNITVEC(P_P7_P22>)
UVEC7> = UNITVEC(P_P7_P23>)
UVEC8> = UNITVEC(P_P8_P24>)
UVEC9> = UNITVEC(P_P6_P25>)
UVEC10> = UNITVEC(P_P12_P26>)

VELOCITY1 = DT(STRETCH1)
VELOCITY2 = DT(STRETCH2)
VELOCITY3 = DT(STRETCH3)
VELOCITY4 = DT(STRETCH4)
VELOCITY5 = DT(STRETCH5)
VELOCITY6 = DT(STRETCH6)
VELOCITY7 = DT(STRETCH7)
VELOCITY8 = DT(STRETCH8)
VELOCITY9 = DT(STRETCH9)
VELOCITY10 = DT(STRETCH10)

%-----------------------------------------------------------------------------------------------
% VELOCITIES OF POINTS ON THE FEET FOR CALCULATING SPRING
% FORCES

VOP1X = DOT(V_P1_N>,N1>)
VOP1Y = DOT(V_P1_N>,N2>)
VOP2X = DOT(V_P2_N>,N1>)
VOP2Y = DOT(V_P2_N>,N2>)
VOP4X = DOT(V_P4_N>,N1>)
VOP4Y = DOT(V_P4_N>,N2>)
VOP9X = DOT(V_P9_N>,N1>)
VOP9Y = DOT(V_P9_N>,N2>)
VOP10X = DOT(V_P10_N>,N1>)
VOP10Y = DOT(V_P10_N>,N2>)
VOP11X = DOT(V_P11_N>,N1>)
VOP11Y = DOT(V_P11_N>,N2>)

R1Y = -K1*POP1Y-K4*VOP1Y
R1X = (-K7*POP1X-K12*VOP1X)*R1Y
R2Y = -K2*POP11Y-K5*VOP11Y
R2X = (-K8*POP11X-K13*VOP11X)*R2Y
R3Y = -K3*POP2Y-K6*VOP2Y
R3X = (-K9*POP2X-K14*VOP2X)*R3Y
R4Y = -K1*POP10Y-K4*VOP10Y
R4X = (-K7*POP10X-K12*VOP10X)*R4Y
```

```
R5Y = -K2*POP4Y-K5*VOP4Y
R5X = (-K8*POP4X-K13*VOP4X)*R5Y
R6Y = -K3*POP9Y-K6*VOP9Y
R6X = (-K9*POP9X-K14*VOP9X)*R6Y
RXT = R1X+R2X+R3X+R4X+R5X+R6X
RYT = R1Y+R2Y+R3Y+R4Y+R5Y+R6Y

%-----------------------------------------------------------------------------------------------
% FORCES AND TORQUES

% GRAVITY

GRAVITY(G*N2>)

% FORCES ON THE SHOE FROM THE GROUND

FORCE(P1,R1X*N1>+R1Y*N2>)
FORCE(P11,R2X*N1>+R2Y*N2>)
FORCE(P2,R3X*N1>+R3Y*N2>)
FORCE(P10,R4X*N1>+R4Y*N2>)
FORCE(P4,R5X*N1>+R5Y*N2>)
FORCE(P9,R6X*N1>+R6Y*N2>)

% FORCES BETWEEN WOBBLING AND RIGID ELEMENTS

FORCE(P3/P17,(-K10*STRETCH1^3-K11*VELOCITY1)*UVEC1>)
FORCE(P5/P18,(-K10*STRETCH2^3-K11*VELOCITY2)*UVEC2>)
FORCE(P5/P19,(-K15*STRETCH3^3-K16*VELOCITY3)*UVEC3>)
FORCE(P6/P20,(-K15*STRETCH4^3-K16*VELOCITY4)*UVEC4>)
FORCE(P6/P21,(-K15*STRETCH5^3-K16*VELOCITY5)*UVEC5>)
FORCE(P7/P22,(-K15*STRETCH6^3-K16*VELOCITY6)*UVEC6>)
FORCE(P7/P23,(-K10*STRETCH7^3-K11*VELOCITY7)*UVEC7>)
FORCE(P8/P24,(-K10*STRETCH8^3-K11*VELOCITY8)*UVEC8>)
FORCE(P6/P25,(-K17*STRETCH9^3-K18*VELOCITY9)*UVEC9>)
FORCE(P12/P26,(-K17*STRETCH10^3-K18*VELOCITY10)*UVEC10>)

% JOINT TORQUES

TORQUE(TR/LUA,TQTRLUA*LUA3>)
TORQUE(TR/RUA,TQTRRUA*RUA3>)
TORQUE(LUA/LFA,TQLUALFA*LFA3>)
TORQUE(RUA/RFA,TQRUARFA*RFA3>)
TORQUE(TR/RTH,TQTRRTH*RTH3>)
TORQUE(TR/LTH,TQTRLTH*LTH3>)
TORQUE(LTH/LS,TQLTHLS*LS3>)
TORQUE(RTH/RS,TQRTHRS*RS3>)
TORQUE(RS/RF2,TQRSRF2*RF23>)
TORQUE(LS/LF2,TQLSLF2*LF23>)
TORQUE(RF2/RF1,TQRF2RF1*RF13>)
TORQUE(LF2/LF1,TQLF2LF1*LF13>)
```

```
%-----------------------------------------------------------------------------------------------
% CALCULATE CENTRE OF PRESSURE

SIMCOP = (R1Y*POP1X+R2Y*POP11X+R3Y*POP2X+R4Y*POP10X+R5Y*
          POP4X+R6Y*POP9X)/(RYT)

%-----------------------------------------------------------------------------------------------
% CALCULATE KINETIC, POTENTIAL ENERGY AND TOTAL ENERGY
% EXCLUDING FOOT SPRINGS AS THEY REQUIRE MODIFICATION IN
% FORTRAN CODE

KE = KE()

PE = (M*POCMY*(-G))+(0.25*K10*(STRETCH1^4+STRETCH2^4+
     STRETCH7^4+STRETCH8^4)) + (0.25*K17*(STRETCH9^4+
     STRETCH10^4)) + (0.25*K15*(STRETCH3^4+STRETCH4^4+
     STRETCH5^4+STRETCH6^4))

TE = KE+PE

%-----------------------------------------------------------------------------------------------
% CONSTRAINTS

AUXILIARY[1]=U29
AUXILIARY[2]=U30

CONSTRAIN(AUXILIARY[U29,U30])

%-----------------------------------------------------------------------------------------------
% EQUATIONS OF MOTION

ZERO = FR() + FRSTAR()
KANE(TQLUALFA,TQRUARFA)

%-----------------------------------------------------------------------------------------------
% GIVE ANGULAR MOMENTUM AROUND THE MASS CENTRE

H>=MOMENTUM(ANGULAR,CM)
H = DOT(H>,N3>)

%-----------------------------------------------------------------------------------------------
% INPUTS

INPUT TINITIAL=2.1625, TFINAL=2.3625
INPUT INTEGSTP=0.0001, PRINTINT=10
INPUT ABSERR=1.0E-08,RELERR=1.0E-07

INPUT K1=0.17538E+06,K2=8969.3,K3=2511.1,K4=21473,K5=36657,
```

```
      K6=17349,K7=10.390,K8=9.6549,K9=96.10,K10=0.12575E+08,
      K11=466.14,K12=1.0764,K13=0.54708,K14=1.8380,K15=0.12255E+08,
      K16=148.39,K17=0.32612E+07,K18=280.43
INPUT G=-9.81
INPUT [Q{19:28}]=1.0E-07,[U{19:28}]=0.0,NANG=-15
INPUT [Q{1:18}]=0.0,[U{1:18}]=0.0
INPUT IRF1=4.59E-05,ILF1=3.86E-05,IRF2=0.002904647,ILF2=0.002643125
INPUT IRS=0.018051941,ILS=0.016799425,IRTH=0.019360505,
      ILTH=0.016387418,ITR=0.137076443
INPUT IHD=0.033,IRUA=0.02,ILUA=0.016,IRFA=0.0217234743,
      ILFA=0.0233425179
INPUT IWRS=0.045298547,IWLS=0.042484156,IWRTH=0.150116121,
      IWLTH=0.130392546,IWTR=0.818757107
INPUT LRF1=-0.083,LLF1=0.083,LRF21=-0.173,LRF22=-0.119,LLF21=0.173,
      LLF22=-0.119
INPUT LRS=-0.448,LLS=0.436,LRTH=-0.451,LLTH=0.423,LTR=0.589,
      LHD=0.266
INPUT LRUA=0.316,LLUA=0.298,LRFA=0.433,LLFA=0.455
INPUT LWRS=-0.448,LWLS=0.436,LWRTH=-0.451,LWLTH=0.423,LWTR=0.589
INPUT LRF1O=-0.0415,LLF1O=0.0415,LRF2O1=-0.102500185,
      LRF2O2=-0.02441107,LLF2O1=0.070499815,LLF2O2=-0.02441107
INPUT LRSO=-0.224,LLSO=0.218,LRTHO=-0.2255,LLTHO=0.2115
INPUT LTRO=0.2945,LHDO=0.135,LRUAO=0.144,LLUAO=0.138,
      LRFAO=0.16718733,LLFAO=0.168284015
INPUT LWRSO=-0.269372493,LWLSO=0.171293022,LWRTHO=-0.26453205,
      LWLTHO=0.175862041,LWTRO=0.30100882
INPUT MRF1=0.155919835,MLF1=0.14519131,MRF2=1.13030231,
      MLF2=1.14843707
INPUT MRS=1.069261409,MLS=1.049961566,MRTH=1.131269364,
      MLTH=1.086798855,MTR=4.649627333,MHD=5.609,MRUA=2.227,
      MLUA=2.042
INPUT MRFA=1.54709789,MLFA=1.59230609,MWRS=3.196738591,
      MWLS=3.139038434,MWRTH=8.611730636,MWLTH=8.273201145,
      MWTR=25.34937267

%-----------------------------------------------------------------------------------------------
% OUTPUTS

OUTPUT T,H,KE,PE,TE,POCMX,POCMY,VOCMX,VOCMY
OUTPUT T,Q1,Q2,Q3,Q4,Q5,Q6,Q7,Q8
OUTPUT T,U1,U2,U3,U4,U5,U6,U7,U8
OUTPUT T,Q9,Q10,Q11,Q12,Q13,Q14,Q15,Q16
OUTPUT T,U9,U10,U11,U12,U13,U14,U15,U16
OUTPUT T,ARSHOE,ALSHOE,ARHIPE,ALHIPE,ARKNEE,ALKNEE,ARANKE,
       ALANKE,ARBALE,ALBALE
OUTPUT T,ARSHOF,ALSHOF,ARHIPF,ALHIPF,ARKNEF,ALKNEF,ARANKF,
       ALANKF,ARBALF,ALBALF
OUTPUT T,WRSHOE,WLSHOE,WRHIPE,WLHIPE,WRKNEE,WLKNEE,
       WRANKE,WLANKE,WRBALE,WLBALE
OUTPUT T,WRSHOF,WLSHOF,WRHIPF,WLHIPF,WRKNEF,WLKNEF,
```

```
            WRANKF,WLANKF,WRBALF,WLBALF
OUTPUT T,RFARUA,LFALUA
OUTPUT T,TQTRRUA,TQTRLUA,TQRUARFA,TQLUALFA
OUTPUT T,TQTRRTH,TQTRLTH,TQRTHRS,TQLTHLS
OUTPUT T,TQRSRF2,TQLSLF2,TQRF2RF1,TQLF2LF1
OUTPUT T,STRETCH1,STRETCH2,STRETCH3,STRETCH4,STRETCH5
OUTPUT T,STRETCH6,STRETCH7,STRETCH8,STRETCH9,STRETCH10
OUTPUT T,VELOCITY1,VELOCITY2,VELOCITY3,VELOCITY4,VELOCITY5
OUTPUT T,VELOCITY6,VELOCITY7,VELOCITY8,VELOCITY9,VELOCITY10
OUTPUT T,R1X,R1Y,R2X,R2Y,R3X,R3Y,R4X,R4Y,R5X,R5Y,R6X,R6Y,RXT,
            RYT,SIMCOP
OUTPUT T,POP1X,POP1Y,POP2X,POP2Y,POP4X,POP4Y
OUTPUT T,POP9X,POP9Y,POP10X,POP10Y,POP11X,POP11Y
OUTPUT T,POP1X,POP1Y,POP2X,POP2Y,POP3X,POP3Y,POP4X,POP4Y,
            POP5X,POP5Y,POP6X,POP6Y,POP7X,POP7Y,POP8X,POP8Y,
            POP9X,POP9Y,POP10X,POP10Y,POP11X,POP11Y,POP12X,
            POP12Y,POP13X,POP13Y,POP14X,POP14Y,POP15X,POP15Y,
            POP16X,POP16Y,POP27X,POP27Y,POCMX,POCMY
OUTPUT T,POP17X,POP17Y,POP18X,POP18Y,POP19X,POP19Y,POP20X,
            POP20Y,POP21X,POP21Y,POP22X,POP22Y,POP23X,POP23Y,
            POP24X,POP24Y,POP25X,POP25Y,POP26X,POP26Y

%-------------------------------------------------------------------------------------------------
% UNITS

UNITS T=S,H=KG.M^2.RAD/S,[KE,PE,TE]=JOULES,G=M/S^2,SIMCOP=M
UNITS [Q{17:28}]=M,[U{17:28}]=M/S
UNITS [Q{1:16}]=DEGS,[U{1:16}]=RADS/S,[Q{29:30}]=DEGS,
        [U{29:30}]=RADS/S,NANG=DEGS
UNITS [ARSHOE,ALSHOE,ARHIPE,ALHIPE,ARKNEE,ALKNEE,ARANKE,
        ALANKE,ARBALE,ALBALE,ARSHOF,ALSHOF,ARHIPF,ALHIPF,
        ARKNEF,ALKNEF,ARANKF,ALANKF,ARBALF,ALBALF]=DEGS
UNITS [WRSHOE,WLSHOE,WRHIPE,WLHIPE,WRKNEE,WLKNEE,
        WRANKE,WLANKE,WRBALE,WLBALE,WRSHOF,WLSHOF,WRHIPF,
        WLHIPF,WRKNEF,WLKNEF,WRANKF,WLANKF,WRBALF,WLBALF]
        =DEGS/S
UNITS [K{1:3}]=N/M,[K{4:6}]=N.S/M,[K{7:9}]=N/M,[K{12:14}]=N.S/M,
        [K10,K15,K17]=N/M^3,[K11,K16,K18]=N.S/M
UNITS [LRF1,LLF1,LRF21,LRF22,LLF21,LLF22,LRS,LLS,LRTH,LLTH,LTR,
        LHD,LRUA,LLUA,LRFA,LLFA,LWRS,LWLS,LWRTH,LWLTH,LWTR,
        LRF1O,LLF1O,LRF2O1,LRF2O2,LLF2O1,LLF2O2,LRSO,LLSO,LRTHO,
        LLTHO,LTRO,LHDO,LRUAO,LLUAO,LRFAO,LLFAO,LWRSO,LWLSO,
        LWRTHO,LWLTHO,LWTRO]=M
UNITS [IRF1,ILF1,IRF2,ILF2,IRS,ILS,IRTH,ILTH,ITR,IHD,IRUA,ILUA,IRFA,
        ILFA,IWRS,IWLS,IWRTH,IWLTH,IWTR]=KG.M^2
UNITS [MRF1,MLF1,MRF2,MLF2,MRS,MLS,MRTH,MLTH,MTR,MHD,MRUA,
        MLUA,MRFA,MLFA,MWRS,MWLS,MWRTH,MWLTH,MWTR]=KG
UNITS [POP{1:27}X,POP{1:27}Y]=M
UNITS STRETCH{1:10}=M,VELOCITY{1:10}=M/S
UNITS [TQRSRF2,TQLSLF2,TQRTHRS,TQLTHLS,TQTRRTH,TQTRLTH,
```

```
        TQTRRUA,TQTRLUA,TQRUARFA,TQLUALFA,TQRF2RF1,TQLF2LF1]=N.M
UNITS [RFARUA,LFALUA]=DEGS
UNITS [RXT,R1X,R2X,R3X,R4X,R5X,R6X,RYT,R1Y,R2Y,R3Y,R4Y,R5Y,R6Y]
        =N

%-------------------------------------------------------------------------------------------------
SAVE C:\AL\SAM-AL\ TRIPLEJUMP.ALL
CODE DYNAMICS() C:\AL\SAM-AL\TRIPLEJUMP.FOR, SUBS

%-------------------------------------------------------------------------------------------------
% END END END END END END END END END END END END END END END
%-------------------------------------------------------------------------------------------------
```

APPENDIX 3

TESTING PROCEDURES, PRE-SELECTION MEDICAL QUESTIONNAIRE, AND INFORMED CONSENT FORM

DATA ACQUISITION FOR THE ANALYSIS OF HUMAN MOVEMENTS
LAY SUMMARY

This study comprises a biomechanical analysis of human movement. This analysis requires kinematic (how you are moving) and kinetic (what forces you produce) data for the triple jump.

The data of actual human movements are required to give detailed information about the current techniques used. The data collected will then be used to understand and explain techniques currently used, determine the contributions of different techniques to performance and injury, as well as to optimise performance.

The kinematic and kinetic data of the triple jump will be obtained in a number of different ways:

- Video and cinematographic recordings.
- Automatic displacement acquisition system. This is similar to being videoed but reflective markers will be taped to you and only their image recorded.
- Force readings from your foot contacting a force plate situated on the runway.

The subject specific parameters will be obtained from:

- Anthropometric measurements. Measuring certain lengths, widths and circumferences of your body with a tape measure in order to construct a computer simulation 'model' of your body.
- Muscular torque readings from an isovelocity dynamometer. This involves measuring your strength at different joints through a range of angles and speeds.

Data will be acquired in the High Performance Athletics Centre (HiPAC) and Powerbase gym at Loughborough University. The data collection sessions will last no longer than four hours, with the subject actively involved for only a fraction of the total time:

- Actual performance of movements: 30 minutes
- Anthropometric measurements: 30 minutes
- Isovelocity dynamometer: 45 minutes

The study in which you have been invited to participate will involve a biomechanical analysis of your triple jump technique. The study will involve you being videoed, using a number of different cameras, as you perform the whole triple jump to obtain kinematic data and each phase separately in order to obtain kinetic data. This will be followed at a later date by strengths tests on an isovelocity dynamometer.

It may be necessary to shave certain areas of your body to attach monitoring equipment using adhesive tape. The data collected will be used to help increase our understanding of the mechanics of human movements.

You will perform the data collection in a suitable environment. The risk of injury during the triple jump data collection will be minimal since we will only ask you to perform movements with which you are familiar and comfortable. It is considered that no increased risks, discomforts or distresses are likely to result from the data collection of the triple jump above those associated with the normal performance of those movements. You will undergo a familiarisation protocol for the isovelocity dynamometer prior to capturing data to minimise any potential for injury.

The information obtained from the study will be collected and stored in adherence with the Data Protection Act. Whilst certain personal and training information will be required, you will be allocated a reference number to ensure that your identity and personal details will remain confidential. If you agree to take part in the study, you are free to withdraw from the study at any stage, without having to give any reasons. An opportunity will be provided in this event for you to discuss privately your wish to withdraw. A contact name and phone number will be provided to you for use if you have any queries about any part of your participation in the study.

PRE-SELECTION MEDICAL QUESTIONNAIRE

LOUGHBOROUGH UNIVERSITY
DEPARTMENT OF PHYSICAL EDUCATION, SPORTS SCIENCE AND RECREATION MANAGEMENT

Please read through this questionnaire, BUT DO NOT ANSWER ANY OF THE QUESTIONS YET. When you have read right through, there may be questions you would prefer not to answer. Assistance will be provided if you require it to discuss any questions on this form. In this case please tick the box labelled "I wish to withdraw" immediately below. Also tick the box labelled "I wish to withdraw" if there is any other reason for you not to take part.

	tick appropriate box
I wish to withdraw	☐
I am happy to answer the questionnaire	☐

If you are happy to answer the questions posed below, please proceed. Your answers will be treated in the strictest confidence.

1. Are you at present recovering from any illness or operation? YES/NO*

2. Are you suffering from or have you suffered from or received medical treatment for any of the following conditions?

   a. Heart or circulation condition YES/NO*
   b. High blood pressure YES/NO*
   c. Any orthopaedic problems YES/NO*
   d. Any muscular problems YES/NO*
   e. Asthma or bronchial complaints YES/NO*

3. Are you currently taking any medication that may affect your participation in the study? YES/NO*

4. Are you recovering from any injury? YES/NO*

5. Are you epileptic? YES/NO*

6. Are you diabetic? YES/NO*

7. Are you allergic to sticking plasters? YES/NO*

8. Do you have any other allergies? If yes, please give details below YES/NO*

……
……
…..……
……..…

9. Are you aware of any other condition or complaint that may be affected by participation in this study? If so, please state below;

……
……
…..……
……..……
…….

* Delete as appropriate

INFORMED CONSENT FORM (SUBJECTS)

PURPOSE
To obtain kinematic and kinetic data during human movements

PROCEDURES
The kinematic data of human movements will be obtained using:

- Video and cinematographic recordings
- Automatic displacement acquisition system

Body inertia parameters will be ascertained from various body measurements.
Muscular torque data will be gathered using an isovelocity dynamometer.

ACTIVITIES

- Full triple jump
- Individual hop, step, and jump phases.
- Strength tests on an isovelocity dynamometer.

A number of trials will be requested with suitable breaks to minimise fatigue and boredom.

During the measurements a number of researchers will be present, at least one of whom will be of the same sex as you.

QUESTIONS
The researchers will be pleased to answer any questions you may have at any time.

WITHDRAWAL
You are free to withdraw from the study at any stage, with or without having to give any reasons.

CONFIDENTIALITY
Your identity will remain confidential in any material resulting from this work.

I have read the outline of the procedures which are involved in this study, and I understand what will be required by me. I have had the opportunity to ask for further information and for clarification of the demands of each of the procedures and understand what is entailed. I am aware that I have the right to withdraw from the study at any time with no obligation to give reasons for my decision. As far as I am aware I do not have any injury or infirmity which would be affected by the procedures outlined.

Name ……

Signed …… (subject) Date ……

In the presence of:

Name ……

APPENDIX 4

DESCRIPTION OF MARKER PLACEMENT FOR TRIPLE JUMP DATA COLLECTION

Marker #	Body Segment	Marker Label(s)	Marker Position
1,2	**Legs**	RTOE, LTOE	Centre line of foot. Centre of marker is 3cm from tip of big toe.
3,4		RANKM, LANKM	Medial side of ankle bone. The line joining the centres of the 2 ankle markers should define the ankle flexion axis.
5,6		RANKL, LANKL	Lateral side of ankle bone.
7,8		RMTPL LMTPL	Lateral metatarsophalangeal – little toe - joint. The line joining the two MTP markers should define the MTP flexion axis.
9,10		RMTPM LMTPM	Medial metatarsophalangeal - big toe – joint.
11,12		RHEE, LHEE	Centre line of foot, placed on back of heel of shoe.
13,14		RKNEM, LKNEM	Medial side of knee, the line joining the centres of the 2 knee markers should define the knee flexion axis.
15,16		RKNEL,LKNEM	Lateral side of knee.
17,18	**Pelvis**	RASI,LASI	Bony protrusion of the right and left anterior super iliac.
19,20		RPSI, LPSI	Dimple created by the right and

			left posterior suprailiac.
21		LHIP	Position not crucial (only used for asymmetry purposes). Roughly level with the other pelvis markers and approximately above the hip joint centre.
22	**Thorax**	LUM1	First lumbar vertebra.
23		T10	Tenth thoracic vertebra.
24		STRN	Sternum.
25		CLAV	Clavicle.
26		C7	Seventh cervical vertebra.
27		RBAK	Position not crucial. Somewhere in the centre of the right scapula.
28,29	**Arms**	RSHOP,LSHOP	Posterior of shoulder.
30,31		RSHOA,LSHOA	Anterior of shoulder.
32,33		RSHOT,LSHOT	Top of shoulder.
34,35		RELBM,LELBM	Medial side of elbow. Line joining centre of elbow markers should define flexion axis of the elbow (particularly when reasonably straight). Probably positioned on bony protrusion.
36,37		RELBL,LELBL	Lateral side of elbow. Probably positioned on anterior side of bony protrusion.
38,39		RWRA,LWRA	Thumb side of wrist. The centre of the 2 wrist markers should define the flexion axis of the wrist. Marker should be placed on the side of the wrist.

40,41		RWRB,LWRB	Little finger side of wrist. Again the marker should be placed on the side of the wrist.
42	**Head**	RFHD	Right temple.
43		LFHD	Left temple.
44		RBHD	Back right of head.
45		LBHD	Back left of head.

APPENDIX 5

INDIVIDUAL AND MEAN CAMERA RESIDUALS

Camera number	Residual (mm)
1	0.699
2	0.388
3	0.689
4	0.778
5	0.321
6	0.598
7	0.624
8	0.572
9	0.664
10	0.485
11	0.945
12	0.607
13	0.798
14	0.602
15	0.582
16	0.568
17	0.556
18	0.479
Mean residual	0.609
Residual range	0.624
Static reproducibility	0.944 %

APPENDIX 6

ROTOTRANSLATION OF COORDINATE DATA

In order to define the new coordinate system of the volume, a matrix describing the plane of the floor was calculated using an optimisation process. Thirty 25 mm retroreflective markers were situated along the lines defining the approach lane for the triple jump and on the force plate (Figure A6.1).

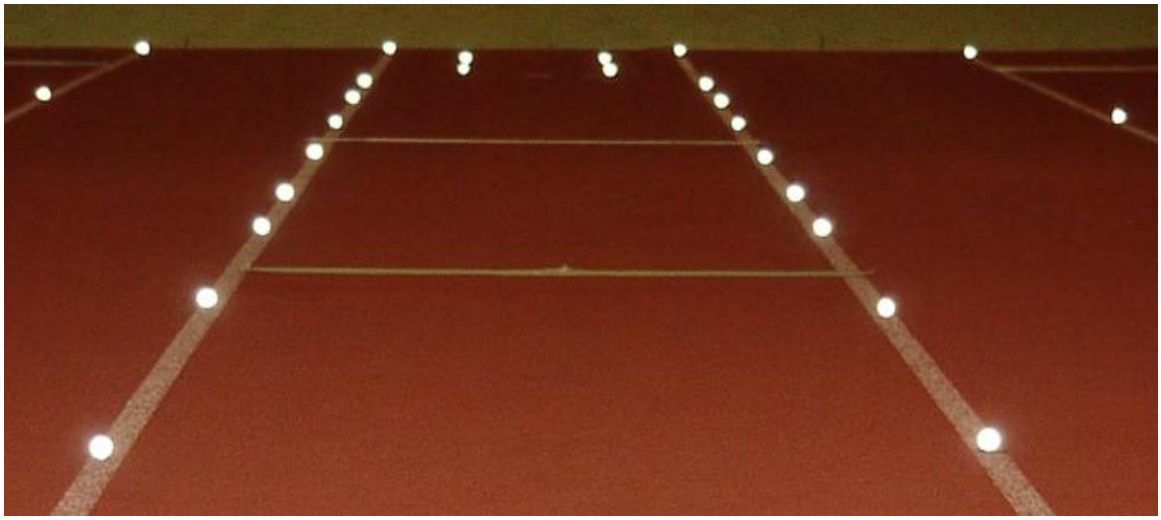

Figure A6.1 Marker positioning for calculation of rotation and translation matrix.

The direction of the lines, and therefore the general direction of motion, was used to define the x axis by calculating the sum of all the vectors that could be made between any two markers along either of the lines. This was calculated twice; once using the markers on the lines defining the approach lane and once using only the markers on the force plate.

Once calculated, the x axis was taken to originate in the centre of the force plate and a z axis was defined by taking the cross product of the x axis and a vector in the plane of the force plate defined using a marker on the force plate. A y axis was subsequently defined by taking the cross product of the x and z axes.

The new coordinate system was calculated by minimising the following function in an iterative fashion (Challis, 1995):

$$\underset{R}{Min} \sum_{i=1}^{n} \left\| b_i - Rc_i \right\|^2 , \qquad \text{(A6.1)}$$

where R is the attitude matrix mapping the i_{th} marker in the old coordinate system c_i to the i_{th} marker in the new one b_i. This assumes both coordinate systems have the same origin and there is no scaling (Challis, 1995).

The two attitude matrices corresponding to the different marker sets mentioned above were then evaluated using the range of the distances of the markers on the approach lines from the calculated axes. In the case of R_0, calculated from the markers on the force plate alone, there was a range of 8.1 mm in the z axis and 49.9 mm and 50.0 mm in the y axis for the left and right lines respectively. In the case of R_1, calculated from markers on the two lines, the range was 6.6 mm in the z axis and 5.8 mm and 4.6 mm in the y axis. Therefore R_1 was preferred.

Having calculated the attitude matrix R_1, a 4x4 matrix also containing the translation necessary to map the origin of the coordinate system to the centre of the force platform was constructed. The rotation and translation were then applied to the coordinates in the following fashion:

$$\begin{pmatrix} -0.968825436 & 0.244820351 & 0.037950905 & -3183.393388 \\ -0.243470175 & -0.969205466 & 0.036919363 & 113.2863626 \\ 0.045820836 & 0.026528505 & 0.998597361 & 498.0157306 \\ 0 & 0 & 0 & 1 \end{pmatrix} \times \begin{pmatrix} x \\ y \\ z \\ 1 \end{pmatrix}. \qquad \text{(A6.2)}$$

The first three columns of the matrix in equation A6.2 represent the rotation of the coordinate data and the last column represents the translation. The rotation and translation were applied to coordinate data in .c3d files using Matlab toolbox for C3Dserver. The rotated and translated data were then available for analysis within Bodybuilder in Vicon.

APPENDIX 7

VICON RECONSTRUCTION PARAMETERS

Maximum acceleration

Maximum acceleration is the maximum expected acceleration of the markers, the default value is 50 mm/s/s and upon manipulation of this value no improvements were shown, therefore it was considered acceptable.

Maximum noise factor

Maximum noise factor indicates how tolerant the reconstruction process is to noise in the marker movement. A higher value indicates more tolerance of erratic movements. If this value was increased from the default value of seven to 15 it led to a decreased segment number. However this also led to a slight increase in misidentification of marker positions and cross over of trajectories. It was deemed necessary to keep this higher value though as triple jumping involves high impacts and, as such, high levels of noise in the marker positions.

Intersection limit

The intersection limit is the upper limit of the separation between rays from two cameras in order for them to contribute to the reconstruction of a marker. For camera residuals of 2.0 mm Vicon suggests this value should be set to 12. In this case the mean camera residual was smaller than 2.0 mm so the value was reduced but no improvements were shown so it was left at 12. The intersection limit and residual factor are interdependent, the residual factor should be set such that multiplying by the intersection limit and dividing by the average camera residual leads to a value between three and ten. In this case the best results were achieved using a residual factor of 0.5 this leading to a value of just under ten using the method above.

Predictor radius

The predictor radius should be set to roughly half the minimum marker separation. This set a limit to the space used in predicting where a given marker may appear in a subsequent

frame. Larger values may result in more unbroken trajectories but can also lead to incorrect association of a marker to a trajectory, leading to a swap. Vicon stated this value is roughly 30 mm for normal human activities. Deviations from this value did not yield improvements in marker tracking so it was considered acceptable.

Minimum cameras to start trajectories

Vicon stated that the minimum cameras to start trajectories should always start at zero and only increase if you are confident that there is an excessive contribution of cameras to trajectory reconstruction. A higher value may eliminate stray reflections and marker ghosting. In this case the volume was very large and often only a few cameras could see markers so this value was left at zero.

APPENDIX 8

VICON BODYLANGUAGE MODEL

```
{*Vicon Bodylanguage model for calculation of joint centres and joint angles adapted for
triple jump model*}
{*Start of macro section*}
{*====================*}

macro REPLACE4(p1,p2,p3,p4)

{*Replaces any point missing from set of four fixed in a segment*}

s234 = [p3,p2-p3,p3-p4]
p1V = Average(p1/s234)*s234
s341 = [p4,p3-p4,p4-p1]
p2V = Average(p2/s341)*s341
s412 = [p1,p4-p1,p1-p2]
p3V = Average(p3/s412)*s412
s123 = [p2,p1-p2,p2-p3]
p4V = Average(p4/s123)*s123

{* Now only replaces if original is missing  11-99 *}

p1 = p1 ? p1V
p2 = p2 ? p2V
p3 = p3 ? p3V
p4 = p4 ? p4V
endmacro

MACRO DisplayAxes( ASeg )

ASeg#O = ASeg(0)
ASeg#X = ASeg(0) + 200 * ASeg(1)
ASeg#Y = ASeg(0) + 200 * ASeg(2)
ASeg#Z = ASeg(0) + 200 * ASeg(3)
OUTPUT( ASeg#O, ASeg#X, ASeg#Y, ASeg#Z )

ENDMACRO

{*Initialisations*}
{*===============*}

{*Define optional marker points*}

OptionalPoints(LFHD,RFHD,LBHD,RBHD)
```

```
OptionalPoints(LSHOP,LSHOA,LELBL,LELBM,LELBF,LELBB,LWRA,LWRB,LHND
A,LHNDB)
OptionalPoints(RSHOP,RSHOA,RELBL,RELBM,RELBF,RELBB,RWRA,RWRB,RHN
DA,RHNDB)
OptionalPoints(RASI,LASI,RPSI,LPSI)
OptionalPoints(LKNEM,LKNEL,LANKL,LANKM,LHEE,LMTPL,LMTPM,LTOE)
OptionalPoints(RKNEM,RKNEL,RANKL,RANKM,RHEE,RMTPL,RMTPM,RTOE)

{*Set Deadband, except for static trials*}

If $Static<>1 Deadband = $Deadband EndIf

Gorigin = {0,0,0}
Global = [Gorigin,{1,0,0},{0,-1,0},xyz]


{*KINEMATICS*}
{*================================================*}

{*Ankle markers used to locate ankle JC (midpoint) and also used in second defining line
for tibiae definitions*}
{*Therefore, they should be placed on axis of ankle and be square on when looking from
the front*}
{*Included an offset to shift the medial markers out by 12.5 mm since half markers were
used*}

LANKOS = ((LANKM-LANKL)/ABS(LANKM-LANKL))*12.5
RANKOS = ((RANKM-RANKL)/ABS(RANKM-RANKL))*12.5
LANKM = LANKM+LANKOS
RANKM = RANKM+RANKOS
LANK = (LANKM+LANKL)/2
RANK = (RANKM+RANKL)/2

{*Knee markers used to locate knee JC (midpoint) and also used in second defining line
for femura definitions*}
{*Therefore, they should be placed on axis of knee and be square on when looking from
the front*}
{*Included an offset to shift the medial markers out by 12.5 mm since half markers were
used*}

LKNEOS = ((LKNEM-LKNEL)/ABS(LKNEM-LKNEL))*12.5
RKNEOS = ((RKNEM-RKNEL)/ABS(RKNEM-RKNEL))*12.5
LKNEM = LKNEM+LKNEOS
RKNEM = RKNEM+RKNEOS
LKNE = (LKNEM+LKNEL)/2
RKNE = (RKNEM+RKNEL)/2

LSHO = (LSHOA+LSHOP)/2
RSHO = (RSHOA+RSHOP)/2
SHO = (LSHO+RSHO)/2
```

```
LELB = (LELBL+LELBM)/2
RELB = (RELBL+RELBM)/2

LWRI = (LWRA+LWRB)/2
RWRI = (RWRA+RWRB)/2

LHND = (LHNDA+LHNDB)/2
RHND = (RHNDA+RHNDB)/2

LMTP = (LMTPL+LMTPM)/2
RMTP = (RMTPL+RMTPM)/2

OUTPUT(LMTP,RMTP,LSHO,RSHO,SHO,LELB,RELB,LWRI,RWRI,LKNE,RKNE,L
ANK,RANK)

{*Head Segment*}
{*============*}

{*Replace marker if one is missing*}

Replace4(LFHD,RFHD,RBHD,LBHD)
OUTPUT(LFHD,RFHD,RBHD,LBHD)

{*Original method used as will be calculating offset value, so better to use average than
calculate precisely for particular markers*}

LHead = (LFHD+LBHD)/2
RHead = (RBHD+RFHD)/2
FHead = (LFHD+RFHD)/2
BHead = (LBHD+RBHD)/2
CHead = (LHead+RHead)/2
Head = [CHead,BHead-FHead,LHead-RHead,YXZ]

{*Calculate the COM of the head in order to calculate an angle between head and torso*}

COMHead={(-0.4*%lengthhead),(-0.1*%lengthhead),0}*Head
OUTPUT(COMHead)
Head = [COMHead,COMHead-SHO,RHead-LHead,XYZ]
DisplayAxes(Head)

{*Pelvis, Sacrum and Hips*}
{*================================================*}

{*Replace marker if one is missing*}

Replace4(LASI,RASI,RPSI,LPSI)
OUTPUT(LASI,RASI,RPSI,LPSI)

If $Static==1 Then
```

```
        {*Save average leg length as parameter*}
        LLegLength = DIST(LASI,LKNE)+DIST(LKNE,LANK)
        RLegLength = DIST(RASI,RKNE)+DIST(RKNE,RANK)
        MP_LegLength = (LLegLength+RLegLength)/2
        PARAM(MP_LegLength)
EndIf

SACR = (LPSI+RPSI)/2
PELF = (LASI+RASI)/2

Pelvis = [PELF,RASI-LASI,SACR-PELF,xzy]

{*Locate position of Hip JCs using method of Davis et al. 1991, but working in mm not
m*}

LATD = 0.1288*MP_LegLength-48.56
RATD = LATD
C = MP_LegLength*0.115-15.3
InterASISDist=DIST(LASI,RASI)
aa = InterASISDist/2
mm = $MarkerDiameter/2
COSBETA = 0.951
SINBETA = 0.309
COSTHETA = 0.880
SINTHETA = 0.476
COSTHETASINBETA = COSTHETA*SINBETA
COSTHETACOSBETA = COSTHETA*COSBETA

LHJC = {C*SINTHETA - aa,C*COSTHETASINBETA - (LATD + mm) * COSBETA -
C*COSTHETACOSBETA - (LATD + mm) * SINBETA}*Pelvis

RHJC = {-C*SINTHETA + aa,C*COSTHETASINBETA - (RATD + mm) * COSBETA -
C*COSTHETACOSBETA - (RATD + mm) * SINBETA}*Pelvis

HJC = (LHJC+RHJC)/2

OUTPUT(LHJC,RHJC,HJC)

Pelvis = (LHJC+RHJC)/2 + Attitude(Pelvis)
DisplayAxes(Pelvis)

{*Foot Segment*}
{*================================================*}

{*Main Foot Segment*}

LFoot = [LANK,LMTP-LANK,LANK-LANKL,XYZ]
RFoot = [RANK,RMTP-RANK,RANKL-RANK,XYZ]

NLMTP = LMTP+13*LFoot(1)-27*LFoot(2)
```

```
NRMTP = RMTP+13*RFoot(1)-27*RFoot(2)

LFoot = [LANK,NLMTP-LANK,LANK-LANKL,XYZ]
RFoot = [RANK,NRMTP-RANK,RANKL-RANK,XYZ]

output(NLMTP,NRMTP)

DisplayAxes(RFoot)
DisplayAxes(LFoot)

{*Forefoot Segment*}

LFFoot = [LMTP,LTOE-LMTP,LMTPM-LMTP,XYZ]
RFFoot = [RMTP,RTOE-RMTP,RMTP-RMTPM,XYZ]

NLTOE = LTOE-17*LFFoot(1)-20*LFFoot(2)
NRTOE = RTOE-17*RFFoot(1)-20*RFFoot(2)

LFFoot = [NLMTP,NLTOE-NLMTP,LMTPM-LMTP,XYZ]
RFFoot = [NRMTP,NRTOE-NRMTP,RMTP-RMTPM,XYZ]

output(NLTOE,NRTOE)

DisplayAxes(RFFoot)
DisplayAxes(LFFoot)

{*Tibiae*}
{*================================================*}

LTibia = [LKNE,LANK-LKNE,LANK-LANKL,XYZ]
RTibia = [RKNE,RANK-RKNE,RANKL-RANK,XYZ]

{*NOTE - FLEXION EXTENSION (AND ABDUCTION/ADDUCTION) NOT
NECESSARILY ABOUT ANATOMICAL AXIS*}

DisplayAxes(RTibia)
DisplayAxes(LTibia)

{*Femura*}
{*================================================*}

LFemur = [LHJC,LKNE-LHJC,LKNE-LKNEL,XYZ]
RFemur = [RHJC,RKNE-RHJC,RKNEL-RKNE,XYZ]

{*NOTE - FLEXION EXTENSION (AND ABDUCTION/ADDUCTION) NOT
NECESSARILY ABOUT ANATOMICAL AXIS*}

DisplayAxes(RFemur)
DisplayAxes(LFemur)
```

```
{*Trunk Segment for triple jump model*}

Trunk = [HJC,SHO-HJC,RHJC-HJC,XYZ]

DisplayAxes(Trunk)

{*Humerus Segments*}
{*================*}

LHumerus = [LSHO,LELB-LSHO,LELB-LELBL,XYZ]
RHumerus = [RSHO,RELB-RSHO,RELBL-RELB,XYZ]

DisplayAxes(RHumerus)
DisplayAxes(LHumerus)

{*Radius (and Ulnar) Segments*}
{*=========================*}

LRadius = [LELB,LWRI-LELB,LELB-LELBL,XYZ]
RRadius = [RELB,RWRI-RELB,RELBL-RELB,XYZ]

DisplayAxes(RRadius)
DisplayAxes(LRadius)

{*Joint Angles*}
{*============*}

{*Trunk: Global >> Trunk (VCM)*}

TrunkAngles = <Trunk,Global,zyx>

{*Hips: Trunk >> Femora (VCM)*}

LHipAngles = <LFemur,Trunk,zyx>
RHipAngles = <RFemur,Trunk,zyx>

{*Knees: Femora >> Tibiae (VCM)*}

LKneeAngles = <LTibia,LFemur,zyx>
RKneeAngles = <RTibia,RFemur,zyx>

{*Ankles: Tibiae >> Feet (VCM)*}

LAnkleAngles = <LFoot,LTibia,zyx>
RAnkleAngles = <RFoot,RTibia,zyx>

{*MTP: Feet >> Forefeet (VCM)*}

LMTPAngles = <LFFoot,LFoot,zyx>
RMTPAngles = <RFFoot,RFoot,zyx>
```

{*Neck: Head >> Trunk *}

NeckAngles = <Head,Trunk,zyx>

{*Shoulders: Trunk >> Humeri*}

LShoulderAngles = <LHumerus,Trunk,zyx>
RShoulderAngles = <RHumerus,Trunk,zyx>

{*Elbows: Humeri >> Radii*}

LElbowAngles = <LRadius,LHumerus,zyx>
RElbowAngles = <RRadius,RHumerus,zyx>

OUTPUT(RShoulderAngles,LShoulderAngles,RElbowAngles,LElbowAngles,RHipAngles
,LHipAngles)

OUTPUT(RKneeAngles,LKneeAngles,RAnkleAngles,LAnkleAngles,RMTPAngles,LMT
PAngles,TrunkAngles,NeckAngles)

APPENDIX 9

ANTHROPOMETRIC MEASUREMENTS FOR SEGMENTAL INERTIA PARAMETERS

NAME Andrew Bell AGE 22 DATE 16/03/07

All measurements in millimetres

TORSO

Level	hip	umbilicus	ribcage	nipple	shoulder	neck	→	nose	ear	top
Length	0	193	256	385	534	589	0	100	153	266
Perimeter	950	793	821	956		381		508	614	
Width	327	279	277	314	321					
Depth					184					

LEFT ARM

Level	shoulder	midarm	elbow	forearm	wrist	→	thumb	knuckle	nails
Length	0		298	352	569	0	54	91	184
Perimeter	324	284	261	270	167		232	214	115
Width					60		92	87	51

RIGHT ARM

Level	shoulder	midarm	elbow	forearm	wrist	→	thumb	knuckle	nails
Length	0		316	383	572	0	47	91	177
Perimeter	345	277	269	255	175		232	214	125
Width					60		90	87	48

LEFT LEG

Level	hip	crotch	midthigh	knee	calf	ankle	→	heel	arch	ball	nails
Length	0	80		423	572	859	0	7		150	196
Perimeter		565	505	379	374	227		341	259	245	148
Width										94	55
Depth								117			

RIGHT LEG

Level	hip	crotch	midthigh	knee	calf	ankle	→	heel	arch	ball	nails
Length	0	83		451	609	899	0	6		161	212
Perimeter		555	505	365	376	225		327	255	237	157
Width										95	57
Depth								122			

Height (M) 181.9 Mass (KG) 72.6 Shoe Mass (KG) 0.6

Shoe Heel Thickness (mm) 20 Shoe Ball Thickness (mm) 15

APPENDIX 10

TORQUE VELOCITY PROFILES SYMBOL DEFINITIONS

T_{max} - The maximum torque in the eccentric phase

T_0 - The isometric torque

ω_{max} - The angular velocity at which the curve reaches zero torque

ω_c - Defined by the vertical asymptote $\omega = -\omega_c$ of the Hill hyperbola (see Fig. A10.1).

k - Ratio of the slopes of the eccentric and concentric functions at $\omega = 0$. The value of k was set at 4.3, the theoretical value which Huxley (1957) predicted in his original model.

a_{min} - The lowest level of activation in the eccentric phase

ω_1 - The angular velocity at the point of inflection of the function (see Fig A10.2)

m - Parameter governing the rate at which the activation increases with angular velocity ($1/m$ was proportional to the slope at the point of inflection).

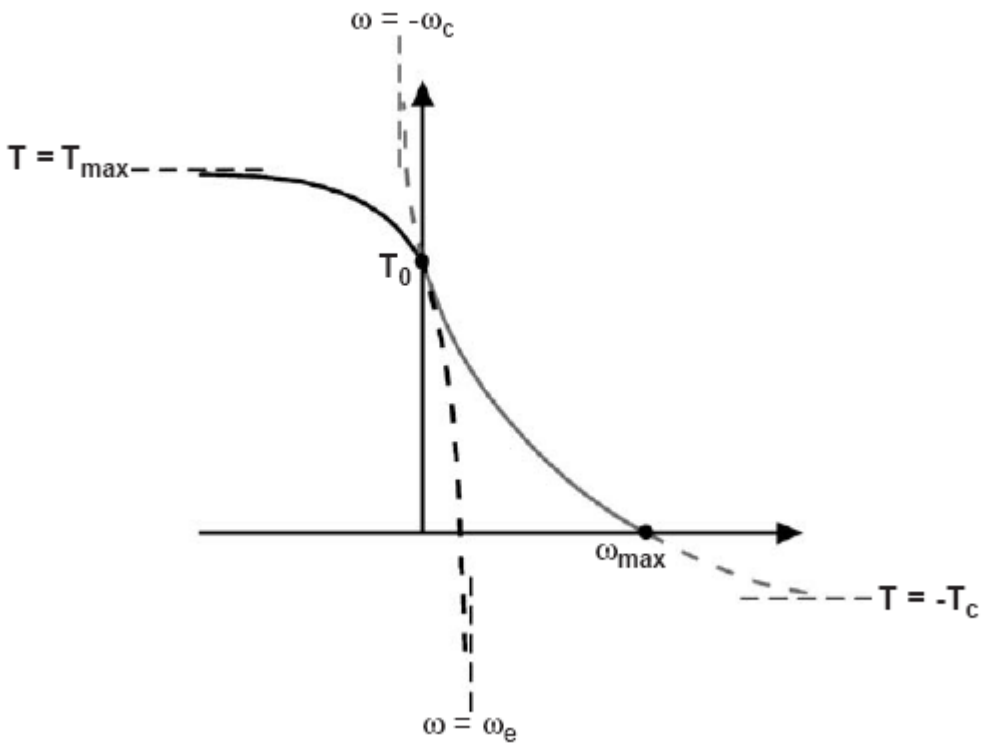

Figure A10.1. Four-parameter maximum torque function taken from Yeadon et al. (2006).

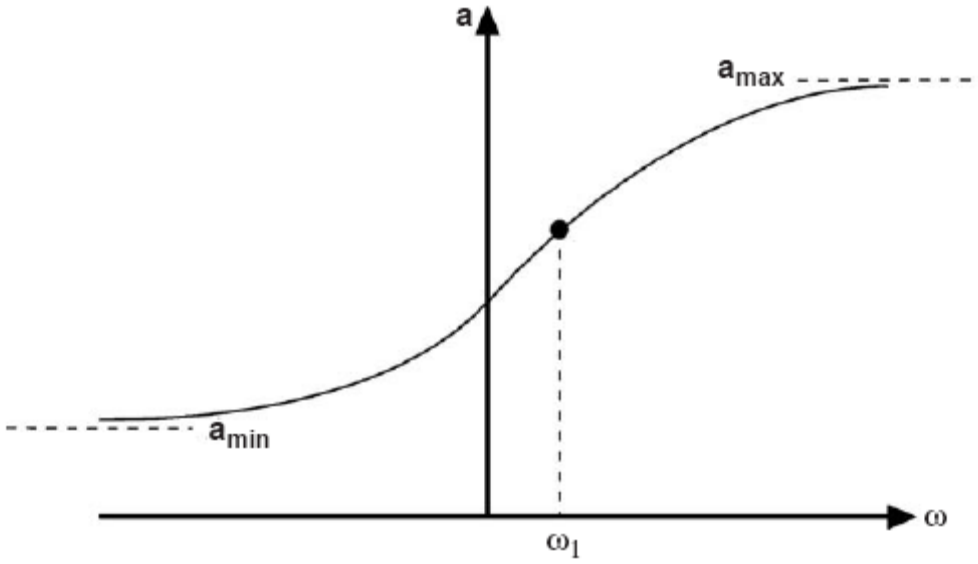

Figure A10.2. The three-parameter differential activation function, taken from Yeadon et al. (2006).

APPENDIX 11

VALUES FOR THE NINE-PARAMETER TORQUE FIT

	Hip Ext	Knee Ext	Ank Plant	Ball Ext	Sho Flex
T_{max} (N)	668	540	464	155	138
T_0 (N)	514	416	272	91	106
w_{max} (rad/s)	26	36	30.8	30.8	36
w_c (rad/s)	7.94	5.44	15.38	15.38	5.83
a_{min} (-)	0.77	0.99	0.88	0.88	0.84
m (rad/s)	1.06	0	0.4	0.4	0.3
w_1 (rad/s)	0.81	-0.36	1.38	1.38	-0.18
k_2 (deg^{-2})	1.64	0.74	0.37	10	0.78
θ_{opt} (deg)	4.93	4.31	4.22	4.22	3.35
$RMS_{weighted}$	24	20	14		
$RMS_{absolute}$ (N)	53	51	30		
% $RMS_{absolute}$ of T_{max}	8	9	6		

	Hip Flex	Knee Flex	Ank Dorsi	Ball Flex	Sho Ext
T_{max} (N)	313	574	107	36	159
T_0 (N)	241	361	64	21	122
w_{max} (rad/s)	28	34.1	26	26	36
w_c (rad/s)	4.2	5.18	3.9	3.9	5.83
a_{min} (-)	0.75	0.74	0.99	0.99	0.84
m (rad/s)	0.26	0.83	0.44	0.44	0.3
w_1 (rad/s)	0.06	1.57	-1.57	-1.57	-0.18
k_2 (deg^{-2})	1.64	0.52	0.44	10	1.08

θ_{opt} (deg)	3.02	2.19	2.13	2.13	3.96
$RMS_{weighted}$	15	16	5		6
$RMS_{absolute}$ (N)	34	33	12		16
% $RMS_{absolute}$ of T_{max}	11	6	11		10

APPENDIX 12

OPTIMISED STIFFNESS AND DAMPING PARAMETERS WITH NO PENALTIES FOR FOOT DEPRESSION

Parameter	Value
Vertical Toe Stiffness (N/m)	296540
Vertical Ball Stiffness (N/m)	6391
Vertical Heel Stiffness (N/m)	1162
Vertical Toe Damping (Ns/m)	199900
Vertical Ball Damping (Ns/m)	2082
Vertical Heel Damping (Ns/m)	122130
Horizontal Toe Stiffness (N/m)*	0.00
Horizontal Ball Stiffness (N/m)*	0.91
Horizontal Heel Stiffness (N/m)*	19.1
Horizontal Toe Damping (Ns/m)*	2.91
Horizontal Ball Damping (Ns/m)*	0.40
Horizontal Heel Damping (Ns/m)*	0.20
Wobbling Mass Stiffness Shank (N/m^3)	5040000
Wobbling Mass Stiffness Thigh (N/m^3)	8806300
Wobbling Mass Stiffness Torso (N/m^3)	5000900
Wobbling Mass Damping Shank (Ns/m)	1685
Wobbling Mass Damping Thigh (Ns/m)	111
Wobbling Mass Damping Torso (Ns/m)	323

* These values are multiplied by vertical force to calculate the horizontal force

APPENDIX 13

OPTIMISED STIFFNESS AND DAMPING PARAMETERS WITH PENALTIES FOR FOOT DEPRESSION

Parameter	Value
Vertical Toe Stiffness (N/m)	453260
Vertical Ball Stiffness (N/m)	147360
Vertical Heel Stiffness (N/m)	291880
Vertical Toe Damping (Ns/m)	463390
Vertical Ball Damping (Ns/m)	113740
Vertical Heel Damping (Ns/m)	249560
Horizontal Toe Stiffness (N/m)*	64
Horizontal Ball Stiffness (N/m)*	126
Horizontal Heel Stiffness (N/m)*	107
Horizontal Toe Damping (Ns/m)*	0.10
Horizontal Ball Damping (Ns/m)*	1.15
Horizontal Heel Damping (Ns/m)*	1.40
Wobbling Mass Stiffness Shank (N/m^3)	636850000
Wobbling Mass Stiffness Thigh (N/m^3)	11392000
Wobbling Mass Stiffness Torso (N/m^3)	1885100
Wobbling Mass Damping Shank (Ns/m)	1734
Wobbling Mass Damping Thigh (Ns/m)	90
Wobbling Mass Damping Torso (Ns/m)	196

Initial Horizontal Velocity Hop (m/s)	7.68
Initial Vertical Velocity Hop(m/s)	-0.99
Initial Angular Velocity of Trunk Hop (rad/s)	1.00
Initial Horizontal Velocity Step (m/s)	7.32
Initial Vertical Velocity Step (m/s)	-2.49
Initial Angular Velocity of Trunk Step (rad/s)	0.85
Initial Horizontal Velocity Jump (m/s)	6.83
Initial Vertical Velocity Jump(m/s)	-2.25
Initial Angular Velocity of Trunk Jump(rad/s)	0.83

* These values are multiplied by vertical force to obtain the horizontal force

APPENDIX 14

TORQUE GENERATOR ACTIVATION TIMINGS FOR MATCHED SIMULATIONS OF ALL THREE PHASES

Hop	a_0	ts_1	tr_1	a_1	ts_2	tr_2	a_2
Right Hip Ext	0.1270	-0.0350	0.0700	1.0000	0.0714	0.0881	0.0000
Left Hip Ext	0.0238	0.0876	0.0895	0.7937			
Right Knee Ext	0.3333	-0.0350	0.0700	0.9968	0.0352	0.0967	0.0000
Left Knee Ext	0.0238	0.0936	0.0786	0.5476	0.0929	0.0705	0.0000
Right Ank Plant	0.3651	-0.0272	0.0835	0.9968	0.0952	0.0790	0.0000
Left Ank Plant	0.0000	0.0000	0.0700	0.0000			
Right Ball Ext	0.0317	0.0933	0.0867	0.6508			
Left Ball Ext	0.2000	0.0000	0.0700	0.2000			
Right Sho Flex	0.3016	-0.0261	0.0719	0.9206	0.0500	0.0767	0.0000
Left Sho Flex	0.2381	-0.0206	0.0905	0.7460	-0.0198	0.0852	0.0000
Right Hip Flex	0.0000	0.0886	0.0957	0.7619			
Left Hip Flex	0.8254	0.0164	0.0890	0.9365	0.0127	0.0976	0.0000
Right Knee Flex	0.3032	-0.0322	0.0771	0.0000	0.0227	0.0886	0.8254
Left Knee Flex	0.0000	0.0706	0.0933	0.4762			
Right Ank Dorsi	0.3127	-0.0161	0.0954	0.0000			
Left Ank Dorsi	0.2000	-0.0300	0.0700	0.2000			
Right Ball Flex	0.0000	0.0000	0.0700	0.0000			
Left Ball Flex	0.5000	-0.0300	0.0700	0.8000			
Right Sho Ext	0.0079	0.0829	0.1002	0.8095			
Left Sho Ext	0.4603	0.0850	0.1105	0.5714			

Step	a_0	ts_1	tr_1	a_1	ts_2	tr_2	a_2
Right Hip Ext	0.3492	-0.0344	0.0767	1.0000	0.0989	0.1000	0.0000
Left Hip Ext	0.0000	0.0819	0.0767	0.3175			
Right Knee Ext	0.3889	-0.0328	0.0724	0.9968	0.0716	0.1000	0.0000
Left Knee Ext	0.0000	0.0850	0.0790	0.0714	0.0333	0.0738	0.0000
Right Ank Plant	0.1905	-0.0317	0.0851	0.9905	0.1262	0.0938	0.0000
Left Ank Plant	0.0000	0.0000	0.0700	0.0000			
Right Ball Ext	0.1587	0.1236	0.0895	0.8333			
Left Ball Ext	0.2000	0.0000	0.0700	0.2000			
Right Sho Flex	0.3968	-0.0228	0.0819	0.9683	0.0246	0.0762	0.0000

Left Sho Flex	0.2540	-0.0039	0.0800	0.7302	-0.0468	0.0700	0.0000
Right Hip Flex	0.0079	0.1157	0.0757	0.9365			
Left Hip Flex	0.9048	0.0437	0.0952	0.9048	0.0968	0.0852	0.0000
Right Knee Flex	0.3857	-0.0067	0.0986	0.0000	0.0506	0.0781	0.6667
Left Knee Flex	0.1667	0.0014	0.0827	0.9127			
Right Ank Dorsi	0.4556	-0.0033	0.1062	0.0000			
Left Ank Dorsi	0.1000	-0.0300	0.0700	0.1000			
Right Ball Flex	0.0000	0.0000	0.0700	0.0000			
Left Ball Flex	0.5000	-0.0300	0.0700	0.5000			
Right Sho Ext	0.1349	0.1102	0.0875	0.3651			
Left Sho Ext	0.4841	-0.0276	0.0954	1.0000			

Jump	**a_0**	**ts_1**	**tr_1**	**a_1**	**ts_2**	**tr_2**	**a_2**
Right Hip Ext	0.0159	0.1086	0.0771	0.9762			
Left Hip Ext	0.1746	-0.0344	0.0767	0.9841	0.1500	0.0919	0.0000
Right Knee Ext	0.0000	0.0968	0.0914	0.0000	0.1000	0.0714	0.0000
Left Knee Ext	0.3730	-0.0344	0.0716	0.9778	0.0906	0.0976	0.0000
Right Ank Plant	0.0000	0.0000	0.0700	0.0000			
Left Ank Plant	0.1429	-0.0261	0.0906	0.9714	0.1119	0.1144	0.0000
Right Ball Ext	0.0000	0.0000	0.0700	0.0000			
Left Ball Ext	0.1032	0.1238	0.0824	0.7381			
Right Sho Flex	0.3254	-0.0080	0.0976	0.4603	-0.0500	0.0795	0.0000
Left Sho Flex	0.4365	-0.0317	0.0905	0.9810	0.0471	0.0857	0.0000
Right Hip Flex	0.0794	-0.0243	0.0871	0.9302	0.1000	0.0767	0.0000
Left Hip Flex	0.0000	0.1252	0.0948	0.6270			
Right Knee Flex	0.5000	0.0014	0.0967	0.6349			
Left Knee Flex	0.3032	-0.0194	0.0886	0.0000	0.1162	0.0719	0.5635
Right Ank Dorsi	0.1000	-0.0300	0.0700	0.1000			
Left Ank Dorsi	0.3159	-0.0328	0.0995	0.0000			
Right Ball Flex	0.5000	-0.0300	0.0700	0.5000			
Left Ball Flex	0.0000	0.0000	0.0700	0.0000			
Right Sho Ext	0.2222	0.0657	0.1057	0.5635			
Left Sho Ext	0.0079	0.1012	0.0700	0.6111			

APPENDIX 15

TORQUE GENERATOR ACTIVATION TIMINGS FOR OPTIMISED SIMULATIONS OF ALL THREE PHASES

Hop	a_0	ts_1	tr_1	a_1	ts_2	tr_2	a_2
Right Hip Ext	0.4206	-0.0350	0.0702	1.0000	0.0696	0.1074	0.0000
Left Hip Ext	0.0000	0.0959	0.0967	0.7293			
Right Knee Ext	0.4524	-0.0178	0.0781	1.0000	0.0517	0.0808	0.0000
Left Knee Ext	0.0036	0.1192	0.0861	0.5131	0.0925	0.0740	0.0000
Right Ank Plant	0.1916	-0.0266	0.0867	1.0000	0.1040	0.0806	0.0000
Left Ank Plant	0.0000	0.0000	0.0700	0.0000			
Right Ball Ext	0.0074	0.0933	0.0806	0.8344			
Left Ball Ext	0.2000	0.0000	0.0700	0.2000			
Right Sho Flex	0.4206	-0.0161	0.0719	0.8968	0.0183	0.0705	0.0000
Left Sho Flex	0.0476	-0.0339	0.0748	0.9762	0.0373	0.0781	0.0000
Right Hip Flex	0.0032	0.1085	0.1116	0.8096			
Left Hip Flex	0.8048	0.0160	0.0824	0.9429	0.0154	0.0964	0.0000
Right Knee Flex	0.3349	-0.0067	0.0897	0.0000	0.0600	0.0757	0.7429
Left Knee Flex	0.0413	0.0877	0.0920	0.5808			
Right Ank Dorsi	0.4365	0.0023	0.0782	0.0000			
Left Ank Dorsi	0.2000	-0.0300	0.0700	0.2000			
Right Ball Flex	0.0000	0.0000	0.0700	0.0000			
Left Ball Flex	0.5000	-0.0300	0.0700	0.8000			
Right Sho Ext	0.0000	0.1046	0.0748	0.8254			
Left Sho Ext	0.0000	0.1021	0.0748	0.6349			

Step	a_0	ts_1	tr_1	a_1	ts_2	tr_2	a_2
Right Hip Ext	0.3647	-0.0350	0.0702	1.0000	0.0970	0.0931	0.0000
Left Hip Ext	0.0000	0.1482	0.0923	0.1508			
Right Knee Ext	0.2148	-0.0350	0.0721	1.0000	0.0610	0.0740	0.0000
Left Knee Ext	0.0000	0.1034	0.0899	0.0000	0.0328	0.0989	0.0000
Right Ank Plant	0.1397	-0.0330	0.0789	1.0000	0.1356	0.0921	0.0000
Left Ank Plant	0.0000	0.0000	0.0700	0.0000			
Right Ball Ext	0.0000	0.1038	0.0713	0.9841			
Left Ball Ext	0.2000	0.0000	0.0700	0.2000			
Right Sho Flex	0.1746	-0.0183	0.0886	0.9762	0.0475	0.0862	0.0000

Left Sho Flex	0.1746	-0.0206	0.0971	0.6667	0.0259	0.0905	0.0000
Right Hip Flex	0.0000	0.1492	0.0797	0.9286			
Left Hip Flex	0.5000	0.1033	0.0959	0.9481	0.0638	0.1020	0.0000
Right Knee Flex	0.3734	-0.0333	0.0821	0.0000	0.1141	0.0823	0.6746
Left Knee Flex	0.1267	-0.0288	0.0706	0.9810			
Right Ank Dorsi	0.3832	-0.0296	0.0906	0.0000			
Left Ank Dorsi	0.1000	-0.0300	0.0700	0.1000			
Right Ball Flex	0.0000	0.0000	0.0700	0.0000			
Left Ball Flex	0.5000	-0.0300	0.0700	0.5000			
Right Sho Ext	0.0000	0.1024	0.0862	0.8730			
Left Sho Ext	0.0000	0.1476	0.0852	0.6270			

Jump	a_0	ts_1	tr_1	a_1	ts_2	tr_2	a_2
Right Hip Ext	0.0000	0.1481	0.0862	0.8317			
Left Hip Ext	0.1726	-0.0350	0.0711	1.0000	0.1662	0.0922	0.0000
Right Knee Ext	0.0000	0.0795	0.0893	0.0000	0.1016	0.0793	0.0000
Left Knee Ext	0.4325	-0.0307	0.0713	1.0000	0.0843	0.0909	0.0000
Right Ank Plant	0.0000	0.0000	0.0700	0.0000			
Left Ank Plant	0.0436	-0.0092	0.0918	1.0000	0.1225	0.1177	0.0000
Right Ball Ext	0.0000	0.0000	0.0700	0.0000			
Left Ball Ext	0.0048	0.1173	0.0742	1.0000			
Right Sho Flex	0.5000	-0.0011	0.0995	0.9127	0.0794	0.0838	0.0000
Left Sho Flex	0.4127	-0.0272	0.0757	0.9444	0.0814	0.0829	0.0000
Right Hip Flex	0.2214	-0.0296	0.0932	0.9524	0.0984	0.0773	0.0000
Left Hip Flex	0.0063	0.1450	0.0907	0.4333			
Right Knee Flex	0.4968	-0.0350	0.0859	1.0000			
Left Knee Flex	0.3317	-0.0081	0.0984	0.0000	0.1284	0.0734	0.4148
Right Ank Dorsi	0.1000	-0.0300	0.0700	0.1000			
Left Ank Dorsi	0.4302	-0.0130	0.1046	0.0000			
Right Ball Flex	0.5000	-0.0300	0.0700	0.5000			
Left Ball Flex	0.0000	0.0000	0.0700	0.0000			
Right Sho Ext	0.0000	0.1484	0.0910	0.7222			
Left Sho Ext	0.0000	0.1357	0.0819	0.7302			